Design and Implementation of System Components for Radio Frequency Based Asset Tracking Devices to Enhance Location Based Services

R. Asif

Ph.D.

UNIVERSITY OF BRADFORD

2017

Design and Implementation of System Components for Radio Frequency Based Asset Tracking Devices to Enhance Location Based Services

Study of angle of arrival techniques, effects of mutual coupling, design of an angle of arrival algorithm, design of a novel miniature reconfigurable antenna optimised for wireless communication systems

Rameez Asif

B.Eng., M.Sc., M.Phil.

Submitted for the Degree of
Doctor of Philosophy
Faculty of Engineering and Informatics
University of Bradford

2017

Design and Implementation of System Components for Radio Frequency Based Asset Tracking Devices to Enhance Location Based Services

Study of angle of arrival techniques, effects of mutual coupling, design of an angle of arrival algorithm, design of a novel miniature reconfigurable antenna optimised for wireless communication systems

Keywords

Angle of Arrival, Direction of Arrival, ESPIRIT Signal to Noise Ratio (SNR), Multiple Signal Classification (MUSIC), Antenna Array, Mutual Coupling, Reconfigurable Antenna, Log Spiral Antenna, Impedance Bandwidth

Abstract

The angle of arrival estimation of multiple sources plays a vital role in the field of array signal processing as MIMO systems can be employed at both the transmitter and the receiver end and the system capacity, reliability and throughput can be significantly increased by using array signal processing. Almost all applications require accurate direction of arrival (DOA) estimation to localize the sources of the signals. Another important parameter of localization systems is the array geometry and sensor design which can be application specific and is used to estimate the DOA.

In this work, various array geometries and arrival estimation algorithms are studied and then a new scheme for multiple source estimation is proposed and evaluated based on the performance of subspace and non-subspace decomposition methods. The proposed scheme has shown to outperform the conventional Multiple Signal Classification (MUSIC) estimation and Bartlett estimation techniques. The new scheme has a better performance advantage at low and high signal to noise ratio values (SNRs).

The research work also studies different array geometries for both single and multiple incident sources and proposes a geometry which is cost effective and efficient for 3, 4, and 5 antenna array elements. This research also considers the shape of the ground plane and its effects on the angle of arrival estimation and in addition it shows how the mutual couplings between the elements effect the overall estimation and how this error can be minimised by using a de-coupling matrix.

At the end, a novel miniaturised multi element reconfigurable antenna to represent the receiver base station is designed and tested. The antenna radiation patterns in the azimuth angle are almost omni-directional with linear polarisation. The antenna geometry is uniplanar printed log-spiral with striplines feeding network and biased components to improve the impedance bandwidth. The antenna provides the benefit of small size, and re-configurability and is very well suited for the asset tracking applications.

Acknowledgement

First and Foremost, I would like to thank **Allah (S.W.T)** for giving me this opportunity to take on this challenge and achieve this landmark.

The completion of this thesis would not have been possible without the help and support of the following people. I would like to express my extreme appreciation and gratitude to my supervisor and mentor *Prof R. A. Abd-Alhameed***.** He has been very generous in his time and always a source of encouragement and inspiration to me. Also, I would like to thank, *Dr. J.M. Noras*, *Dr. SMR Jones* and *Dr. C. H. See* for their ideas, support, and guidance throughout this work.

In addition, I would also like to extend my gratitude to the industrial colleagues from Seven Technologies Company, UK, *Dr. Taherah Ghazaany* and *Dr. Sharon Zhu* for their excellent help and support to join their work on antenna array design for localization purposes.

Moreover, I extend my thanks to all the members of the Radio Frequency and antenna lab, workshop, and computer officers, for their great support and help.

I wish to express my deepest thanks to my friends *Mohammad Al-Sadoon and Ammar Ali* for their endless support throughout my research.

Finally, special thanks are also given to my family for their support and encouragement through all my pursuits over this period of time.

Dedication

I would like to dedicate my whole life and work to my parents. There are not enough words in any dictionary that can express my gratitude to my parents. Throughout my life despite of all the constraints they provided me with all the comfort. My mother who dedicated her life to me and always prayed and asked Allah Almighty for just one thing and that was my success. She provided me with every possible support and comfort. Whenever I lost the motivation or got worried she was right there to console and encourage me. My father who was a constant source of inspiration for me, he believed in my abilities, supported my decisions, encouraged me at every step and made me believe in myself. Throughout my career I never had to worry about anything because he was always there to take care of things for me. I consider myself blessed to have such loving, dedicated and supportive parents. I know I can never thank my parents enough for all the sacrifices they have made for me. I pray that may Allah Almighty give them a healthy long life so that they can see their dreams coming true. Ameen.

Table of Contents

LIST OF FIGURES

LIST OF TABLES

Acronyms

AFLT	Advanced Forward Link Trilateration
A-GPS	Assisted Global Positioning System
AOA	Angle of Arrival
AWGN	Additive White Gaussian Noise
BSS	Base Station Subsystem
BW	Bandwidth
CDMA	Code Division Multiple Access
CGI	Cell Global Identity
CST	Computer Simulation Technology, (https://www.cst.com)
DAS	Distributed Antenna System
DOA	Direction of Arrival
DRSS	Difference Received Signal Strength
E-911	Enhanced 911
EFLT	Enhanced Forward Link Trilateration
E-OTD	Enhanced Observed Time Difference
ESPIRIT	Estimation of Signal Parameters Via Rotational Invariance Techniques
FB	Facebook
FOU	Four Square
GIS	Geographic Information System

GLA	Google Latitude
GNSS	Global Navigation Positioning Satellite System
GOW	Gowalla
GPRS	General Packet Radio Service
GPS	Global Positioning System
GSM	Global System for Mobile Communications
HT	Hybrid Techniques
IPDL	Idle Period on the Down Link Trilateration
IR	Infra-Red
LMU	Location Measurement Unit
LOS	Line of Sight
MAC	Media Access Control
MEMS	Micro Electro-Mechanical Systems
MIMO	Multiple Input Multiple Output
MISO	Multiple Input Single Output
ML	Maximum Likelihood
MS	Mobile Stations
MUSIC	Multiple Signal Classification
NLOS	Non-Line of Sight
NEC	Numerical Electromagnetic Code, https://www.nec.com
OUTLIERS	Observations That Do Not Follow the Pattern of The Majority of The Data

RAU	Remote Antenna Units
RFID	Radio Frequency Identification
RSS	Received Signal Strength
RTD	Real Time Difference
SIMO	Single Input Multiple Output
SISO	Single Input Single Output
SNR	Signal to Noise Ratio
TDM	Time Division Multiplexing
TDOA	Time Difference of Arrival
THP	Tomlinson Harashima Precoding
TOA	Time of Arrival
TTFF	Time to First Fix
VANETS	Vehicular Ad-Hoc Networks
WAG	Wireless Assisted GPS
WAVE	Wireless Access for Vehicular Environment
WCDMA	Wireless Code Division Multiple Access
WLAN	Wireless Local Area Network

LIST OF NOTATIONS

τ	*Signal Propagation Time*
d	Distance between two nodes
t_a	Arrival time of signal on a^{th} node
c	Speed of light
t_s	Start time of the signal
x_a	Position of a^{th} node on x-axis
y_a	Position of a^{th} node on y-axis
t_b	Arrival time of signal on b^{th} node
t_e	Arrival time of signal on e^{th} node
x_b	Position of b^{th} node on x-axis
y_b	Position of b^{th} node on y-axis
x_e	Position of e^{th} node on x-axis
y_e	Position of e^{th} node on y-axis
x_m	Position of $mobile$ on x-axis
y_m	Position of $mobile$ node on y-axis
φ	Azimuthal Angle
θ	Elevation Angle
A	Peak amplitude
β	Wave Vector
λ	Wavelength

f	Frequency
M	Total number of omni directional antennas
d	Distance between two antennas
ω	Angular Frequency
a_m	Steering factor of the m^{th}
t_d	Wave propagation time
R	Radius of the circle
$\mathrm{u_m(t)}$	Input Signal at M omni-directional antennas
$\mathrm{y(t)}$	Output signal
$\mathbf{a}(\varphi)$	Steering Vector
L	Number of Signals
k	Total number of iterations

1. INTRODUCTION

1.1 Introduction

In the exponentially increasing market of wireless communications location based services serve as the key enabling technology. Location based services (LBS) exists from short range Bluetooth and ad hoc to long range telecom networks. Location based services in a broad sense are considered to provide the basic information about the whereabouts of the service users by using the location of the wireless devices within the network. The latter is the critical issue among all to uniquely identify the device.

1.2 Location Aware Services

The demand for the location aware services has considerably increased with the increase of mobile and wireless devices. e.g. in the field of medical science patient management and movement [1-5], concept of smart spaces that enables the physical space and human interaction [6-10], in the field of [11] logistics for the transportation of goods [12, 13], inventory management and warehousing [14-17], environmental monitoring services use sensor network for real time weather predictions and to determine the source of pollutants that are present in air and water [18] and content sharing using mobile peer to peer connections [19-21].

1.3 Background and Motivation

Estimation problem and in specific parameter estimation has been a topic of great interest for the engineer's due to its applications and their ever-growing requirement for an improved performance [15 - 17]. With the expansion in the applications the accurate estimation of temporal and spatial parameters found wide spread interest. Sensor array processing has been an area of active research during the past decade because of the requirement to gather data from all sensors to provide an estimation. Array sensor processing relies on the prior knowledge of the geometry of the array and the characteristics and number of array elements. The most regarded achievement of this method is the source location estimation using radars and sonars. One of the earliest angle of arrival (AoA) techniques was suggested in 1961 [22] and named as the classical beamformer method. The fundamental principle of this method suggests to apply an equal weighting on each antenna element to construct the steering vector in a certain specific direction [23]. This approach is ideal to rotate the steering vector of array mechanically in a specific direction and measuring the output power. However, due to the high level of side lobes, output power is the sum of the power from the direction of array steering vector and from other directions where the side lobes are pointing. Thus, the revolving power depends on the size of antenna array and beamwidth of main lobe. In 1969, author in [24] proposed an algorithm to estimate the power of incoming signals. This algorithm is known as minimum variance distortionless response (MVDR) method. The idea of this approach is to estimate a signal from one direction and consider all other signals as interference. MVDR method has

much better resolution compared with the classical beamformer method. On the other hand, when the signals are similar or highly correlated the resolution of MVDR becomes worse than classical beamformer algorithm [25]. In 1971, author in [26, 27] developed a technique to control the cancellation of interference signals adaptively. This technique was called as the Howells-Applebaum method. At the time, authors in [28, 29] utilized a least mean square to minimize error between the output of antenna array and self-training of reference signal. This technique is known as least mean square (LMS) method, which uses the steepest descent or gradients methods to find the optimum weights. The convergence of approach is mainly based upon on the eigenvalues spread. The eigenvalues become larger as the convergence time increases [30]. The convergence time of this method is dependent on the gradient step size parameter, which is given in [31]. As they were affected by the Rayleigh fading channel conditions, this method suffers from many problems such as poor resolution, wide main beam and higher side lobes level. These issues limited the ability of delay and sum methods to separate closely spaced signals and acquire satisfying performance and high resolution [32]. However, MVDR method can overcome the poor resolution problem associated with the delay-and-sum method, and gives a significant improvement compared with this type of techniques.

Unlike traditional techniques, subspace algorithms utilize the structure of the received signal, instead of exploiting the statistic characteristics of received data; which is leading into a significant improvement in resolution. This type of

algorithms provides better resolution and performance compared with previous types. In 1972, a maximum entropy (ME) algorithm was proposed by [33]. The main idea of this method is to determine the pseudo spectrum that maximizes the entropy function subject to conditions. In 1973, author in [34] proposed an AOA method which is called Pisarenko harmonic decomposition (PHD), which exploits the Eigen structure of covariance matrix to estimate the direction of incoming signals. The main idea of this technique is to minimize the mean squared error (MSE) of the antenna array output under the specific condition that makes the norm of weight vector equal to unity. This approach has better resolution compared with Classical Beamformer, MVDR and ME methods [35]. In 1975, [36] proposed a linear prediction error method to estimate the direction of incoming sources by minimizing the mean squared prediction error between the output of antenna array and actual output. In 1979, a Minimum Norm algorithm was proposed by [37] and then developed in 1983 by [38]. This method is employed by optimizing the weight vector of array output. The limitation of this algorithm is that it is only applicable on the uniform linear arrays (ULA). In (1983) [161] proposed Root MUSIC technique to reduce the computational complexity of MUSIC method. The main idea of this approach is to search for the roots, which are associated with direction of arrival signals. This method is faster than MUSIC because it does not need the manifold and give better accuracy even when the angle of arrivals is close to each other. The main limitation of this method is that it is also applicable on the uniform linear antenna array. Moreover, not all roots give the correct location of AOA, therefore requires extra processing to select the right roots. In 1986, a multiple emitter

location and signal parameter estimation (MUSIC) method was suggested by [39]. MUSIC is an Eigen structure technique, which provides fair estimates for the angles of arrival, number of signals, and the strength of each waveform. The idea of this algorithm is dependent on the orthogonality between the noise subspace and steering vector of antenna array. In 1989, [40] suggested the Cyclic MUSIC algorithm, which utilized the spectral coherence characteristics of the received signal and made it has ability to solve signals spaced more accurately. Additionally, the Cyclic MUSIC algorithm averts the condition that the total number of incoming signals on the array are less than the number of antenna elements. Many efforts have been made to simulate and develop this algorithm [41-50]. Also In 1989, [51] suggested an Estimation of Signal Parameters via Rotational Invariance Technique (ESPRIT) to estimate the direction of arrival signals. ESPRIT method assumes that the type of sources are narrowband as well as number of received signals is less than number of the antenna elements. The main idea of this technique depends on exploiting the rotational invariance of the signal subspace, which is produced by two arrays with a translational invariance structure. It is very much necessary to separate these subarrays as translationally and not rotationally. In 1991, [52] proposed the propagator method to estimate the DOA of signal. This technique has low complexity since it does not require decomposition of the eigenvalues and eigenvector of the covariance matrix. However, it utilizes the whole covariance matrix to obtain the propagation operator. Thus, this technique is only suitable in the presence of AWGN and its performance will significantly deteriorate under

spatial non-uniform noise. The performance of this method was analysed and evaluated in addition to its advantages and drawbacks in [53].

Many efforts and attempts have been done to improve performance and increase resolution of the conventional MUSIC algorithm. One of these attempts was achieved in 1991 by [54]. He proposed a Root-MUSIC algorithm to find roots that represent the location of incident signals. Root-MUSIC method depends on polynomial rooting [55]. Simply, the goal of this method is to reduce the complexity of MUSIC by finding the roots that are associated with received signals. However, this algorithm is only applicable on the uniform linear arrays. In 1997, [56] suggested Norm Root MUSIC to reduce the complexity of root computational and minimize the order of the polynomial [56]. Briefly, the idea of this technique is to apply the rules of Root MUSIC method on the Min-Norm algorithm. This algorithm gives better resolution than MUSIC. However, this approach is only suitable for uniform linear array and this limits its application. Additionally, the roots sometimes do not give the correct indication toward the angles of arrival especially at poor SNR. In 2004, [57] presented a method for signal direction estimation based on the spatial filter. This method combined subspace approach with spatial filter algorithm to obtain good performance for angles estimation at medium signal to noise ratio. Further, it can solve sources under resolution threshold. In 2013, [58] presented a method to estimate the direction of received signals by combing the delay profile estimation method with AoA estimation technique. The advantage of this method is that it uses delay profile technique to separate the incoming signal under multipath

conditions and then employs AoA approach to estimate the direction of the incoming signals. In 2015, [59] proposed hybrid MUSIC and hybrid ESPRIT methods to estimate the direction of angles of arrival in hybrid antenna array technique. The hybrid antenna array approach employs the same analogue to digital converter (ADC). The purpose of this work was to estimate multiple received signals simultaneously instead of one AoA. The essential idea is to divide the incoming information into several orthogonal frequency division multiple (OFDM) symbols. Enormous efforts have been made to improve the accuracy of the estimation algorithms to provide better location estimates to improve the quality of the location based services and some algorithms are very highly regarded but there is a room for improvement in this field to present a faster and reliable algorithm and this will be the first focus of this work.

In addition to the estimation problem the design of a small enough antenna array for localization applications using TETRA VHF/UHF frequencies is another great challenge [60]. These frequencies are a preferred choice for radio frequency based tracking systems and applications due to their longer wavelengths and thus the ability to travel longer distances and easy detection but due to the longer wavelengths the conventional techniques of antenna design result in large dimensioned sensors which are not suitable due to the space constraints in most modern tracking hardware. The smaller designs that have been proposed in the literature suffer from limited bandwidth due to their small size. But size is a major constraint as the mobile tracking devices need to be discrete and customer friendly

and can have more than one tracking solution built in such as a combination of radio frequency and Global Positioning System (GPS) which then add additional space requirements for the GPS receivers. A new sensor array design which is small, reliable and easy to manufacture is of great importance and this important parameter is another focus of this thesis.

Another challenge that is faced by the world of wireless communication in general is that of the multipath effects of the channel which in result change the signal covariance matrix and result in wrong angle of arrival estimation.
All the needs of these fast-growing applications and current technological limitations motivated this research.

1.4 Aims, Objectives and New Contributions

The aim of this research is to contribute on the system level towards the study, design and implementation of system components for the tracking devices that can be used to enhance the user or asset location estimate and to provide improved location based services. The system level components that are focussed in this work include the angle estimation algorithm, antenna design suitable for integration in a tracking device in the form of an array, and transmission scheme.

Objectives identified towards this aim were to:

- Review and understand the Location Aware Services their applications and importance.

- Understand the parameter estimation problem and model and simulate current estimation algorithms.
- Contribute new technique that enhance the capability of the current localization framework.
- Design an antenna that can be employed in a practical tracking system, which is reliable, has a suitable radiation pattern and easy to manufacture.

The major contributions of this work are

- A new signal subspace based angle of arrival estimation algorithm is proposed in Chapter 3 and the mathematical model is derived. Simulations and measurements have been carried out to evaluate the performance of the proposed algorithm and the results prove that the proposed algorithm can indeed enhance the performance of the conventional widely accepted angle estimation algorithms.
- Evaluation of the mutual coupling methods namely conventional impedance method and receiving mutual impedance method by calculating the decoupling matrices and applying them to the data to measure performance improvements to propose the best algorithm to be used for localization purposes is described in Chapter 4. In localization systems, the antenna arrays are employed as receivers so the receiving mutual coupling method is proposed which is easier to implement and has the same complexity as the conventional mutual impedance method.

- In mobile devices used for localization, size, reliability, cost and performance of the receiver are of utmost importance. For this purpose, Design of a novel reconfigurable miniaturised antenna suitable for localization applications is presented in Chapter 5.
- Orthogonal Frequency Division Multiplexing (OFDM) systems have been applauded for their ability to combat multipath and for this reason OFDM based wideband transmission scheme for angle of arrival estimation has been evaluated.

1.5 Organization of the Thesis

Chapter 2: This chapter provides an introduction of the location based services. It describes the different positioning systems including the indoor positioning systems, the RFID based systems and the GPS. Provides details about the outdoor localization systems using terrestrial base stations and techniques that are employed by the current systems to provide localization services. Then a review of the latest trends and applications of the location aware services is presented.

Chapter 3: This chapter opens with an introduction to the term localization its applications followed by a mathematical derivation of antenna arrays that can be used as receivers in a localization system. Mathematical models of some of the well-known direction of arrival (DOA) estimation techniques are presented followed by the mathematical model of the new signal subspace based angle of arrival estimation algorithm. This chapter further considers the performance of the

proposed algorithm under different constraints and provides a comparison between the proposed algorithm and other methods including phase interferometry, MUSIC and Bartlett, Minimum variance distortionless response etc. to highlight the advantages of the proposed algorithm.

Chapter 4: Mutual coupling between antenna arrays which is a big problem is discussed in this chapter with examples. Two different mutual coupling compensation methods namely conventional and received impedance based methods are presented. These methods were then evaluated in terms of performance improvement in the angle of arrival and ease of implementation. Calculation of the decoupling matrices for both methods is described and the results are studied. The decoupling matrices were then applied to the data from different array geometries and the performance was evaluated in terms of angle estimation error for antenna arrays with mutual coupling and with mutual coupling compensated.

Chapter 5: With the current knowledge of the design of the antennas it is very hard to design an antenna that is small, has sufficient bandwidth and gain and is capable of surface mounting for TETRA VHF/UHF frequencies. Such a novel reconfigurable antenna is presented in this chapter. The design and implementation of this antenna is detailed in terms of antenna geometry, design methodology and the switch design. Results and discussion are then presented

which focus on the antennas performance in terms of reflection coefficient, reconfigurability, radiation pattern and gain.

Chapter 6: This chapter entirely comprises of the measurement data received using arrays of the prototype antenna. Different geometry configurations were measured and the results were processed using MATLAB and the angle of arrival estimation methods were applied including the proposed method to deduce the angle estimations. The results obtained are then detailed and discussed.

Chapter 7: This chapter provides the mathematical description of how the OFDM system can be employed in angle of arrival estimation. Angle of arrival estimation performance is then presented for different number of antenna elements with different Bandwidth and the results are discussed

Chapter 8: This chapter summarizes the whole thesis and provides the outcomes of this research. The conclusions gathered from each chapter and how this work can be further extended is discussed in this chapter.

2. LOCATION BASED SERVICES: A REVIEW

2.1 Introduction

Location Based Services (LBS) involve rendering different services to a subscriber based on user location [61, 62], ranging from security [63], infotainment [64], healthcare [65-70], retailing [71] , tracking [72] and so on. These can be done in either position-aware technology in which a device is aware of its own position or other devices track the location of the device [73]. LBS was first pursued to offer efficient safety to subscriber by determining exact user geographical location [74] and later infotainment services which can be delivered to the user using the geographical location identity of the mobile devices [75, 76]. Some LBS have the capability of detecting when the boundaries between regions or zones have been crossed while others can detect the location services based on service logic capability [77, 78]. These LBS techniques can as well be applied in the tracking services of old and disabled persons [79], monitoring health of patients [80, 81], navigational services at the airports [82], traffic telematics [83], fleet management [84, 85], enquiry and information services, crime fighting [86], toll systems [87], marketing [88], gaming [89], geography mark-up and community services [74, 90, 91]. Some modern applications include location enabled web services [92] such as social networking [93] including Gowalla (GOW), Facebook (FB), Four Square (FOU), Google Latitude (GLA), etc. The location of the user is disclosed to enhance the social networking scenario. LBS are based on second generation

(2G), third generation (3G), fourth generation (4G) long term evolution (LTE) and fifth generation (5G) mobile positioning systems [94-96]. In 2G and 3G systems radio resource control (RRC), IS-801, and radio resource location services protocol to meet the criteria for the location based emergency services and applications, the current 4G standard supports techniques such as assisted global navigation satellite system (a-GNSS), enhanced cell-ID (ECID) and observed time difference of arrival (OTDOA) using the LTE positioning protocol (LPP) which enables localization over LTE [97]. There are five different technologies that have been proposed for the upcoming 5G systems which include device-centric architecture, massive multiple input multiple output (Massive MIMO), millimetre wave (MW), smarter devices and support for the machine to machine (M2M) communications and most of those will help improve the location accuracy as suggested in [98, 99]

As the geographical position of the user changes, location management first requires the network to authenticate the user and update the location profile of the user [100-102]. The second step is the delivery of the call in which the network identifies the updated location profile of the user and finds the present position of the mobile terminal [103, 104]. There are different positioning systems for mobile terminals in LBS which differ in reliability, accuracy, and time. These include satellite positioning systems [105], network based positioning systems and local positioning systems [106, 107].

The US government upholds a self-regulatory environment for corporations, such that the firms are permitted to access, use, and sell consumer proprietary information. European regulations, for example in Germany, contrast with this by restricting with stricter laws about access to and use of private information. This dichotomy limits the adoption of LBS by subscribers (who are aware), for example in retail LBS services. In fact, location tracking services generate more concerns for privacy than position-aware services. This is solved by offering the user the option of turning off location data services.

Other major challenges facing LBS include measuring the mobility of the client, location reliant obstacles and delivering services with high performance [108] and security [109, 110]. LBS Actors involve regulation and standardization organizations, location information providers, logistics providers and users. The localization infrastructure for LBS include LBS indoor systems, LBS satellite systems, LBS Global Positioning Systems (GPS), outdoor systems using terrestrial base stations (BSs). Present geo-location techniques for LBS are categorized into Global Navigation Satellite System (GNSS) based [111], cellular network based, or the combination of both [112]. GNSS based methods depends largely on the visibility of the satellite and the geometry of the receiver satellite. It can create problems in urban areas and in indoor locations [113-116] . In the past years, more attention was paid to outdoor localization but with the rapid advancement in the technology in the recent year’s indoor localization techniques have also become popular [117-119]. Information gained from indoor spatial localization has been

used to deal with disaster management [120] in case of natural disaster and emergency cases [121-124]. Indoor localization methods do not depend on GPS [125-127].

2.2 Positioning Methods for LBS

In this section, a discussion is presented on LBS using different positioning methods. Both indoor and outdoor positioning methods are discussed.

2.2.1 Indoor Positioning Systems

Indoor localization uses various techniques such as Radio Frequency Identification (RFID) [70, 128], Bluetooth [119, 129-134] and Wi-Fi technologies. An indoor location system is comprised of a set of antennas containing wireless tags. These antennas transfer data wirelessly by means of tags which are attached to an object or a person or an animal. The antennas communicate wirelessly with tags, which are attached to humans, or to desired positions. The method for communication might include Bluetooth, RFID, Wireless Local Area Network (WLAN) and Infrared (IR) [135-137]. In the case of outdoor localization, GPS is required which depends on Line of Sight (LOS) to the GPS satellites. Satellite-based GPS systems are only suitable for outdoor localization but localization within the indoor environments such as buildings can be attained using assisted GPS (a-GPS) [138]. Infrared-based systems such as active badges are also used for indoor localization but their drawback is that they require supplementary hardware and have short range transmitters. An indoor positioning system detects the position of a person or an

object in an indoor space such as hospital, organization, home, etc. [139]. Indoor positioning such as indoor mobility systems need accuracy of the location of the user. In indoor Wi-Fi based systems, the influence of multipath propagation must be considered, namely the reflection and absorption of the signals. When the signal strength is matched with the values of the earlier recorded database, it is necessary to consider a range of values due to the multipath that are reasonably similar.

Advancement in the Wi-Fi technology and in smart devices has made it easier for locating people indoors. For this purpose, the trilateration method is used which calculates the distance from a close-by access points through Media Access Control (MAC) addresses. In this case, the recorded signal strength values are used to estimate the distance of a user [140-142]. Unconnected Wi-Fi micro location based applications do not depend on cellular networks. Location enabled Wi-Fi networks in buildings, campuses and indoor public places deliver micro Geographic Information Systems (GIS) application opportunities for education, business, health care, supply chain management etc.

The indoor positioning system comprises of three layers, namely the location sensing system, software location abstraction and location based applications. The quality criteria for the localization methods include localization accuracy, availability and consistency, applicability, power consumption, the size of the hardware, software processing load and the supported positioning modes, signalling and

network dependent load, cost, standardization, and latency.

2.2.2 Radio Frequency Identification (RFID)

Radio Frequency Identification (RFID) uses a chip containing a radio frequency electromagnetic field coil. It transmits a coded identification number transmitted by the electromagnetic field coil when it is queried by the reader device [143]. RFID chips are usually integrated in products and are also implanted in animals for their identification. For transferring data, RFID uses a wireless system comprising of radio frequency electromagnetic fields and are rapidly replacing the bar codes. RFIDs are used for various purposes such as toll collection, access management and for tracking of animals, goods or people [144]. RFID system comprises of a reader and numerous active or passive tags. An active tag contains an internal battery which is readable from a remote distance [145-147]. The limitation of RFID tags is that they cannot work in an environment where there is shortage of power, gate count and memory storage. Hence, privacy and security are the major hurdles in the deployment of the RFID technology [148-151] .

For transmitting and receiving data, RFID tags and readers use well-defined radio frequencies and protocols defined by International Telecommunications Unit (ITU) and European Telecommunication Standards Institute (ETSI) for Europe [152, 153] and the frequency ranges which are used for RFID systems include low frequencies (LF) ranging from 100 kHz to 500 kHz [154], high frequencies (HF)

from 10 MHz to 15 MHz [155] and ultra-high frequencies (UHF) ranging from 850 to 950 MHz [156, 157] .

2.2.3 Global Positioning Systems (GPS)

Global Positioning System (GPS) is a successful commercial system providing LBS including reliable navigational, positioning, and timing services. This satellite navigational system is formed by the 24 satellites circling around the earth's orbit and their compatible receivers here on earth. GPS receivers can calculate accurate speed, location, and time.

The GPS services are widely employed in industries like for mineral exploration and for the management of wildlife habitation, in forestry, in tracking people and objects, land surveying, map-making, and scientific applications such as study of seismic activity, management of telecom networks, etc. GPS does not provide accuracy in urban areas and in indoor places as the walls of tall buildings block the signals from the satellites [158]. GPS is a satellite based navigation system, it requires a Line of Sight (LOS) between the signals from the satellites and their receiving antenna. If a land vehicle is used, the Line of Sight principle will not be met as signals cannot reach the antenna when a land vehicle moves in an urban environment [159]. The limitation of GPS technology is that buildings and foliage greatly intercept GPS signals.

For precise calculations GPS requires at least three satellites. If the altitude of the user is also required, an additional satellite will be required for that. Any number of satellites can be used in GPS, but only three satellites are used due to satellite failure, poor geometry, constellation build-up and long acquisition time. GPS is extensively used as GPS receivers are cheap and it gives the precise location of the user.

Assisted GPS also known as A-GPS or aGPS is a system which can recuperate the Time to First Fix (TTFF) that is; the start-up operation of a Global Satellite-based Positioning System. A-GPS incorporates the mobile network with the GPS for providing precision of 5 to 10 meters. This system provides better coverage and adjusts the system within seconds. It also uses fewer satellites, saves power and can be used indoor [160]. Hence, A-GPS is more precise and has a shorter acquisition time of less than 10 seconds. The cost per unit of this system is quite cheaper than the GPS but it requires some changes at the Base Station (BS) Level. The receiver of A-GPS can detect weaker signals as compared to the receiver in the GPS. A-GPS is cheaper due to decreased search space and sensitivity support.

2.3 Outdoor Systems Using Terrestrial Base Stations

The Outdoor systems using Terrestrial BS's comprise

- Global System for Mobile Communications GSM (with Enhanced Observed Time Difference (E-OTD)).

- Global System for Mobile Communications GSM (with CELL-ID).
- Code Division Multiple Access (CDMA) / General Packet Radio Service (GPRS) (with A-GPS)
- CDMA/GPRS (with A-GPS) - Advance Forward Link Trilateration (AFLT) + A-GPS.
- Wirelessly Assisted GPS and AFLT.
- Wideband Code Division Multiple Access (WCDMA) (with Idle Periods in the Downlink (IPDL), Time Alignment Idle Periods in the Downlink (TA-IPDL) and Observed Time Difference of Arrival with Positioning Elements (OTDOA-PE)).
- Systems with Smart Antennas and Distributed Antenna Systems (DAS) and Wi-Fi Access Points (Aps).

These systems are discussed next.

2.3.1 GSM (with Enhanced-Observed Time Difference (E-OTD))

This is a triangulation system based on the network finding locations by calculating signals' arrival times [161]. It mainly calculates based on Angle of Arrival (AOA) and Time Difference of Arrival (TDOA) [162, 163]. This is a standard technique which is used for calculating the location of mobile phones by using multi-lateration. It has an accuracy of localization within 50 - 125 m and acquisition time about 5 seconds. This system requires changes in both the software and the hardware of the GSM system, e.g. E-OTD offers a process to allow pseudo-synchronization. The transmission time counterbalance can be assessed by using

a Location Measurement Unit (LMU) between the two base stations. This quantity is referred to as Real Time Difference (RTD). Pseudo-synchronization can be achieved using RTD.

2.3.2 GSM (With CELL-ID)

This system is simple but its accuracy depends on the size of the cell. This system can be improved by using hybrid methods. The combination of different methods to constitute a hybrid method allows for the increased reliability, precision, applicability and accessibility [164-166]. This method can combine any standardized method with any of the measurements from the physical layer such as Evolved Cell Global Identifier (E-CGI) and CELL ID + Round Trip Time (RTT), Angle of Arrival (AOA)+ Round Trip Time (RTT) while the other methods use two complete location techniques, such as Observed Time Difference of Arrival (OTDA) + Angle of Arrival (AOA).

2.3.3 CDMA/GPRS (With A-GPS)

Code Division Multiple Access (CDMA) provides the main radio modelling positioning methods which depends on the Time Difference of Arrival (TDOA) trilateration. This system works on two positioning technologies namely Advance and Enhanced Forward Link Trilateration (AFLT), (EFLT) [167].

2.3.4 CDMA/GPRS (With A-GPS) - AFLT+AGPS

Advance Forward Link Trilateration (AFLT) accepts a methodology like that of Idle Period Downlink (IPDL) [168], but it uses GPS other than Location Measurement Unit (LMU) to locate all BS's and requires supplementary units to utilize the preliminary information to measure the mobile station's (MS's) position [169].

2.3.5 Wireless Assisted GPS and AFLT: GPS One a Hybrid Solution

This technique of localization is distinctive to CDMA networks, as they are integrally synchronous in their functioning. It calculates the phase delay between the signals which has been sent to a pair of BSs. After that it compares this to the same data taken from another pair of BSs. The GPS type is a joint Wireless Assisted GPS (WAG) and Advance Forward Link Trilateration (AFLT) technology proposed by Qualcomm. It is developed based upon the WAG [170-172].

2.3.6 WCDMA (With IPDL, TA-IPDL and OTDOA-PE)

This is a spread-spectrum modulation methodology primarily used in 3G mobile networks. The channels with higher bandwidth than the transmitted data are employed in this scheme. In IPDL based positioning in WCDMA, the system makes no effort to avoid loss of data as compared to the compressed mode. IPDL method is the prime 3GPP standard reference for this operation [169].

2.3.7 Distributed Antenna Systems (DAS)

In sky-scrapers, DAS are usually used to reduce the antenna receiver separation [173, 174]. Within a building, there is a Central Unit (CU) that controls the Remote Antenna Units (RAU) installed on every floor. DAS lessens the transmission power and provides higher rates of data transmission for the Mobile Terminals indoors.

2.3.8 WIFI Technology with Access Points (AP)

Wi-Fi is a Local Area Network (LAN) technology which was invented to add mobility to the private wired LAN. It is not just getting connection to a computer or to a network. It is now being used in gaming gadgets, MP3 players, phones, etc. It uses a decentralized and end-user-centric method for providing services to its users. It is an IEEE 802.11ad wireless Ethernet standard which supports wireless LAN [175-177].

Wi-Fi technology is used to efficiently locate persons and objects, improve workflow and WLAN planning, improve productivity by proper allocation, reduces loss, improve customer satisfaction and security [178, 179]. The most commonly used standard in Wi-Fi is IEEE 802.11b/g which works in the 2.4 GHz band. At this frequency, the broadcasting signals are altered due to noise and distorted due to the obstacles (such as wall, buildings, objects, humans, etc.). The WLAN infrastructure comprises of wireless Access Points (APs) which are connected to a LAN. When the Wi-Fi-supported mobile device enters a cell, the mobile device receives the MAC address of the AP [180].

Wi-Fi APs are universal and are providing significant connectivity for extensive variety of mobile networking devices. Management tasks such as enhancing AP placement and sensing distorted APs wants a user to effectively verify the location of the wireless APs. The wireless APs issues a MAC address which is a unique identifier to distinguish it from the other APs. The APs play the role of a verifier [181-183]. The physical or virtual port comprises of two logical ports namely Authentication Port Access Entity (PAE) and Service PAE. The authentication PAE is permanently open whereas the service PAE opens just upon positive authentication for a default time of an hour [184]. The internal transmission lines are small in diameter but the cable run is less as it is of few inches [185].

Researchers have proposed the use of commodity smartphones for locating APs in real time [186]. This method does not require the use of outdoor measurements or any specialized equipment. By revolving a smartphone around the body of the user, one can successfully imitate the operations of a directional antenna. The results have shown that the signal strength artefacts can be detected on numerous smartphone positions for multiple outdoor environments. In the meantime, researchers have developed a system called Borealis which gives accurate guidance related to the direction and after few measurements it directs the user to the desired AP. this system gives accurate values as compared to other real time localization systems. It detects signal inclinations created by the blocking obstacles which precisely measure the direction of the AP [187].

2.4 Techniques of the Existing LBS Methods

The techniques for estimating the existing localization based services include Localization by Cell-ID, Localization using Prediction (Dead -Reckoning Method), Angle of Arrival (AOA), Time of Arrival (TOA), Finger-Printing, Observed Time Difference of Arrival (OTDOA) and Hybrid localization techniques employing AOA-TOA. These are explained below:

2.4.1 Localization by CELL-ID

The localization by Cell-ID involves Cell Global Identity (CGI) that results in locating a region as large as the cell itself [188, 189]. This positioning method can be stretched to sectorial cell positioning and can also be combined with TOA-based distance calculation methods. Generally, in GSM networks, three antennas are fixed at most of the Base Transceiver Station (BTS) locations, with the purpose that sectorial cell positioning is recognized automatically.

The identification (ID) codes like Subscriber Identifiers (Mobile Stations (MS)) are required in order to localize by Cell-ID and also the following identifiers can also be used: Location Area (LA) and Routing Identifiers (Mobile Switching Centre (MSC)) [190].

2.4.2 Localization by Prediction (Dead-Reckoning Method)

Localization by dead-reckoning or prediction involves localizing the position of a moving target by using the memory of the last position of the target [191, 192].

Various applications of dead-reckoning methods include air navigation, automotive navigation, marine navigation, animal navigation, personal navigation systems, etc. Automotive navigation systems overcome the limitations of the GPS and GNSS technology. In robots, the dead-reckoning method reduces the requirement for ultrasonic sensors [193, 194]. Multi-scale dead-reckoning algorithms are used for network localization which is anchor-free and does not need any network topology. It uses local distance and angular information for close-by sensors.

2.4.3 Localization by Angle of Arrival (AOA)

Angle of Arrival (AOA) based measurement found significant fame in wireless networks for localization [195-200]. The properties that characterize the direction of the radio waves propagation on the antenna array can be calculated using this method.

The applications of AOA include geodesic location or geo-location of mobiles [201]. Numerous receivers present on a base station can estimate the AOA of the mobile's signal and calculate the location of the mobile. AOA is also used for finding the location of military or spy radio transmitters. It is also used for localizing objects with active or passive ranging in submarines. It is also used in interferometry in optics.

AOA positioning is a simple method. In mobile communications, the base stations measures the AOA with respect to an absolute reference, say north, for example

[74, 202]. The absolute angles can be calculated keeping in view that the location of the base station (x_b, y_b) are known and the position (x_u, y_u) of the user can be measured by transecting two lines which are passing across the base stations with the angles which are measured [203].

The AOA positioning precision decreases with increasing distance between the positioning system and the mobile. So, AOA may not be suitable for many applications of positioning. In WLAN, the Access Points are near the mobile and can provide positioning precision with time based systems having equivalent signal bandwidth [204]. A major drawback of Angle of Arrival measurements is that it uses an array of sensors (microphones, antennas and ultrasonic sensors). Due to size and high costs, arrays are considered unsuitable for integration, but as radio communications attains higher frequencies, the dimensions of the antenna contracts and micro electro-mechanical systems (MEMS) progresses. The integration becomes possible in the presence of the array empowered node platforms. By incorporating multiple antennas in the same dimensions, a platform can be designed using four antenna elements, which does not cost very much.

2.4.4 Localisation by Time of Arrival (TOA) and Observed Time Difference of Arrival (OTDOA)

Information can either be collected by a Mobile Station (MS) from the Base Station (BS) or sent by the MS towards BS [74]. In the earlier case, the TOA information for the MS is collected by the BS and in the latter case, the information of OTDOA

is collected by MS transmitted from BS. TOA and OTDOA have high precision due to high time resolution signals. TOA location based algorithms include Analytical method (AM), Taylor Series method (TS), Approximate Maximum Likelihood method (AML), Least Squares method (LS) and Two-Stage Maximum Likelihood method (TSML). A brief review of location based techniques and the context in which they are applied are presented in Table 2-1 and Table 2-2 below.

Table 2-1: Location Based Technology for the Network Solutions

Localization Technology	**Abbreviation**	**Working**	**Obstructed Areas**
Cellular Identification	Cell ID	It detects the base station which is used by the mobile	99%
Enhanced Cellular Identification	E- Cell ID	Calculates the Mobile strength of the receiver	99%
Time of Arrival	TOA	It calculates the total time passed between the transmissions of signals from the mobile to the base station.	-
Angle of Arrival	AOA	It utilizes antennas at the base stations to detect the direction of the incoming signals. It needs 2 base stations with the Antennas.	As the distance of the user to the base station increases, its accuracy decreases. Its performance is poor in urban areas.
Observed Time Difference of Arrival; Time Difference of Arrival and Uplink Time Difference	OTDOA/ TDOA	It measures the Time Difference of Arrival of signals through handset from mobile units at multiple base stations.	The degradation of signal occurs in the urban areas.

Table 2-2: Location Based Technology for the Handset Solutions

Localization Technology	Abbreviation	Working	Obstructed Areas
Enhanced Observed Time Difference	E-OTD	It matches the Time Difference of signals sent to the mobile and to LMU by the base station. The software in the mobile handset measures the position. It needs 3 base stations.	The signals degrade in buildings and urban areas.
Assisted - GPS	A-GPS	It measures the mobile unit position by utilizing the satellites and Global Positioning Receiver	50 to 70%

2.4.5 Hybrid Localization AoA-ToA Based

Hybrid localization involves both AOA and TOA. These two and more techniques are combined to attain a more precise position location. The accuracy of TOA or AOA depends on the environment [205]. However, the mobile prefers TOA where there are many scatterers and otherwise, AOA.

2.4.6 Localization by Finger-Printing

Finger-printing is a method in which the reference measurements at the possible way-points are involved to increase localization precision. When the GPS systems are not working, then indoor positioning systems such as locating finger prints of wireless local area networks are used. It uses finger-printing techniques, that is; it receives signal strength with respect to a location and derives the location on the basis of this data [206, 207]. It involves two stages, on line phase and offline stage. In the online stage, a site survey is done for the Received Signal Strength Indices (RSSIs) from the access points (AP). The vector created using the RSSI values at a point can be considered as the location fingerprint for that point. In offline stage,

many location fingerprints are gathered at each point. The drawback of this method is that it requires a lot of time [208].

Location finger-printing involving ultra-wideband radio frequency signals is a provides a substitute to the traditional positioning methods which are based on the angle estimation, range and the strength of the received signals [209]. This type of finger-printing method is useful for indoor environments and uses multipath propagation information. It requires large bandwidth RF signals. The location finger-printing method comprises of two stages i.e. the training stage and the localization stage. In the first stage the location finger prints are gathered from the known position by the system, while in the localization finger-printing method, the location fingerprints are gathered from the agents with unknown positions and are matched with the training data. There are numerous approaches for matching these positions with the training data such as neural networks, Bayesian approaches, vector machines, etc. [210]. The large bandwidth gives less restrictions and the benefit is that a single broadcaster serves for suitable localization performance. The limitation of this method is that a large quantity of training data is needed, so the training phase becomes tedious and time consuming.

The drawback of finger-printing is that it can attain precision of just few meters. More research is needed for the probabilistic method. The finger-printing method is effective in Wireless LAN positioning but the problem lies in locating the unknown

location. Two approaches have been used for solving this problem. The deterministic approach and the probabilistic approach [211]. In the deterministic method, the standard sample scan of each wireless LAN access point calculated for each reference point is then used to generate the database of the fingerprint. As the difference in the sample scan calculated at each segment is big, and it does not consider a lot of information present in the database, so a probabilistic method has been used to remove this discrepancy [212]. Information related to the average signal strength and the difference in each access point varies and it must be considered to maximize accuracy.

Bayesian method has been used by the researchers to remove limitations of finger-printing method [213]. For each fingerprint, the probability distribution is created using the regularity in the occurrence of each signal strength value. The main drawback of finger-printing method is that just a few meters' accuracy is achieved. More research is needed in probabilistic methods for removing the discrepancies [214].

2.5 Latest Trends and Modern Applications of Location Based Services

LBS Services are useful for orientation and localization [215], navigation [216], searching [217], identification [218] and event search [219]. Information services [220, 221] are the earliest application of the LBS technology. Presently, they are integrated into vehicles for route finding and are also used for emergency and

health services [222, 223]. LBSs have appeared as the most interactive technology for mobile computing due to the fast developments in the wireless and positioning technology. In order to further improve the efficiency of these services, data caching techniques have been used which removes the faults of the restricted wireless bandwidth in mobile environments [224]. Modern applications of LBS include the following:

2.5.1 Enhanced – 911 (E911) and Enhanced – 112 (E112) Services

The motivation behind the development of LBS technology applications in United States by the Federal Communications Commission (FCC) in 1996 was to locate mobile devices during emergency calls [225]. This service was named Enhanced - 911 or E911 [226]. The need arose as calls from the mobile phones showed a growing percentage of emergency calls which reached 45 million in 2001. A similar service with the name of E112 was promoted in European Union countries [227, 228]. About 40 million calls were made through the mobile phones in 2011 out of which 15% were not addressed due to the insufficient or non-availability of the location of the callers. Public Safety Answering Points (PSAPs) were used to find the location and number of the caller [229] . The network based solutions such as Automatic Location Identification (ALI) for wireless carriers are used to find the location of the user within 150 to 300 meters of their location [230].

2.5.2 Mobile Guides

Mobile guides are information rich, movable and location sensitive digital guides which provide information that is related to the surroundings of the user [231, 232]. They are the largest group of LBSs applications which are portal and information rich digital guides [233, 234]. The mobile guides were categorized on the basis of geo-positioning (GPS, Wi-Fi, etc.), architecture, adaptation (handling), situational factors, interfacing, network access and map boundaries [233, 235-237]. Mobile guides are also being used for mobile social networking [238]. Mobile guides exist in different categories such as resource adapted (having regular patterns for use), resource adaptive (has a single strategy for the use of resources) and resource adapting (uses multiple strategies).

2.5.3 Transport Location Based Services

Intelligent Transport Systems (ITS) is a rapidly growing technological concept for the incorporation of the information between the extensive variety of organizations working in transport planning and functioning [239-241]. The intelligent systems hold the capability of performing situational analysis and adaptive rationalizing [242]. The future of transportation system is effective, time saving, economical, and will be much safer for the well-informed users than now. ITS have grown to the establishment of institutions like the ITS and Services for Europe (ERTICO) [243, 244]. The International Standard systems such as ISO 14813 (ISO 2007) have also played a vital role in its advancement. The technologies used for ITS, are known as telematics and include wireless communications, geo-positioning, spatial

databases and mobile computing platforms. The transport LBS include but are not limited to services like assistance for the drivers [245-247], information for the passenger, management of the vehicles and applications involving vehicle-to-vehicle communication [248]. The services provided by traffic telematics includes automatic configuration of appliances and features inside the vehicles, navigation, detection of faults and broadcasting of caution messages [249, 250]. Traffic telematics are also used to calculate the distance between the various vehicles in a fleet and between a vehicle and its destination [251]. Today computer hardware and software are used in vehicles for monitoring fuel usage and releases, engine performance, brake performance and for handling electrical systems [252]. The user services for travel and traffic management comprise collection and broadcasting of information and dispensation for the external transportation system. These services are used for providing commands to different traffic control devices [253]. Traffic telematics promotes exchange of data between service providers and the vehicles which helps in improving traffic management processes [254]. Today with the advancement of the wireless communication systems, vehicles are fitted with wireless communication devices which enable them to communicate with other vehicles [255]. Vehicular networks can also enable vehicles to transmit information in case of any accident or obstacles. Fleet management is another interactive service in transportation system. The fleet management systems provide freight services, public transportation and emergency services. The fleet asset and management units are wireless handsets

or devices that track the fleet of vehicles and facilitates in faster transportation through different modes [256].

2.5.4 Location Based Gaming

Location based games are the computer games in which the game development depends upon the real-world location of the player (user) [257-259]. Multiplayer games include street games and urban games. The characteristics of location based gaming include movement, communication in public, specification of the location and incorporation of the digital world and the real physical world [260]. In pervasive gaming, real world games, supplemented with the functionality and the power of computer and the entertainment provided by the computers are brought to life [261-264].

2.5.5 Location Based Health and Assistive Technology

LBSs play a vital role in fulfilling the navigational needs of the visually impaired people [265-268]. MoBic (Mobility of Blind and elderly people) was the first system to be used to help the elderly and visually impaired. This system helped the visually impaired and elderly people in finding destination and location of the route [269]. It informs the traveller about the journey through a map. It was made up of a MoPS (MoBic Pre-Journey System) and a MoODS (MoBic Outdoor System). A MoPS considers the account preferences of the users, distance and time for travelling in order to measure the direction. The MoODS uses the information measured by MoPS to keep the user informed through warning and audio guides.

A famous wireless pedestrian navigation system is Drishti which is used both indoors and outdoors for the guidance of visually impaired and special persons. It provides route and destination information to the users. This system uses Routing according to the user preferences and also take in account the shortest route [270]. The dead-reckoning method can be used for outdoor movement and for indoor environments protective ultrasonic sensing is used [271]. Information of the route is downloaded on the device of the user. Any new information related to the direction or obstacle is uploaded by the device to keep the server updated. It guides the users through various transportation means such as buses, trains, footpaths, trams, etc. It takes use of the mobile devices with Global Positioning System capabilities, wireless connection and voice production. Location based health services have also been developed to track the mobility of the patients and old persons [272]. Ambient Assistant Living (AAL) system is an LBS system which provides location information in indoor environments. For example; it gives help to old people living alone to perform their daily tasks. It also provides information to elderly people about the location of shopping stores and public places. It also helps to find a specific product within a shop [273]. Location based health services have also been used for monitoring the health of children [274] and for measuring health and fitness [275]. In [276] the research was conducted on around developing an assistive technology to improve the mobility of manual wheelchair's user. During the research, questionnaires were also designed based on the seven key principles of universal design. Per the questionnaires, the users of manual wheelchair are fatigued and suggested a change in the type of hub (rather than its

location) to improve the speed of the wheelchair. The solution has been developed on the following: parameter changes (wheelchair), mechanical substitution and self-service. In [277] a system is presented that supports cognitively impaired people in their daily activities. The most interesting part of the research is to generate user friendly names for streets and various routes based on user context – especially for people who aren't accustomed to using new technologies e.g. elderly people. The system also enables the relatives of the user to establish tasks that must be performed at specific locations and to monitor the activities of the user to detect potentially risky situations.

2.5.6 Mobile Marketing

Mobile advertising or marketing is an interactive LBS which works in the same way as directory services. It involves all the activities undertaken in order to communicate with the customers by using mobile devices for promoting the sale of products or services and for providing information to the customers about the products and services [278]. It has two categories namely pull model and push model. The information can be requested using the pull mode from the marketer, while it can be sent from the marketer to the customer in push mode although it is not requested by the customer [279]. Interactive and personalization of the content message is possible in mobile marketing [108]. In [280], a method is presented to implement some trust level so that only genuine mobile users can use the system and identify malicious users. For this purpose, it is proposed by the authors to store the IMEI number of the mobile devices in a central controller. The system can also

be deployed on cloud server for storing the distributed data. In [281], a business model is presented for internet and mobile based marketing for smart parking operators with a focus on personalisation of advertisements. This method can be used to increase parking operator's revenues and thus attract more investments in the future. Among the variety of mobile services, significant attention has been dedicated to mobile marketing specifically to mobile customer relationship management (CRM) services. In [282] authors investigate which type of mobile marketing has a significant relationship with which type of CRM. The research done in this project also proves that future is brighter for mobile advertising rather than any other type of advertising.

In [283], the potential of using mobile marketing for increasing the value for customers and retailers has been has been explored. It has been observed that the consumer behaviour on mobile shopping is an extension of their behaviours developed on internet connected PCs. However, new behaviours are also integrated during this such as camera, scanners and GPS. This concept is specifically useful for development of managerial concepts related to mobile marketing.

The growth of Location Based Social Networks (LBSNs) has greatly enhanced the people's urban experience through social media and so the number of users has increased exponentially. Vast amount of data related to human behaviour is available – Big Data - and so there is an opportunity to apply advanced data

analysis tools and algorithms to build our learning on this data. In [284], the background, framework and distinct properties of location based mobile social networking are presented – illustrating the application of data mining to real world location based social networks.

In [285] the authors have investigated the customers' privacy concerns, and their attitude towards the Mobile based Location Based Advertising (LBA). The sample data comprised of 224 cases in which consumers' acceptance of LBA was found. It was found that although customers viewed LBA in a positive way, the information privacy concern influenced their overall perception of the LBA and its types, namely push (product/service information relayed) versus pull (customer information collection + processing). It is crucial to understand the customers' attitude and acceptance of LBA before adopting either a push or a pull model.

2.5.7 Community Based Services

These services are location supported having personal interaction component and a central communication system [286]. Online social networks are using Location Based Services to assist social networking and for discovering places [287]. Virtual mobile communities comprise users who communicate with each other and interact with each other electronically through mobile devices [288]. Community based services have facilitated visually impaired persons as they provide advanced navigation in urban areas where satellite systems have failed to do so as the signals get degraded due to obstacles such as buildings. Community based

location services enable the community members to interact with each other through services such as mapping my friends (finding the physical location of friends), friend alert (when friends visit each other they get alerts) and portable messages [289]. Localization and tracking of pedestrians involves a combination of active and passive positioning systems. It involves multi sensor systems which not only detects the location of objects and person but also provides precision related to the position [290]. The GSM signal strength finger-printing provides better indoor and outdoor localization techniques. This method is useful for delivering warning messages related to weather or in case of emergency traffic situations. It is also useful for tracking people inside a building [291].

In [292], a system for real-time event detection, tracking, monitoring and visualisation has been developed. The main motive behind the project was to help Information/Data Analysts to gain a better comprehension of complex events as they unfold in the world. At the end, the information is used to categorise security relevant events which are then tracked, geo-located, summarised, and visualised for the end user.

Lighting systems are undergoing a revolution from fluorescent lamps or tubes to light emitting diodes that offer an energy efficient solution and longer lifetime. In [293], a low-cost deployment solution has been presented for a system that uses the characteristics of visible light to complement existing wireless communication systems. The proposed system has following three features: (a) It provides a

provable and secure wireless communication capability – the user is authenticated based on their location (b) It also offers high precision indoor positioning system (c) and most importantly it offers broadcast of information with a high frequency reuse factor. So, the system presents a novel approach to authentication based on user's location.

2.5.8 Crime Fighting

LBSs have the potential to be used in fighting terrorism as the suspects can be watched and tracked through this service. RFID services can be used for biometric passports and for managing disaster. GPS devices are used for monitoring emergency response teams at crime sights [294]. Control and management of information for national security can be done through the use of LBSs as terrorists' organizations can use the government websites for planning terrorist attacks [295]. Theft of vehicles and bikes are also controlled by installing tracking devices in them [296]. [296] emphasized that location based services offers remarkable benefits in safety and security areas such as by tracking criminals, lost vehicles, mobiles, etc. and by responding to the emergency calls. The emergency response time has been greatly reduced due to the use of location based services [297]. Law enforcement agencies are increasingly using facial recognition software as a crime-fighting tool. Mobile Cloud Computing (MCC) enforces the idea of moving most of the processing and storage capability of the mobile phone to the cloud. In [298], an efficient architecture has been presented that enables the face recognition algorithms to run on the smartphone and reduce overall processing

time. Digital media has greatly enhanced the capability of information systems. Although, the humanity has benefited from this revolution, it has also resulted in new methods of forged authentication. Therefore, in, the methodologies to fight against these forgery attacks has been presented.

Urban crime rates are expected to increase keeping in line with the population growth by the year 2030. Studies have shown that crime only increases in certain areas of an urban landscapes. This has attracted the attention of spatial crime analysis that primarily focuses on crime hotspots that are basically the areas with disproportionally higher crime density. The problem might arise if areas outside of hotspots are overlooked and proper analysis techniques aren't applied. Therefore, in [299] Crimetracer, has been developed that enables an accurate crime location prediction outside of hotspots. A probabilistic model of spatial behaviour is proposed within the activity space of the known offenders.

The fear of crime has been the central theme in criminological research from the 1970s onwards. The research methodologies used in these projects have been well documented and revolve around neighbourhood effects. However, the specific location of home has been largely overlooked during these researches. Therefore, in [300], the fear of crime was examined from a location based approach and took neighbourhood and location of one's home into perspective. The demographic data was also used in relation to the research to find the variations in fear of crime

across racial/ethnic groups.

2.5.9 Real Time Shopping

LBSs involving indoor positioning have made it possible for the exploration of products and things existing in the physical world as simple as it can be performed on the internet. In stores, indoor positioning technology has been utilized to find products on shelves and for other in-store services. Hence, by doing so, the shoppers involve themselves in real time shopping experience, similar to as they do on the internet [301].

In [302], context aware automated service system was developed that basically worked as “Intelligent Shopping-aid Sensing System (iS^3). For recognition, collection and delivery of user contexts, RFID is used. Another benefit of using RFID is that the information of products e.g. locations, specifications and characteristics are collected quickly. Local applications were also developed that enabled real time interactions between central system and end users.

The scientific community is continuously exploring new services that make effective use of the developing wireless technologies. In [303] the authors focus on connecting various sources of information based on the protocol stack of IEEE 802.11 and Bluetooth interfaces. The corresponding software architecture along with the preliminary results for the tracking of visitors in smart shopping environments has been presented.

2.5.10 Information and Entertainment

LBSs such as Facebook, Gowalla, Where, GeoLife2 [304] and Foursquare [305] utilize the geo-location function of a mobile phone or smart phone to deliver infotainment to people. Facebook places controls the prevailing Facebook network of more than 500 million users for sharing, connecting with friends and finding local transactions [306]. Hence, these services provide free advertising and promotion of products and services [307]. It permits the customers to “Check in” places such as hotels, airports, restaurants for transacting physical and intangible rewards. Yelp website provides rating and reviews and their mobile applications allow customers to check and review stores, hotels and restaurants. Similarly, WHERE facilitates its customers in locating things and providing suggestions to them regarding purchasing products or services.

2.5.11 Location Based Services in Politics

During the 2009 elections, many social networking sites such as Facebook, Twitter, Youtube, etc. provided platform to the politicians to express their views and policies in front of the public. Lots of politicians such as the president of the United States, Barack Obama and former president of Pakistan, General Pervaiz Musharaff used Facebook to express themselves before the public. In the case of Barack Obama political campaign, there was found a cause and effect between the votes and social media. Foursquare issued an “I Voted” badge and a website that was a combined effort with the Pew Center, Google and Rock the Vote. It truly demonstrated that location based services can influence elections. It was a test run

for the 2012 presidential elections. The users were encouraged to check in at their voting location and to attain the distinct limited-edition badge. This project had 50,416 check-ins obtained from 23,560 variant venues. It was considered that the Foursquare badge got minimum one person out to vote.

This idea followed the idea of Howard Dean's online micro donation. It was found that approximately 15% of Americans with ages 18 and over took part in the 2008 presidential election using social media networks such as Facebook.

Hence, LBSs can be used in almost all fields of life for improving the standard of living and making communication system better. However, the use of LBSs may not have succeeded well in collecting real time images such as photos. Meanwhile, the use of LBS in the MOPSI applications, as by using the split smart swap clustering method, the disorder problem in map visualization can be reduced and photo collections can be clustered through the use of grid based clustering with bounding box method [308]. LBSs are also used for localizing the position of the Robots and mapping the environment [309]. LBS applications are also used in Geographical Information Systems as it provides spatial analysis opportunities [310]. The beginning of mobile communication technologies, such as General Packet Radio Service (GPRS) and then the evolution of Universal Mobile Telecommunications System (UMTS) has empowered users of mobile devices to use internet regardless of time and place [311]. LBS services involve client/server relation, while LBA involves IT applications based on geo-spatial locating. Both use

real time for location objects or users and are suitable for mobile applications [312]. It has been reported that LBSs can provide multiple services ranging from tourist navigation to rescue systems for managing disaster. These services were developed separate from the geographic information Service (GIS) stream used for the wireless services, but today more than 80% of data being supplied is the spatial form (2D map) Hence, location based services are also a special kind of GIS [313].

So far, LBS are basically mobile applications which provide information that are related to the location of the users. These services are quickly capturing the market and have tremendous growth opportunities [314]. The position of a user or object can be informal, absolute or relative to a certain point whether they are located through Bluetooth, infrared, RFID, mobile or through satellites [315]. Today LBSs have a well-established role in value added services and their applications are continuously growing [316]. Calculating the distance error through uncertainty and confidence constraints is useful in locating the position of a user or object but the Distance error produces inconsistent location estimates [316]. Reinforcing LBS needs focusing on a number of issues such as software, hardware, network structure, security, database, etc. [317]. The application of the location based technologies depend on well-established and accessible multi layered client server technologies. The fundamental infrastructure to assist LBS applications is developed to assist mobile client functions with wireless communication [131].

Another application of location based services deployed by the government is to assist people with the management of emergencies via their mobile phones. Therefore, in [318] the viability of location based mobile emergency services has been assessed. The study was conducted in a three-pronged way: (a) exploring the challenges of location based services and their use at a national/country level for emergency management (b) investing the impact of these of these services in terms of behaviours and attitudes (c) understanding the social acceptance or rejection of these services and outlining the factors that determine their acceptance. The common theme found in the results is the trust factor: the collection of personal location information adversely affected the trust level.

2.6 Conclusion

Location based services have been elaborately reviewed in this chapter. It is used to give services in both public and business sectors. Some of which include tracking services for old and disabled persons, monitoring health of patients, navigational services at the airports, traffic telematics, fleet management, enquiry and information services, crime fighting, toll systems, marketing, gaming, geography mark-up and community services.

The localization infrastructure for LBS include LBS indoor systems, LBS satellite systems, LBS GPS system, outdoor systems using terrestrial BSs and LBS Outdoor Systems using terrestrial BSs. The techniques for the existing localization were also enumerated. Different solutions for improving the existing LBS

technology and services were described. The modern applications of Location Based Services include Enhanced – 911 (E911) and Enhanced–112 (E112) Services, mobile guides, transport location based services, location based gaming and location based health and assistive technology. The emergency and location based health applications have assisted in saving lives of people and improving the standard of living of people. The prospects of LBS are very high as with further research the existing technologies can be improved and new ones can be created.

Table 2-3: Applications of Location Based Services Discussed in This Chapter

LBS Technique	Category	Application (Example if any)	Positioning	Architecture	Presentation	Delivery	Use Case	Adaptivity
Enhanced 911 or E911	Emergency Services	Rescue, emergency and Disaster Management	GPS	Client/Server	MAP/Book	Push/ Pull	Mobile Search	Adapted
Enhanced 112 or E112	Emergency Services	Rescue, emergency and Disaster Management	GPS	Client/Server	MAP/Book	Push/ Pull	Mobile Search	Adapted
Mobile Guides	Digital Guides	Provides information about the surroundings of the user. Tourism/ Guide	GPS/WiFi	Client/Server	MAP/Book	Push/ Pull	Mobile Search/Tour/ Navigation	Adapted/ Adaptivity
i)Archetypal Mobile Guide	Mobile Digital Guides	Tourism and Transport	GPS	Client/Server	MAP/Book	Push/ Pull	Mobile Search/Tour/ Navigation	Adapted/ Adaptivity
ii) Location based video	Mobile Digital Guides	Museum (Sotto Voce, LISTEN, etc.)	GPS/WiFi/IR	Broadcast	Book/Speech /SoundScape	Push/ Pull	Mobile Search/Tour/ Navigation	Adaptive/ Adapted
iii) Speech Oriented Systems and Speech based Navigation Describers	Mobile Digital Guides	(Transport and Museum) BPN, REAL, etc.	GPS/WiFi/IR	Broadcast	MAP/Speech /VR	Push/ Pull	Mobile Search/Tour/ Navigation	Adapting
iv) Event triggered systems	Mobile Digital Guides	Phone Guides, Marble Museum, etc.	RFID/Tags	Event Trigger	MAP/Book/Speech/Video Imagery	Push/ Pull	Mobile Search/Tour	Adapted/ Adaptive
Vehicular Ad-Hoc Networks (VANETS)	MANETS	Vehicle to Vehicle (V2V) and Inter Vehicle communications (IVC).	Wireless Access for Vehicular Environment (WAVE)	Event Trigger	MAP/Book/Speech/Video Imagery	Push/ Pull	V2V and IVC	Adapting

			Communication devices					
Intelligent Transport Systems and Services for Europe (ERTICO).	Intelligent Systems	Driver assistance, passenger information, vehicle management, vehicle-to-vehicle applications and Fleet Management.	Telematics (wireless, geo positioning, spatial databases and mobile computing)	Broadcast and Client/Server	MAP/Book	Push/ Pull	Mobile Search/Tour	Adapting
Outdoor and Computer Board Games	Location Based Gaming	Street and urban games. Geocaching.	GPS	Client/Server	MAP/Book	Push/ Pull	Mobile Search/Tour/ Navigation	Adaptive /Adapting
Technology for Visually impaired and elderly people	Location Based Health and Assistive Technology	Assistance of visually impaired and elderly people (MoBic, MoPS, MoODS, NOPPA	GPS. DGPS and Dead Reckoning and Ultrasound sensing.	Client/Server	MAP/Book/Speech	Push/ Pull	Mobile Search/Tour/ Navigation	Adapting
Mobile Advertising	Mobile Marketing	Online marketing and advertising	GPS	Client/Server	MAP/Book	Push/ Pull	Mobile Search/Tour/	Adapting
Community Based Services	Location Based Community Services (LBCS)	Online social networking (Mapping my friends Friend Alert Portable Messages.	GSM	Client/Server	MAP/Book	Push/ Pull	Mobile Search/Tour/	Adapting
Crime Fighting LBS	Location based security and safety services	Crime Fighting (tracking criminals, lost vehicles, mobiles, etc.)	RFID and GPS	Broadcast	MAP/Book/Speech/video imagery	Push/ Pull	Mobile Search/Tour/ Navigation	Adapting
Geographical Information	MOPSI applications	Robots and mapping the environment (SLAM)	GPRS and UMTS	Client/Server	MAP/Book/Speech/video imagery	Push/ Pull	Mobile Search/Tour/ Navigation	Adapting

Systems								
LBS in politics	Location Based Community Services (LBCS)	Political campaigns	GPS/WiFi/ GPRS	Broadcast Client/Server	MAP/Book/Speech/video imagery	Push/ Pull	Voting/political rallies Facebook, Gowalla, Where and Foursquare	Adapting
Information and Entertainment	Location Based Community Services (LBCS)	Online social networking	GPS/WiFi/ GPRS	Client/Server	MAP/Book/Speech/video imagery	Push/ Pull	Search/Shopping/in-store services Facebook, Gowalla, Where and Foursquare	Adapting

3. NEW SIGNAL SUBSPACE BASED ANGLE OF ARRIVAL ESTIMATION ALGORITHM

3.1 Introduction

Latest advancement in technology and consumer demand has created a great deal of interest in the subject of identifying the spatial relationship between different objects. This procedure is referred to as *localisation* and has found wide spread applications [319-321]. When the earth is used as the reference frame in localization operations it is referred to as *Geolocation.* The data collected for these applications however is useless without the accurate location information of the transmitter node. The direction-finding algorithms have a key role to play in the smart antenna technology of the future as the Global Positioning System (GPS) technology has restrictions due to the requirement of Line of Sight (LOS) between the satellite and the GPS receiver [322]. These algorithms are required to precisely estimate the bearing angle on the receiver array which is highly important for both military and non-military services. The accuracy of these algorithms is extremely important when it concerns the emergency response services. The massive enhancement in the smart antenna technologies in the past decade has triggered an increased interest in the field of direction finding (DF). In smart antenna technology, multiple antenna elements can be combined using digital signal processing (DSP) to adjust the antenna radiation pattern per surrounding channel.

These smart antenna systems can improve the capacity of the cellular wireless networks through beam steering [323]. To steer the beam into the direction of the right user who is requesting access to the network resources it is important that the right estimate of the user location be calculated. In [324] and [325, 326] the authors have provided detailed references and quantification of the performance of the existing localisation techniques. Localization techniques have been applied to a variety of applications including autonomous mobile robot navigation [327-330], Underwater navigation [331], public health and social medial [332] [333, 334], emergency services [335] etc.

This chapter is arranged as follows. Section 3.2 presents the mathematical model for deducing the direction of arrival using antenna arrays and then presents a review for some of the well-known Angle of Arrival estimation techniques which have been employed in this work 1) Interferometry 2) Classical Beamformer 3) Capon's Minimum Variance Distortionless Response (MVDR) and 4) Super resolution Eigen decomposition based Multiple Signal Classification (MUSIC) algorithm. Section 3.3 presents the mathematical model of the Novel proposed algorithm. Results and discussion are presented in Section 3.4 followed by the conclusion in Section 3.5.

3.2 DOA Estimation Algorithms Using Antenna Arrays

The direction of arrival problem relates to the estimation of (φ, θ) where φ stands for the azimuthal angle and θ stands for the elevation angle of the impinging plane

wave on an antenna or an array of antennas. The plane wave is assumed to be of constant frequency and has infinite parallel wave fronts with constant amplitudes. In a (1-D i.e. one-dimensional plane the estimation problem reduces to only the estimation of the azimuthal angle φ;

The expression for the plane wave that impinges at point $\mathbf{x}$ at time t can be written as:

$$\mathrm{s}(\mathbf{x},\mathrm{t}) = \mathrm{A}\mathrm{e}^{\mathrm{j}(\boldsymbol{\beta}.\mathbf{x}-\omega\mathrm{t})} \qquad 3\text{-}1$$

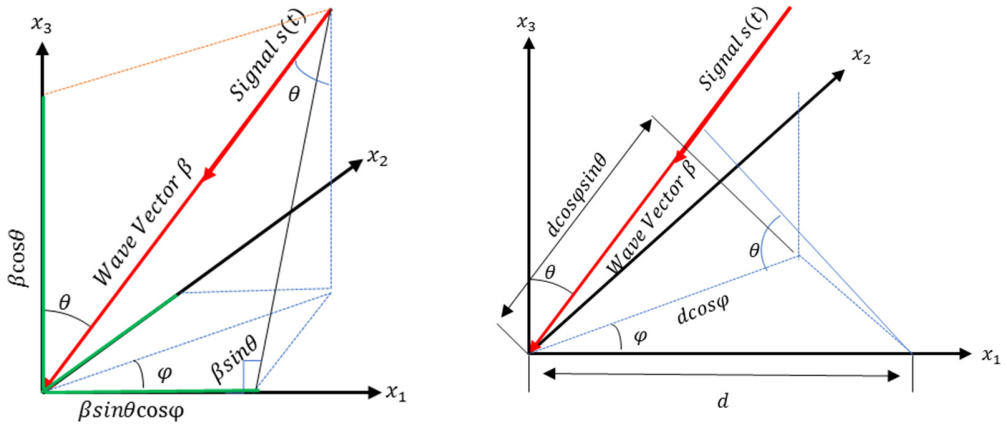

(a) (b)

Figure 3-1: Geometry representing the DOA of the signal as an azimuth and elevation angle pair on an antenna array

where A is the peak amplitude, $\beta = \frac{2\pi}{\lambda}$ is the wave factor, $\lambda = \mathrm{c}/\mathrm{f}$ is the wavelength of frequency f, c is the speed of light and ω is the angular frequency defined as

$\omega = 2\pi f$. Using the above equation 3-1, the arriving signal at an antenna located at (x_1, x_2, x_3) with origin $(0,0,0)$ can be defined as:

$$s(\mathbf{x}, t) = s(\mathbf{0}, t)e^{j\beta(x_1 \cos\varphi \sin\theta + x_2 \sin\varphi \sin\theta + x_3 \cos\theta} \quad 3\text{-}2$$

If there are M omnidirectional isotropic antennas that have a unity gain arranged in a uniform linear array (ULA) with uniform spacing d between them on the x_1-axis then the arriving signal at the mth element can be described as:

$$s_m(t) = s\big((md, 0,0), t\big) = s(\mathbf{0}, t)a_m(\varphi, \theta) \quad 3\text{-}3$$

where, a_m is the steering factor of the m^{th} element and is equal to:

$$a_m(\varphi, \theta) = e^{j\beta md \cos\varphi \sin\theta} \quad 3\text{-}4$$

The above equation 3-4 describes a progressive phase shift

$$\beta md \cos\varphi \sin\theta = \frac{2\pi}{\lambda} md \cos\varphi \sin\theta = 2\pi f \frac{md \cos\varphi \sin\theta}{v = f\lambda} = \omega t_d \quad 3\text{-}5$$

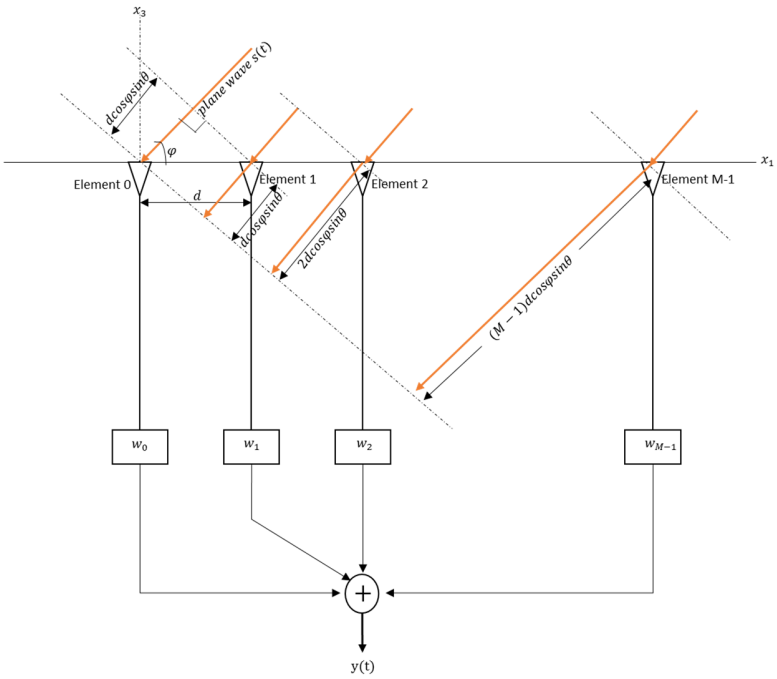

Figure 3-2: Uniform Linear Array

Equation 3-5 represents the time t_d it will take the plane wave to propagate $md\cos\varphi\sin\theta$ in the direction of the incident wave.

Now for the case of uniform circular array (UCA) with element spacing of $\frac{2\pi R}{M}$ arranged on a circle of radius R the arriving signal at the m^{th} element can be described as

$$s_m(t) = s(Re^{\frac{j2\pi m}{M}}, t) = s(\mathbf{0}, t)a_m(\varphi, \theta) \quad 3\text{-}6$$

where in this case, the antenna factor for the m^{th} antenna can be described as:

$$a_m(\varphi, \theta) = e^{j\beta R\sin\theta\cos(\varphi - \frac{2\pi m}{M})} \quad 3\text{-}7$$

For simplicity from here onward unless otherwise stated it is assumed that the elevation angle $\theta = 90$ making $sin\theta = 1$.

3.2.1 Interferometry

The principle of interferometry states that if a plane wave arrives at an antenna array with an angle it will be received by two different elements with a time delay due to the difference in the length of the path. This path length difference results in a phase difference between signals received by antennas.

$$\Delta\varphi = \left(\frac{2\pi}{\lambda}\right) d\cos\varphi\, sin\theta \quad 3\text{-}8$$

To estimate the angles some baselines should be defined. To form two baselines three antenna elements are necessary which can be placed on an equilateral triangle. The phase measurement techniques are analogue, digital and Fourier transform.

In correlative interferometry at each wave angle the measured phase differences are compared with the reference phase differences for the direction finding (DF) antenna. The column of measured phase angles is moved through the matrix of reference phase angles and the values with maximum correlation are used. This value corresponds to the angle of arrival of the incoming signal.

The reference phase differences or “array manifold” is measured during the calibration process, in which a model is designed to understand the behaviour of the antennas. The theoretical array response values might be considerably different in practical so it is very important that the non-ideal aspects of the system should be considered while making a theoretical model to increase accuracy of the practical systems. A signal is transmitted to the receiver using known locations and regular azimuthal and frequency stepping. The differential phase and the amplitude values are then used to form a calibration table. Figure 3-3 depicts an example of the correlative interferometry. The data set is from an antenna array of 5-elements and the columns in the data matrix represent the direction and are used to form a comparison vector. The measured phase differences are contained in the upper data vector. In the reference and measurement vector matrices each column is correlated between the two matrices. Thus, the angle that will be linked with the comparison vector matrix because of the maximum correlation will be the true angle.

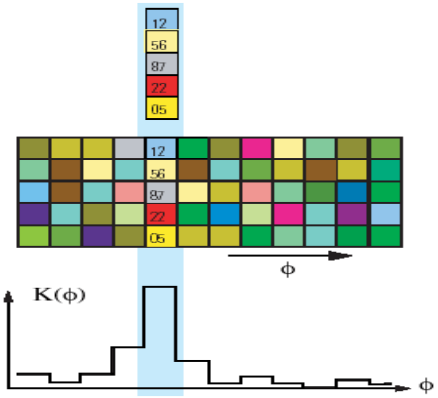

Figure 3-3: Correlative Interferometer

3.2.2 Conventional or Classical Beamformer

This method was proposed in [336] .If there are M omnidirectional isotropic antennas that have a unity gain arranged in a uniform linear array with uniform spacing d between them on the $\mathbf{x_1}$ axis as shown in Figure 3-2 then the input at each element in the presence of noise can be written as

$$\mathrm{u_m(t)} = \mathrm{a_m(\varphi)s(t)} + \mathrm{n_m(t)} \qquad 3\text{-}9$$

where $\mathrm{a_m(\varphi)}$ for a ULA with $\sin\theta = 1$ can be written as:

$$\mathrm{a_m(\varphi)} = \mathrm{e^{j\beta m(d/\lambda)\cos\varphi}} \qquad 3\text{-}10$$

The conventional beamforming method introduces a phase delay in the signals and weights and then sum them together as the output $\mathrm{y(t)}$ which can be written as:

$$\mathrm{y(t)} = \mathbf{w}^{\mathrm{H}}\mathbf{u(t)} \qquad 3\text{-}11$$

Substituting the value of $\mathbf{u(t)}$ from equation 3-9 into equation 3-11 gives:

$$\mathrm{y(t)} = \mathbf{w}^{\mathrm{H}}(\mathbf{a}(\varphi)\mathrm{s(t)} + \mathbf{n(t)}) \qquad 3\text{-}12$$

$$y(t) = [w_0^* \; w_1^* \; \dots \; w_{M-1}^*]\left(\begin{bmatrix} a_0(\varphi) \\ a_1(\varphi) \\ \vdots \\ a_{M-1}(\varphi) \end{bmatrix} s(t) + \begin{bmatrix} n_0(t) \\ n(t) \\ \vdots \\ n_{M-1}(t) \end{bmatrix}\right) \quad 3\text{-}13$$

where $\mathbf{a}(\varphi)$ is the steering vector and $\mathbf{w}$ are the weights or beamforming vector.

The pseudospectrum of the DAS beamformer can be written as:

$$P_{DAS} = \mathbf{E}\{|y_t|^2\} = E\{|\mathbf{w}^H \quad \mathbf{u}(t)|^2\} = E\{\mathbf{w}^H\mathbf{u}(t)\mathbf{u}^H(t)\mathbf{w}\} \quad 3\text{-}14$$

$$= \mathbf{w}^H\mathbf{E}\{\mathbf{u}(t)\mathbf{u}^H(t)\}\mathbf{w}$$

$$= \mathbf{w}^H\mathbf{R}_{uu}\mathbf{w}$$

R_{uu} is the autocorrelation matrix of the data received from the array.

$$R_{uu} = \mathbf{E}\{\mathbf{u}(t)\mathbf{u}^H(t)\} = \mathbf{E}\{[\mathbf{a}(\varphi)s(t) + \mathbf{n}(t)][s(t)\mathbf{a}^H(\varphi) + \mathbf{n}^H(t)]\} \quad 3\text{-}15$$

$$= \sigma_s^2\mathbf{a}(\varphi)\mathbf{a}^H(\varphi) + \sigma_n^2 I_{MxM}$$

where $\sigma_s^2 = \mathbf{E}\{s^2(k)\}$ represents the signal power and $\sigma_n^2 = \mathbf{E}\{n^2(k)\}$ is the noise power.

If a signal $s(t)$ with an azimuthal angle of φ_0 arrives at the array, then the maximum output of the beamformer with no noise present would be maximum for $\mathbf{w} = \mathbf{a}(\varphi_0)$ thus aligning the phases of the antenna element input so that the components of the incoming signal can add constructively. Thus, the estimated angle can be any value of φ that will maximise the following:

$$P_{DAS}(\varphi)|_{\mathbf{w}=\mathbf{a}(\varphi)} = \mathbf{w}^H R_{uu}\mathbf{w}|_{\mathbf{w}=\mathbf{a}(\varphi)} = \mathbf{a}^H(\varphi)R_{uu}\mathbf{a}(\varphi) \quad 3\text{-}16$$

Equation 3-16 is referred to as the spatial spectrum of the DAS (Conventional) beamformer whose peaks can be determined to estimate the azimuth angle of arrival.

3.2.3 Capon's Minimum Variance Distortionless Response Algorithm

This method was proposed in [337] to improve the poor resolution of the beamformer method as shown in Figure 3-4. This method also measures the received signal power in all directions possible and suppresses the contribution of the unwanted signals by modifying the spatial spectrum. This modification is accomplished by solving the constrained minimization equation below and then the resultant constrained optimal weight vector $\boldsymbol{w}_c$ in Equation 3-14.

$$\mathrm{Min_w}\mathbf{E}\{|\mathrm{y_t}|^2\} = \mathrm{Min_w}\mathbf{w}^{\mathrm{H}}\mathrm{R_{uu}}\mathbf{w}\ \text{condition: } \mathbf{w}^{\mathrm{H}}\mathbf{a}(\varphi) = 1 \qquad 3\text{-}17$$

Equation 3-17 can be solved using the Lagrange multiplier

$$\mathrm{J} = \frac{1}{2}\mathbf{w}^{\mathrm{H}}\mathrm{R_{uu}}\mathbf{w} + \lambda(\mathbf{w}^{\mathrm{H}}\mathbf{a} - 1); \qquad 3\text{-}18$$

$$\left\{\begin{array}{ll} \dfrac{\partial}{\partial \mathbf{w}}\mathrm{J} = \mathrm{R_{uu}}\mathbf{w} + \lambda\mathbf{a} = \mathbf{0}; \quad \mathbf{w} = \mathrm{R_{uu}^{-1}}\lambda\mathbf{a} & (1) \\ \dfrac{\partial}{\partial \lambda}\mathrm{J} = 0;\ \mathbf{w}^{\mathrm{H}}\mathbf{a} = 1 \rightarrow \lambda\mathbf{a}^{\mathrm{H}}\mathrm{R_{uu}^{-H}}\mathbf{a} = 1;\ \lambda = \dfrac{1}{\mathbf{a}^{\mathrm{H}}\mathrm{R_{uu}^{-H}}\mathbf{a}} & (2) \end{array}\right\} \qquad 3\text{-}19$$

Equation 3-19 results in

$$\mathbf{w_c} = \mathrm{R_{uu}^{-1}}\lambda\mathbf{a} = \frac{\mathrm{R_{uu}^{-1}}\mathbf{a}(\varphi)}{\mathbf{a}^{\mathrm{H}}(\varphi)\mathrm{R_{uu}^{-1}}\mathbf{a}(\varphi)} \qquad 3\text{-}20$$

Substituting Equation 3-20 in Equation 3-17 results in Capon's Pseudospectrum:

$$\mathrm{P_{Capon}}(\varphi) = \mathbf{w}^{\mathrm{H}}\mathrm{R_{uu}}\mathbf{w} = \left(\frac{\mathrm{R_{uu}^{-1}}\mathbf{a}(\varphi)}{\mathbf{a}^{\mathrm{H}}(\varphi)\mathrm{R_{uu}^{-1}}\mathbf{a}(\varphi)}\right)^{\mathrm{H}}\mathrm{R_{uu}^{-1}}\ \frac{\mathrm{R_{uu}^{-1}}\mathbf{a}(\varphi)}{\mathbf{a}^{\mathrm{H}}(\varphi)\mathrm{R_{uu}^{-1}}\mathbf{a}(\varphi)} = \frac{1}{\mathbf{a}^{\mathrm{H}}(\varphi)\mathrm{R_{uu}^{-1}}\mathbf{a}(\varphi)} \qquad 3\text{-}21$$

The disadvantage of using the MVDR method is that it requires computation of inverse matrix which can become ill conditions in the presence of highly correlated signals.

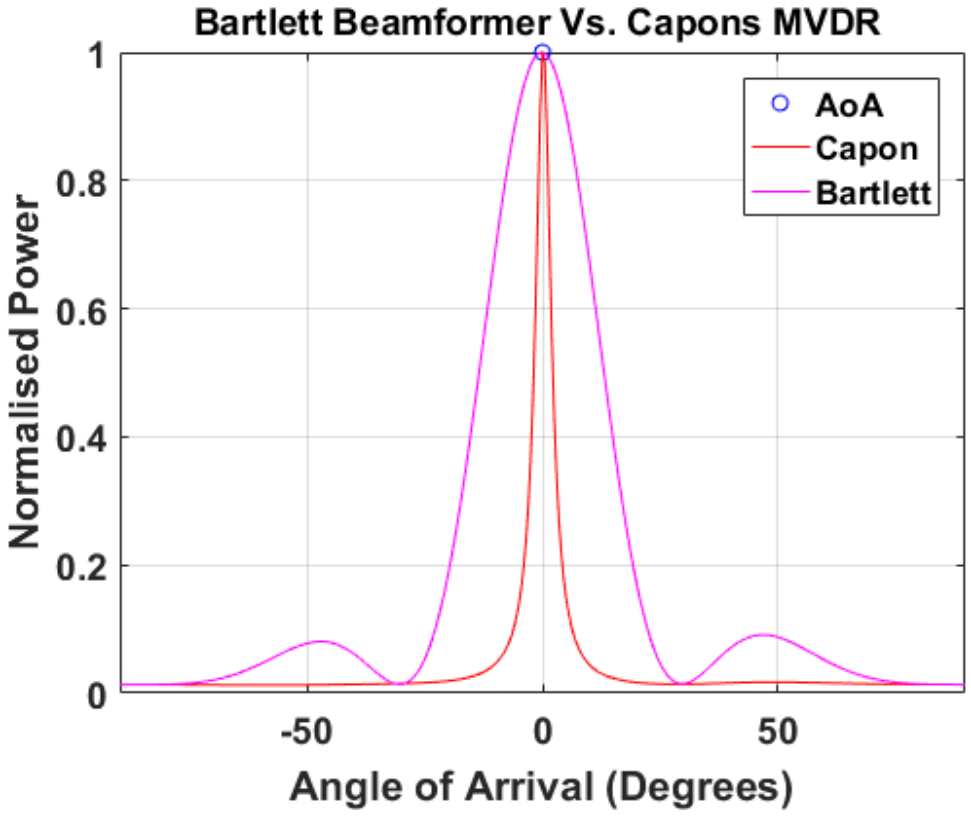

Figure 3-4: Performance Comparison Between the Beamformer and Minimum Variance Distortionless Response

3.2.4 Subspace Based DOA Estimation Method of Multiple Signal Classification (MUSIC)

Schmidt proposed this method to estimate the direction of an incoming plane wave in the presence of noise [39].

The linear combination of L incident signals and noises arriving at an M-element array can be written in a form of a as:

$$\mathbf{u}(\mathrm{t}) = \sum_{\mathrm{t}=0}^{\mathrm{L}-1} \mathbf{a}(\varphi_{\mathrm{l}})\mathrm{s}_{\mathrm{l}}(\mathrm{t}) + \mathbf{n}(\mathrm{t}) = \mathrm{A}\,\mathbf{s}(\mathrm{t}) + \mathbf{n}(\mathrm{t}) \qquad 3\text{-}22$$

$$\begin{bmatrix} u_0(t) \\ u_1(t) \\ \vdots \\ u_{M-1}(t) \end{bmatrix} = \begin{bmatrix} a_0(\varphi_o) & \dots & a_0(\varphi_{L-1}) \\ a_1(\varphi_o) & \dots & a_1(\varphi_{L-1}) \\ \vdots & \dots & \vdots \\ a_{M-1}(\varphi_o) & \cdots & a_{M-1}(\varphi_{L-1}) \end{bmatrix} \begin{bmatrix} s_0(t) \\ s_1(t) \\ \vdots \\ s_{L-1}(t) \end{bmatrix} + \begin{bmatrix} n_0(t) \\ n_1(t) \\ \vdots \\ n_{M-1}(t) \end{bmatrix} \quad 3\text{-}23$$

where $\mathbf{a}(\varphi_l) = [a_0(\varphi_l)\, a_1(\varphi_l) \dots a_{M-1}(\varphi_o)]^T$ is the antenna array steering vector of size $Mx1$ for the l^{th} signal that has a direction of arrival (DOA) (φ_l) and $\mathbf{s}(t) = [s_0(t)\, s_1(t) \dots s_{L-1}(t)]^T$ is the vector containing L signals that are arriving on the antenna array.

The steps in the computation of the MUSIC algorithm are:

- Step 1: Collect the array input vector samples.

$$\{u(nT), n = 0, \dots \dots . N - 1\} \text{where N: Number of snapshots} \quad 3\text{-}24$$

- Step 2: Calculate the array correlation matrix as:

$$\widehat{R}_{uu} = \frac{1}{N} \sum_{n=0}^{N-1} \mathbf{u}(nT)\mathbf{u}^H(nT) = AR_{ss}A^H + \sigma_n^2 I \quad 3\text{-}25$$

where $R_{ss} = \mathbf{E}\{\boldsymbol{s}\boldsymbol{s}^H\}$ is the signal correlation matrix and $\sigma_n^2 I$ is the noise correlation matrix.

- Step 3: Apply Eigen decomposition to the input correlation matrix $\hat{R}_{uu}$ as:

$$\hat{R}_{uu}V = V\Lambda \quad 3\text{-}26$$

where

$$V = [v_o\ v_1\ \dots v_{M-1}] \quad 3\text{-}27$$

and

$$\Lambda = \begin{bmatrix} \lambda_0 & 0 & \dots & 0 \\ 0 & \lambda_0 & \dots & 0 \\ \vdots & \vdots & \ddots & \vdots \\ 0 & 0 & \dots & \lambda_{M-1} \end{bmatrix} \quad 3\text{-}28$$

Step 4: Estimate the total number of signals $\hat{L} = M - N_n$, where, N_n is the total number of the smallest eigenvalues that create the Matrix V_n of form MxN_n containing the noise eigenvectors that correspond to the smallest eigenvalues.

$$V_n = [\boldsymbol{v}_0\ \boldsymbol{v}_0 \ldots\ \boldsymbol{v}_{N_n} - 1] \quad \text{3-29}$$

- Step 5: Compute the MUSIC pseudospectrum using:

$$P_{MUSIC}(\varphi) = \frac{1}{\boldsymbol{a}^H(\varphi) V_n V_n^H \boldsymbol{a}(\varphi)} \quad \text{3-30}$$

- Step 6: Select the $\hat{L}$ highest peaks of the pseudospectrum to estimate the DOA.

Super-resolution techniques allow estimating the AOA of multiple co-channel signals. It has a DF accuracy about 1° and can search for azimuth and elevation at the same time.

A brief comparison of different direction of arrival estimation techniques is provided in Table 3-1

Table 3-1: Comparison of different AOA/DOA estimation algorithms

	Sensitivity to noise	**Sensitivity to calibration**	**Sensitivity to multipath**	**Ability to separate closely spaced multipath**	**Complexity**
DAS (spectral estimation methods)	High	Moderate	High	Low	Low
MUSIC	Low	Higher	Low	High	High
Root-MUSIC	Lower	High	Lower	High	High
ESPRIT	Lower	Low	Low	High	High
Fusion (DAS & root-MUSIC)	Low	Moderate	Lowest	Very high	Moderate

3.3 Mathematical Model of the Proposed Angle of Arrival (AoA) Estimation Technique

The proposed technique makes use of the signal subspace to provide an estimate of the direction of arrival. The steps of the proposed algorithm are summarised as follows:

- Step 1: Collect the array input vector samples.

$$\{\mathrm{u(nT)}, \mathrm{n} = 0, \ldots\ldots \mathrm{N}-1\} \text{where N: Number of snapshots} \quad \text{3-31}$$

- Step 2: Calculate the array correlation matrix as:

$$\widehat{\mathrm{R}}_{\mathrm{uu}} = \frac{1}{\mathrm{N}}\sum_{\mathrm{n=0}}^{\mathrm{N-1}} \mathbf{u}(\mathrm{nT})\mathbf{u}^{\mathrm{H}}(\mathrm{nT}) = AR_{ss}A^{H} + \sigma_n^2 I \quad \text{3-32}$$

where $R_{ss} = \mathbf{E}\{\boldsymbol{ss}^{H}\}$ is the signal correlation matrix and $\sigma_n^2 I$ is the noise correlation matrix.

- Step 3: Apply Eigen decomposition to the input correlation matrix $\hat{R}_{uu}$ as:

$$\hat{R}_{uu}V = V\Lambda \quad \text{3-33}$$

where

$$V = [v_o\ v_1\ \ldots v_{M-1}] \quad \text{3-34}$$

and

$$\Lambda = \begin{bmatrix} \lambda_0 & 0 & \ldots & 0 \\ 0 & \lambda_0 & \ldots & 0 \\ \vdots & \vdots & \ddots & \vdots \\ 0 & 0 & \ldots & \lambda_{M-1} \end{bmatrix} \quad \text{3-35}$$

Step 4: Estimate the total number of signals $\hat{L} = M - N_n$, where, N_n is the total number of the smallest eigenvalues.

Step 5: Estimate the signal subspace V_s.

$$V_s = [\boldsymbol{v}_0\ \boldsymbol{v}_0 \ldots \boldsymbol{v}_{\hat{L}} - 1]$$

The signal subspace is computed using the eigenvectors that correspond to the $\hat{L}$ largest eigenvalues.

Step 6: Compute:

$$\mathrm{P}(\varphi) = \bar{\mathrm{a}}(\varphi)\, V_s\, V_s^H\ \bar{\mathrm{a}}(\varphi)^{\mathrm{H}} \qquad 3\text{-}36$$

This will result in the peaks in the direction of arrival. However, the peaks produced by the above equation result in a very wide side lobed spectrum which results in erroneous estimation at low power levels and for this reason it is proposed to search for the nulls in the direction of arrival which can be achieved by subtracting all the values of $\mathrm{P}\ (\varphi)$ from its max value.

$$\mathrm{P}_{\mathrm{diff}}(\varphi) = \mathrm{P}\ (\varphi)_{\mathrm{max}} - \mathrm{P}\ (\varphi) \qquad 3\text{-}37$$

The pseudo spectrum of the proposed technique then can be written as:

$$P_{prop}\ (\varphi) = \frac{1}{P_{diff}(\varphi) + \varepsilon} \qquad 3\text{-}38$$

where ε =1/ λ_{Max} is added to remove any singularities that might be present. Finally, the error can then be calculated between the true direction of arrival and the estimated direction. The absolute error for each incoming signal can be mathematically described as

$$\mathrm{er(i)} = \left|\ \mathrm{Real}_{\mathrm{Ang}}(\mathrm{i}) - \mathrm{Estimated}_{\mathrm{Ang}}(\mathrm{i})\right| \qquad 3\text{-}39$$

and the average error for each impinging ray ($e_{av\text{-}angle}$) can be calculated as:

$$e_{\mathrm{av-angle}} = \frac{\sum_{\mathrm{i=1}}^{\mathrm{k}} |\mathrm{er(i)}|}{\mathrm{k}} \qquad 3\text{-}40$$

where i represents the total number of iterations used to generate the L angles. The average total error ($e_{av\text{-}total}$) is:

$$e_{\mathrm{av-total}} = \frac{\sum_{k=1}^{L}(\mathrm{er_k})}{L} \qquad 3\text{-}41$$

The proposed method can be described using the flow diagram below:

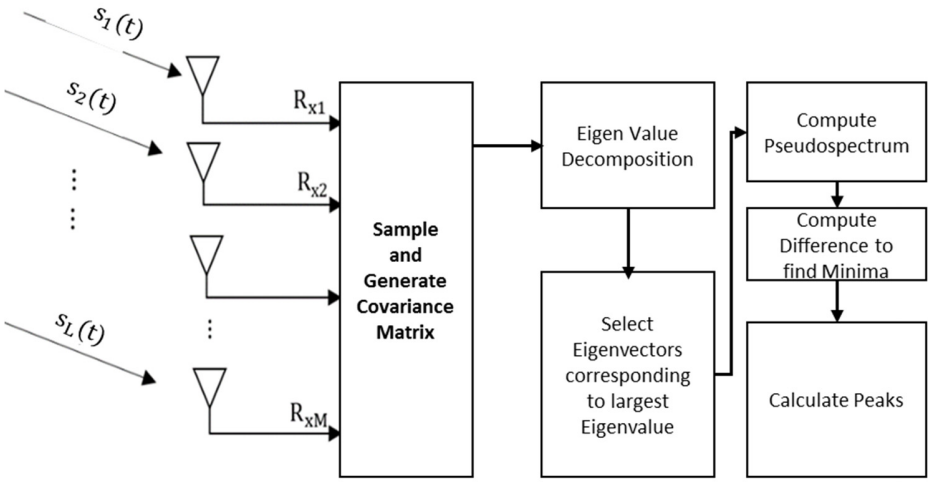

Figure 3-5: Flow Diagram of the Proposed AoA Method

This technique has the advantage of less computation complexity over the more widely accepted Multiple Signal Classification (MUSIC) technique for applications that require fast processing of low number of incoming signals especially in asset tracking.

3.4 Results and Discussion

The performance of the proposed algorithm was evaluated using different setups and some of those are discussed in this section

3.4.1 Performance Evaluation of the Proposed Algorithm

A 10-element uniform linear antenna array was constructed using MATLAB, with inter-element spacing of $(\frac{\lambda}{2})$ to compare the performance of the proposed algorithm. The simulation parameters used are listed in Table 3-2.

Table 3-2: Simulation Parameters Using the ULA for the Performance Comparison of the Proposed Algorithm

Parameter	Value
Number of Elements	10
SNR	20 dB
Antenna Spacing	$\lambda/2$
True Angle	0 Degree
Number of Snapshots	100
Noise	AWGN

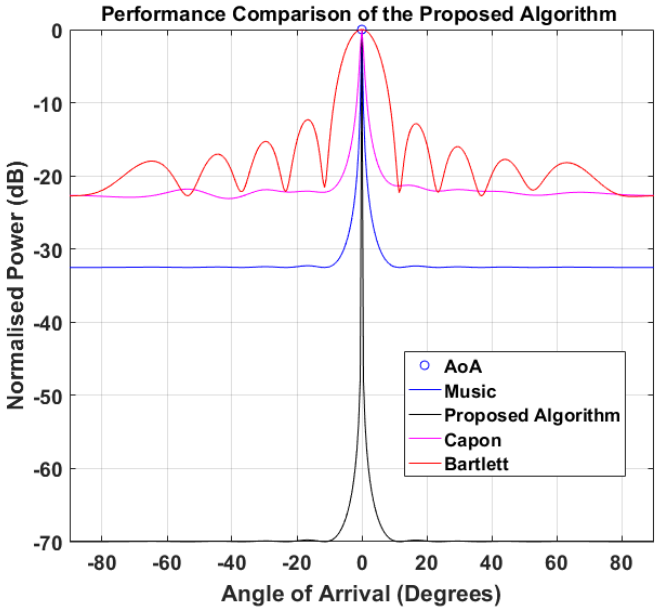

Figure 3-6: ULA for The Performance Comparison of the Proposed Algorithm

The Capon's algorithm is famous for its ability to improve the spectral resolution as shown in Figure 3-4, and something of the similar nature is evident from the results produced in Figure 3-6 where the proposed algorithm clearly shows its ability to have superior resolution and a much higher normalised power that the signal can be accurately estimated at lower power thresholds.

a) Effect of Number of SNR on the Proposed Algorithm

The same 10-element ULA was used to understand the effect of the number of snapshots on the proposed angle estimation method for multiple closely spaced angles. The simulation parameters are as shown in Table 3-3

Table 3-3: Simulation Parameters Using the ULA for the Study of the Effects of Total Number of Snap Shots on the Proposed Angle of Arrival Estimation Algorithm

Parameter	Value
Number of Elements	10
SNR	0 dB
Antenna Spacing	$\lambda/2$
True Angle	[-20, 0, 20] Degrees
Number of Snapshots	100, 500 1000
Noise	AWGN

The results obtained in Figure 3-7 show that even with 100 data snapshots the proposed algorithm could resolve three closely spaced angles, the performance however can be further increased as for N = 1000, with a higher number of data snapshots.

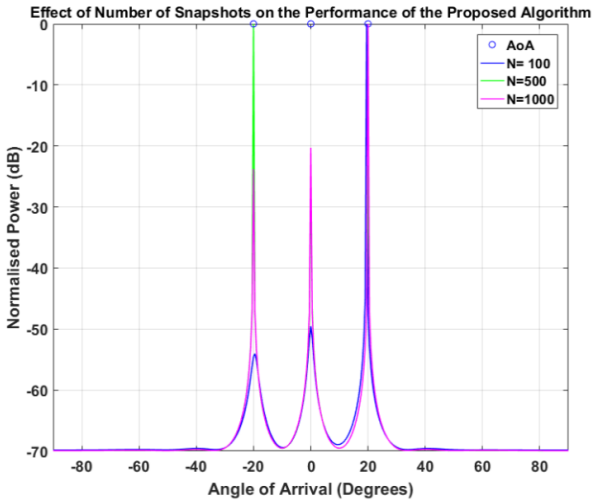

Figure 3-7: Effects of Total Number of Snap Shots on the Proposed Angle of Arrival Estimation Algorithm

b) Effect of SNR on the Accuracy of Proposed AoA Algorithm

To evaluate the effect of signal to noise ratio (SNR) the same 10-element ULA was used and the simulation parameters are described in Table 3-4. The results obtained in Figure 3-8 show that even at SNR of -20 dB the estimator could identify the three different peaks at the normalised power level of approx. -40 dB. However, as the SNR increases three highly identifiable peaks emerge to point in the direction of the source signals.

Table 3-4: Simulation Parameters Using the ULA

Parameter	Value
Number of Elements	10
SNR	[-20 -10 0 10 20] dB
Antenna Spacing	$\lambda/2$
True Angle	[-20, 0, 20] Degrees
Number of Snapshots	100

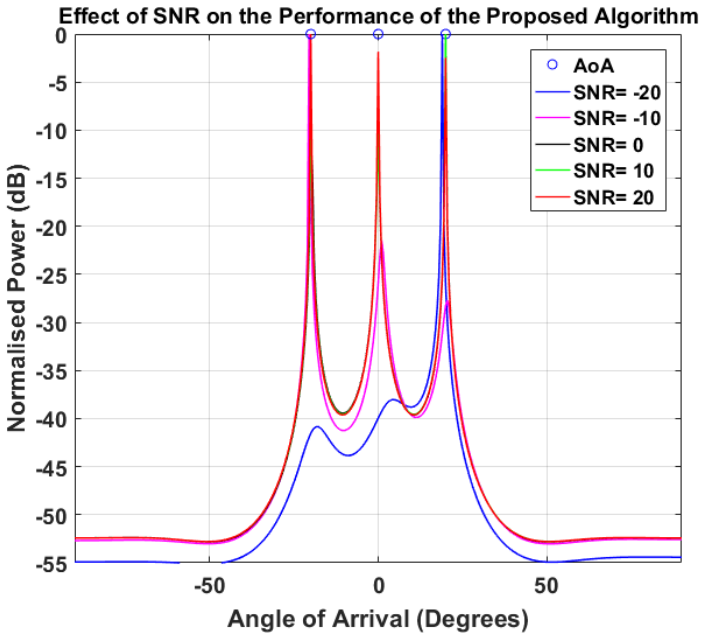

Figure 3-8: Effects of SNR on the Proposed Angle of Arrival Estimation Algorithm

All the results obtained using the simulation model built in MATLAB support the enhanced performance of the proposed algorithm. However, when designing a practical antenna array system, the designer must face many challenges including the required geometry and size of the antenna array according to the application specifications, in addition depending on the application the choice of antenna as different antennas has different radiation patterns and gains etc. These requirements then introduce further variables in the estimation system. To further test the performance of the proposed algorithm in a more real-world scenario different antenna arrays and geometries were constructed using computer simulation technology (CST) software and Numerical Electromagnetic Code (NEC).

c) Execution Time

In practical localization applications, it is necessary that the processing algorithm be computationally fast. In Figure 3-9 the comparison is made for the time of execution of four different algorithms that are used in this study for a total of 1000 iterations, it is suggested by the results that the proposed algorithm has the fastest execution performance as compared to any of the other methods presented.

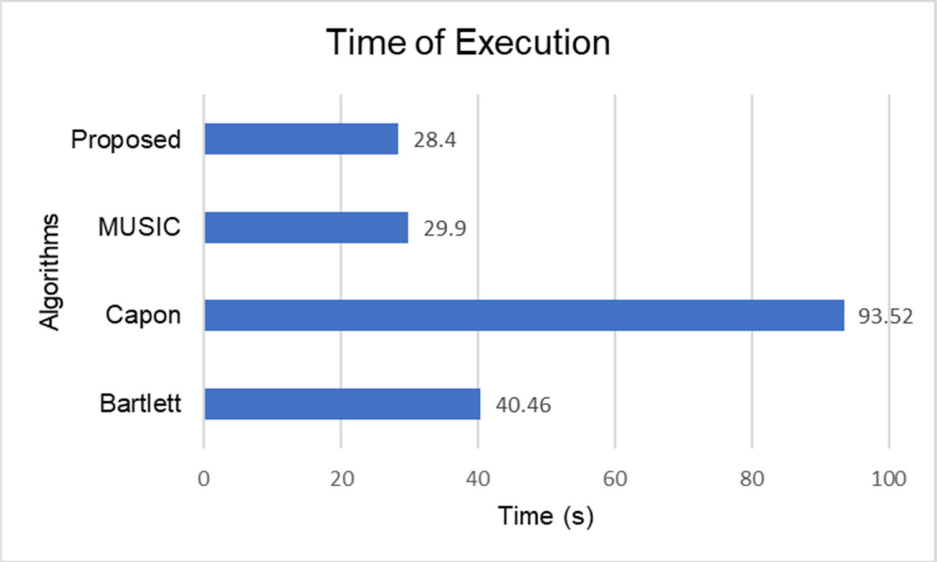

Figure 3-9: Time of Execution Comparison

d) Signals with Different Power Levels

Five signals are constructed such that each signal is arriving from a different source or because of a multipath scatter with different direction of arrival and has different received power due to the path travelled. The directions and amplitude power of these signals are [-60^0, -30^0, 0^0, 30^0, 60^0] and [1, 0.8, 0.6, 0.3, 0.1] Watts.

The results obtained in Figure 3-10 suggest that the proposed algorithm can estimate both the direction of arrival and the received power of each arriving signal.

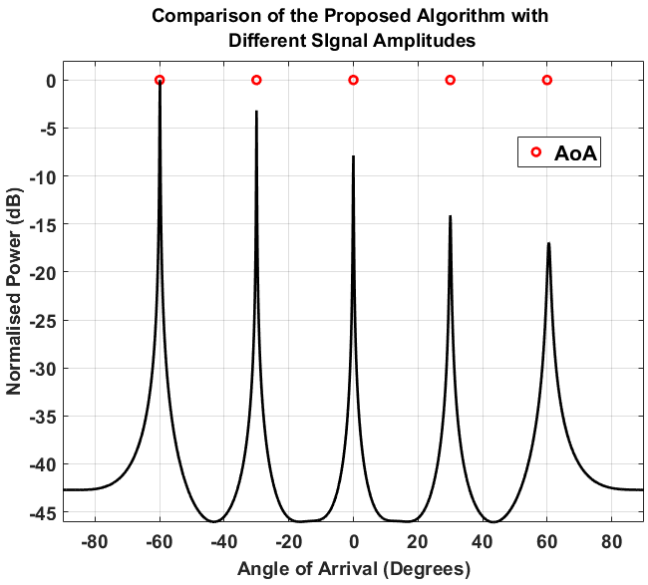

Figure 3-10: Signals with Different Amplitudes

e) Effect of Number of Elements and Inter-Element Spacing

Three different true angles were used to evaluate the effect of number of elements and inter element spacing on the angle of arrival estimation of the proposed algorithm. The simulation criteria are defined in Table 3-5.

Table 3-5: Simulation Parameters

Parameter	Value
Number of Elements	6, 8, 10
SNR	0 dB
Antenna Spacing	$\lambda/2$, $\lambda/4$
True Angle	[-20, 0, 20] Degrees
Number of Snapshots	100

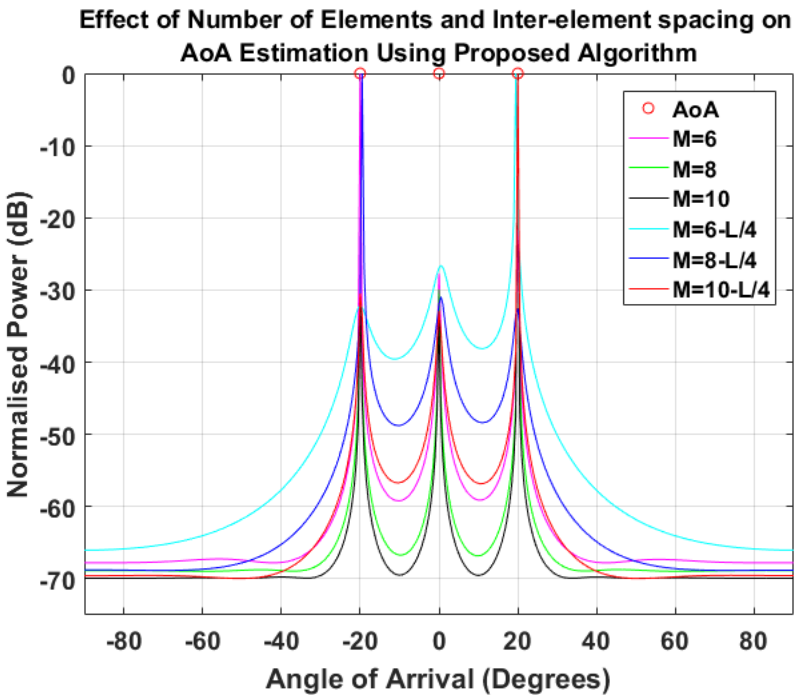

Figure 3-11: Effects of number of elements and Inter-element spacing on the Proposed Angle of Arrival Estimation Algorithm

The results in Figure 3-11 show the performance of the proposed algorithm with the change in the number of elements and the element spacing from $\lambda/2$ to $\lambda/4$ which is expressed as “L/4” in Figure 3-11. The estimation algorithm has the best performance with the highest number of elements when the inter element spacing is $\lambda/2$. Even 10 elements with $\lambda/4$ show worse performance than 6 elements with $\lambda/2$. This explains how the interelement spacing degrades the performance and how it creates a challenge for the antenna array designer for localization systems when the space constraints are present.

f) Performance Comparison of the Proposed Algorithm in the Presence of Correlated Sources

Correlation or similarity between signals reduces the performance of direction estimation algorithms. Hence, a simulation was run for two received signals with 95% correlation coefficients incident on linear array consisting of ten elements spaced by d = 0.5λ. The performance of the various methods is shown in Figure 3 12. Although MUSIC and Capon give correct estimates for both signals, their performance significantly deteriorates. The Bartlett method gives reasonable performance and accuracy, but the proposed algorithm is the most accurate, with sharpest peaks and very low side lobe levels.

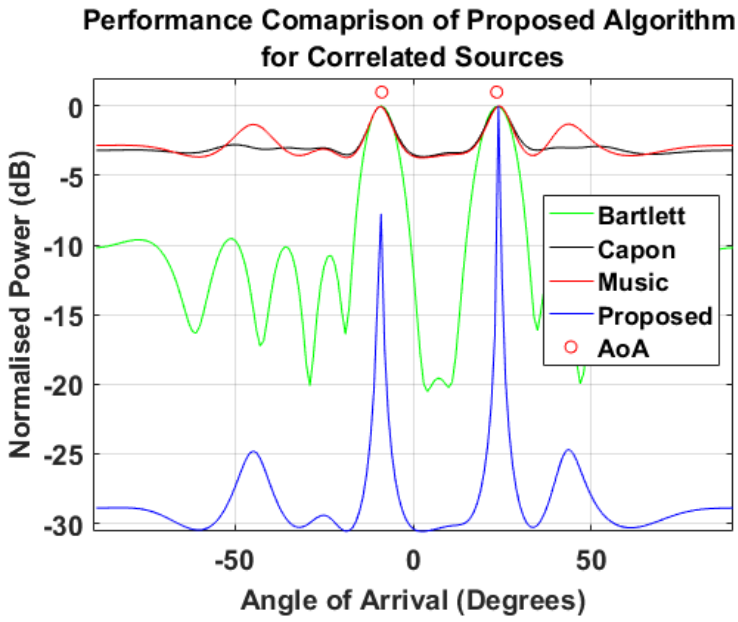

Figure 3-12: Performance Comparison of the Proposed Algorithm in the Presence of Correlated Sources

3.4.2 3-element IFA Antenna Array

A three-element inverted F antenna (IFA) based array was constructed using the computer simulation technology (CST) antenna design software. The elements were separated at 120 degrees in azimuth plane over $1\lambda\, x\, 1\lambda$ square finite conducting ground plane with antenna spacing of $\lambda/4$, where λ is the wavelength at the desired carrier frequency of 400 MHz, the selection of $\lambda/4$ spacing between the antenna elements was to keep the overall antenna array footprint to the minimum. The transmitter and the receiver array were placed in the same plane thus only azimuth angle calculations were done. The transmitter was placed in the far field zone i.e. at least 3 meters away from the receiver array. The construction of the simulation environment is shown in Figure 3-13.

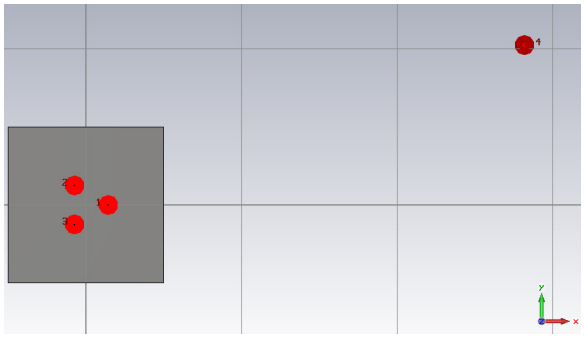

Figure 3-13: Three element array structure in CST

Four different angle of arrival estimation algorithms were compared, namely, Interferometry, Bartlett, Proposed method and Multiple Signal Classification technique (MUSIC). The receiver array was turned at 20-degree step size for the whole azimuth plane (i.e. 360 degrees) and additive white Gaussian noise (AWGN)

was introduced to the received signal. The results in terms of estimation error at SNR of 0dB from the four algorithms are plotted in Figure 3-14.

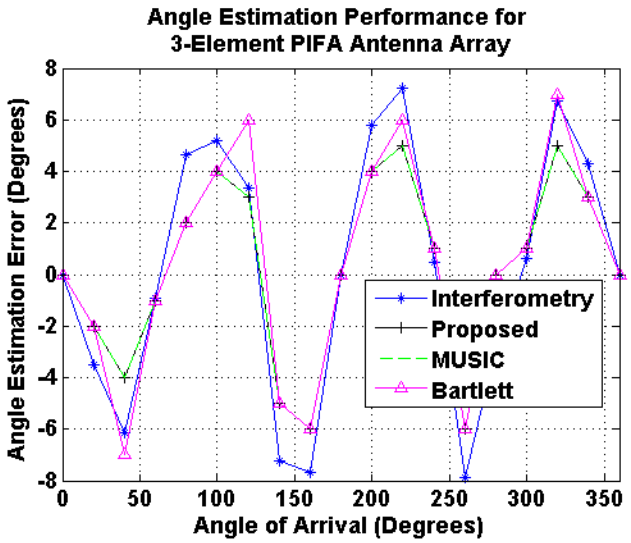

Figure 3-14: Angle of arrival estimation error using interferometry, Covariance and MUSIC

As envisaged, the super-resolution signal subspace based proposed algorithm and noise subspace based MUSIC algorithm outperform the conventional Bartlett algorithm and the interferometry method for determination of angle of arrival in terms of angle error. The results also suggest that both subspace based methods show similar angle estimation error performance. The maximum estimation error from the signal subspace techniques was 6 degrees which is acceptable considering the low antennas spacing between the elements of the antenna array and low SNR.

3.4.3 Interferometry vs. Proposed Algorithm

Next a comparative study has been carried out to evaluate the performance of the proposed algorithm against the phased interferometry algorithm and to understand the effect of the ground plane (finite/infinite) on the angle estimation. Three antenna and four antenna circular array geometries have been used for this study and simulated using Numerical Electromagnetics Code (NEC) antenna design software. The diagram of the two geometries is presented in Figure 3-15 (a) and (b). In the study, the size of the finite ground plane was $1\lambda \times 1\lambda$. The ground plane was made up of conducing material with properties like that of copper.

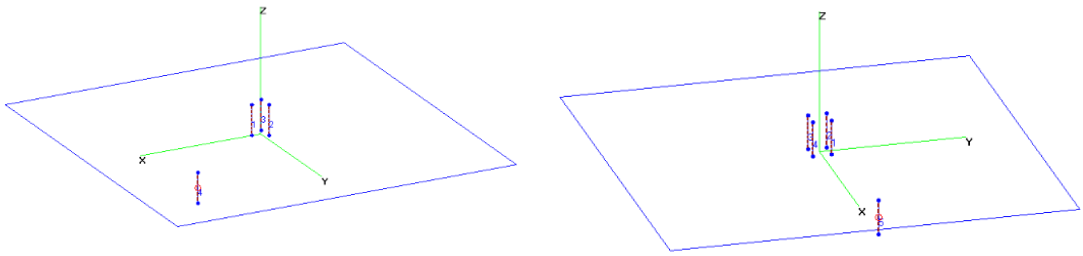

(a) (b)

Figure 3-15: Simulation setup with (a) Three Elements (b) Four Elements

a) True Angle = 0 degrees

The study was conducted for a total of 72 angles using a single transmit source, i.e. the receiver array was rotated at 5-degree step size, but for illustration purposes only a few angles have been chosen and the results are discussed. It

was assumed for simplicity that there is no additive noise present. The antennas however, do have mutual coupling present between them.

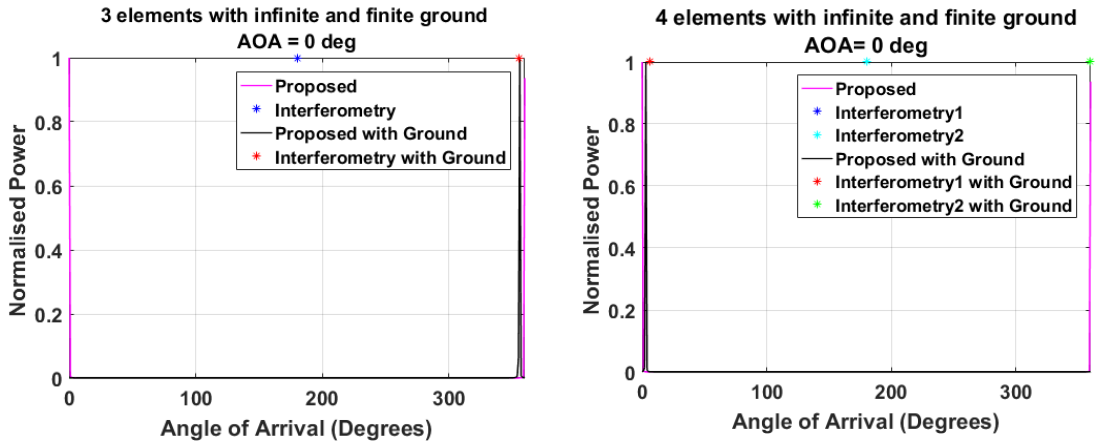

(a) (b)

Figure 3-16: AOA = 0, (a) 3 Elements with Infinite and Finite Ground Plane (b) 4 Elements with Infinite and Finite Ground Plane

The results obtained in Figure 3-16 (a) for the 0 degree as the true angle of arrival suggested an ambiguity in the interferometry method as the solution was unable to resolve the correct angle using 3 elements with infinite ground, the proposed method did provide an accurate estimate to the true bearing angle. However, when a finite ground plane was introduced the interferometry method and the proposed method were both able to closely estimate the true bearing angle with a 1 degree angle estimation error. The same true angle was then tested using a 4-element circular antenna array and the results in Figure 3-16 (b) show that with infinite ground the interferometry solution pointed in the opposite direction of the true bearing angle i.e. 180-degree error and a big angle ambiguity, whereas the proposed algorithm could closely resolve the true angle. Again, it was seen that the

introduction of a finite ground plane helps resolve the ambiguity present in the interferometry algorithm. In addition to improving the antenna radiation the ground planes also reduce the unwanted reflections which can explain the improvement in the angle estimation performance of the interferometry algorithm.

b) True Angle = 10 degrees

Second example presented is of 10 degree as the true bearing angle, for this angle again the solution for interferometry algorithm is 180 degrees in error for a three element array with infinite ground plane and there is a large error in the proposed algorithm also as shown in Figure 3-17 (a), but when an infinite ground plane is introduced the angle estimated points towards the true bearing angle, which supports the theory, that a finite ground plane actually improves the angle estimation by reducing reflections.

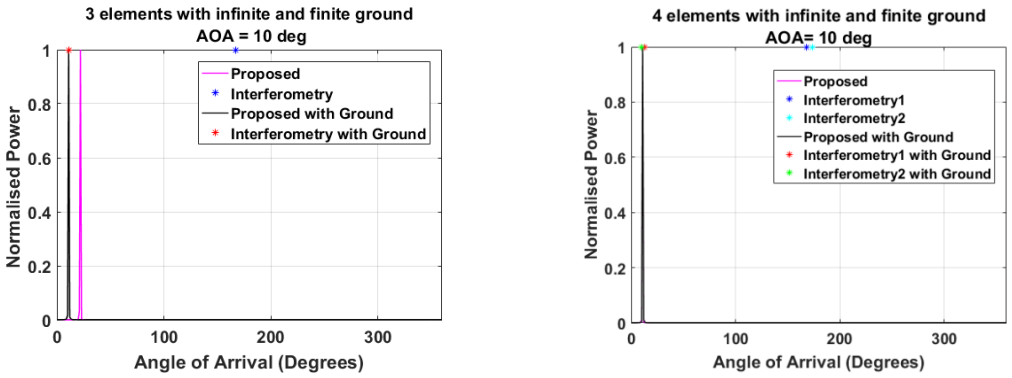

(a) (b)

Figure 3-17: AOA = 10, (a) 3 Elements with Infinite and Finite Ground Plane (b) 4 Elements with Infinite and Finite Ground Plane

In Figure 3-17 (b) by increasing the number of elements in the antenna array the estimation error in the proposed algorithm is negligible even with infinite ground however the interferometry algorithm still cannot accurately estimate the angle information and suggests the solution to be in 180 degrees opposite direction. This is a good example to show that the eigen structure based proposed method does show enhanced angle estimation resolution with an additional antenna element but that is not enough in the case of phase interferometry to increase the algorithms performance. To further illustrate this issue of angle ambiguity caused by the interferometry algorithm a few more examples of different bearing angles are presented below.

c) True Angle = 45 degrees

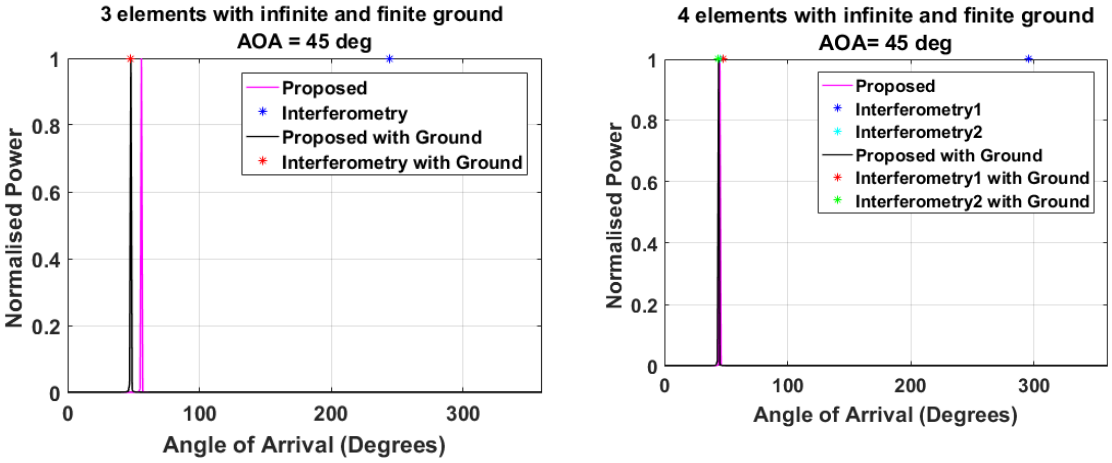

(a) (b)

Figure 3-18: AOA = 45, (a) 3 Elements with Infinite and Finite Ground Plane (b) 4 Elements with Infinite and Finite Ground Plane

In Figure 3-18 the true bearing angle is 45 degrees, in Figure 3-18 (a) with a 3-element array it can be seen the interferometry solution is again approx.180 degrees in error.

All the results obtained in section 3.4.3 suggest that the interferometry algorithm is finite ground plane dependent. Next, the same setup is repeated for multiple arriving angles.

3.4.3.1 Multiple Sources Case

Multiple transmitter sources were introduced to simulate the effect of a multipath environment on angle estimation where various copies of the same transmitted signal reach the receiver with time delays caused by the difference in length of the path travelled by the ray in a narrowband system.

a) True Angle = 45 and 300 degrees

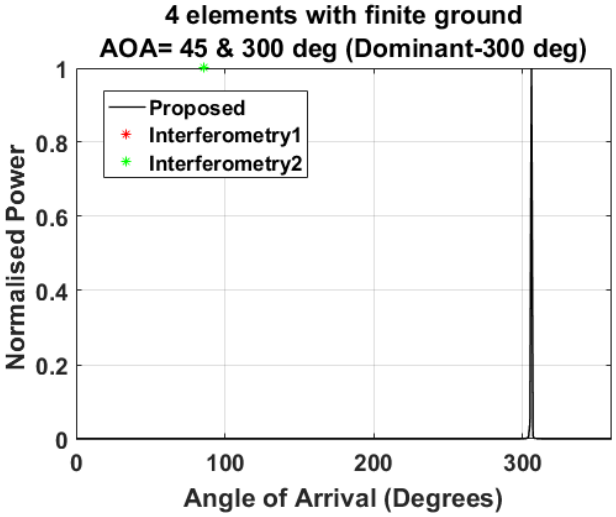

Figure 3-19: Four element array, Multiple Source Case

The first comparison that is shown in Figure 3-19 is of two angles, 45 degrees and 300 degrees. It is assumed that both the rays arrive at the receiver at the same time but with different magnitudes and the ray arriving from 300 degrees has 5 times the power as compared to the one arriving from 45 degrees. The results suggested that none of the solutions proposed by the interferometry method point toward either of the two angles. The proposed algorithm does provide a solution and point towards the dominant angle as in the case of Line of Sight environment the dominant ray will be the true angle as it will travel the shortest distance between the transmitter and receiver array.

b) True Angle = 0 and 90 degrees

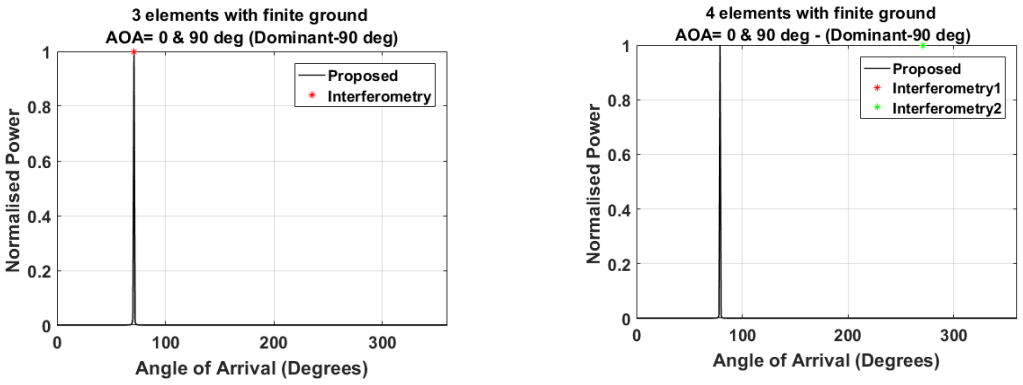

(a) (b)

Figure 3-20: (a) Three element array (b) Four element array, Multiple Source Case

This example is presented as it shows some very interesting results regarding the phase interferometry based angle of arrival estimation solution. Figure 3-20 (a)

represents the solution using a 3-element circular array for both the proposed algorithm and the phase interferometry algorithm. Results suggest that both solutions are in agreement that the dominant angle is the true bearing angle however theoretically and from previous knowledge it is known that increasing the number of elements and the addition of the finite ground plane helps improve the angle estimation accuracy, which is not seen for the case of phase interferometry in Figure 3-20 (b) rather the phase interferometry has shown an ambiguity with the addition of an extra antenna element, this shows the unstable behaviour of the algorithm and even though it is computationally easy to implement but not if all factors are considered such as signal processing based corrections that the algorithm require to correct the angle ambiguities.

3.4.4 Individual Algorithm Performance for Different Array Geometries

In this sub section, the effect of different array geometries on an individual angle of arrival algorithm is discussed. It was assumed that there are multiple rays arriving at the receiver with same power levels and complex noise was present.

From the results obtained in Figure 3-21 it is safe to say that five-element arrays show the best estimation accuracy. The results also suggest that the 5-element ring array can provide greater accuracy than the concentric ring array of 5 elements.

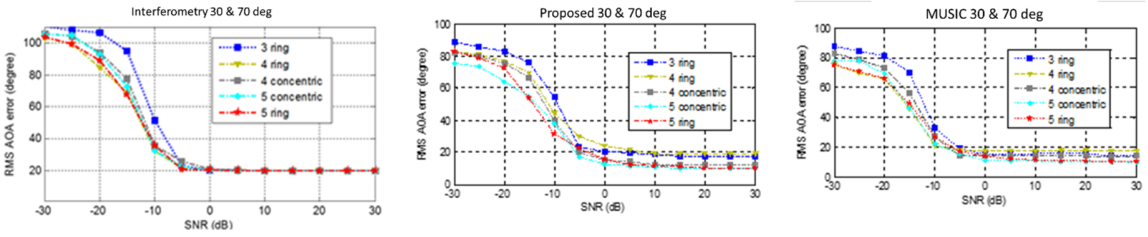

(a) (b) (c)

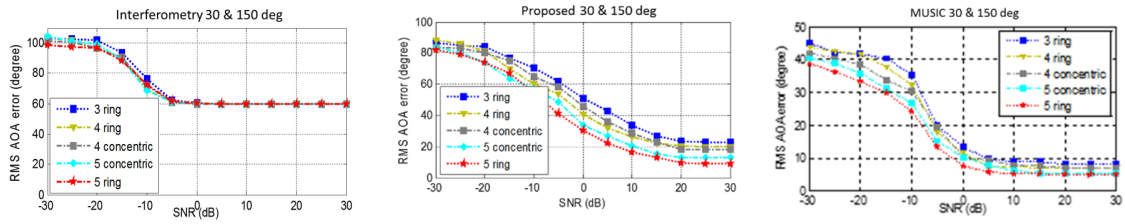

(c) (d) (e)

Figure 3-21: Comparison of Array Geometries for (a) Interferometry (b) Proposed (c) MUSIC for Multiple Rays

3.4.5 Narrowband vs. Wideband

In this sub section, the role of the bandwidth in angle estimation is studied. A comparison of Angle of Arrival algorithms is presented in terms of RMSE.

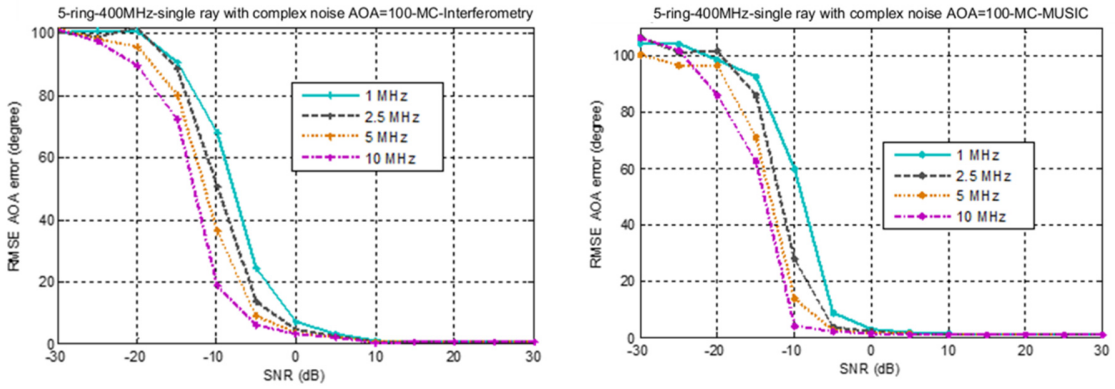

(a) (b)

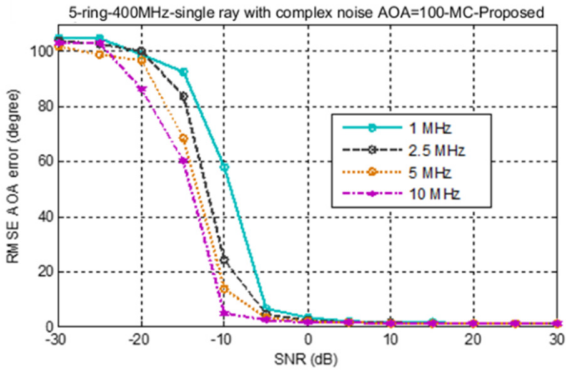

(c)

Figure 3-22: Comparison of the Performance of AoA Techniques Using Different Bandwidths

The results achieved showed how the available bandwidth improves the angle of arrival estimation accuracy for all algorithms. These results also support that the proposed algorithm can provide the same if not better the estimation accuracy as that of the MUSIC algorithm.

3.4.6 Effect of Number of Elements on the Angle Estimation Ambiguities

In this section the study is presented which looked at the fact that at least how many antennas are required in an array ideally to remove any angle ambiguities such as those shown by the interferometry algorithm in Section 3.4.3 where the true bearing angle was suggested to be in 180 degrees in error e.g. true bearing angle of 0 degree was solved by interferometry method and resulted in the solution of estimated angle as 180 degree as shown in Figure 3-16 (a) which makes it imperative to understand this phenomenon and its relation to the number of antenna elements regardless of the constraints of physical space available to

mount these receiver antenna arrays in practical mobile localization and tracking devices.

inverted F antennas (IFA) based receiver arrays were used for this study. Firstly, three element antenna array with element spacing of $\lambda/4$ was evaluated. The results obtained suggested that using this type of antenna geometry can cause some angle ambiguities between several angles, e.g. as can be seen from Figure 3-23 (a) in a 3D view and Figure 3-23 in a 2D view that if the true angle of arrival was 60 degrees there are two peaks in the solution one at 60 degrees and the second one at approx. 240 degrees, also the same is true in the case of 120 degree that there are two peaks and the second peak is lying at 180 degrees in the opposite direction at 300 degrees. These results thus suggest that 3-element spaced at $(\frac{\lambda}{4})$ are not sufficient to resolve the true angle completely and unambiguously.

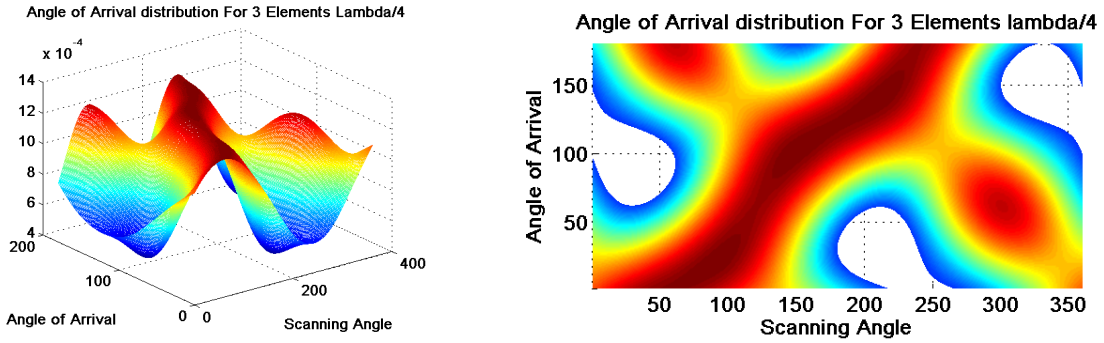

(a) (b)

Figure 3-23: Angle Ambiguities in a 3-element (λ/4) Array (A) 3D (B) 2D

The next logical solution was to keep the number of elements the same but increase the inter element spacing within the array to $(\frac{\lambda}{2})$ thus reducing the degrading effects of the mutual coupling between the antenna elements. The results obtained in Figure 3-24 suggest that even though the performance has improved to a certain extent but there still exists high correlation between some of the angles thus this geometry also fails to resolve the ambiguities completely without any further processing.

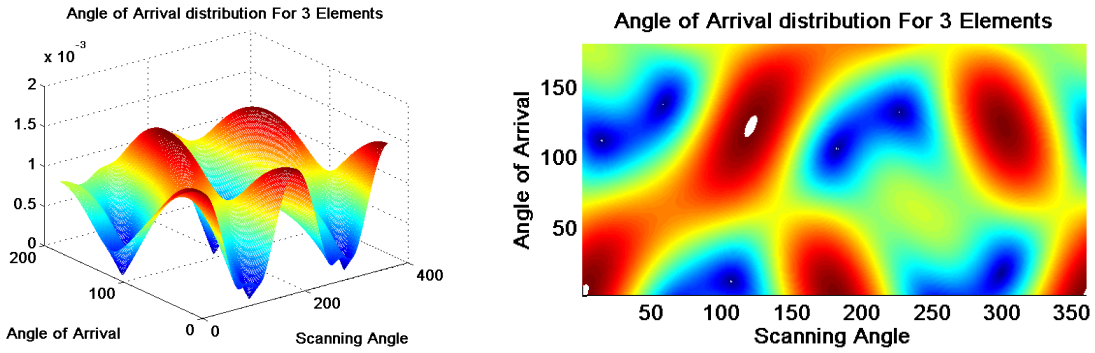

(a) (b)

Figure 3-24: Angle Ambiguities in a 3-element (λ/2) Array (A) 3D (B) 2D

The study was repeated for several geometries with different inter-element spacing including circular and concentric designs until finally a geometry emerged which can resolve these ambiguities and that is the uniform circular design with 5-elements as shown in Figure 3-25.

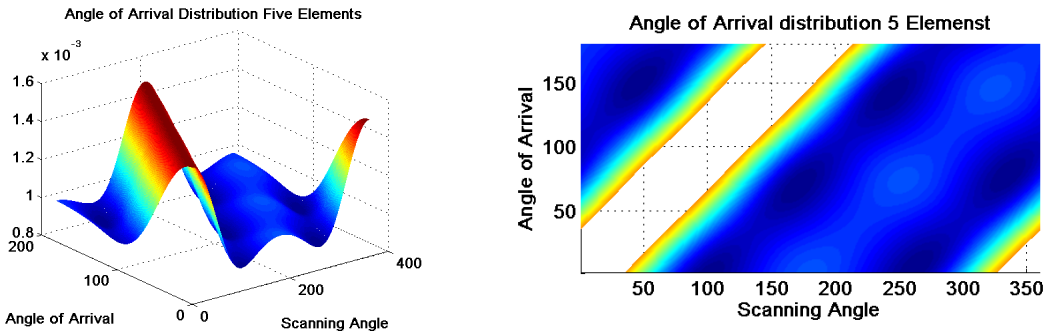

(a) (b)

Figure 3-25: Angle Ambiguities in a 5-element (λ/4) Array (A) 3D (B) 2D

3.5 Conclusion

A novel high-resolution direction of arrival estimation algorithm based on the signal subspace decomposition has been presented in this chapter. The core idea of the technique is to find the difference between the maximum absolute value of the pseudo-spectrum and the absolute value of the pseudo-spectrum thus minimizing the denominator and producing larger peaks in the direction of arrival of the incoming signal. The proposed method exploits the signal subspace with array steering vector as opposed to the MUSIC algorithm that exploits the noise subspace with array steering vector. The proposed algorithm has been tested and evaluated using different criteria. As was expected, increased SNR, number of antennas in the array and number of samples will significantly increase the resolution and make the peaks sharper of the proposed algorithm. In addition, the increase in available bandwidth will also increase the performance of the proposed

algorithm. This chapter has also covered the mathematical backgrounds of the proposed algorithm and some of the conventional algorithms and compared the performance of the proposed algorithm with those conventional algorithms. The results have proved that the proposed algorithm provides superior performance as opposed to any of the previously known direction of arrival estimation algorithms along with faster computation time which is an essential part of any real-time localization system.

4. Effects of Mutual Coupling In Antenna Arrays On Angle of Arrival Estimation

When dealing with antenna arrays there is a common problem of mutual coupling. Mutual coupling results in degraded performance of the array signal processing algorithm which results in wrong direction of arrival (DOA) estimates.

Enormous studies have been done on the compensation of mutual coupling effect and various approaches have been developed [338-346]. Conventionally the mutual coupling can be defined through mutual impedances between the array elements in their transmitting mode. However, several studies have shown that the mutual coupling effects the transmitting and receiving antenna arrays differently and should therefore be treated differently.

In this chapter, detailed effects of mutual coupling in antenna arrays are presented, then a few decoupling methods are reviewed which are applied in this work to assess the performance level of the proposed algorithm. In the end, these

decoupling methods were applied to different direction-finding algorithms and performance was compared against the proposed algorithm to draw a conclusion.

4.1 Mutual Coupling Behaviour

In antenna arrays when the number of antennas increases, every increasing element will be affected by the electromagnetic field of the other radiating element, in addition to the one produced by itself. This results in the induction of coupling current and this phenomenon is referred to as mutual coupling. The mutual coupling effect is inversely proportional to the antenna array element spacing, i.e. if the spacing between the elements is increased the effect of mutual coupling will decrease and vice versa. The effects of mutual coupling can be studied in terms of mutual impedances. Mutual impedance is a complex value that relates to the position of the elements of the antenna array in the geometrical plane.

In [338] it was shown that the effects produced by the mutual coupling when the antennas are in transmit mode are different than when the antennas are in the receive mode. If there are two antenna elements *m* and *n* the effects of mutual coupling in two different modes for these elements is different and is shown in Figure 4-1. In transmit mode if an antenna element *n* is excited using a source, with condition that antenna *m* is passive and not transmitting, the generated power travels to the element *n* and then as shown in Figure 4-1 (a) with a label (0) will radiate into the free space which is labelled as (1). Antenna element *m* will also

receive some of that energy resulting in an induced current and in Figure 4-1 it is labelled as (2). Some of the energy from the induced current is radiated back into the free space which is labelled as (3), the label (4) shows the energy that is dissipated into the passive load connected to the antenna element *m.* When the energy is radiated due to the induced current on the antenna element *m,* it is quite possible that the antenna *n* will also receive some part of that energy as shown by label (5) making it an infinite loop process which will be repeated if the antenna element *m* is excited. If the excitation is provided to all the antenna elements the total field can be looked at as the sum of the radiated field and the fields that are re-scattered from all the elements.

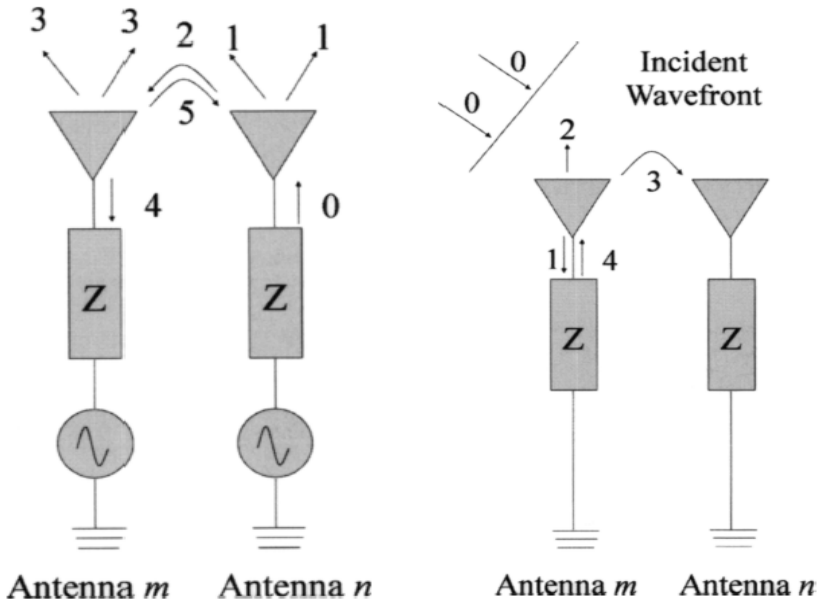

(a) (b)

Figure 4-1 (a) Mutual coupling paths in transmitting mode; (b) Mutual coupling paths in receiving mode

In Figure 4-1 (b) an antenna array in the receive mode is shown. The incident ray from the free space labelled as (0) hits the antenna element *m* resulting in an induced current. Energy is radiated to the free space by the induced current (2), and some part of that energy move towards the load (1). Antenna element *n* also receives some part of that energy (3). Some part of the energy will also be reflected and will travel in to the free space (4). Again, like the transmit mode antennas, in receive mode once the antenna element *n* receives some part of the energy from element *m,* it will result in an induced current. The same process takes place if the incident wave hits the antenna element *n*. If the incident ray impinges on all the elements at the same time the total field can be calculated by calculating the sum of the radiated fields and the re-scattered fields of all the antenna elements. To analyse mutual coupling effects on an *N* element antenna array, choose any two elements and then repeat the procedure for all possible pairs.

In the direction-finding radio systems, the received signal matrix is processed to obtain the direction information. In an antenna array, corresponding vectors are changed due to the mutual coupling. Mutual coupling changes the structure of the received signal correlation matrix and thus results in degraded DOA estimates. Proper estimates and decoupling methods are required to improve the accuracy of the direction-finding algorithms.

4.2 Review of Decoupling Methods

4.2.1 Conventional Mutual Impedance Method

The conventional mutual impedance method is also known as the open-circuit voltage method. In conventional mutual impedance method as explained in [347] , the mutual coupling is defined using the mutual impedance, in network analysis it is usually referred to as the Z parameter. The mathematical relationship between the voltages at antenna terminals and the voltage at terminal k can be written as:

$$V_k = I_1 Z_{k,1} + I_2 Z_{k.2} + \cdots + I_i Z_{k,i} + \cdots + I_k Z_{k,k} + \cdots + I_N Z_{k,N} + V_{ock} \qquad (4\text{-}1)$$

where $Z_{k,i}$ represents the ratio between the excitation current I_i and the induced open circuit voltage of terminal k at terminal i, $Z_{k,k}$ represents the self-impedance of the antenna element k, The open circuit voltage is represented by V_{ock} while all other antenna elements are in the open-circuit condition. The detailed mathematical background of this technique can be found in [347] which shows that mathematically the terminal voltages and the open circuit voltages are related as:

$$\begin{bmatrix} 1+\frac{Z_{11}}{Z_L} & \frac{Z_{12}}{Z_L} & \cdots & \frac{Z_{1N}}{Z_L} \\ \frac{Z_{21}}{Z_L} & 1+\frac{Z_{22}}{Z_L} & \cdots & \frac{Z_{2N}}{Z_L} \\ \vdots & \vdots & \ddots & \vdots \\ \frac{Z_{N1}}{Z_L} & \frac{Z_{N2}}{Z_L} & \cdots & 1+\frac{Z_{NN}}{Z_L} \end{bmatrix} \begin{bmatrix} V_1 \\ V_2 \\ \vdots \\ V_N \end{bmatrix} = \begin{bmatrix} V_{oc1} \\ V_{oc2} \\ \vdots \\ V_{ocN} \end{bmatrix} \qquad (4\text{-}2)$$

For most of the applications the conventional mutual impedance can be calculated by assuming the antenna array as a network of N-ports. The open circuit voltages V_{ock} can then be determined together with the measured.

Although this method was popularly used in the previous researches and practices, there are a few issues when the conventional mutual impedance method is applied to the receiving antenna arrays:

1. This method is derived under the assumption that mutual coupling follows the path shown in Figure 4-1(a), where the antenna elements are radiating with an active source. While for a receiving array, the actual mutual coupling is characterised by Figure 4-1 (b), where the antenna elements are passively excited by a far-field plane wave;
2. Load impedance is used to terminate the antenna elements in practical situations rather than open circuit.
3. In the 'open-circuit voltages' concept it is assumed that the antenna elements that are open-circuit do not radiate. This concept is not true as the electromagnetic fields will still be generated by the antenna elements due to the induced current.

4.2.2 Receiving Mutual Impedance Method

This method assumes the following conditions for the calculations

- Impedance Z_L (Load Impedance) value used to terminate the antenna elements is known.
- The elements in the antenna array are in receiving mode and they are excited through an external incoming wave.

Assume an antenna array containing *N* number of elements and are all terminated using the same impedance load, Z_L then under excitation by the incoming wave the voltage at the terminal *K* can be written as*:*

$$V_k = Z_L I_k = U_k + W_k \tag{4-3}$$

Because of the incoming signal, the terminal voltage at *K* is represented by U_k, the voltage caused by the other elements due to the mutual coupling is represented by W_k and can be mathematically written as:

$$W_k = I_1 Z_t^{k,1} + I_2 Z_t^{k,2} + \cdots + I_{k-1} Z_t^{k,k-1} + I_{k+1} Z_t^{k,k+1} + \cdots + I_N Z_t^{k,N} \tag{4-4}$$

The receiving mutual impedance among two different antenna elements i.e. *k* and *i* is represented by $Z_t^{k,i}$ and the value of the induced current is represented by I_i, where the subscript *i* is the element number. The defined mutual impedance at the receiving antenna terminal is shown by the subscript *t* and the values of U_k and V_k are related as follows.

$$\begin{bmatrix} 1 & -\frac{Z_t^{12}}{Z_L} & \cdots & -\frac{Z_t^{1N}}{Z_L} \\ -\frac{Z_t^{21}}{Z_L} & 1 & \cdots & -\frac{Z_t^{2N}}{Z_L} \\ \vdots & \vdots & & \vdots \\ -\frac{Z_t^{N1}}{Z_L} & -\frac{Z_t^{N2}}{Z_L} & \cdots & 1 \end{bmatrix} \begin{bmatrix} V_1 \\ V_2 \\ \vdots \\ V_N \end{bmatrix} = \begin{bmatrix} U_1 \\ U_2 \\ \vdots \\ U_N \end{bmatrix} \tag{4-5}$$

The value of the receiving mutual impedance is dependent on the currents and voltages at the terminal. As standard, the current distribution on an antenna will vary with the direction i.e. both with azimuth and elevation of the external signal

and thus the value of the receiving mutual impedance will be dependent as function to that direction of the signal.

In the case of an omni-directional antenna, e.g. a dipole, the current distribution at the resonance frequency is independent of the azimuth angle of the impinging signal if the signal is arriving from the plane that is perpendicular to antenna axis (θ = 90°). This means that the resultant mutual impedance will be the same irrespective of the incoming signals azimuth angle [348] making it a very suitable choice for applications such as direction of arrival. The current distribution also does not change significantly in the case where the incoming signal is close to the horizontal plane (e.g., θ = 70°), the current distribution also does not change considerably, and the value of the receiving mutual impedance calculated in the horizontal plane, still provides a rational approximation that can be used for decoupling purposes.

4.3 Performance Evaluation of Angle of Arrival Algorithms with Mutual Coupling and with Coupling Compensated

4.3.1 Simulation Setup

To evaluate the performance of AOA estimation algorithms in the presence of mutual coupling and with coupling compensated using different coupling compensation techniques a simple propagation scenario was built in Computer

Simulation Technology (CST) software. This simulation setup includes a single transmitter antenna, 3 meters away from the centre of the receiver antenna array, and three receiver antennas in an equilateral triangle shape, as shown in Figure 4-2 (a). The transmitter antenna was modelled using a half wavelength dipole, which radiates omni-directionally in the azimuth plane. The receiver antennas were modelled using two types of antennas as shown in Figure 4-2(b) and Figure 4-2(c), quarter wavelength monopole antenna of length 17.83 cm, which has isotropic radiation patterns in the azimuth plane, and Inverted F antenna (IFA) dimensions of which are shown in Figure 4-2 (c), which has non-symmetrical radiation patterns. A finite size square ground plane $1\lambda\, x\, 1\lambda$ was used for both types of receiver antennas. Both the transmitter antenna and the receiver antennas were designed individually to work at 400MHz frequency band.

In the simulation, the transmitter and receiver antennas were placed at same level in elevation plane, therefore only azimuth plane was observed in terms of AOA estimation. During the observation, the transmitter antenna was rotated anti-clockwise with a 5-degree step size within the range of 0-359 degrees. Therefore, overall 72 incoming signals with azimuth angle Φ were investigated with a 5-degree resolution.

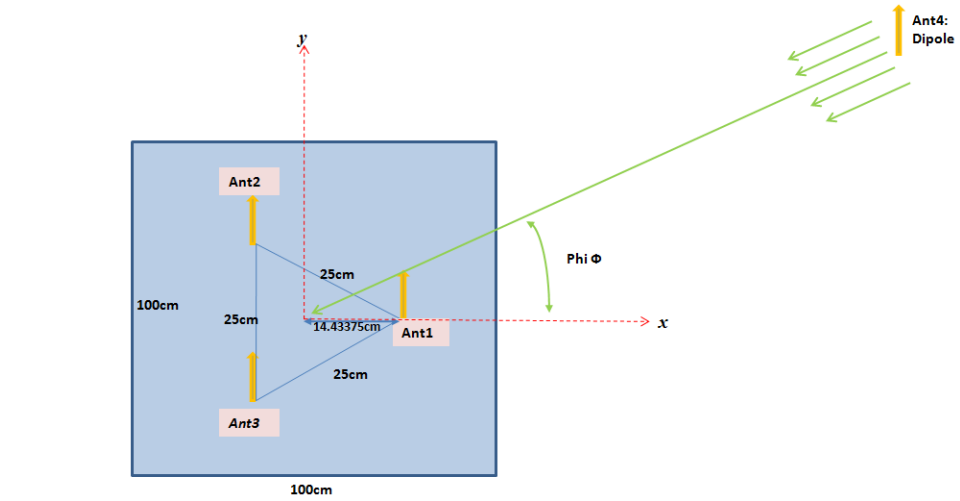

(a)

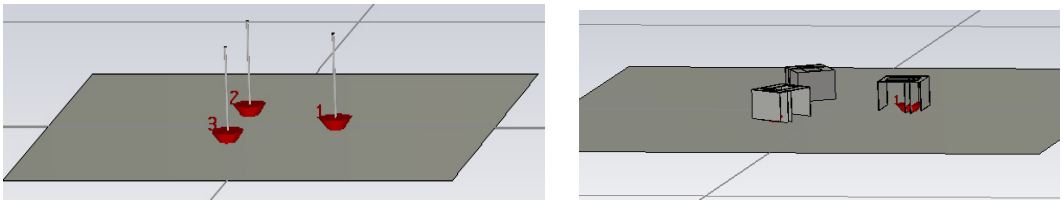

(b) (c)

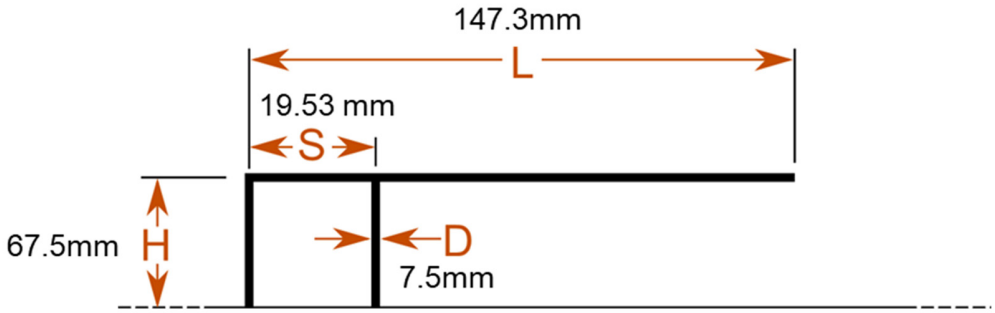

(d)

Figure 4-2: (a) Receiver antennas geometry in simulation (b) Monopole antennas (c) IFA antennas (d) IFA Antenna Dimensions

4.3.2 AOA Estimation Error in Presence of Mutual Coupling

Three of the direction-finding algorithms whose mathematical models were presented in Chapter 3 namely the proposed algorithm, Multiple Signal Classification (MUSIC) and interferometry were used to study the effects of mutual coupling on the AOA estimation. Figure 4-3 demonstrates the AOA estimation errors for a monopole array in presence of mutual coupling when a wideband signal with BW equal to 25 MHz radiated by transmitter. The simulation was run from 390 MHz to 415 MHz with 25 kHz step size (1001 samples).

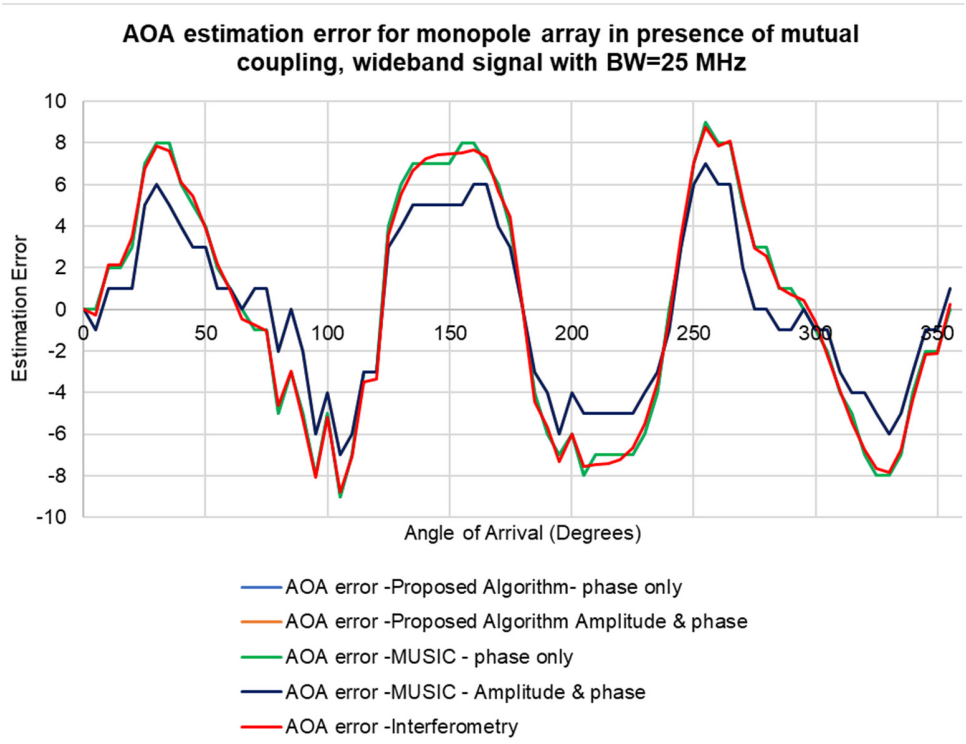

Figure 4-3: AOA estimation error for monopole array in presence of mutual coupling, wideband signal with BW=25 MHz

The results obtained in Figure 4-3: AOA estimation error for monopole array in presence of mutual coupling, wideband signal with BW=25 MHz show the superior performance of the proposed algorithm and the MUSIC algorithm. It is also evident from the results that as the interferometry algorithm only accounts for the phase difference between the elements to predict the angle of arrival if the amplitude of the received signal is normalised the performance of the other two algorithms with only the phase information seem to match the performance of the interferometry algorithm.

4.4 Applied Decoupling Methods to Direction Finding Algorithms

Because the receiver antenna elements are spaced only quarter wavelength apart, the mutual coupling effect between the elements could be the major reason that caused the high AOA estimation error. The mutual coupling effects of the setups shown in Figure 4-2 are investigated next in this section. Decoupling matrices using different compensation methods were generated and employed in the direction-finding algorithms for performance evaluation. Two objectives were observed for each compensation method, the first one was to test the AoA estimation error after mutual coupling compensation to find the most effective method, and the second aim was to find out the angular dependence of the decoupling matrix on incoming signals for each type of antenna.

4.4.1 Conventional Impedance Method

The open circuit mutual impedance was obtained by considering two antennas in the array at a time while leaving the other elements in loaded status as in practice [347]. The two antennas were treated as a two-port network, and the S parameters, S_{11}, S_{12}, S_{21}, and S_{22} were calculated. This process was repeated for all possible pairs in the array, and the S parameter matrix was obtained. The impedance parameters, Z, was then transferred from the S parameters using

$$Z = Z_o[I + S][I - S]^{-1} \tag{4-6}$$

where Z_0 is the system impedance, Z and S are $N \times N$ matrices from the N elements array, and I is the N-by-N identity matrix. Z matrix in Equation (4-6) was applied into Equation (4-2) together with the loaded impedance Z_L and the received voltage V at each terminal and the open circuit voltage at each antenna element without coupling was recovered.

4.4.1.1 Monopole Antenna Array

First, the monopole antenna arrays were simulated in CST to get all the parameters and then the data was exported to MATLAB for the decoupling matrix calculation. For angular dependence investigation, four angles were studied and the corresponding decoupling matrices are listed in Table 4-1.

Table 4-1: Monopole antenna transmission mode decoupling matrix for different incoming signals

30 Degree	90 Degree
$\begin{bmatrix} 1.7795-0.0778i & -0.0313-0.4692i & -0.0308-0.4675i \\ -0.0252-0.4783i & 1.7827-0.0855i & -0.0146-0.467i \\ -0.0255-0.4776i & -0.0154-0.468i & 1.7832-0.0854i \end{bmatrix}$	$\begin{bmatrix} 1.7794-0.0787i & -0.0311-0.4698i & -0.0314-0.4684i \\ -0.0235-0.4789i & 1.7823-0.0862i & -0.0151-0.4684i \\ -0.0244-0.4781i & -0.0157-0.469i & 1.7828-0.0858i \end{bmatrix}$
200 Degree	**325 Degree**
$\begin{bmatrix} 1.82-0.0878i & -0.0028-0.4468i & -0.0009-0.446i \\ 0.0047-0.471i & 1.8229-0.0969i & 0.0196-0.4519i \\ 0.0057-0.4701i & 0.0186-0.452i & 1.8234-0.0973i \end{bmatrix}$	$\begin{bmatrix} 1.7795-0.0779i & -0.0309-0.4676i & -0.0311-0.4691i \\ -0.0256-0.4778i & 1.7830-0.0854i & -0.0154-0.4683i \\ -0.0252-0.4782i & -0.0148-0.4672i & 1.7826-0.0856i \end{bmatrix}$

Table 4-1 shows that for monopole antenna array, the decoupling matrix remains consistent for most of the angles, as claimed in many literatures. The decoupling matrix for each angle was then applied to various direction-finding algorithms to compensate the mutual coupling effect.

The calculated AOA estimation errors before and after coupling compensation are compared in Table 4-2. The accuracy of AOA estimation algorithms was much improved for all the observed angles.

Table 4-2: AOA estimation error using transmission mode coupling compensation for monopole array

AOA-Ref (deg)	AOA error - Proposed- Phase only		AOA error - Proposed Amplitude and Phase		AOA error - MUSIC Phase only		AOA error - MUSIC Amplitude and Phase		AOA error - Interferometry	
	Before	**After**	**Before**	**After**	**Before**	**After**	**Before**	**After**	**Before**	**After**
30	8	-3	6	-3	8	-3	6	-3	7.86	-2.63
90	-5	3	-2	3	-5	3	-2	3	-5.28	3.3
200	-6	1	-4	1	-6	1	-4	1	-5.98	0.7841
325	-8	1	-5	1	-8	1	-5	1	-7.64	1.4128

4.4.1.2 IFA Antenna Array

The conventional mutual impedance method was also applied to IFA antenna arrays. Four different incoming signal angles were studied for this occasion. The decoupling matrices are listed in Table 4-3. For IFA antennas, for some angles, the decoupling matrix remain stable, but for other angles, the change is significant. Again, these matrices were applied to different direction-finding algorithms to observe the AOA estimation error after coupling compensation. Table 4-4 shows that for IFA antenna array, the transmitting mode decoupling matrix did not reduce the estimation error. For some angles, the error even got much worse and was indicated by a few direction-finding algorithms.

Table 4-3: IFA antenna array transmission mode decoupling matrix for different incoming signals

15 Degree	120 Degree
$\begin{bmatrix} 2.0342+0.1108i & 0.9906+0.1693i & 0.9901+0.1696i \\ 0.1123+0.1831i & 2.2702+0.1127i & 0.8665+0.0615i \\ 0.1124+0.1839i & 0.8677+0.0623i & 2.2719+0.1131i \end{bmatrix}$	$\begin{bmatrix} 2.7299+0.4858i & 1.2278+0.4304i & 1.2278+0.4304i \\ 1.5506+0.4493i & 2.8179+0.4045i & 1.4069+0.3344i \\ 1.553+0.4512i & 1.407+0.3349i & 2.8177+0.4046i \end{bmatrix}$
205 Degree	**320 Degree**
$\begin{bmatrix} 2.7418+0.474i & 1.2403+0.4186i & 1.2329+0.4101i \\ 1.5641+0.4379i & 2.8282+0.39284i & 1.4094+0.3138i \\ 1.5785+0.4353i & 1.4313+0.3194i & 2.8341+0.388i \end{bmatrix}$	$\begin{bmatrix} 2.7272+0.4942i & 1.229+0.4446i & 1.2258+0.4382i \\ 1.545+0.4515i & 2.8161+0.4111i & 1.4105+0.335i \\ 1.5486+0.4602i & 1.4086+0.3487i & 2.8165+0.4124i \end{bmatrix}$

Table 4-4: AOA estimation error before and after transmission mode compensation for IFA array

AOA-ref (deg)	**AOA error - Proposed- phase only**		**AOA error - Proposed Amplitude and phase**		**AOA error - MUSIC phase only**		**AOA error - MUSIC Amplitude and phase**		**AOA error - Interferometry**	
	before	**after**	**before**	**after**	**before**	**after**	**before**	**after**	**before**	**after**
15	-4	-6	-4	-6	-4	-6	-4	-6	-2.41	-6.3
120	-1	-1	-1	0	-1	-1	-1	0	-1.38	-0.83
205	-4	-1	-2	-8	-4	-1	-2	-8	-3.77	-0.67
320	-3	7	-1	-6	-3	7	-1	-6	-3.12	6.92

4.4.2 Receiving Impedance Method

The receiving mutual impedance was calculated using the received power wave (the S_{12} parameter). Using the transmitter antenna in free space to create the plane wave source, and the receiving antenna array was placed at a fixed position. The following steps were then used to retrieve the corresponding S_{12} parameters:

(1) Measure S_{12} at element 1's terminal with element 2's terminal connected to a load. Denote this as S_{12_1};

(2) Measure S_{12} at element 2's terminal with element 1's terminal connected to a load. Denote this as S_{12_2};

(3) Measure S_{12} at element 1's terminal with element 2 removed from the array. Denote this as S'_{12_1};

(4) Measure S_{12} at element 2's terminal with element 1 removed from the array. Denote this as S'_{12_2};

Then the measured receiving mutual impedances were calculated as follows:

$$Z_t^{12} = \frac{S_{12\_1} - S'_{12\_1}}{S_{12\_2}} Z_0 \tag{4-7}$$

$$Z_t^{21} = \frac{S_{12\_2} - S'_{12\_2}}{S_{12\_1}} Z_0 \tag{4-8}$$

For an *N*-element array, the mutual impedances can be measured by considering two elements at a time with all the rest elements loaded, and repeating the above procedure for all the possible pairs of elements in the array. After all the *Z*

parameters, have been measured, the decoupling matrix can be obtained using Equation (4-5) and then the uncoupled voltage *U* matrix at each element can be recovered for direction finding application.

Again, this method was tested on different types of receiving antenna arrays: monopole and IFA arrays. The result analysis will be discussed in the following sections.

4.4.2.1 Monopole antenna array

The decoupling matrices using the receiving mode method for monopole antenna array are studied for a few incoming ray angles. Results for four typical angles are listed in Table 4-5 where it is seen that the decoupling matrices for 30, 90 and 325 degrees are relatively consistent. For 200 degrees, the matrix has more obvious difference at some components, but overall for monopole antenna arrays, the decoupling matrix is not very angular dependent. To validate this conclusion, the 30 degrees and 325 degree matrices are applied to all the 72 angles to observe the estimation error improvement, and the results are listed in Figure 4-4 and Figure 4-5. From the results, it is obvious that for a single incoming ray, only one matrix applying to all angles improves the AOA estimation error for all direction-finding methods.

Table 4-5: Monopole antenna transmission mode decoupling matrix for different incoming signals

30 Degree	90 Degree
$\begin{bmatrix} 1 & 0.0873-0.2233i & 0.0901-0.2205i \\ 0.0956-0.2168i & 1 & 0.0987-0.2167i \\ 0.0938-0.2106i & 0.0974-0.2145i & 1 \end{bmatrix}$	$\begin{bmatrix} 1 & 0.0908-0.2251i & 0.0963-0.2086i \\ 0.105-0.2138i & 1 & 0.0883-0.214i \\ 0.095-0.2108i & 0.0952-0.2188i & 1 \end{bmatrix}$
200 Degree	**325 Degree**
$\begin{bmatrix} 1 & 0.1013-0.2122i & 0.0949-0.2188i \\ 0.0139-0.1827i & 1 & 0.1423-0.2388i \\ 0.1658-0.2293i & 0.087-0.3028i & 1 \end{bmatrix}$	$\begin{bmatrix} 1 & 0.0897-0.2205i & 0.0865-0.2232i \\ 0.0936-0.2104i & 1 & 0.0973-0.2147i \\ 0.0961-0.2177i & 0.0987-0.2171i & 1 \end{bmatrix}$

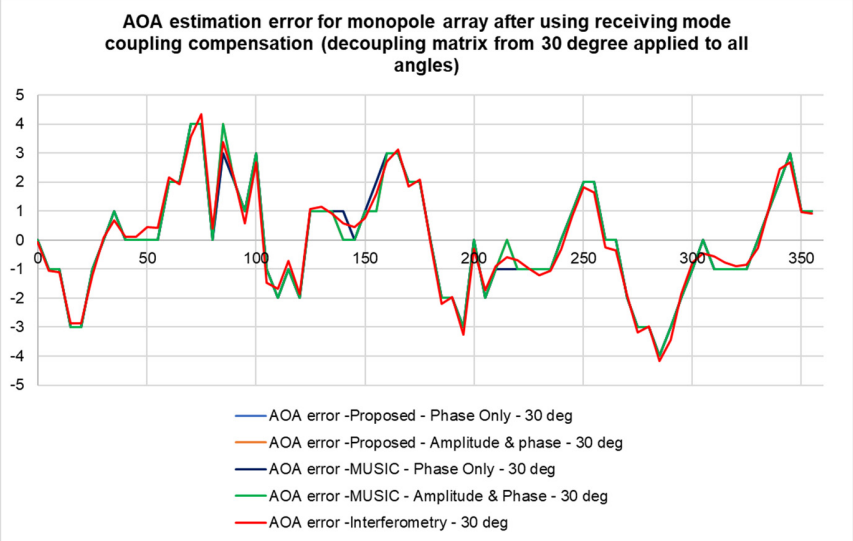

Figure 4-4: AOA estimation error for monopole array after using receiving mode coupling compensation (DM 30 degrees applied to all angles)

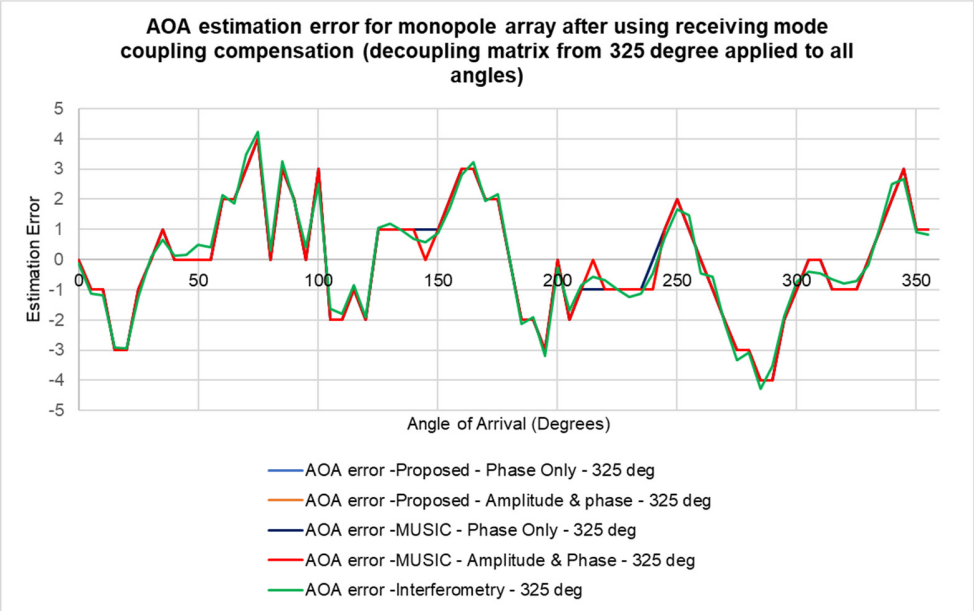

Figure 4-5: AOA estimation error for monopole array after using receiving mode coupling compensation (DM 325 degrees applied to all angles)

4.4.2.2 Receiving Impedance Method for two coming rays

CST simulation results were used to model two signals from different angles arriving at the receiver. The dominant signal arrives from different azimuth between 0 and 360 degrees, while the second ray's AOA is fixed at 60 degrees. The decoupling matrix calculated from a 325-degree signal was applied to all the combined signals. Table 4-6 compares the estimation error before and after compensation for all 72 angles, and the results show that for multiple incoming signals, the mutual coupling compensation sometimes does not improve the estimation error. The reason for this is that for a three-element circular array, the

maximum solved incoming rays is one, therefore the number of antenna elements is not sufficient to solve two incoming rays.

Table 4-6: AOA estimation error for monopole array before and after using receiving mode coupling compensation (decoupling matrix from 325 degrees applied to all angles)-two rays received

AOA -ref (deg)	AOA error - Proposed- phase only		AOA error - Proposed Amplitude and phase		AOA error - MUSIC phase only		AOA error - MUSIC Amplitude and phase		AOA error - Interferometry	
	Before	After	Before	After	Before	After	Before	After	Before	After
0	12	7	12	7	12	7	12	7	11.53	7.03
5	12	6	11	6	12	6	11	6	11.57	6.43
10	13	6	12	6	13	6	12	6	12.54	6.31
15	12	5	12	5	12	5	12	5	11.91	5.12
20	12	5	11	5	12	5	11	5	11.92	5.23
25	14	7	13	7	14	7	13	7	13.56	7.42
30	13	8	12	8	13	8	12	8	13.11	8.22
35	12	8	11	8	12	8	11	8	11.68	7.85
40	9	6	9	7	9	6	9	7	9.29	6.25
45	8	5	7	6	8	5	7	6	7.61	5.42
50	5	4	5	4	5	4	5	4	5.32	4.05
55	3	2	3	2	3	2	3	2	2.94	2.42
60	1	2	1	2	1	2	1	2	0.99	1.52
65	-1	0	-1	0	-1	0	-1	0	-1.13	0.14
70	-2	0	-2	0	-2	0	-2	0	-2.39	-0.01
75	-4	0	-3	-1	-4	0	-3	-1	-3.65	-0.31
80	-7	-4	-7	-4	-7	-4	-7	-4	-7.44	-4.09
85	-7	-3	-6	-3	-7	-3	-6	-3	-7.29	-2.72
90	-10	-5	-10	-6	-10	-5	-10	-6	-10.35	-5.14
95	-14	-8	-13	-8	-14	-8	-13	-8	-13.67	-7.58
100	-12	-5	-12	-6	-12	-5	-12	-6	-12.23	-5.28
105	-16	-9	-16	-9	-16	-9	-16	-9	-16.29	-9.38
110	-16	-9	-16	-9	-16	-9	-16	-9	-15.99	-9.35
115	-14	-8	-14	-8	-14	-8	-14	-8	-13.91	-8.26
120	-14	-10	-14	-10	-14	-10	-14	-10	-14.46	-9.85
125	-8	-7	-8	-7	-8	-7	-8	-7	-8.33	-6.74
130	-6	-7	-6	-7	-6	-7	-6	-7	-5.98	-6.53
135	-4	-7	-4	-7	-4	-7	-4	-7	-4.05	-6.55
140	-2	-7	-3	-7	-2	-7	-3	-7	-2.38	-6.54

145	-1	-6	-2	-6	-1	-6	-2	-6	-0.89	-6.33
150	0	-6	-1	-6	0	-6	-1	-6	0.45	-5.80
155	1	-5	0	-5	1	-5	0	-5	1.46	-4.94
160	2	-4	0	-4	2	-4	0	-4	2.28	-4.12
165	2	-4	1	-4	2	-4	1	-4	2.36	-3.82
170	1	-5	-1	-5	1	-5	-1	-5	1.09	-4.85
175	0	-5	-1	-5	0	-5	-1	-5	0.38	-5.01
180	-3	-8	-5	-8	-3	-8	-5	-8	-3.47	-8.25
185	-8	-12	-9	-12	-8	-12	-9	-12	-8.12	-12.14
190	-10	-13	-10	-12	-10	-13	-10	-12	-9.56	-12.54
195	-11	-14	-12	-14	-11	-14	-12	-14	-11.45	-14.09
200	-10	-11	-10	-10	-10	-11	-10	-10	-9.91	-11.20
205	-11	-12	-11	-11	-11	-12	-11	-11	-11.24	-11.84
210	-10	-9	-10	-8	-10	-9	-10	-8	-9.64	-9.02
215	-9	-8	-9	-6	-9	-8	-9	-6	-9.19	-7.63
220	-9	-7	-9	-5	-9	-7	-9	-5	-8.73	-6.67
225	-8	-6	-8	-5	-8	-6	-8	-5	-8.02	-5.88
230	-7	-5	-7	-4	-7	-5	-7	-4	-6.80	-4.99
235	-5	-4	-5	-3	-5	-4	-5	-3	-4.72	-3.64
240	-1	-1	-1	-1	-1	-1	-1	-1	-1.34	-1.38
245	4	2	4	2	4	2	4	2	3.70	2.32
250	9	6	9	5	9	6	9	5	8.63	6.17
255	11	8	11	6	11	8	11	6	11.32	8.33
260	11	8	11	6	11	8	11	6	10.74	7.52
265	11	9	11	7	11	9	11	7	10.96	8.83
270	8	6	7	5	8	6	7	5	7.69	6.24
275	6	5	6	4	6	5	6	4	6.12	5.20
280	6	6	6	5	6	6	6	5	6.06	6.05
285	5	6	5	5	5	6	5	5	4.74	5.83
290	4	7	5	6	4	7	5	6	4.34	6.85
295	4	8	5	7	4	8	5	7	3.92	7.77
300	2	7	3	7	2	7	3	7	2.07	7.16
305	1	7	2	6	1	7	2	6	0.69	6.63
310	-1	6	1	6	-1	6	1	6	-0.54	6.08
315	-1	6	0	6	-1	6	0	6	-1.37	5.77
320	-2	6	0	6	-2	6	0	6	-1.70	5.75
325	-1	6	0	6	-1	6	0	6	-1.32	6.12
330	0	7	1	7	0	7	1	7	0.13	7.02
335	3	8	3	8	3	8	3	8	3.00	8.27
340	7	10	7	10	7	10	7	10	6.82	9.78
345	10	10	10	10	10	10	10	10	9.50	10.07
350	9	8	10	8	9	8	10	8	9.47	8.41
355	12	9	12	9	12	9	12	9	12.32	8.99

4.4.2.3 IFA Antenna Array

The receiving mode method was used to generate the decoupling matrices for the IFA antenna array. The Table 4-7 shows that the decoupling matrix is much more angle-dependent for this non-isotropic type of antennas. The decoupling matrices for four different angles are completely different from each other, therefore more attention is needed when implementing mutual coupling compensation in practice. The true angles are calculated using the receiving mode matrices as shown in Table 4-8. In contrast to the transmitting mode method, the receiving mode method shows considerable improvement in the true angle estimation. The maximum estimation error after compensation is 1 degree for all direction-finding algorithms.

Table 4-7: IFA antenna array receiving mode decoupling matrix for different incoming signals

15 Degree	**120 Degree**
$\begin{bmatrix} 1 & -0.0863+0.6201i & -0.5858+0.497i \\ -0.1183-0.1478i & 1 & 0.0798-0.0413i \\ -0.3754-0.0218i & 0.1678-0.5364i & 1 \end{bmatrix}$	$\begin{bmatrix} 1 & -0.0921-0.0151i & 0.0251-0.0631i \\ 0.0248-0.0411i & 1 & 0.0282-0.0579i \\ 0.0081-0.0538i & -0.0911-0.0257i & 1 \end{bmatrix}$
205 Degree	**320 Degree**
$\begin{bmatrix} 1 & -0.0582-0.1163i & -0.0583-0.1599i \\ 0.0122-0.0208i & 1 & -0.0387-0.1468i \\ 0.0152-0.0163i & -0.0124-0.1113i & 1 \end{bmatrix}$	$\begin{bmatrix} 1 & 0.0332-0.0044i & 0.0042-0.1233i \\ -0.047-0.1212i & 1 & -0.0614-0.1034i \\ -0.0163-0.1331i & 0.0237-0.0152i & 1 \end{bmatrix}$

Table 4-8: AOA estimation error before and after receiving mode compensation for IFA array

AOA-ref (deg)	AOA error - Proposed- phase only		AOA error - Proposed Amplitude and phase		AOA error - MUSIC phase only		AOA error - MUSIC Amplitude and phase		AOA error - Interferometry	
	Before	After	Before	After	Before	After	Before	After	Before	After
15	-2	1	-4	1	-2	1	-4	1	-2.4	1.2415
120	-1	-1	-1	-1	-1	-1	-1	-1	-1.38	-0.8
205	-4	1	-2	1	-4	1	-2	1	-3.8	0.53
320	-3	0	-1	0	-3	0	-1	0	-3.12	-0.23

4.5 Comparison of Proposed Angle of Arrival Estimation Algorithm for Different Antenna Array Geometries with Mutual Coupling and Coupling Compensated

Multi-element antenna arrays were constructed on a $1\lambda\, x\, 1\lambda$ square conducting surface with element spacing of $\lambda/4$ to compare the performance of the proposed algorithm using different antenna geometries against the phase interferometry, Bartlett and MUSIC AoA algorithms and to evaluate the improvement in angle estimation by applying decoupling matrices. The receiver array was rotated at 10-degree steps for the whole azimuth plane and the results are discussed below.

4.5.1 5-element Circular Ring Array

A 5-element uniform circular antenna array (UCA) with element separation of 72 degrees was evaluated first. It was assumed that a single ray is impinging on the receiver array and complex noise was added to the received signal. The signal to noise ratio was kept at 0 dB.

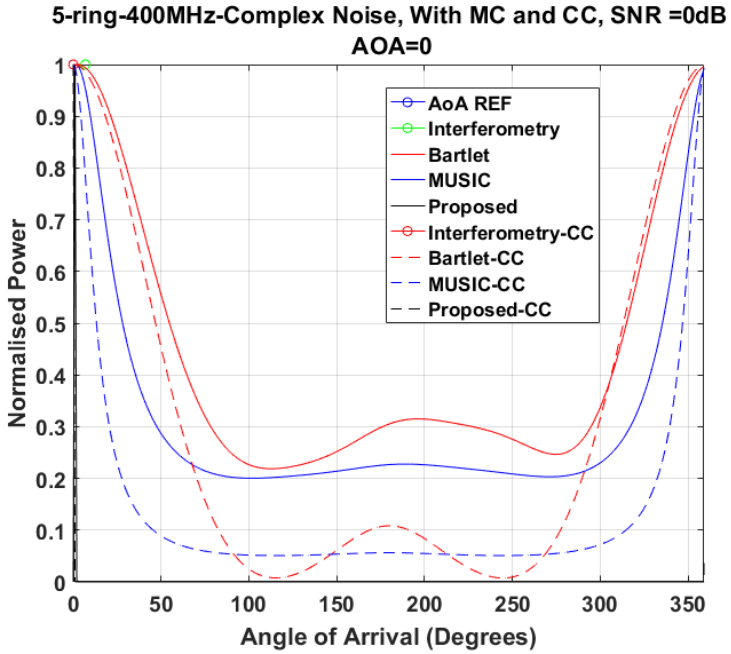

Figure 4-6: Performance Evaluation of the AOA Algorithms for a 5- element UCA with Mutual Coupling and Coupling Compensated for a True Angle of 0 Degrees

The results obtained in Figure 4-6 show how the estimation error performance was improved for the Interferometry, Bartlett and MUSIC algorithms. The interferometry algorithm had estimation error which was removed after the decoupling matrix was applied, and for the Bartlett and MUSIC algorithms the lobes sharpened after the decoupling matrix was applied. The proposed algorithm showed superior

performance with no side lobes and no estimation error occurred for this angle so the estimation angle before and after the coupling compensation remains the same.

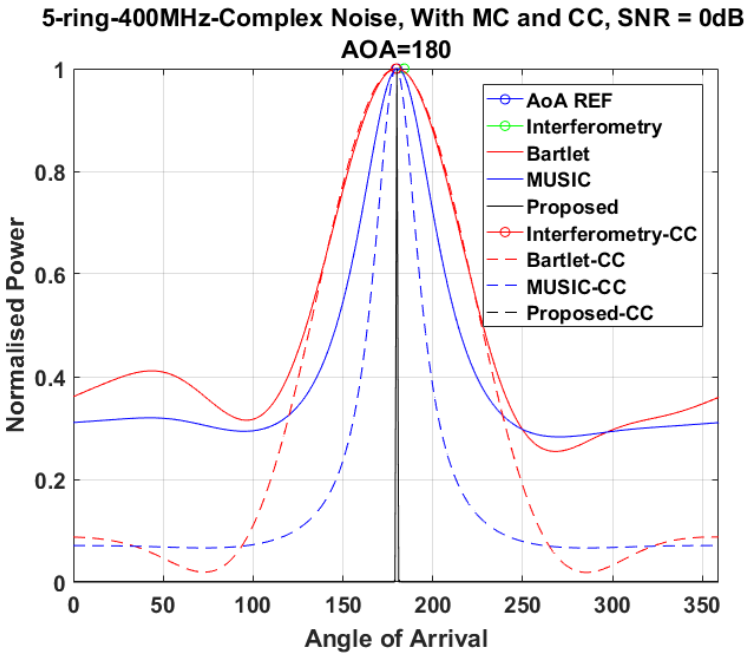

Figure 4-7: Performance Evaluation of the AOA Algorithms for a 5- element UCA with Mutual Coupling and Coupling Compensated for a True Angle Of 0 Degrees

In Figure 4-7 another angle was evaluated to be a true angle and again it can be seen that the estimation performance of the proposed algorithm is far superior to any of the know AoA techniques. The performance of the proposed algorithm remains unchanged after the application of the decoupling matrix as there were no estimation errors and no side lobes however, the decoupling matrix does provide improvement in terms of improved side lobes for Bartlett and MUSIC and removes the angle estimation error in interferometry algorithms.

Table 4-9: Performance Analysis of Five Element Circular Ring Array

Max. Error (Degrees) Without Coupling Compensation	Max. Error (Degrees) After Coupling Compensation	Number of Angles Improved	Number of Angles Unchanged	Number of Angles worsened
4	3	13	19	4

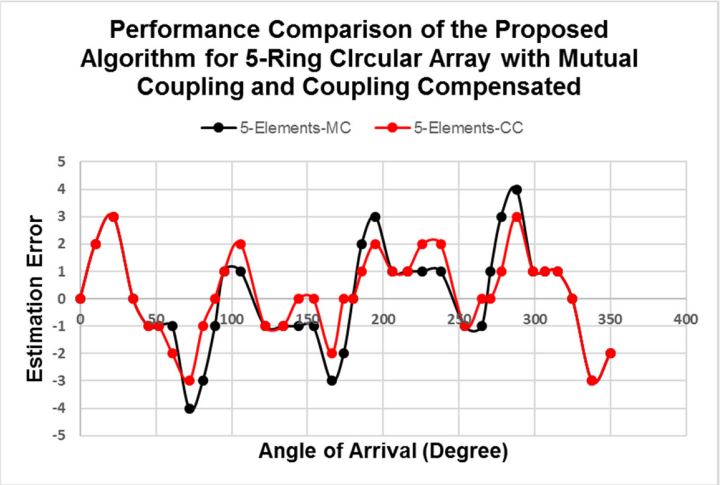

Figure 4-8: Comparison of the Performance of the Proposed Algorithm for a 5-Ring Circular Array with Mutual Coupling and with Mutual Coupling Compensated

From Table 4-9, the maximum angle error was 4 degrees for the proposed angle of arrival estimation method when there was mutual coupling present between the antenna elements. The maximum error was reduced by 1 degree by applying the received mutual impedance decoupling method. The results for all the 36 angles are listed in Table 4-10.

Table 4-10: Angle Estimation Performance of the Five Element Circular Ring Array with Mutual Coupling and with Coupling Compensated

5 Element Circular Ring Array				
AoA_REF	**Without Coupling Compensation**	**After Coupling Compensation**	**Error Without Coupling Compensation**	**Error After Coupling Compensation**
0	0	0	0	0
10	8	8	2	2
20	17	17	3	3
30	30	30	0	0
40	41	41	-1	-1
50	51	51	-1	-1
60	61	62	-1	-2
70	74	73	-4	-3
80	83	81	-3	-1
90	91	90	-1	0
100	99	99	1	1
110	109	108	1	2
120	121	121	-1	-1
130	131	131	-1	-1
140	141	140	-1	0
150	151	150	-1	0
160	163	162	-3	-2
170	172	170	-2	0
180	180	180	0	0
190	188	189	2	1
200	197	198	3	2
210	209	209	1	1
220	219	219	1	1
230	229	228	1	2
240	239	238	1	2
250	251	251	-1	-1
260	261	260	-1	0
270	269	270	1	0
280	277	279	3	1
290	286	287	4	3
300	299	299	1	1
310	309	309	1	1
320	319	319	1	1
330	330	330	0	0
340	343	343	-3	-3
350	352	352	-2	-2

A total of 13 angles were improved out of which the error was reduced to 0 degrees for 7 angles. In total for 24 angles the total error was reduced to 1 degree or less. The other main benefit of the proposed algorithm which is also evident from the results is that due to the sharper peaks average error for different power thresholds is very less while on the other hand in the MUSIC algorithm, the coupling compensation helps reduce the size of the lobes and make it sharper but the average error is still greater than the proposed algorithm. This technique is further tested using a 4–element circular ring array where the receiver elements are placed at 0 degrees, 90 degrees, 180 degrees and 270 degrees in the azimuth plane and in the level plane with the transmitter antenna. 1λ x 1λ square conducting surface with element spacing of λ/4 was used for the next simulations. The total error performance comparison of this five-element circular ring geometry with mutual coupling and with mutual coupling compensated is shown in Table 4-10.

4.5.2 4-element Circular Ring Array

A 4-element uniform circular antenna array (UCA) with element separation of 90 degrees was constructed. It was again assumed that only a single ray is impinging on the receiver array and complex noise was added to the received signal. The signal to noise ratio was kept at 0 dB as was for the previous experiment with 5-element uniform circular array to provide consistency in the comparison results between the different array geometries. The results obtained are discussed below.

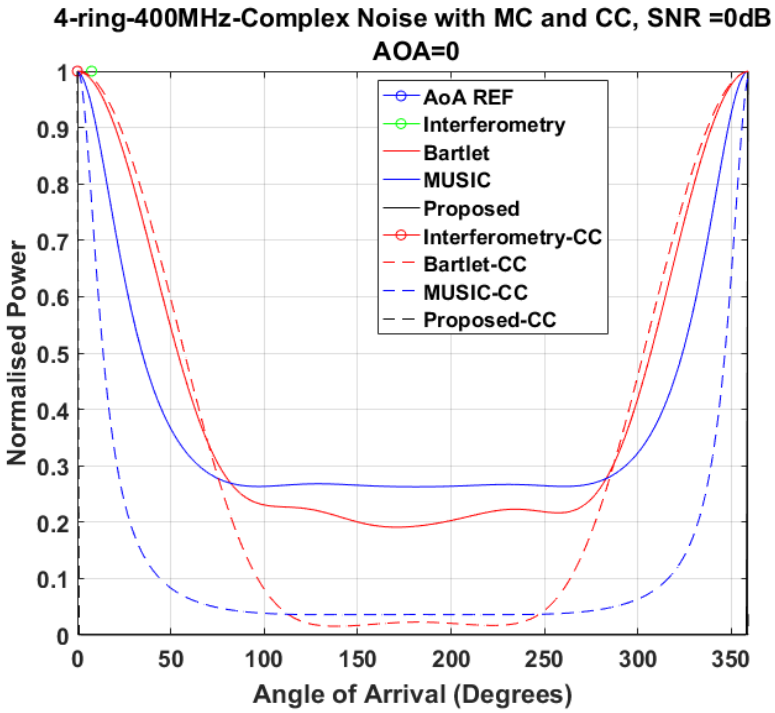

Figure 4-9: Performance Evaluation of the AOA Algorithms for a 4- element UCA with Mutual Coupling and Coupling Compensated for a True Angle of 0 Degrees

The results obtained in Figure 4-9 show very similar results to those of the results obtained for the 5-element array in Figure 4-6 for the true angle of 0 degrees that the estimation error performance was improved for the Interferometry, Bartlett and MUSIC algorithms. The interferometry algorithm had an estimation error which was resolved after the decoupling matrix was applied, and for the Bartlett and MUSIC algorithms the spectrum became more streamlined with smaller side lobes after the decoupling matrix was applied. The proposed algorithm showed superior performance with no side lobes and no estimation error occurred for this angle so the estimation angle before and after the coupling compensation remains the same.

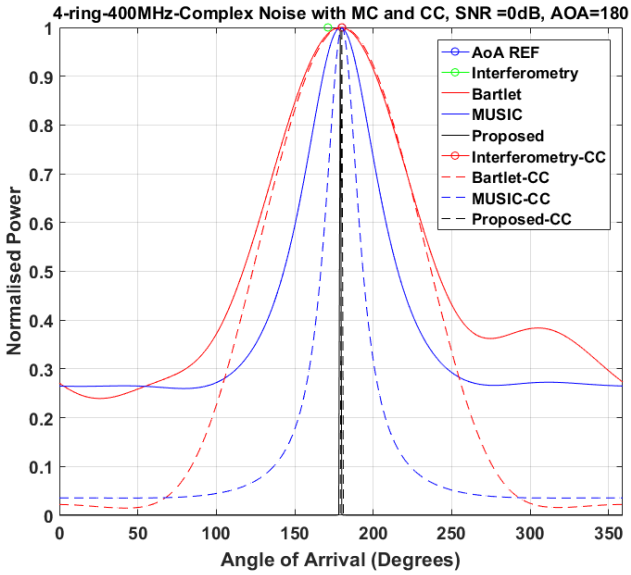

Figure 4-10: Performance Evaluation of the AOA Algorithms for a 5- element UCA with Mutual Coupling and Coupling Compensated for a True Angle Of 180 Degrees

In Figure 4-10, 180 degrees was evaluated to be a true angle and again it can be seen that the estimation performance of the proposed algorithm is very similar to that of the 5-element array as shown in Figure 4-7 and far superior to any of the other evaluated AoA techniques. The performance of the proposed algorithm remains unchanged after the application of the decoupling matrix as there were no estimation errors and no side lobes however, the decoupling matrix does provide improvement in terms of narrower side lobes for Bartlett and MUSIC and removes the angle estimation error in interferometry algorithm. The performance of the 4-element array for all angles before and after the application of the decoupling matrix is discussed next.

Table 4-11: Performance Analysis of Four Element Circular Ring Array

Max. Error (Degrees) Without Coupling Compensation	Max. Error (Degrees) After Coupling Compensation	Number of Angles Improved	Number of Angles Unchanged	Number of Angles Worsened
5	2	23	13	0

From Table 4-11 the maximum angle error in degrees was 5 degrees when there was mutual coupling present between the antenna elements. The max error was reduced by 3 degrees by applying the received mutual impedance based decoupling method. Total 23 angles were improved out of which the error was reduced to 0 degrees for 10 angles. All the angles after the mutual coupling compensation had 1 degree or less estimation error. Figure 4-11 provides a good visual understanding on the improvements in the performance of the proposed estimator with mutual coupling present and compensated. It can be suggested here that in the presence of complex noise and with an SNR of 0 dB angle error of 2 degrees is quite acceptable.

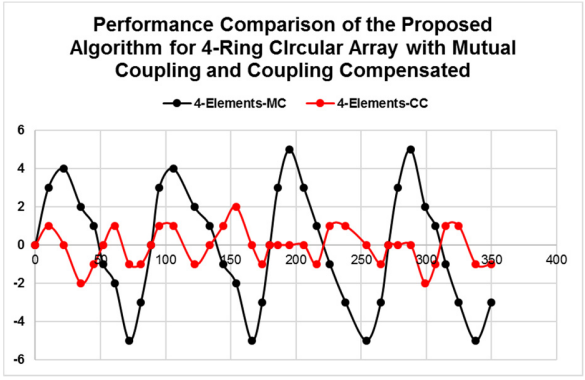

Figure 4-11: Performance of the Proposed Algorithm for a 4-ring Circular Array

A comparison between the estimation performance of the proposed algorithm with a 5-element UCA and a 4-element UCA in the presence of mutual coupling and after the application of the decoupling matrix is presented in Figure 4-12.

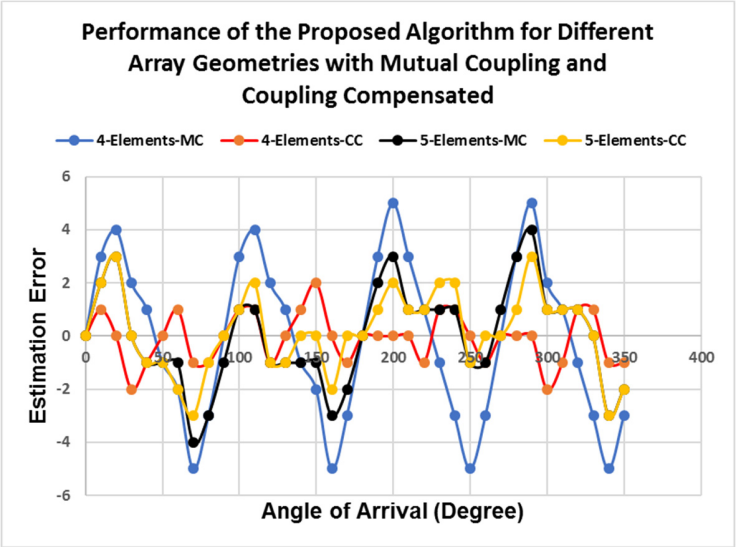

Figure 4-12: Performance of The Proposed Algorithm for a 5-ring and a 4-ring Circular Array with Mutual Coupling and with Mutual Coupling Compensated

It is clear from the results that the increased number of elements provided a higher estimation accuracy when there was mutual coupling present between the antenna elements but on the other hand once the degrading effects of the mutual coupling were removed the angle estimation performance for both arrays is very similar with the advantage of one less element in the array thus resulting is easier implementation and lower cost as well as less processing. The detailed results of all angles for a 4-element array with mutual coupling and with coupling compensated are presented in Table 4-12.

Table 4-12: Angle Estimation Performance of the 4-element Circular Ring Array with Mutual Coupling and with Coupling Compensated

4 Element Circular Ring Array				
AoA_REF	Without Coupling Compensation	After Coupling Compensation	Error Without Coupling Compensation	Error After Coupling Compensation
0	0	0	0	0
10	7	9	3	1
20	16	20	4	0
30	28	32	2	-2
40	39	41	1	-1
50	51	50	-1	0
60	62	59	-2	1
70	75	71	-5	-1
80	83	81	-3	-1
90	90	90	0	0
100	97	99	3	1
110	106	109	4	1
120	118	121	2	-1
130	129	130	1	0
140	141	139	-1	1
150	152	148	-2	2
160	165	160	-5	0
170	173	171	-3	-1
180	180	180	0	0
190	187	190	3	0
200	195	200	5	0
210	207	210	3	0
220	219	221	1	-1
230	231	229	-1	1
240	243	239	-3	1
250	255	250	-5	0
260	263	261	-3	-1
270	270	270	0	0
280	277	280	3	0
290	285	290	5	0
300	298	302	2	-2
310	309	311	1	-1
320	321	319	-1	1
330	333	329	-3	1
340	345	341	-5	-1
350	353	351	-3	-1

4.6 Conclusion

In this chapter, the mutual coupling effect on antenna arrays was discussed. It is important to compensate this negative effect in direction finding applications. Different mutual coupling compensation methods were introduced and the implementation method was explained. The decoupling matrices using these methods were then generated and applied to simulation data. After validating these matrices by various direction-finding algorithms, compared to other methods, the receiving mode method is easy to apply, requiring the same amount of calculation and memory space as the open-circuit voltage method. In summary, per the results provided by simulation the receiving mode decoupling method can provide more improvements in terms of AOA estimation in situations requiring real-time processing, such as adaptive direction finding.

5. NOVEL RECONFIGURABLE ELECTRICALLY SMALL ANTENNA FOR ASSET TRACKING

The increase in demand of the wireless technology applications and the scarcity of the microwave spectrum has caused a tremendous increase in the requirement of new and efficient antenna design techniques. In a tracking system, it is ideal that both the transmitter antenna and receiver arrays are small and discrete. In practise, the tracking systems might employ more than one localisation solution such as a combination of radio frequency (RF) and GPS thus greatly affecting the available space for the antenna array as there will be a requirement of a GPS receiver antenna. In addition to the small design the antenna must also provide suitable and reliable performance. The lower frequencies are also of great interest for the localization purposes because of their longer wavelengths but the design of antennas for those frequencies poses a challenge because the conventional techniques result in structures that are physically too big and thus integration of those antennas into mobile devices with low profiles is very challenging. In this regard the electrically small antenna have been regarded as a viable solution [349-351] but the design of such antennas is challenging due to the limitations as

described in [352] and then revisited in [349], the author in [353] also details the limitations applicable on electrically small antennas.

In [354, 355] the authors have proposed miniaturized low profile antennas that exhibit omni-directional radiation pattern with vertical polarisation. In [356] authors have proposed low profile antennas that can be installed on automotive. An omni-directional antenna radiation pattern is of paramount importance for applications where the sensor deployment is random such as in localization applications and in non-line of sight situations. Per [354] for line of sight or non-line of sight applications the antenna with a vertical polarization is less prone to path loss. The large wavelength at the low frequencies results in a high Q value and narrow bandwidth for the electrically small antennas due to their compact size. Therefore, an electrically small antenna with decent operational bandwidth for low frequency applications is highly desirable.

Reconfigurable antennas are active antennas that has the capability to modify their properties such as bandwidth, frequency, radiation pattern and polarization according to the application needs [357, 358]. This frequency reconfigurability is a beneficial trade in antennas for diverse applications, as it reduces the bandwidth requirement, because the antenna does not have to operate on all frequencies simultaneously thus improving the antenna functionalities without increasing the size and design complexity [359, 360]. Other desirable features of frequency reconfigurable antennas include low profiles and cost and their ability to be used

for a range of applications making them highly desirable for modern wireless systems [361].

Several works have been published where authors have achieved the frequency reconfigurability by altering the antenna's effective length by using methods such as RF-Micro-Electro-Mechanical Systems RF-MEMS for the purpose of frequency tuning [362-364]. In 11 the authors have employed varactor diodes to redirect the surface currents, thereby producing a change in capacitance which in turn allows for smooth frequency change, the use of RF-P-I-N diodes is another way for achieving tuneable frequency bands as reported in [365-368]. The antenna frequency reconfigurability using RF-MEMS exhibits lower loss and higher Q factors in comparison with varactor and PIN diodes [369]. On the other hand, PIN diodes have low cost, relatively high power handling capability, faster switching speed, good isolation, low insertion loss and are easier to fabricate for optimal performance [370]

The solution to the problem of limited bandwidth of the electrically small antennas at low frequencies can be solved using the frequency reconfigurability if the antenna does not have to operate at all frequencies simultaneously. It is a common practice among telecom industry to have frequency reconfigurable antennas in the mobile devices for worldwide connectivity.

In this chapter, the design and implementation of an electrically small reconfigurable low profile logarithmic spiral antenna for low frequency applications is presented. The antenna exhibits an omni-directional radiation pattern. The low profile, low cost and ease of manufacturing makes this antenna the best suited candidate for localization applications. The antenna was designed using Computer Simulation Technology and the prototype was built and tested using an anechoic chamber.

The chapter is organized as follows. Firstly, in Section 5.1 the design and implementation of the antenna is discussed followed by Section 5.2 which will highlight the results of the antenna design including return loss and radiation pattern. The chapter is concluded in Section 6.3

5.1 Antenna Design and Implementation

As the front-end of the wireless communication link, the antenna performance has a huge impact on the system quality, e.g. link budget, direction finding accuracy, etc. On the other hand, the antenna design need to consider the system requirement, for example to meet the bandwidth requirement of the modulation scheme and to qualify the polarisation and radiation pattern requirement of the direction-finding algorithms. The antenna should be designed under consideration of the entire integrated hardware devices and its possible working environment.

Finally, a good antenna design should have long life, low power consumption, and suitable to work under various environmental conditions.

The antenna design requirements for any localization system in general can be summarised as below.

- **Radiation pattern:** Approximately omni-directional radiation pattern in the azimuthal plane and wide beamwidth in the vertical direction.
- **Input impedance:** The input impedance should be well matched to the source impedance over the whole bandwidth of operation, even in the presence of detuning from the objects in the proximity.
- **Efficiency:** Able to achieve a high conversion of the input RF power into radiation over the whole range of conditions of use.
- **Manufacturability:** Ease of manufacturing and low cost.
- **Size:** As small as possible, consistent with meeting the performance requirements. Increasingly, the ability to fit into a consumer product of acceptable size.

5.1.1 Antenna Geometry

The proposed antenna is designed using an FR-4 as a substrate with a thickness of 1.6 mm, the substrate has a tangential loss of 0.02 and the relative permittivity ε_r of 4.3. The geometry of the antenna is shown in Figure 5-1. The antenna is comprised of two double sided printed boards.

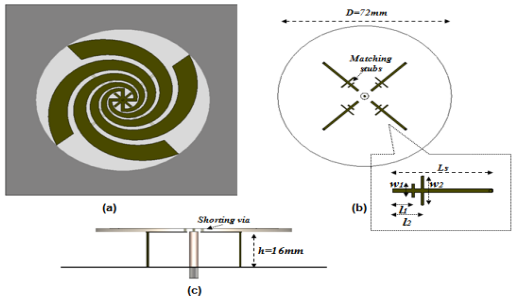

Figure 5-1: Geometry of The Proposed Antenna

The top of the first double sided printed board consists of multi arm logarithmic spirals as shown in Figure 5-2 (a). The logarithmic spirals are preferred as these geometries usually provide wider bandwidth when compared to thin strip square spirals. The log-spiral multi-arm design has a total inner radius = 6 mm, and the spiral progress is 0.26 with the increment angle of 5°. Each arm consists of 1.12 turns.

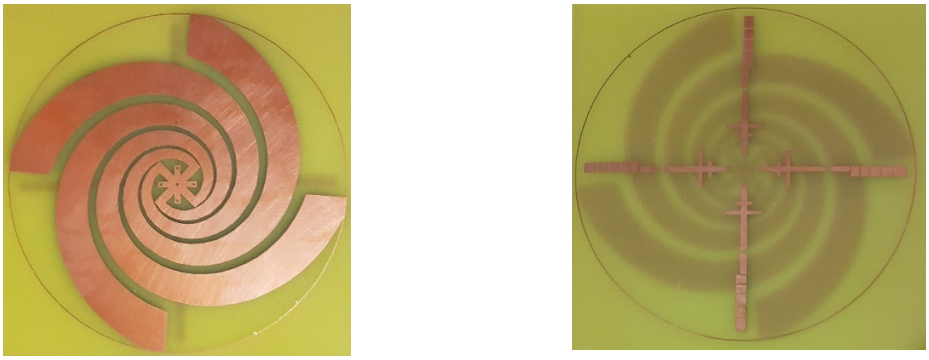

(a) (b)

Figure 5-2: (a) Top Layer with Multi Element Log Spirals (b) Matching Circuit with Tuning Extensions

The bottom layer consists of the matching circuit and the tuning extensions as shown in Figure 5-2 (b), the total diameter of the substrate is D = 72 mm. The total length of the matching circuit is Ls = 25 mm and the length of the tuning extension circuit is Lt = 11 mm as shown in Figure 5-3. The matching strip width on the bottom of the substrate is s1 = 1 mm, and the width of the parallel matching stubs s2 = 0.5 mm. The shorting vias are used to connect the logarithmic spirals to the matching circuit and the shorting pins are used to connect to the ground plane. There are total 4 shorting vias and 4 shorting pins. The total height of the antenna is h = 16 mm.

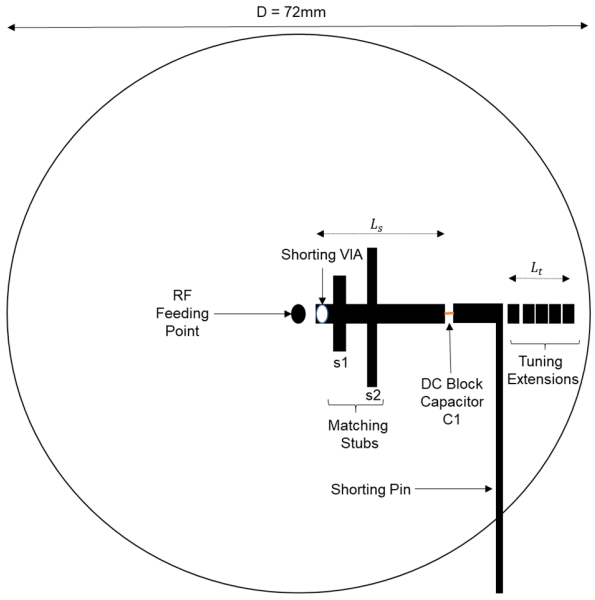

Figure 5-3: Matching Circuit with Tuning Extensions

PIN diodes are added between the tuning extensions and the tuning extensions are then connected to the tuning circuit on the bottom of the second double sided

printing board which is also made of FR-4 substrate and has copper ground plane on the top side as shown in Figure 5-4(a) and the tuning circuit on the bottom as shown in Figure 5-4 (b). The tuning circuit is then used to provide the 3V DC voltage to turn the diodes ON/OFF thus changing the current distribution and allowing for frequency reconfigurability.

(a) (b)

Figure 5-4: (a) Antenna Mounted on The Ground Plane (b) Tuning Circuit

5.1.2 Design Methodology

The addition of the tuning extensions causes a change in the total matching circuit and thus results in new resonant frequencies which is very useful because at lower frequencies with higher wavelengths and electrically small antenna designs the Q values are high thus very small bandwidths. The frequency reconfigurability provides the added advantage of extra bandwidth for the antenna designs working in lower frequency bands. The total size of the proposed antenna is $\lambda/43$ and the resonant frequency is 400 MHz. The addition of the tuning circuit does not affect the antenna's fundamental frequency. Various steps that were adopted for the

design and optimization of this antenna are illustrated in a way of a flow chart in Figure 5-5.

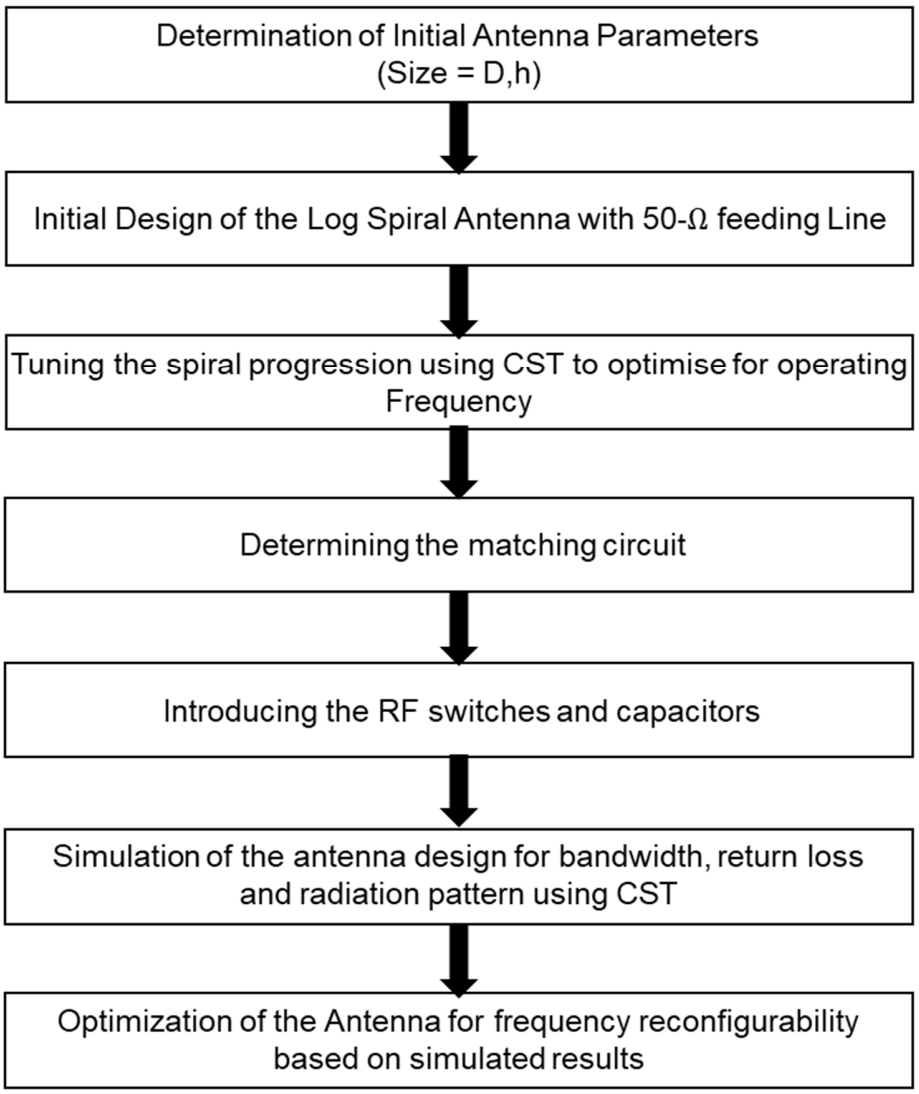

Figure 5-5: Antenna Design Methodology

5.1.3 Switch Design

To implement the electronic frequency reconfigurability, PIN diodes were used to replace the ideal shunt switches. PIN diodes are ideal for this antenna design due

to their small size, high reliability, fast switching speed and negligible capacitance and resistance in the OFF and ON states. The circuit diagram of the PIN diode acting as a shunt is shown in Figure 5-6

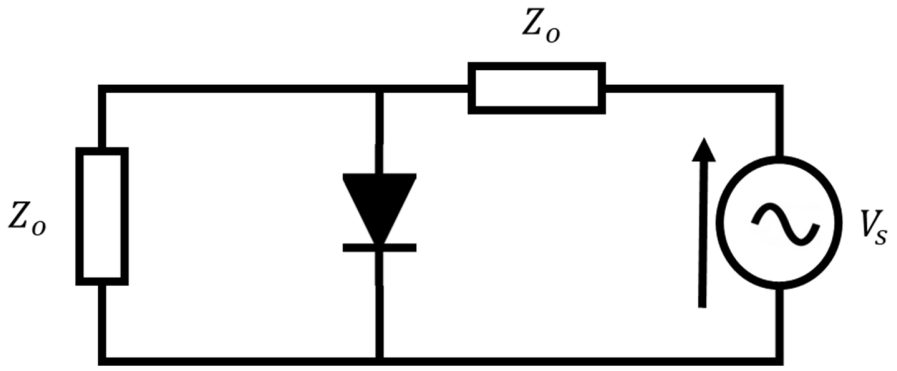

Figure 5-6: PIN Diode as A Shunt

The ON/OFF states equivalent circuits of the PIN diode based on Figure 5-6 are illustrated in Figure 5-7 (a) and (b); where L_s and C_T define the packaging effect values while the rest of the components model the electrical properties for the PIN diode junction in (a) OFF (b) ON states.

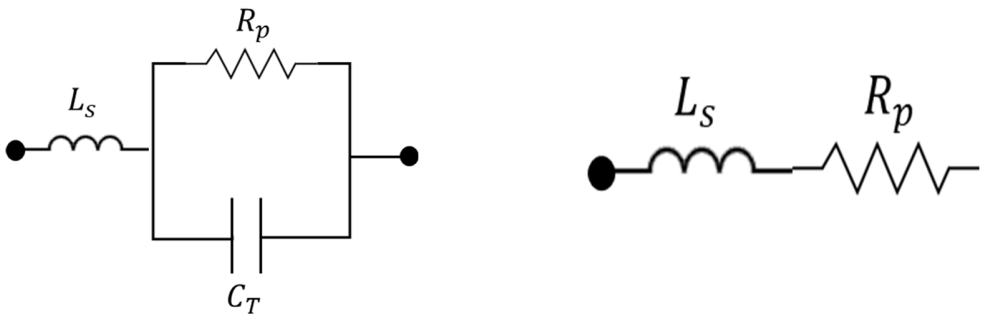

(OFF) (ON)

(a) (b)

Figure 5-7: PIN Diode as A Shunt

The circuit diagram of the electrical tuning circuit is illustrated in detail in Figure 5-8.

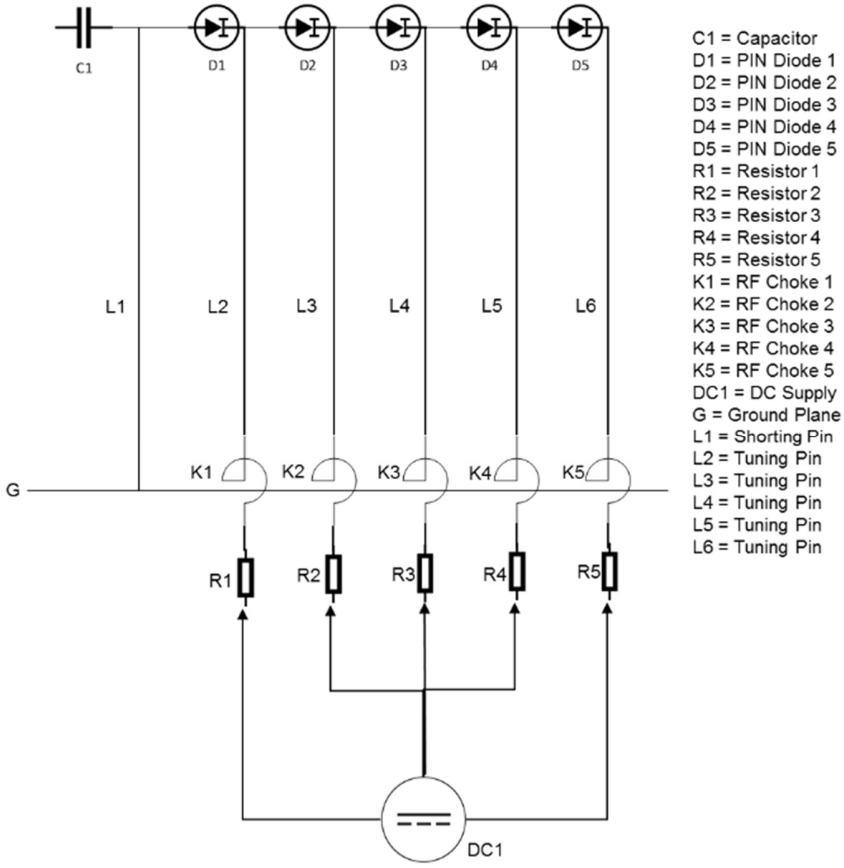

Figure 5-8: Antenna Tuning Circuit

5.2 Results and Discussions

The simulations of the reconfigurable antenna with the PIN diodes was carried out to achieve an agreement between the simulated and measured results. The simulations were carried out using the CST Microwave Studio Design Suite.

Return loss, radiation patterns and antenna gain were simulated and the values were then checked against the measurement results obtained using the prototype

antenna measured in an anechoic chamber with the HP 8510C network analyser. Both the simulated results and measured results show great agreement.

5.2.1 Reflection Coefficient

The possible switching states that can be obtained using the five PIN diodes are summarised in Table 5-1. The diodes provide the antenna tuning over a band of 390 MHz – 415 MHz. CST design studio was used to first evaluate impedance bandwidth $(\text{for } S_{11} < -10 \text{ dB}) \text{ for}$ the five basic states with one diode ON and the remaining diodes in the OFF state. Similarly, the prototype antenna was analysed the network analyser to validate the results S_{11} for the same setup. The simulated results are presented in Figure 5-9 (a) and the measurement results are presented in Figure 5-9 (b).

Table 5-1: Possible Frequency Reconfiguration Combinations for the Proposed Antenna Design

SEQUENCE	DIODE 1	DIODE 2	DIODE 3	DIODE 4	DIODE 5
1	ON	OFF	OFF	OFF	OFF
12	ON	ON	OFF	OFF	OFF
13	ON	OFF	ON	OFF	OFF
14	ON	OFF	OFF	ON	OFF
15	ON	OFF	OFF	OFF	ON
123	ON	ON	ON	OFF	OFF
124	ON	ON	OFF	ON	OFF
125	ON	ON	OFF	OFF	ON
134	ON	OFF	ON	ON	OFF
135	ON	OFF	ON	OFF	ON
145	ON	OFF	OFF	ON	ON
1234	ON	ON	ON	ON	OFF
1245	ON	ON	OFF	ON	ON
12345	ON	ON	ON	ON	ON

2	OFF	ON	OFF	OFF	OFF
23	OFF	ON	ON	OFF	OFF
24	OFF	ON	OFF	ON	OFF
25	OFF	ON	OFF	OFF	ON
234	OFF	ON	ON	ON	OFF
245	OFF	ON	OFF	ON	ON
2345	OFF	ON	ON	ON	ON
3	OFF	OFF	ON	OFF	OFF
34	OFF	OFF	ON	ON	OFF
35	OFF	OFF	ON	OFF	ON
345	OFF	OFF	ON	ON	ON
4	OFF	OFF	OFF	ON	OFF
45	OFF	OFF	OFF	ON	ON
5	OFF	OFF	OFF	OFF	ON

It can be seen from Figure 5-9 (a) that the return loss for all the resonant frequencies is better than -20 dB. In the corresponding Figure 5-9 (b) it can also be seen that the return loss for all resonant frequencies is again better than -20 dB with minor differences which can be attributed to the fabrication error. Thus, both the simulated and the measured results are in good agreement.

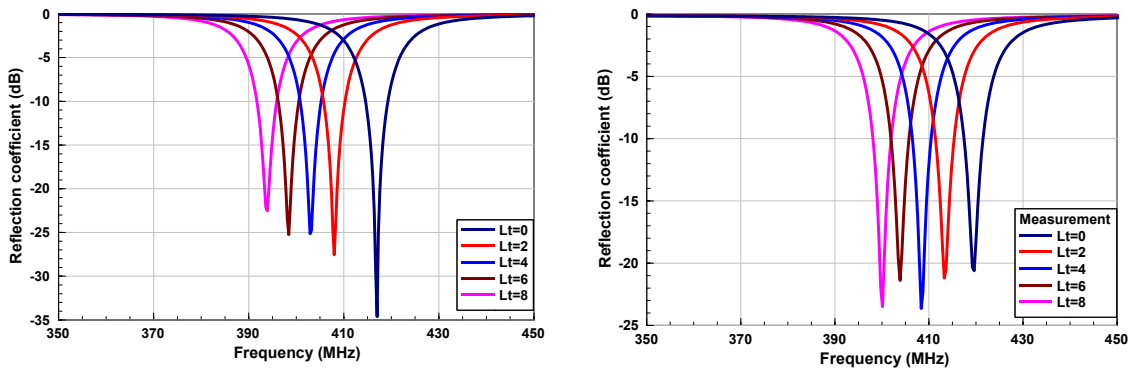

(a) (b)

Figure 5-9: (a) Simulated Reflection Coefficient (b) Measured Reflection Coefficient

The prototype antenna is shown in Figure 5-10 (a) and the measured return loss for six different states is presented in Figure 5-10 (b) with no diode, with diode 1 ON only, with diode 1 and 2 ON, with diode 1 and 3 ON, with diode 1 and 4 ON and with diode 1 and 5 ON, all the results show the reflection coefficient to be better than -20 dB.

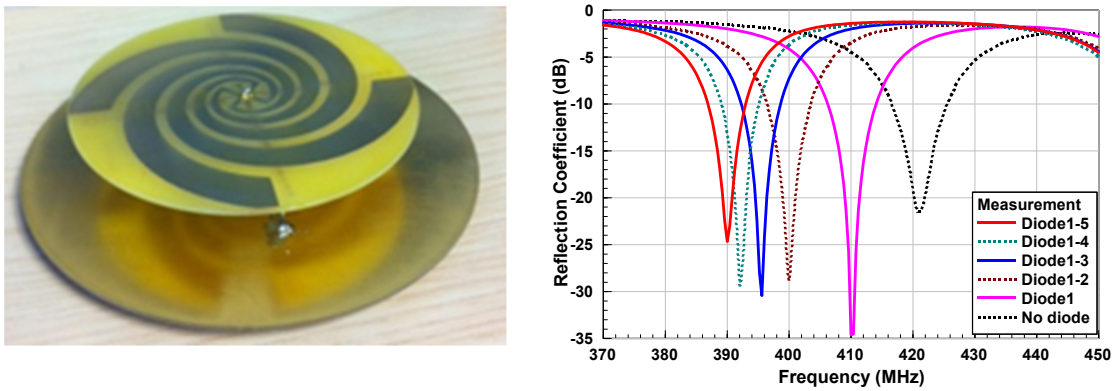

(a) (b)

Figure 5-10: (a) Prototype Antenna (b) Measured Return Loss Using Diode Combinations

5.2.2 Radiation Pattern

The normalised radiation pattern of the antenna at 400 MHz is shown in Figure 5-11, from which the radiation pattern of the antenna in the H-plane is omni-directional, while in the E-plane the antenna exhibits a radiation pattern that looks like a figure-of-eight. Due to the small ground plane size of the antenna for the 400 MHz resonant frequency the cross-polarization level decrease by 5 -10 dB from the co-polar level, the antenna has a measured gain of 0.3 dB and the simulated gain

of 0.5 dB. In Figure 5-11 the E-co and E-x represent the co-polarization and cross-polarization characteristics, respectively.

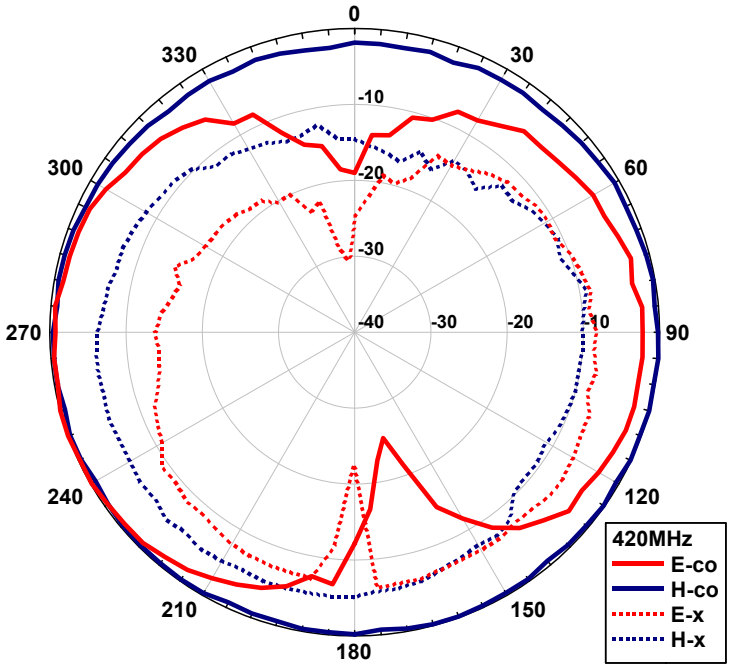

Figure 5-11: Measured Radiation Pattern of the Prototype Antenna in E-Plane and H-Plane Co polarization and Cross polarization

The Figure 5-12 represents the radiation patterns in the electrical and magnetic field planes for different frequency points achieved by using the PIN diode combinations. These radiation patterns indicate that the designed prototype antenna meets the objectives of the designs for an electrically small reconfigurable antenna that is well suited for the tracking system integration with 25 MHz bandwidth.

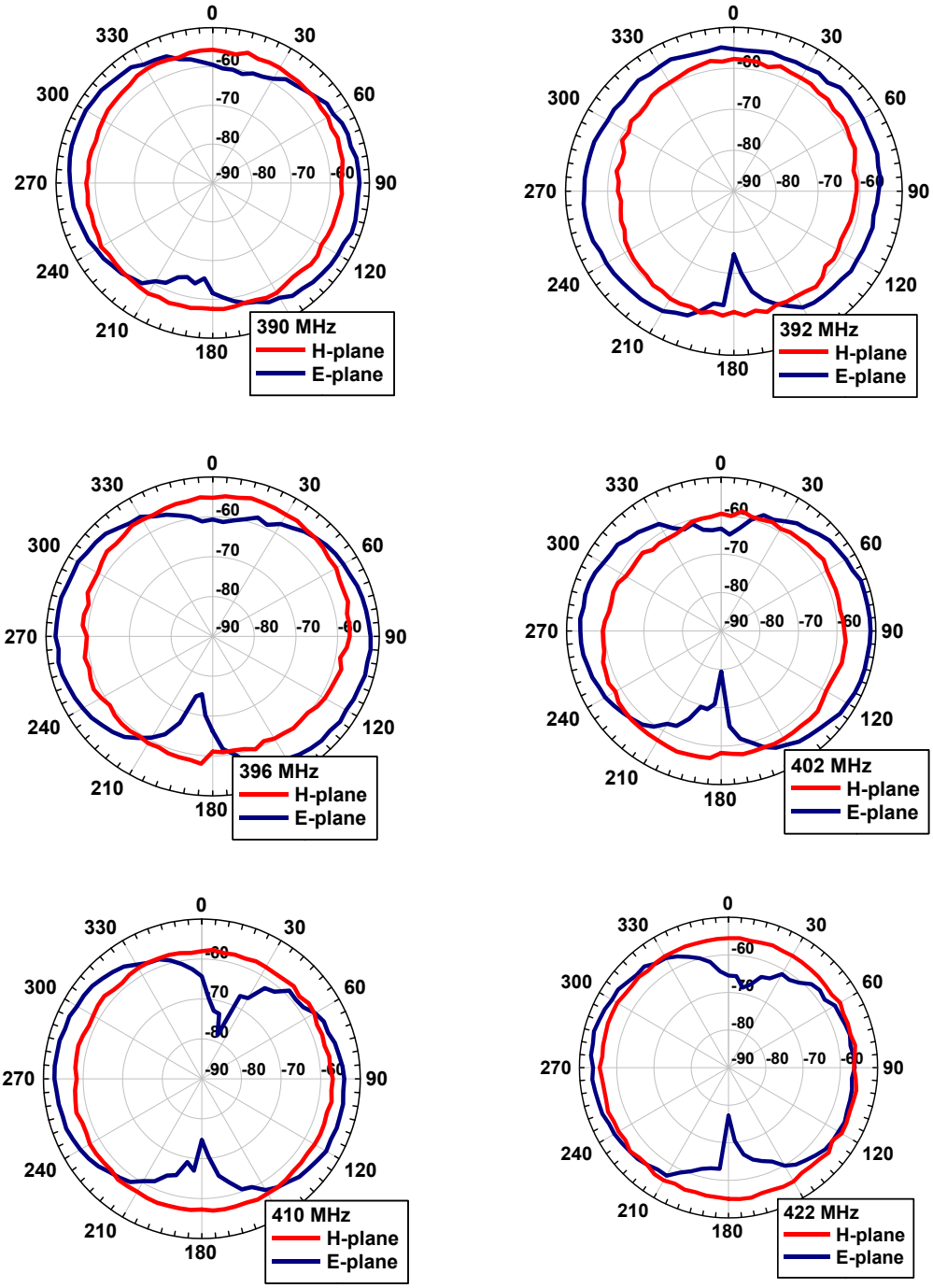

Figure 5-12: Measured Radiation Pattern of the Prototype Antenna for Various Operating Frequencies

5.2.3 Gain

The proposed antenna has a simulated gain of -3 dB and measured gain of -5 dB. The variation in the result can be attributed to the non-ideal absorbers and the coaxial cable length in the anechoic chamber.

5.3 Conclusion

A new miniaturized low profile reconfigurable antenna design is presented. The antenna has a low profile (16mm) and a compact size (diameter = 72 mm) and provides a vertical polarized monopole like the omni-directional radiation pattern. The use of the log-spirals in the design allows for the sensor structure to provide better performance and a wide band and is very suitable for TETRA wideband and wideband VHF/UHF frequency applications. The antenna has a sufficient gain and provides considerable efficiency with a small finite ground plane making it a very suitable choice for applications that require antenna surface mountings with size constraints.

6. MEASUREMENT RESULTS FOR THE PROPOSED ANGLE OF ARRIVAL ESTIMATION TECHNIQUE EMPLOYING AN ARRAY OF PROPOSED ELECTRICALLY SMALL RECONFIGURABLE MULTI-ELEMENT ANTENNA

6.1 Introduction

After simulating the proposed angle of arrival estimation design for various antenna geometries under different environments using different radiators i.e. monopole and inverted F antenna (IFA) based arrays, it is now necessary to test the performance of the proposed algorithm described in Chapter 3, with an antenna array consisting of the proposed antenna detailed in Chapter 5 to get a good agreement between the simulated results and the measured results.

6.2 Simulation Setup 4-Ring Circular Array

Different antenna array geometries were constructed using the prototype antenna. The first array geometry was a ring of 4 elements arranged in a uniform circular array (UCA) with inter-element spacing of $\lambda/4$ at an operating frequency of 400MHz and elemental separation of 90 degrees using a circular finite ground plane of 1m x 1m A 400 MHz log periodic reference antenna was used as a transmitter for the measurements. The measurement setup is summarised for the

4-element UCA in Table 6-1 and shown in Figure 6-1 The real and imaginary values obtained from each antenna were then imported into MATLAB to perform the digital signal processing (DSP).

Table 6-1: Measurement Parameters for the 4 – Elements Uniform Circular Array

Parameter	Value
Number of Elements	4
SNR	0 dB
Antenna Spacing	$\lambda/4$
Number of Snapshots	100
Noise	AWGN

.

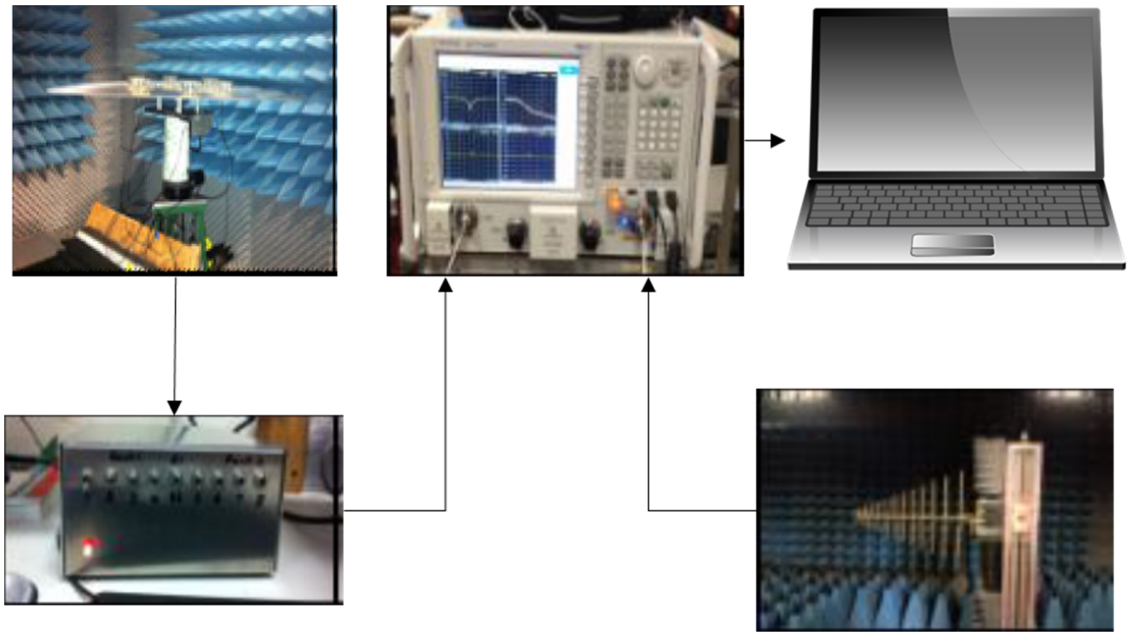

Figure 6-1: Simulation Setup for Prototype Antenna Array Testing

6.2.1 Results and Discussion

In the measurements, the receiver array was rotated at 10-degree step size for the whole azimuth plane of 360 degrees and the results were captured and processed. Figure 6-2 shows the angle estimation performance of the four algorithms for the angle of arrival reference or true angle of 0 Degrees. The Bartlett algorithm produced enormous side lobes and the resolution is not good.

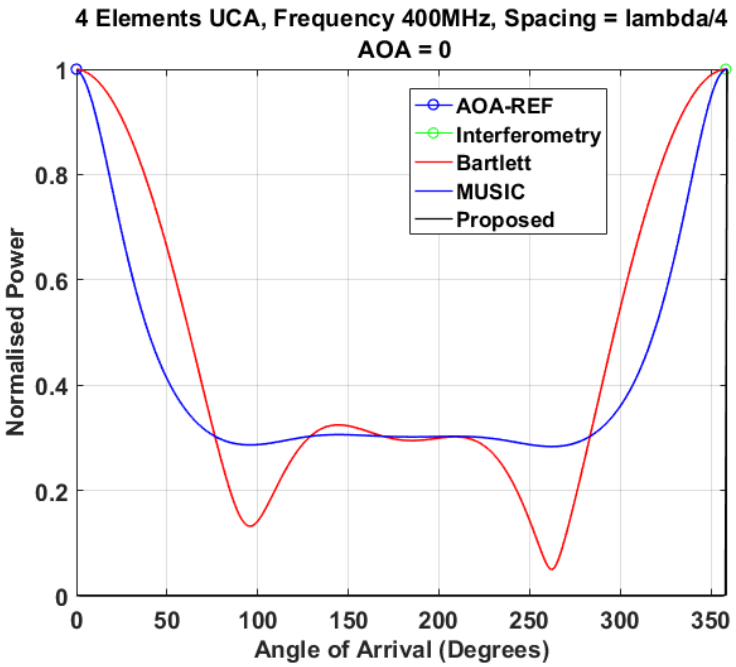

Figure 6-2: Performance Comparison Using 4-element UCA for True Angle of 0 Degree

Even though all algorithms could resolve the true angle with 1 degree error only the proposed algorithm produced a very fine peak. For the interferometry algorithm, it has been seen during simulations in Chapter 3 that the estimator has an acceptable performance when there is a finite ground plane available which is

visible from Figure 6-2. Performance of the angle estimation algorithms is plotted for another true angle of 180 degrees in Figure 6-3: and again, pretty similar results are obtained where the proposed algorithm produces a very fine peak in the direction of the true angle whereas the Bartlett algorithm and the MUSIC algorithm have very wide side lobes.

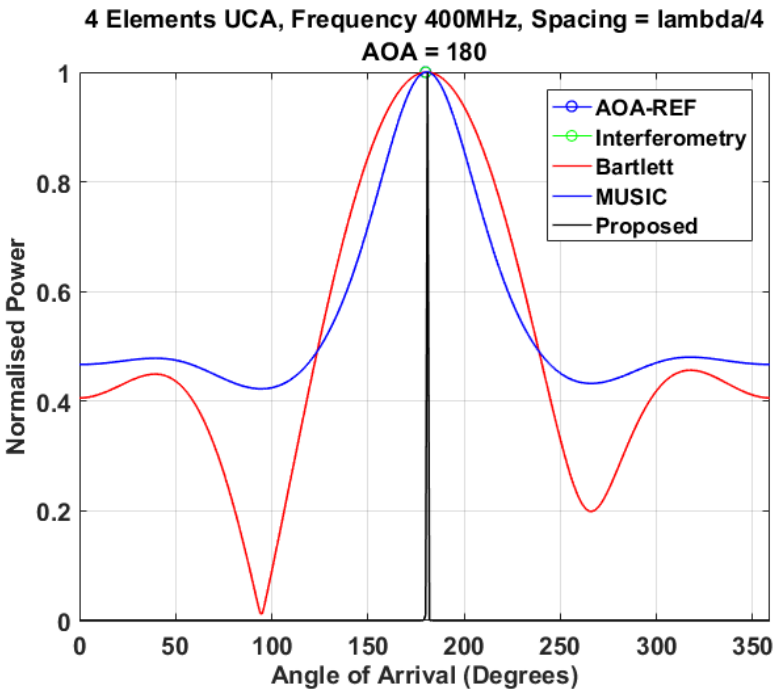

Figure 6-3: Performance Comparison Using a 4-element UCA for a True Angle of 180 Degrees

The overall comparison of all algorithms for all 36 angles in the azimuth plane is presented in Figure 6-4 and the performance of all algorithms is quite similar except for some angles where interferometry algorithm has shown a big angle error

performance and that is because of the angle ambiguities caused by the number of elements present in the antenna array are not sufficient to completely resolve the angle for the interferometry algorithm as discussed in Section 3.4.5.

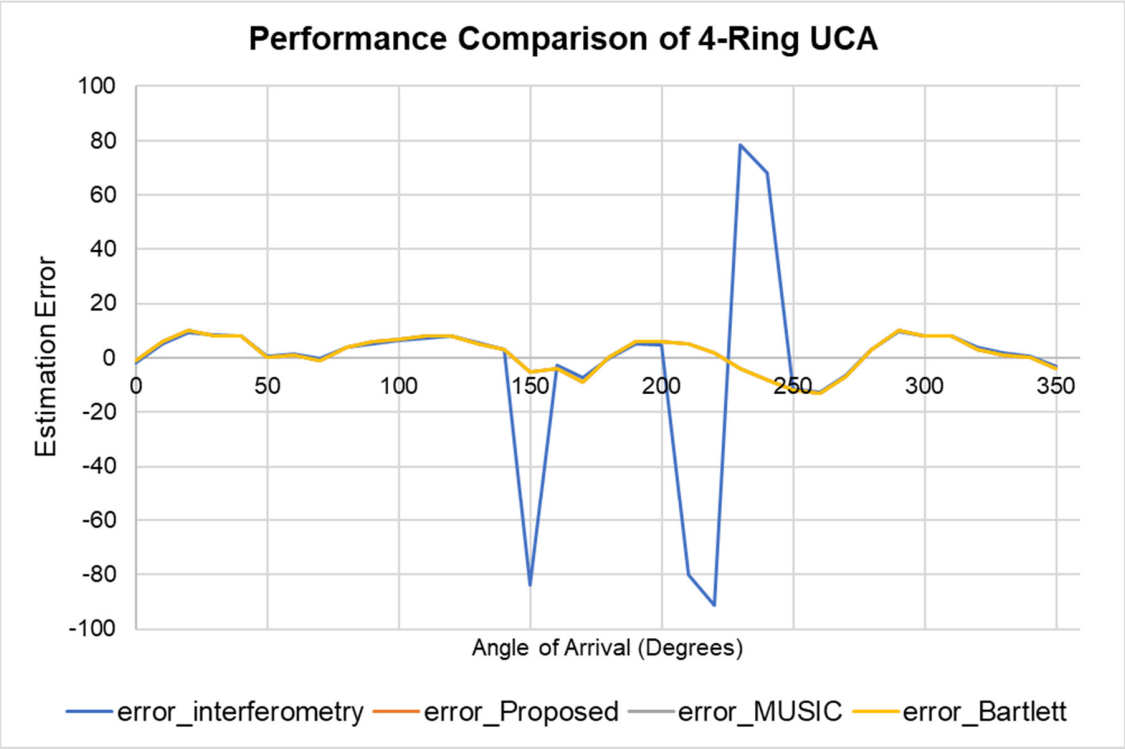

Figure 6-4: Performance Comparison Using a 4-element UCA for the Whole Azimuth Plane

From the measurement results obtained for the 4-element array the performance advantage of the proposed algorithm is quite clear. The proposed solution with its advantage of sharper peaks and quite reliable estimation performance makes this algorithm a better choice for applications that require information regarding the source angle of arrival.

The angle estimation performance comparison between the simulated results and the measured results are presented in Figure 6-5. The results show that even though the measurement error was a little higher than the simulated but it is within acceptable limits without any sort of addition digital signal processing for a 4-element array with a quarter wavelength spacing.

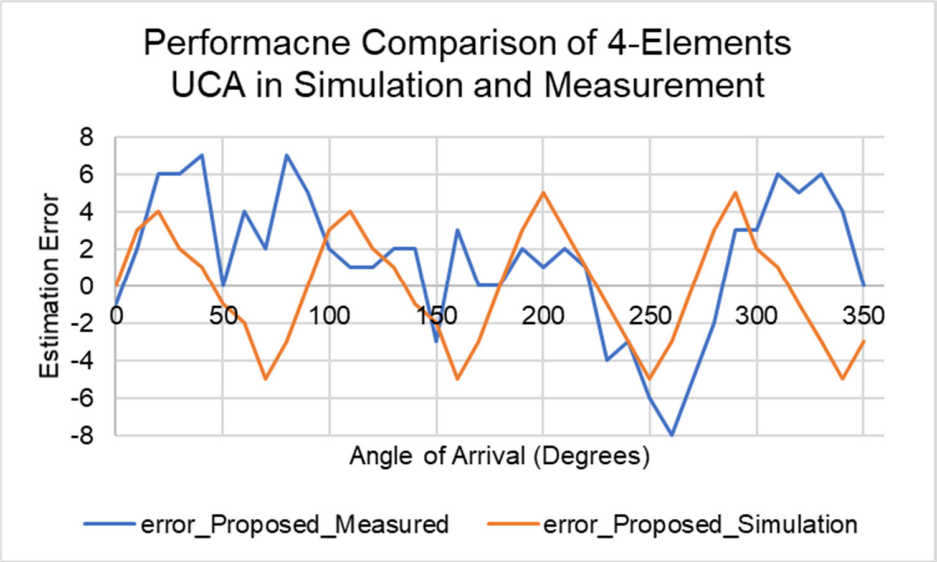

Figure 6-5: Performance Comparison of 4-element UCA for the Whole Azimuth Plane Using Simulated and Measured Data

Next the performance of the proposed algorithms was compared using multiple impinging rays. From Figure 6-6 the proposed algorithm, Bartlett and MUSIC algorithms could closely resolve the two incoming rays while the Interferometry algorithm completely failed to estimate the true angle.

Up to this point it has been shown how all the algorithms could resolve the correct angle for a single source. Next it will be shown how the performance of these algorithms relate under power thresholds.

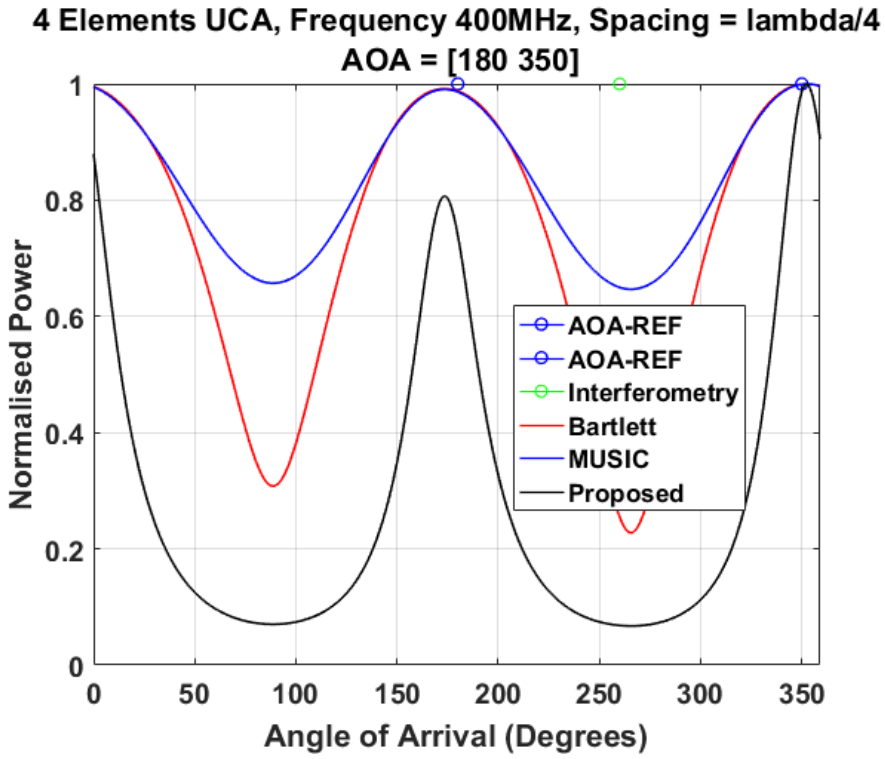

Figure 6-6: Performance Comparison Using a 4-element UCA for Multiple Received Rays

6.3 Average Error Performance Comparison Using Restricted Power Threshold

To verify the performance of the proposed method and to compare it against the widely-accepted MUSIC and phase interferometry algorithms the results from the

same 4-element array were used. The performance of these algorithms was compared using the power threshold limits. The results suggested that the wider side lobes produced by the MUSIC algorithms cause the estimator to result in more than one true angle of arrival estimation thus the total average error increases and thus reducing the performance efficiency. For all three threshold levels of 0.25%, 0.50% and 0.75% the phase interferometry technique outperforms the super resolution techniques.

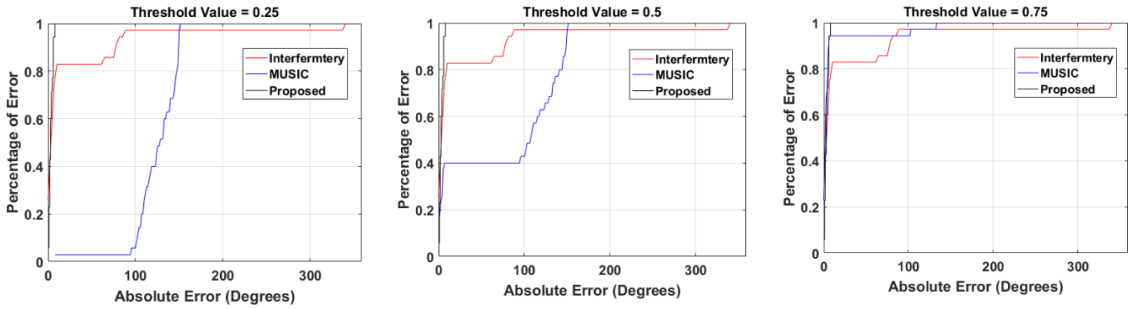

(a) (b) (c)

Figure 6-7: Average Error Performance of AoA Algorithms at Power Thresholds of (a) 25% (b) 50% (c) 75%

6.4 Simulation Setup 3-Ring Circular Array

The second array geometry was a ring of 3-elements arranged in a uniform circular array (UCA) with inter-element spacing of $\lambda/4$ at an operating frequency of 400MHz and elemental separation of 120 degrees using a circular finite ground plane of 1m x 1m. A 400 MHz log periodic reference antenna was used as a transmitter for the measurements. The measurement setup is summarised for the

3-element UCA in Table 6-2 The real and imaginary values obtained from each antenna were then imported into MATLAB to perform the digital signal processing (DSP).

Table 6-2: Measurement Parameters for the 3 – Elements Uniform Circular Array

Parameter	Value
Number of Elements	3
SNR	0 dB
Antenna Spacing	$\lambda/4$
Number of Snapshots	100
Noise	AWGN

6.4.1 Results and Discussion

In the measurements, the receiver array was rotated at 10-degree step size for the whole azimuth plane of 360 degrees and the results were captured and processed and are shown in Figure 6-8.

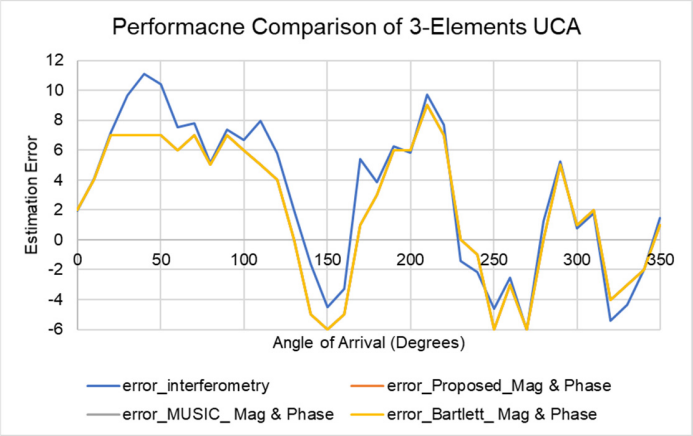

Figure 6-8: Performance Comparison Using a 3-element UCA for the Whole Azimuth Plane

The pattern of estimation algorithms remains consistent where Bartlett, MUSIC and Proposed algorithms have consistent performance but interferometry algorithms suffers from degraded estimation performance.

When compared with the 4-element UCA the 3-element presents a higher error. This error is still within acceptable levels depending upon the application type and the design cost constraints.

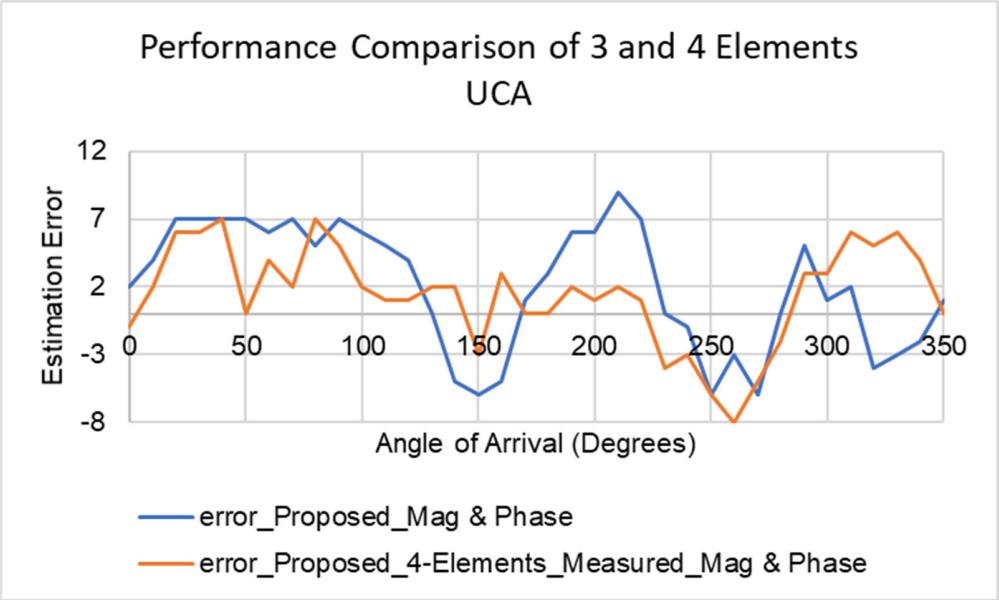

Figure 6-9: Performance Comparison Using 3 and 4-element UCAs for the Whole Azimuth Plane

6.5 Conclusion

The performance of the antenna array consisting of 4 elements and 3 elements of the proposed sensor was measured using the anechoic chamber and the angle of arrival estimation algorithms were applied and compared. The results showed that the proposed direction of arrival estimation scheme provides very sharp peaks in the direction of the source which in turn improves the overall average estimation error at low power levels. The other algorithms suffer from big side lobes which at low power levels result in the estimation of multiple angles and increase average estimation error.

7. ORTHOGONAL FREQUENCY DIVISION MULTIPLEXING SCHEME FOR ANGLE OF ARRIVAL APPLICATIONS

7.1 Introduction

With the advancements in wireless communications the number of applications requiring the knowledge of the number and location of the sources is growing rapidly. In the world of array signal processing the primary technique supporting these applications is Angle of Arrival estimation through antenna array [371]. In AOA algorithms, the bearing between the receiver and the transmit signal source is determined based on the angle of the incoming signal. The multipath fading effects of the of the environment such as Doppler shift [372], signal attenuation and low values of signal-to-noise ratio make the process of detection of the signal source extremely difficult [373]. In cases where there is a LOS signal present the problem lies in the separation of the true line of sight signal from the delayed and overlapped replicas arriving at the receiver and the addition of noise further complicates the process. All these problems make it extremely difficult to detect the LOS signal with absolute certainty. To improve the detection of the LOS component the resolution of the channel response in time domain requires enhancement to resolve for paths and enhance the estimation accuracy of the

AOA algorithm. In several scenarios if the wideband system is employed it mitigates the negative effects of the multipath and in turn improve the ability of the localization system to successfully resolve the paths. Majority of the AOA estimation techniques are narrowband estimators. However, the extended versions of these algorithms can be applied to wideband scheme.

This chapter presents a coded OFDM system to be used in the application of localization systems. In a practical wireless transmission, the spectral response of the channel is not flat. The spectral response has nulls present in it which are caused by the reflected signals. These reflected signals cannot only cause the certain frequencies to be cancelled at the receiver but can also result in deep fades in the received signal strength if they arrive at the receiver with the same power as that of the direct signal and destructively interfere. In a narrowband transmission, the entire signal can be lost if the null is present in the frequency response at the transmit frequency. By employing a wideband signal, complete signal loss can be avoided. Another solution to complete signal loss is to split the transmission into many small narrowband carriers by using Orthogonal Frequency Division Multiplexing (OFDM). In such a transmission scheme, multiple carrier frequencies can be used to digitally encode the data. This results in the transformation of the frequency selective channel into several flat fading channels [374]. Any loss of data can be prevented by using coded OFDM in which forward error correction (FEC) codes can be applied to the signal before transmission.

Moreover, as explained earlier, the received signal at the receiver consists of direct line of sight (LOS) signals and non-line of sight (NLOS) signals caused by the reflections from the scatterers present in the propagation path between the transmitter and the receiver. These reflected signals arrive at the receiver with a delay due to the difference in the path length travelled and the received energy is spread in time which is referred to as channel delay spread. The channel delay spread can be described as the time between first and the last significant multipath signal arriving at the receiver. This delay spread is responsible for the inter symbol interference (ISI) in the digital wireless communications. The inter-symbol interference occurs when a delayed multipath signal overlaps the following symbols. One method to reduce the ISI is to divide the bandwidth into several sub channels by using OFDM.

This chapter is arranged as follows: Section 7.2 provides the mathematical model for the orthogonal frequency division multiplexing scheme that can be employed for the angle of arrival estimation followed by Section 7.3 which describes the simulation model. Results and discussion are presented in Section 7.4 followed by the conclusion in Section 7.5

7.2 Mathematical Model for Orthogonal Frequency Division Multiplexing (OFDM) For Angle of Arrival Estimation

Assume the broadband impulse channel response is given by

$$h(\tau) = \sum_{k=1}^{n} a_k e^{j\phi_k} \delta(\tau - \tau_k) \tag{7-1}$$

Apply an input signal:

$$f(t,\omega) = e^{j\omega t} \tag{7-2}$$

Then the output can be simplified to the following:

$$s(t,\omega) = \sum_{k=1}^{n} a_k e^{j\phi_k} e^{j\omega(t-\tau_k)} \tag{7-3}$$

This alternatively can be given by:

$$s(t,\omega) = e^{j\omega t} \sum_{k=1}^{n} a_k e^{j\phi_k} e^{-j\omega\tau_k} = e^{j\omega t} U(\omega) \tag{7-4}$$

Extend U(ω) over baseband bandwidth B (shown in Figure 1) for N frequency samples, then the ith frequency sample might be expressed by:

$$f_i = -\tfrac{B}{2} + (i-1)n\Delta f = -\tfrac{B}{2} + (i-1)n\tfrac{B}{N} = \tfrac{B}{2}(-1 + (i-1)\tfrac{2n}{N}) \tag{7-5}$$

where

$$N\Delta f = B \tag{7-6}$$

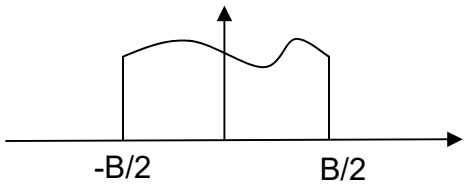

Figure 7-1: Assumed bandwidth range

The sampling time can be stated as follows:

$$\frac{1}{2\Delta t} = \frac{B}{2}, \text{ hence } \Delta t = \frac{1}{B} \tag{7-7}$$

Thus, the minimum sampling frequency assumed by:

$$f_s \geq 2\frac{B}{2} = B \tag{7-8}$$

The i^{th} uniform frequency sample of $U(\omega)$ can be given by:

$$U(2\pi f_i) = \sum_{k=1}^{n} a_k e^{j\phi_k} e^{-j\omega\tau_k} e^{-j2\pi f_i \tau_k} \tag{7-9}$$

7.3 Simulation Model

The wireless propagation simulation software Wireless Insite by Remcom is utilised in this study as it can provide the most realistic simulation model for real life wireless propagation. It is an electromagnetic simulation tool that helps predict the propagation behaviour of electromagnetic waves in the presence of objects with different electrical properties. The propagation scenario used in this work is of Ottawa city in Canada available from Remcom which can be classified as an urban environment as shown in Figure 7-2.

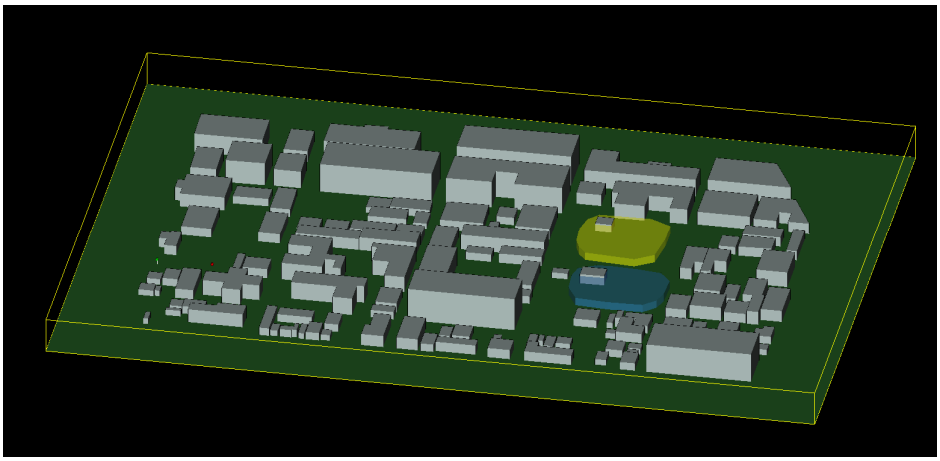

Figure 7-2: Study Area for OFDM

A 3-element array of ideal dipoles spatially distributed in the azimuthal plane with angular separation of 120 degrees at known locations with inter-element spacing of $\lambda/3$ was used to receive the electromagnetic field propagating from the far field transmitter. The output of each element in the antenna array was then used to calculate the angle of arrival. The receiver array and the far field transmitter lie in the same plane so only azimuthal angle calculations were done. Complex Gaussian noise uncorrelated from the signals was added to each element of the array. The IFFT was applied to the received channel transfer function to acquire the impulse response with 10 multipath including the LOS path over the desired band. Each impulse in the frequency range was assigned an AOA and the AOA assigned to the impulse with the highest amplitude was the true bearing angle. The phase adjustments were done on the received components to account for the antenna position within the array so that the impulse response is in line with each receiver channel. The dominant impulse from all received channels was then

passed to the narrow band angle of arrival estimation technique and the performance is evaluated in terms of AOA estimation error

5.2 Results and Discussion

The results from two different array types, 1) 3-element uniform circular ring array with element spacing of 120 degrees and 2) 5-Elements uniform circular array with an element spacing of 72 degrees are presented for available bandwidths of 1MHz and 10 MHz.

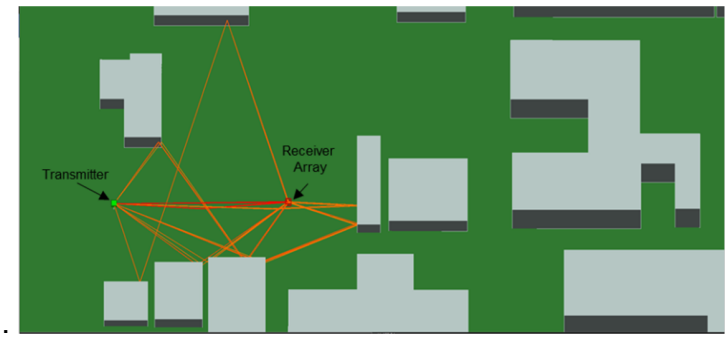

Figure 7-3: Multipaths travelled by the transmitted signal

The Figure 7-4 (a) shows the results for the 3-element UCA where the transmission is split into small narrowband carriers using 1 MHz and b) where the transmission is split using 10MHz for the total of 11 carriers. It is to be noted that there is noise and multipaths presents in the system and the resultant frequency domain and time domain results are close to the true AoA for most carriers but still not sufficient enough clarity to deduce the true AoA. To further improve the performance, the same experiment was repeated with a 5-element UCA.

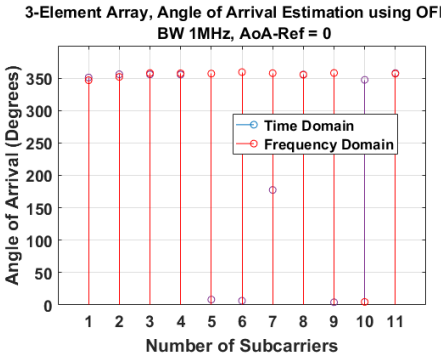

(a)

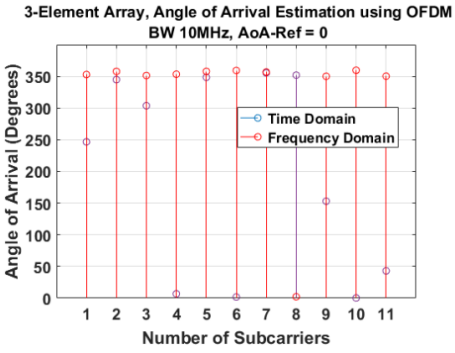

(b)

Figure 7-4: 3-element Circular Ring Array using OFDM

The results obtained in Figure 7-5 clarify the usefulness of the transmission division into narrowband carriers and show how all carriers are in sync with using either time or frequency domain estimation technique. It can also be seen that by increasing the bandwidth as in Figure 7-5 (b) any minute errors present between the time and frequency domain estimation were also resolved.

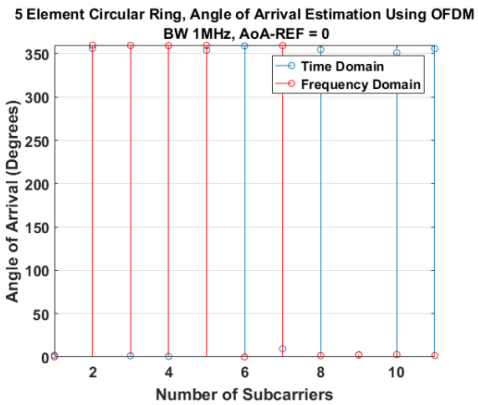

(a)

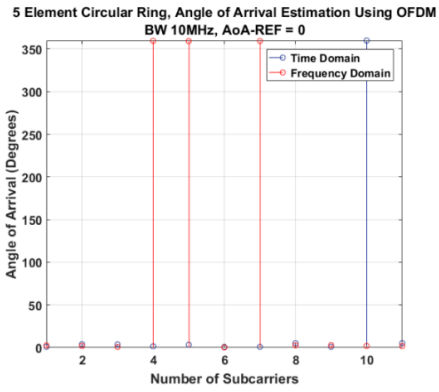

(b)

Figure 7-5: 5-element Circular Ring Array using OFDM

7.4 Conclusion

In this chapter, a multi carrier modulation scheme is evaluated for use in localization systems. OFDM can provide many suitable solutions which the single carrier modulation scheme or the FDM scheme cannot provide. The ability of the OFDM systems to combat multipath make them the most suitable scheme for angle of arrival estimation. The higher time resolution and the higher number of array elements makes it easier to place decisions on the true angle of arrival estimation. In such systems, however for accuracy an assumption must stand that there is a line of sight present between the transmitter and receiver and there will always be a dominant ray present. If this assumption is to be taken out of the equation, then further processing must be applied to cater for non-line of sight (NLOS) scenarios and this can include having a memory bank based on previous calculations to calibrate the localization system in case a sudden dominant NLOS component appears.

8. CONCLUSION AND FUTURE WORK

8.1 Conclusion

An in-depth analysis of the techniques involved in the angle of arrival estimation for several antenna configurations and different scenarios for both narrowband and wideband spectrum estimations were presented. This type of work has high significance in military applications, patient tracking and in providing the location based services to the continuously growing community of mobile users. A new signal subspace based algorithm is designed, implemented and testes using both simulation and measurement models and has shown an improved performance as compared to any of the previously proposed algorithms. In addition, a new and novel miniaturized reconfigurable logarithmic spiral antenna with improved bandwidth performance and reconfigurable frequency bands is designed, implemented and tested using multiple element arrays measure the performance. The results suggest the proposed antenna is highly suitable for localization systems that have size constraints for the antenna array implementation, cost constraints and require reliability and is also suited for mobile wireless devices that require antenna surface mounting. Also, the degrading effects of the mutual coupling on antenna arrays was studied and the procedures were detailed to deduce the decoupling methods which were then applied to different data sets and the performance of the AoA algorithms was evaluated before and after the mutual coupling compensation, Finally an OFDM based transmission scheme was

evaluated by dividing the whole transmission into narrow band carriers which is suitable for AoA estimation systems and is capable of negating the multipath effects of the channel and improve estimation accuracy. A brief thesis summary is presented below.

8.2 Thesis Summary

Chapter 2 – A detailed review of the location based services and their applications both in public and private sector was presented. Location based services have found its place in the next generation wireless communication system applications such as tracking, health, navigation etc. The chapter also presents the infrastructure model for both indoor and outdoor LBS. The existing localization techniques were also reviewed and solutions were presented to improve the existing localization applications and techniques.

Chapter 3 – Mathematical background on the antenna arrays and angle of arrival estimation techniques was presented. A novel high-resolution direction of arrival estimation algorithm based on the signal subspace decomposition has been presented with the core idea of finding the difference between the maximum absolute value of the pseudo-spectrum and the absolute value of the pseudo-spectrum thus minimizing the denominator and producing larger peaks in the direction of arrival of the incoming signal. The proposed method exploits the signal

subspace with array steering vector as opposed to the MUSIC algorithm that exploits the noise subspace with array steering vector. The proposed algorithm has been tested and evaluated using different criteria and has shown great potential to be employed as the next generation localization technique.

Chapter 4 – The degrading effects of mutual coupling on antenna array elements were discussed. Two methods of mutual coupling compensation namely the conventional mutual impedance method and the receiving mutual impedance methods were discussed and evaluated. Based on these methods, decoupling matrices were generated and applied to the simulation data. The results showed that receiving mutual impedance method is easier to implement with the same computational complexity as that of the conventional mutual impedance method and has better results and is a better fit for application requiring real time processing.

Chapter 5 – In this chapter the design and implementation of a novel reconfigurable electrically small antenna for wideband UHF frequencies is presented. The antenna design makes use of the logarithmic spirals with biased components and has considerable stable gain and efficiency with a small ground plane making it a suitable candidate for surface mounting on tracking devices which has size constraints. The performance of this antenna in terms of reflection coefficient, radiation pattern and gain were presented which show the suitability of

the antenna for localization applications with reconfigurable bandwidth, omni-directional radiation pattern, vertical polarisation and small size.

Chapter 6 – In this chapter the performance of the antenna array consisting of 4-elements and 3-elements of the proposed sensor was measured using the anechoic chamber and the angle of arrival estimation algorithms were applied and compared. The results showed that the proposed direction of arrival estimation scheme provides very sharp peaks in the direction of the source which in turn improves the overall average estimation error at low power levels. The other algorithms suffer from big side lobes which at low power levels result in the estimation of multiple angles and increase average estimation error.

Chapter 7 – A multicarrier modulation OFDM based system is evaluated to be used for angle of arrival estimation. The channel characteristics received from the electromagnetic propagation software were converted into time domain using IFFT and spread across the desired band using subcarriers making the system more robust against multipath effects. The time resolution provided by the wideband transmission improved the angle estimation accuracy. The comparison between the time domain and frequency domain estimation is presented and how the bandwidth made an effect on these estimations.

8.3 Recommendations for Future Work

As the topic of source localization is quite wide spread and the market demands are ever growing there is always a margin for improvement. Some of the topics that can be of interest for further research are listed below.

- As most this study was comprised around receiver antenna arrays it was shown in Chapter 4 that received mutual impedance method calculated for one angle helps reduce coupling error in majority of angles but this can be extended further to develop a single mutual coupling compensation method that can be applied to all angles.

- The proposed angle of arrival estimation algorithm can be used to test the performance of angle of arrival estimation with more antenna geometries and can be enhanced to include 3D angle of arrival estimation.

- Another important piece of work that is presented in Chapter 7 is the multi carrier modulation scheme of OFDM for angle of arrival estimation. This work using the proposed technique can be enhanced and further improved by adding space time coding, improved channel estimations, frequency offset estimations, path loss estimations and channel compensation techniques.

REFERENCES

[1] J. E. Bardram and H. B. Christensen, "Pervasive Computing Support For Hospitals: An Overview Of The Activity-Based Computing Project," *IEEE Pervasive Computing*, Vol. 6, No. 1, pp. 44 - 51, January - March 2007. DOI: 10.1109/MPRV.2007.19

[2] J. E. Bardram, "Applications Of Context-Aware Computing In Hospital Work: Examples And Design Principles," *ACM Symposium on Applied Computing*, pp. 1574-1579, March 14 - 17, 2004. DOI: 10.1145/967900.968215

[3] R. Zekavat and R. M. Buehrer, "*Handbook of position location: Theory, practice and advances*, " John Wiley & Sons, Vol. 27, November 2011. ISBN: 978-0-470-94342-7

[4] A. Solanas *et al*., "Smart Health: A Context-Aware Health Paradigm Within Smart Cities," *IEEE Communications Magazine*, Vol. 52, No. 8, pp. 74 - 81, August 2014. DOI: 10.1109/MCOM.2014.6871673

[5] T. A. Khan, H. Asmat, F. Shahzad, M. F. Mushtaq, M. M. S. Missen, and N. Akhtar, "SN2SMS: Location-Aware Social Network Based SMS Health-Care System," *International Journal of Computer Science Issues (IJCSI),* Vol. 11, pp. 144 - 149, July 2014. ISSN (Print): 1694-0814 | ISSN (Online): 1694-0784

[6] P. Steggles and S. Gschwind, "The Ubisense Smart Space Platform," *Third International Conference on Pervasive Computing*, Vol. 191, pp. 73 - 76, 2005. doi=10.1.1.176.362

[7] B. Simon, Z. Miklós, W. Nejdl, M. Sintek, and J. Salvachua, "Smart Space For Learning: A Mediation Infrastructure For Learning Services," *Twelfth*

International Conference on World Wide Web, pp. 20 - 24, May 2003. ISBN 963-311-355-5.

[8] S. Helal, W. Mann, H. El-Zabadani, J. King, Y. Kaddoura, and E. Jansen, "*The Gator Tech Smart House: A Programmable Pervasive Space,*" John Wiley & Sons, Ltd., 2008. DOI: 10.1002/9780470379424.ch37

[9] S. Alletto *et al*., "An Indoor Location-Aware System for an IoT-Based Smart Museum," *IEEE Internet of Things Journal*, Vol. 3, No. 2, pp. 244 - 253, April 2016. DOI: 10.1109/JIOT.2015.2506258

[10] A. Martinez-Balleste, P. A. Perez-martinez and A. Solanas, "The Pursuit Of Citizens' Privacy: A Privacy-Aware Smart City Is Possible," *IEEE Communications Magazine*, Vol. 51, No. 6, pp. 136 - 141, June 2013. DOI: 10.1109/MCOM.2013.6525606

[11] S. A. Applin and M. D. Fischer, "Thing Theory: Connecting Humans to Location-Aware Smart Environments," *3rd Workshop On Location Awareness For Mixed And Dual Reality: LAMDa*'13, pp. 29, March 2013. DOI:10.1145/2451176.2451228

[12] P. M. Singh and M. van Sinderen, "Interoperability Challenges For Context Aware Logistics Services-The Case Of Synchromodal Logistics," *6th International IFIP Working Conference on Enterprise Interoperability*, Vol. 1414, pp. 9 – 9, 2015. ISSN (Print): 1613-0073

[13] I. Durazo-Cardenas, A. Starr, A. Tsourdos, M. Bevilacqua, and J. Morineau, "Precise Vehicle Location As A Fundamental Parameter For Intelligent Self-Aware

Rail-Track Maintenance Systems," *Procedia CIRP*, Vol. 22, pp. 219 - 224, 2014. DOI: https://doi.org/10.1016/j.procir.2014.07.002

[14] L. Evers, M. J. Bijl, M. Marin-Perianu, R. Marin-Perianu, and P. J. Havinga, "Wireless Sensor Networks And Beyond: A Case Study On Transport And Logistics," *University of Twente, Centre for Telematica and Information Technology (CTIT)*, Vol. 05, pp. 1 – 6, 2005. ISBN (Print): 1381 – 3625.

[15] K. Kuladinithi, O. Bergmann, T. Pötsch, M. Becker, and C. Görg, "Implementation of COAP And Its Application In Transport Logistics," *Proceedings of Extending the Internet to Low Power and Lossy Networks (IP+ SN)* , pp. 1 – 6, April 2011.

[16] W. Zhou, S. Piramuthu, F. Chu, and C. Chu, "RFID-Enabled Flexible Warehousing," *Decision Support Systems*, Vol. 98, pp. 99 - 112, June 2017. DOI: https://doi.org/10.1016/j.dss.2017.05.002

[17] D. Ma, N. Saxena, T. Xiang and Y. Zhu, "Location-Aware and Safer Cards: Enhancing RFID Security and Privacy via Location Sensing," *IEEE Transactions on Dependable and Secure Computing*, Vol. 10, No. 2, pp. 57 - 69, March-April 2013. DOI: 10.1109/TDSC.2012.89

[18] P. L. Smith, "Effects Of Imperfect Storm Reporting On The Verification Of Weather Warnings," Bulletin of the American Meteorological Society, Vol. 80, pp. 1099

1105,June1999.DOI:https://doi.org/10.1175/15200477(1999)080<1099:EOISRO>2.0.CO;2

[19] Steinmetz R., Wehrle K. “Chapter 2. What Is This *“Peer-to-Peer”* About?, Peer-to-Peer Systems and Applications”, *Lecture Notes in Computer Science*, Vol 3485. pp. 9 – 16, Springer. 2005. DOI: https://doi.org/10.1007/11530657_2

[20] V. Lenders, E. Koukoumidis, P. Zhang, and M. Martonosi, "Location-Based Trust For Mobile User-Generated Content: Applications, Challenges And Implementations," *9th Workshop On Mobile Computing Systems And Applications*, pp. 60 - 64, 2008. DOI:10.1.1.139.1903

[21] C. Xu, S. Jia, L. Zhong and G. M. Muntean, "Socially Aware Mobile Peer-To-Peer Communications For Community Multimedia Streaming Services," *IEEE Communications Magazine*, Vol. 53, No. 10, pp. 150 - 156, October 2015. DOI: 10.1109/MCOM.2015.7295477

[22] M. Bartlett, "*An Introduction to Stochastic Processes with Special References to Methods and Applications*," Cambridge University Press, New York, 1961.

[23] L. C. Godara, “*Smart antennas,*” CRC press*, January 2004*. ISBN 9780849312069 - CAT# 1206

[24] J. Capon, "High-Resolution Frequency-Wavenumber Spectrum Analysis," *Proceedings of the IEEE*, Vol. 57, No. 8, pp. 1408 - 1418, Aug. 1969. DOI: 10.1109/PROC.1969.7278

[25] F. Gross, "*Smart Antennas For Wireless Communications,*" McGraw-Hill Companies Inc, ed: New York, 2005. ISBN: 9780071447898

[26] S. Applebaum, "*Adaptive Arrays*”, Syracuse University Research Corporation, SPL, TR66-1, August 1966.

[27] S. Applebaum, "Adaptive Arrays," *IEEE Transactions on Antennas and Propagation*, Vol. 24, No. 5, pp 585 – 598, September 1976. DOI: 10.1109/TAP.1976.1141417

[28] B. Widrow and M. Hoff, “Adaptive Switching Circuits,” *IRE WESCON Convention Record: At The Western Electronic Show And Convention*, Vol. 4, pp. 96 - 104, 1960.

[29] B. Widrow, P. E. Mantey, L. J. Griffiths, and B. B. Goode, "Adaptive Antenna Systems," *Proceedings of the IEEE*, Vol. 55, pp. 2143 - 2159, December 1967.

[30] W. Gabriel, "Adaptive Processing Antenna Systems," *IEEE Antennas and Propagation Society Newsletter*, Vol. 25, No. 5, pp. 4 - 11, October 1983. DOI: 10.1109/MAP.1983.27703

[31] L. C. Godara, "Application Of Antenna Arrays To Mobile Communications. II. Beam-Forming And Direction-Of-Arrival Considerations," *Proceedings of the IEEE*, Vol. 85, No. 8, pp. 1195 - 1245, August 1997.DOI: 10.1109/5.622504

[32] J. C. Liberti and T. S. Rappaport, "*Smart Antennas For Wireless Communications: IS-95 And Third Generation CDMA Applications,*" Prentice Hall Communications Engineering And Emerging Technologies Series, Prentice Hall PTR, 1999. ISBN 0137192878, 9780137192878

[33] J. P. Burg, "The Relationship Between Maximum Entropy Spectra And Maximum Likelihood Spectra," *Geophysics*, Vol. 37, pp. 375 – 376, April 1972. DOI: https://doi.org/10.1190/1.1440265

[34] V. F. Pisarenko, "The Retrieval of Harmonics from a Covariance Function," *Geophysical Journal of the Royal Astronomical Society*, Vol. 33, pp. 347 – 366, September 1973. DOI: https://doi.org/10.1111/j.1365-246X.1973.tb03424.x

[35] M. Wax, Tie-Jun Shan and T. Kailath, "Spatio-Temporal Spectral Analysis By Eigenstructure Methods," *IEEE Transactions on Acoustics, Speech, and Signal Processing*, Vol. 32, No. 4, pp. 817 - 827, Aug 1984. DOI: 10.1109/TASSP.1984.1164400

[36] J. Makhoul, "Linear Prediction: A Tutorial Review," *Proceedings of the IEEE*, Vol. 63, No. 4, pp. 561 - 580, April 1975. DOI: 10.1109/PROC.1975.9792

[37] S. S. Reddi, "Multiple Source Location-A Digital Approach," *IEEE Transactions on Aerospace and Electronic Systems*, Vol. AES-15, No. 1, pp. 95 - 105, January 1979. DOI: 10.1109/TAES.1979.308800

[38] R. Kumaresan and D. W. Tufts, "Estimating The Angles Of Arrival Of Multiple Plane Waves," *IEEE Transactions on Aerospace and Electronic Systems*, Vol. AES-19, No. 1, pp. 134 - 139, January 1983. DOI: 10.1109/TAES.1983.309427

[39] R. Schmidt, "Multiple Emitter Location And Signal Parameter Estimation," *IEEE Transactions on Antennas and Propagation*, Vol. 34, No. 3, pp. 276 - 280, March 1986. DOI: 10.1109/TAP.1986.1143830

[40] S. V. Schell, R. A. Calabretta, W. A. Gardner and B. G. Agee, "Cyclic MUSIC Algorithms For Signal-Selective Direction Estimation," *International Conference on Acoustics, Speech, and Signal Processing,* Vol.4, pp. 2278 - 2281, 1989. DOI: 10.1109/ICASSP.1989.266920

[41] T. E. Biedka and B. G. Agee, "Subinterval Cyclic MUSIC-Robust DF With Error In Cycle Frequency Knowledge," *Conference Record of the Twenty-Fifth Asilomar Conference on Signals, Systems & Computers*, Vol.1, pp. 262 - 266, 1991. DOI: 10.1109/ACSSC.1991.186453

[42] K. D. Mauck, "Wideband cyclic MUSIC," *IEEE International Conference on Acoustics, Speech, and Signal Processing*, Vol.4, pp. 288 - 291, 1993. DOI: 10.1109/ICASSP.1993.319651

[43] S. V. Schell, "Performance Analysis Of The Cyclic MUSIC Method Of Direction Estimation For Cyclostationary Signals," *IEEE Transactions on Signal Processing*, Vol. 42, No. 11, pp. 3043 - 3050, November 1994. DOI: 10.1109/78.330364

[44] P. Charg, Y. Wang, and J. Saillard, "An Extended Cyclic Music Algorithm," *IEEE International Conference on Acoustics, Speech, and Signal Processing (ICASSP),* pp. III-3025 - III-3028, 2002.

[45] P. Charge, Yide Wang and J. Saillard, "An Extended Cyclic MUSIC Algorithm," *IEEE Transactions on Signal Processing*, Vol. 51, No. 7, pp. 1695 - 1701, July 2003. DOI: 10.1109/TSP.2003.812834

[46] H. Yan and H. H. Fan, "Improved Cyclic And Conjugate Cyclic MUSIC," *Sensor Array and Multichannel Signal Processing Workshop*, pp. 289 - 293, 2004. DOI: 10.1109/SAM.2004.1502955

[47] H. Yan and H. H. Fan, "Extended Wideband Cyclic MUSIC," *Sensor Array and Multichannel Signal Processing Workshop*, pp. 318 - 322, 2004. DOI: 10.1109/SAM.2004.1502961

[48] Zhigang Liu and Jinkuan Wang, "Unitary Cyclic MUSIC Algorithm In A Multipath Environment," *12th European Signal Processing Conference*, pp. 2155 - 2158, 2004.

[49] M. Sahmoudi and M. G. Amin, "Unitary Cyclic MUSIC for Direction Finding in GPS Receivers," *Fourth IEEE Workshop on Sensor Array and Multichannel Processing,* pp. 70 - 73, 2006. DOI: 10.1109/SAM.2006.1706093

[50] S. Ali and P. Aarabi, "A Cyclic Interface For The Presentation Of Multiple Music Files," *IEEE Transactions on Multimedia*, Vol. 10, No. 5, pp. 780 - 793, August 2008.DOI: 10.1109/TMM.2008.922848

[51] R. Roy and T. Kailath, "ESPRIT-Estimation Of Signal Parameters Via Rotational Invariance Techniques," *IEEE Transactions on Acoustics, Speech, and Signal Processing*, Vol. 37, No. 7, pp. 984 - 995, July 1989. DOI: 10.1109/29.32276.

[52] J. Munier and G. Y. Delisle, "Spatial Analysis Using New Properties Of The Cross-Spectral Matrix," *IEEE Transactions on Signal Processing*, Vol. 39, No. 3, pp. 746 - 749, March 1991. DOI: 10.1109/78.80863

[53] S. Marcos, A. Marsal and M. Benidir, "Performances Analysis Of The Propagator Method For Source Bearing Estimation," *IEEE International Conference on Acoustics, Speech, and Signal Processing,* Vol.4, pp. IV/237 - IV/24, 1994. DOI: 10.1109/ICASSP.1994.389823

[54] K. V. S. Babu, "A Fast Algorithm For Adaptive Estimation Of Root-MUSIC Polynomial Coefficients," *International Conference on Acoustics, Speech, and*

Signal Processing, Vol. 3, pp. 2229 - 2232, 1991. DOI: 10.1109/ICASSP.1991.150830

[55] A. Barabell, "Improving The Resolution Performance Of Eigenstructure-Based Direction-Finding Algorithms," *IEEE International Conference on Acoustics, Speech, and Signal Processing*, pp. 336 - 339, 1983. DOI: 10.1109/ICASSP.1983.1172124

[56] Q. S. Ren and A. J. Willis, "Fast Root MUSIC Algorithm," *Electronics Letters*, Vol. 33, No. 6, pp. 450 - 451, 13 March 1997. DOI: 10.1049/el:19970272

[57] C. S. MacInnes, "Source Localization Using Subspace Estimation And Spatial Filtering," *IEEE Journal of Oceanic Engineering*, Vol. 29, No. 2, pp. 488 - 497, April 2004. DOI: 10.1109/JOE.2004.827290

[58] T. Hayashi, M. Nakano and A. Yamaguchi, "Novel AOA Estimation Method Using Delay Profile In Downlink," *International Workshop on Antenna Technology (iWAT),* pp. 35-38, 2013. DOI: 10.1109/IWAT.2013.6518293

[59] S. F. Chuang, W. R. Wu and Y. T. Liu, "High-Resolution AoA Estimation for Hybrid Antenna Arrays," *IEEE Transactions on Antennas and Propagation*, Vol. 63, No. 7, pp. 2955-2968, July 2015. DOI: 10.1109/TAP.2015.2426795

[60] C. A. Balanis, " *Antenna Theory: Analysis and Design,*" Wiley-Blackwell, 2005. ISBN: 978-0471667827

[61] H. Zhu, F. Liu, and H. Li, "Efficient and Privacy-Preserving Polygons Spatial Query Framework for Location-Based Services," *IEEE Internet of Things Journal,* Vol. 4, pp. 536 - 545, 2017. DOI**:** 10.1109/JIOT.2016.2553083

[62] Y. Song, Z. Hu, X. Leng, H. Tian, K. Yang, and X. Ke, "Friendship Influence on Mobile Behaviour of Location Based Social Network Users," *Journal of Communications and Networks,* Vol. 17, pp. 126 - 132, 2015. DOI: 10.1109/JCN.2015.000026

[63] T. Peng, Q. Liu, and G. Wang, "Enhanced Location Privacy Preserving Scheme in Location-Based Services," IEEE *Systems Journal,* Vol. 11, pp. 219 - 230, 2017.

[64] A. Baiocchi and F. Cuomo, "Infotainment Services Based on Push-Mode Dissemination in An Integrated VANET and 3G Architecture," *Journal of Communications and Networks,* Vol. 15, pp. 179 - 190, 2013. DOI: 10.1109/JCN.2013.000031

[65] E. Jovanov and A. Milenkovic, "Body Area Networks for Ubiquitous Healthcare Applications: Opportunities and Challenges," *Journal of medical systems,* Vol. 35, pp. 1245 - 1254, 2011.

[66] M. S. Hossain, "Cloud-Supported Cyber–Physical Localization Framework for Patients Monitoring," *IEEE Systems Journal,* Vol. 11, pp. 118 - 127, 2017. DOI: 10.1109/JSYST.2015.2470644

[67] P. A. Moreno, M. E. Hernando, and E. J. Gómez, "Design and Technical Evaluation of an Enhanced Location-Awareness Service Enabler for Spatial Disorientation Management of Elderly with Mild Cognitive Impairment," *IEEE Journal of Biomedical and Health Informatics,* Vol. 19, pp. 37 - 43, 2015. DOI: 10.1109/JBHI.2014.2327638

[68] H. Huang, J. Zhou, W. Li, J. Zhang, X. Zhang, and G. Hou, "Wearable Indoor Localisation Approach in Internet of Things," *IET Networks,* Vol. 5, pp. 122 - 126, 2016. DOI:10.1049/iet-net.2016.0007

[69] L. Calderoni, M. Ferrara, A. Franco, and D. Maio, "Indoor Localization in A Hospital Environment Using Random Forest Classifiers," *Expert Systems with Applications,* Vol. 42, No.1, pp. 125 - 134, 2015. DOI: 10.1016/j.eswa.2014.07.042

[70] A. Athalye, V. Savic, M. Bolic, and P. M. Djuric, "Novel Semi-Passive RFID System For Indoor Localization," *IEEE Sensors Journal,* Vol. 13, pp. 528 - 537, 2013. DOI: 10.1109/JSEN.2012.2220344

[71] D. Grewal, A. L. Roggeveen, and J. Nordfält, "The Future of Retailing," *Journal of Retailing,* Vol. 93, pp. 1 - 6, 2017.

[72] K. Zheng, H. Wang, H. Li, W. Xiang, L. Lei, J. Qiao*, et al.*, "Energy-Efficient Localization and Tracking of Mobile Devices in Wireless Sensor Networks," *IEEE Transactions on Vehicular Technology,* Vol. 66, pp. 2714 - 2726, 2017. DOI: 10.1109/TVT.2016.2584104

[73] M. Yassin and E. Rachid, "A Survey of Positioning Techniques and Location Based Services in Wireless Networks," *IEEE International Conference on Signal Processing, Informatics, Communication and Energy Systems (SPICES)*, pp. 1 – 5, 2015. DOI: 10.1109/SPICES.2015.7091420

[74] A. H. Sayed, A. Tarighat, and N. Khajehnouri, "Network-Based Wireless Location: Challenges Faced in Developing Techniques for Accurate Wireless Location Information," *IEEE Signal Processing Magazine,* Vol. 22, pp. 24 - 40, 2005. DOI: 10.1109/MSP.2005.1458275

[75] P. H. Tseng and K. T. Lee, "A Femto-Aided Location Tracking Algorithm in LTE-A Heterogeneous Networks," *IEEE Transactions on Vehicular Technology*, Vol. 66,No. 1, pp. 748 - 762, Jan. 2017. DOI: 10.1109/TVT.2016.2544790

[76] I. D. Constantiou, C. Lehrer, and T. Hess, "Changing Information Retrieval Behaviours: An Empirical Investigation Of Users' Cognitive Processes In The Choice Of Location-Based Services," *European Journal of Information Systems*, Vol. 23, pp. 513 - 528, September 2014. DOI: 10.1057/ejis.2014.12

[77] G. Zhao, X. Qian, and C. Kang, "Service Rating Prediction By Exploring Social Mobile Users; Geographical Locations," *IEEE Transactions on Big Data,* Vol. 3, pp. 67 - 78, 2017. DOI: 10.1109/TBDATA.2016.2552541

[78] J. T. Penttinen, "*The LTE-Advanced Deployment Handbook: The Planning Guidelines for the Fourth Generation Networks",* John Wiley & Sons, 2016.

[79] R. Y. Chan, X. Bai, X. Chen, S. Jia, and X.-h. Xu, "iBeacon and HCI in Special Education: Micro-Location Based Augmentative and Alternative Communication for Children with Intellectual Disabilities," *CHI Conference Extended Abstracts on Human Factors in Computing Systems*, pp. 1533 - 1539, 2016. DOI:10.1145/2851581.2892375

[80] E. S. Lohan, P. F. e Silva, A. Basiri, and P. Peltola, "*Location Based Services Analysis Through Analytical Hierarchical Processes: An e-Health-Based Case Study*," Multi-Technology Positioning, ed: Springer, pp. 283-301, 2017.

[81] A. Grillon, A. Perez-Uribe, H. Satizabal, L. Gantel, D. D. S. Andrade, A. Upegui, et al., "*A Wireless Sensor-Based System for Self-tracking Activity Levels Among Manual Wheelchair Users*," eHealth 360°, ed: Springer, pp. 229-240, 2017.

[82] A. Boulmakoul, L. Karim, A. Elbouziri, and A. Lbath, "A System Architecture for Heterogeneous Moving-Object Trajectory Metamodel Using Generic Sensors: Tracking Airport Security Case Study," *IEEE Systems Journal,* Vol. 9, pp. 283 - 291, 2015. DOI: 10.1109/JSYST.2013.2293837

[83] J. Wahlström, I. Skog, and P. Händel, "Smartphone-Based Vehicle Telematics: A Ten-Year Anniversary," *IEEE Transactions on Intelligent Transportation Systems, Vol.* PP, No. 99, pp. 1 - 24, 2017. DOI: 10.1109/TITS.2017.2680468

[84] W. Lin, J. Liu, Y. Zhou, and J. Huang, "Estimation Of TOA Based MUSIC Algorithm And Cross Correlation Algorithm Of Appropriate Interval," *AIP Conference Proceedings*, pp. 08 – 011, 2017.

[85] Y. Huang and Y. Xu, "Advanced Technology in GIS/GPS-Based Transportation Systems," *Recent Patents on Mechanical Engineering,* Vol. 10, pp. 18-29, 2017.

[86] M. A. Tayebi, M. Ester, U. Glässer and P. L. Brantingham, "CRIMETRACER: Activity Space Based Crime Location Prediction," *IEEE/ACM International Conference on Advances in Social Networks Analysis and Mining (ASONAM 2014)*, pp. 472 – 480, 2014. DOI: 10.1109/ASONAM.2014.6921628

[87] N. M. Drawil, H. M. Amar and O. A. Basir, "GPS Localization Accuracy Classification: A Context-Based Approach," *IEEE Transactions on Intelligent Transportation Systems*, Vol. 14, No. 1, pp. 262 - 273, March 2013. DOI: 10.1109/TITS.2012.2213815

[88] S. Dibb, "*Changing Times for Social Marketing Segmentation*," Segmentation in Social Marketing, ed: Springer, pp. 41 – 59, 2017.

[89] O. Ahlqvist, "*Location-Based Games*," The International Encyclopedia of Geography, 2017.

[90] M. Capra, M. Radenkovic, S. Benford, L. Oppermann, A. Drozd, and M. Flintham, "The Multimedia Challenges Raised by Pervasive Games," *13th annual ACM international conference on Multimedia*, pp. 89 - 95, 2005. DOI: 10.1145/1101149.1101163

[91] Z. Sun, L. Di, G. Heo, C. Zhang, H. Fang, P. Yue, et al., "Geofairy: Towards A One-Stop And Location Based Service For Geospatial Information Retrieval," *Computers, Environment and Urban Systems*, Vol. 62, pp. 156 - 167, March 2017. DOI: https://doi.org/10.1016/j.compenvurbsys.2016.11.007

[92] A. Roy, P. De, and N. Saxena, "Location-Based Social Video Sharing Over Next Generation Cellular Networks," *IEEE Communications Magazine,* Vol. 53, pp. 136 - 143, 2015. DOI: 10.1109/MCOM.2015.7295475

[93] J. Bao, Y. Zheng, D. Wilkie, and M. Mokbel, "Recommendations In Location-Based Social Networks: A Survey," GeoInformatica, Vol. 19, pp. 525 - 565, 2015.

[94] T. Deng, X. Wang, P. Fan, and K. Li, "Modelling and Performance Analysis of a Tracking-Area-List-Based Location Management Scheme in LTE Networks," *IEEE Transactions on Vehicular Technology,* Vol. 65, No. 8 pp. 6417 - 6431, August 2016. DOI: 10.1109/TVT.2015.2473704

[95] K. Katsaros, M. Dianati, R. Tafazolli, and X. Guo, "End-to-End Delay Bound Analysis for Location-Based Routing in Hybrid Vehicular Networks," *IEEE*

Transactions on Vehicular Technology, Vol. 65, No. 9, pp. 7462 - 7475, September 2016. DOI: 10.1109/TVT.2015.2482362

[96] A. Nessa, M. Kadoch, and B. Rong, "Fountain Coded Cooperative Communications for LTE-A Connected Heterogeneous M2M Network," *IEEE Access,* Vol. 4, pp. 5280-5292, 2016. DOI: 10.1109/ACCESS.2016.2601031

[97] P. Zhang, J. Lu, Y. Wang, and Q. Wang, "Cooperative Localization In 5G Networks: A Survey," *ICT Express,* Vol. 3, No. 1, pp. 27 - 32, March 2017 .DOI: 10.1016/j.icte.2017.03.005

[98] R. E. Hattachi, "*Next Generation Mobile Networks Alliance*", NGMN 5G White Paper*,* Vol. 1.0, pp. 1 - 125, February 2015.

[99] F. Boccardi, R. W. Heath, A. Lozano, T. L. Marzetta, and P. Popovski, "Five Disruptive Technology Directions For 5G," *IEEE Communications Magazine,* Vol. 52, No. 2, pp. 74 - 80, February 2014. DOI: 10.1109/MCOM.2014.6736746

[100] L. Hua and J. Dai, "A Location Authentication Scheme Based On Adjacent Users," *IEEE International Conference on Progress in Informatics and Computing*, pp. 158-162. 2014. DOI: 10.1109/PIC.2014.6972316

[101] Z. Dou, I. Khalil, and A. Khreishah, "A Novel and Robust Authentication Factor Based on Network Communications Latency," *IEEE Systems Journal,* Vol. PP, No. 99, pp. 1 - 12, 2017. DOI: 10.1109/JSYST.2017.2691550

[102] M. Thorpe, M. Kottkamp, A. Rössler, and J. Schütz, "*LTE Location Based Services Technology Introduction*," Rohde & Schwarz, 2013.

[103] U. Mahbub, S. Sarkar, V. M. Patel, and R. Chellappa, "Active User Authentication for Smartphones: A Challenge Data Set And Benchmark Results,"

IEEE 8th International Conference on Biometrics Theory, Applications and Systems (BTAS), pp. 1 - 8, 2016. DOI: 10.1109/BTAS.2016.7791155

[104] L. Fridman, S. Weber, R. Greenstadt and M. Kam, "Active Authentication on Mobile Devices via Stylometry, Application Usage, Web Browsing, and GPS Location," *IEEE Systems Journal*, Vol. 11, No. 2, pp. 513 - 521, June 2017. DOI: 10.1109/JSYST.2015.2472579

[105] C. Cummins, R. Orr, H. O'Connor, and C. West, "Global Positioning Systems (GPS) And Microtechnology Sensors in Team Sports: A Systematic Review," *Sports Medicine,* Vol. 43, No.10, pp. 1025 - 1042, 2013. DOI:10.1007/s40279-013-0069-2

[106] R. Pfeil, S. Schuster, and A. Stelzer, "Optimized Parameter Estimation for the LPM Local Positioning System," *IEEE Transactions on Instrumentation and Measurement,* Vol. 62, No.1 pp. 153 - 166, January 2013. DOI: 10.1109/TIM.2012.2212593

[107] R. Gierlich, J. Huettner, A. Ziroff, R. Weigel, and M. Huemer, "A Reconfigurable MIMO System for High-Precision FMCW Local Positioning," *IEEE Transactions on Microwave Theory and Techniques,* Vol. 59, No. 12, pp. 3228 - 3238, December 2011. DOI: 10.1109/TMTT.2011.2169079

[108] R. Di Taranto, S. Muppirisetty, R. Raulefs, D. Slock, T. Svensson, and H. Wymeersch, "Location-Aware Communications For 5G Networks: How Location Information Can Improve Scalability, Latency, And Robustness Of 5G," *IEEE Signal Processing Magazine,* Vol. 31, No. 6, pp. 102 - 112, November 2014. DOI: 10.1109/MSP.2014.2332611

[109] Z. Montazeri, A. Houmansadr and H. Pishro-Nik, "Achieving Perfect Location Privacy in Wireless Devices Using Anonymization," *IEEE Transactions on Information Forensics and Security*, Vol. 12, No. 11, pp. 2683 - 2698, November 2017. DOI: 10.1109/TIFS.2017.2713341

[110] K. Fawaz and K. G. Shin, "Location Privacy Protection For Smartphone Users," *ACM SIGSAC Conference on Computer and Communications Security*, pp. 239 - 250, November 2014. DOI: http://dx.doi.org/10.1145/2660267.2660270

[111] P. D. Groves, "*Principles of GNSS, Inertial, And Multisensor Integrated Navigation System,"* Artech house, 2nd Revised Edition, April 2013. ISBN-13: 978-1608070053

[112] Y. Gao, S. Liu, M. M. Atia, and A. Noureldin, "INS/GPS/LiDAR Integrated Navigation System For Urban And Indoor Environments Using Hybrid Scan Matching Algorithm," *Sensors Journal*, Vol. 15, pp. 23286 - 23302, 2015. DOI:10.3390/s150923286

[113] A. Angrisano, S. Gaglione and C. Gioia, "RAIM Algorithms For Aided GNSS In Urban Scenario," *2012 Ubiquitous Positioning, Indoor Navigation, and Location Based Service (UPINLBS)*, Helsinki, Finland, 2012, pp. 1 - 9. DOI: 10.1109/UPINLBS.2012.6409786

[114] Narula, K. P. Singh and M. G. Petovello, "Accelerated Collective Detection Technique For Weak GNSS Signal Environment," *2014 Ubiquitous Positioning Indoor Navigation and Location Based Service (UPINLBS)*, Corpus Christ, TX, 2014, pp. 81-89. DOI: 10.1109/UPINLBS.2014.7033713

[115] D. Margaria, E. Falletti and T. Acarman, "The Need For GNSS Position Integrity And Authentication In ITS: Conceptual And Practical Limitations In Urban Contexts," *2014 IEEE Intelligent Vehicles Symposium Proceedings*, Dearborn, MI, June 2014, pp.1384 - 1389. DOI: 10.1109/IVS.2014.6856485

[116] T. Váradi, M. Tadić, A. Gulyás, and M. Niculescu, "Language Technology in the Service of Intelligent Transport Systems," *22nd ITS World Congress*, Bordeaux, France, October 2015, pp. 2878 – 2889.

[117] P. Karbownik, G. Krukar, A. Shaporova, N. Franke, and T. von der Grün, "Evaluation of Indoor Real Time Localization Systems on the UWB Based System Case," 2015 International Conference on Indoor Positioning and Indoor Navigation (IPIN2015), Banff, Canada, October 2015.

[118] C. Luo, H. Hong and M. C. Chan, "PiLoc: A Self-Calibrating Participatory Indoor Localization System," *IPSN-14 Proceedings of the 13th International Symposium on Information Processing in Sensor Networks*, Berlin, 2014, pp. 143-153. DOI: 10.1109/IPSN.2014.6846748

[119] Z. Farid, R. Nordin, and M. Ismail, "Recent Advances in Wireless Indoor Localization Techniques and System," *Journal of Computer Networks and Communications,* Vol. 2013, pp. 1 – 13, August 2013. DOI: http://dx.doi.org/10.1155/2013/185138

[120] N. Simon, J. Bordoy, F. Höflinger, J. Wendeberg, M. Schink, R. Tannhäuser*, et al.*, "Indoor Localization System for Emergency Responders with Ultra Low-Power Radio Landmarks," *IEEE International Instrumentation and Measurement*

Technology Conference (I2MTC), pp. 309 - 314, 2015. DOI: 10.1109/I2MTC.2015.7151285

[121] J. Rantakokko, J. Rydell, P. Strömbäck, P. Händel, J. Callmer, D. Törnqvist*, et al.*, "Accurate and Reliable Soldier and First Responder Indoor Positioning: Multisensor Systems and Cooperative Localization," *IEEE Wireless Communications,* Vol. 18, No. 2, pp. 10 - 18, April 2011. DOI: 10.1109/MWC.2011.5751291

[122] R. Zhang, F. Hoflinger, and L. Reindl, "Inertial Sensor Based Indoor Localization And Monitoring System For Emergency Responders," *IEEE Sensors Journal,* Vol. 13, No. 2, pp. 838 - 848, February 2013. DOI: 10.1109/JSEN.2012.2227593

[123] J. O. Nilsson, J. Rantakokko, P. Händel, I. Skog, M. Ohlsson and K. V. S. Hari, "Accurate Indoor Positioning Of Firefighters Using Dual Foot-Mounted Inertial Sensors And Inter-Agent Ranging," *IEEE/ION Position, Location and Navigation Symposium,* pp. 631 - 636, May 2014. DOI: 10.1109/PLANS.2014.6851424

[124] H. Yoon, R. Shiftehfar, S. Cho, B. F. Spencer Jr, M. E. Nelson, and G. Agha, "Victim Localization And Assessment System For Emergency Responders," *Journal of Computing in Civil Engineering*, Vol. 30, pp. 1- 14 , August 2015. DOI: 10.1061/(ASCE)CP.1943-5487.0000483

[125] K. J. Wu, T. S. Gregory, J. Moore, B. Hooper, D. Lewis, and Z. T. H. Tse, "Development of An Indoor Guidance System for Unmanned Aerial Vehicles With Power Industry Applications," *IET Radar, Sonar & Navigation,* Vol. 11, No.1, pp. 212-218, April 2017. DOI: 10.1049/iet-rsn.2016.0232

[126] M. D. Souza, B. Schoots, and M. Ros, "Indoor Position Tracking Using Received Signal Strength-Based Fingerprint Context Aware Partitioning," *IET Radar, Sonar & Navigation,* Vol. 10, No. 8, pp. 1347-1355, October 2016. DOI: 10.1049/iet-rsn.2015.0396

[127] H. Koyuncu and S. H. Yang, "Improved Adaptive Localisation Approach For Indoor Positioning By Using Environmental Thresholds With Wireless Sensor Nodes," *IET Wireless Sensor Systems,* Vol. 5, No. 3, pp. 157-165, June 2015. DOI: 10.1049/iet-wss.2013.0100

[128] Z. Zhang, Z. Lu, V. Saakian, X. Qin, Q. Chen, and L.-R. Zheng, "Item-Level Indoor Localization With Passive UHF RFID Based On Tag Interaction Analysis," *IEEE Transactions on Industrial Electronics,* Vol. 61, No. 4, pp. 2122-2135, April 2014. DOI: 10.1109/TIE.2013.2264785

[129] S. Puri, "Indoor Positioning System Using Bluetooth," *International Journal of Engineering Research,* Vol. 4, No.5, pp: 244-247, May 2015. ISSN: (2319-6890) (online), 2347-5013 (print)

[130] F. Palumbo, P. Barsocchi, S. Chessa and J. C. Augusto, "A Stigmergic Approach To Indoor Localization Using Bluetooth Low Energy Beacons," *12th IEEE International Conference on Advanced Video and Signal Based Surveillance (AVSS)*, pp. 1-6, August 2015. DOI: 10.1109/AVSS.2015.7301734

[131] L. Chen, L. Pei, H. Kuusniemi, Y. Chen, T. Kröger, and R. Chen, "Bayesian Fusion for Indoor Positioning Using Bluetooth Fingerprints," *Wireless Personal Communications,* Vol. 70, No.4, pp. 1735-1745, June 2013. DOI: https://doi.org/10.1007/s11277-012-0777-1

[132] R. Faragher and R. Harle, "An Analysis of The Accuracy of Bluetooth Low Energy For Indoor Positioning Applications," *27th International Technical Meeting of The Satellite Division of the Institute of Navigation (ION GNSS+ 2014), Tampa, FL, USA*, pp. 201-210, September 2014.

[133] J. Niu, B. Wang, L. Shu, T. Q. Duong, and Y. Chen, "ZIL: An Energy-Efficient Indoor Localization System Using Zigbee Radio To Detect WIFI Fingerprints," *IEEE Journal on Selected Areas in Communications,* Vol. 33, No. 7 pp. 1431-1442, July 2015. DOI:10.1109/JSAC.2015.2430171

[134] C. Yang and H.-R. Shao, "WIFI-Based Indoor Positioning," *IEEE Communications Magazine,* Vol. 53, No. 3, pp. 150-157, March 2015. DOI: 10.1109/MCOM.2015.7060497

[135] C. H. Huang, L. H. Lee, C. C. Ho, L. L. Wu, and Z. H. Lai, "Real-Time RFID Indoor Positioning System Based on Kalman-Filter Drift Removal and Heron-Bilateration Location Estimation," *IEEE Transactions on Instrumentation and Measurement,* Vol. 64, No. 3, pp. 728-739, March 2015. DOI: 10.1109/TIM.2014.2347691

[136] S. Karakaya, H. Ocak, G. Küçükyildiz, and O. Kilinç, "A Hybrid Indoor Localization System Based on Infra-Red Imaging and Odometry," *International Conference on Image Processing, Computer Vision, and Pattern Recognition (IPCV)*, pp. 224-228, 2015.

[137] E. Martin-Gorostiza, F. J. Meca-Meca, J. L. Lázaro-Galilea, D. Salido-Monzú, E. Martos-Naya, and A. Wieser, "Infrared Local Positioning System Using Phase Differences," *Ubiquitous Positioning Indoor Navigation and Location Based*

Service (UPINLBS), pp. 238-247, November 2014. DOI: 10.1109/UPINLBS.2014.7033733

[138] M. C. Sundaramurthy, S. N. Chayapathy, A. Kumar and D. Akopian, "Wi-Fi Assistance To SUPL-Based Assisted-GPS Simulators For Indoor Positioning," *IEEE Consumer Communications and Networking Conference (CCNC)*, Las Vegas, NV, pp. 918-922, January 2011. DOI: 10.1109/CCNC.2011.5766641

[139] L. Liu, W. Zhang, C. Deng, S. Yin and S. Wei, "BriGuard: A Lightweight Indoor Intrusion Detection System Based On Infrared Light Spot Displacement," *IET Science, Measurement & Technology*, Vol. 9, No. 3, pp. 306-314, April 2015. DOI: 10.1049/iet-smt.2013.0171

[140] M. N. Husen and S. Lee, "Design Guideline Of Wi-Fi Fingerprinting In Indoor Localization Using Invariant Received Signal Strength," *International Conference on Information and Communication Technology (ICICTM)*, pp. 260-265, May 2016. DOI: 10.1109/ICICTM.2016.7890811

[141] N. Etemadyrad and J. K. Nelson, "A Sequential Detection Approach To Indoor Positioning Using RSS-Based Fingerprinting," *IEEE Global Conference on Signal and Information Processing (GlobalSIP)*, pp. 1127 - 1131, December 2016. DOI: 10.1109/GlobalSIP.2016.7906017

[142] M. Zhou, A. Wilford, Z. Tian, and Q. Zhang, "Composite Peer Hand-Shake Radio Map for Indoor WLAN Localization," *IEEE Sensors Letters,* Vol. 1, No.1, pp. 1-4, February 2017. DOI: 10.1109/LSENS.2017.2679018

[143] K. Finkenzeller, "*Fundamentals and Applications in Contactless Smart Cards, Radio Frequency Identification and Near-Field Communication*," Wiley, 3rd Edition, June 2010. ISBN: 978-0-470-69506-7

[144] S. A. Ahson and M. Ilyas, "*RFID Handbook: Applications, Technology, Security, And Privacy*," CRC press, March 2008. ISBN: 9781420054996

[145] K. Finkenzeller, "*RFID Security: Techniques, Protocols, and System-On-Chip Design,*" Springer, November 2008. ISBN: 978-0-387-76480-1

[146] P. Kolhe, R. Dharaskar, M. Tharkar, S. Joshi, S. Desai, and B. Dapoli, "Information Technology Tool In Library Barcode & Radio Frequency Identification RFID," *International Journal of Innovative Science Engineering and Technology (IJISET),* Vol. 3, No.1, pp. 81 - 86, January 2016. ISSN 2348 – 7968

[147] F. Abate, G. Di Leo, A. Paolillo, and V. Paciello, "An Advanced Traceability System Based On Semiactive RFID Devices," *20th IMEKO TC4 Symposium on Measurements of Electrical Quantities: Research on Electrical and Electronic Measurement for the Economic Upturn, Together with 18th TC4 International Workshop on ADC and DCA Modelling and Testing, IWADC 2014*, pp. 1106 - 1109, September 2014. ISBN-14: 978-92-990073-2-7

[148] L. McIntyre, K. Michael, and K. Albrecht, "RFID: Helpful New Technology or Threat to Privacy and Civil Liberties?," *IEEE Potentials,* Vol. 34, No. 5, pp. 13 - 18, Sept.-October 2015. DOI: 10.1109/MPOT.2015.2410392

[149] H. Knospe and H. Pohl, "RFID Security," *Information Security Technical Report,* Vol. 9, No. 4, pp. 39 - 50, 2004. DOI:/10.1016/S1363-4127(05)70039-X

[150] F. Rahman, M. Z. A. Bhuiyan and S. I. Ahamed, "A Privacy Preserving Framework For RFID Based Healthcare Systems," *Future Generation Computer Systems,* Vol. 72, pp. 339 - 352, July 2017. DOI: /10.1016/j.future.2016.06.001

[151] R. Doss, S. Sundaresan, and W. Zhou, "A Practical Quadratic Residues Based Scheme For Authentication And Privacy In Mobile RFID Systems," *Ad Hoc Networks,* Vol. 11, No. 1 pp. 383-396, January 2013. DOI: /10.1016/j.adhoc.2012.06.015

[152] Information technology--Smart transducer interface for sensors and actuators--Part 7: Transducers to radio frequency identification (RFID) systems communication protocols and transducer electronic data sheet (TEDS) formats," *ISO/IEC/IEEE 21451-7:2011(E) (Revision of 1451.7-2010)*, pp.1 - 92, February 2012. DOI: 10.1109/IEEESTD.2012.6155051

[153] F. Thornton and C. Lanthem, "*RFID Security*," Springer, 1st Edition, June 2005. ISBN: 9781597490474

[154] F. P. Cortes *et al*., "A Low-Power RF/Analog Front-End Architecture For LF Passive RFID Tags With Dynamic Power Sensing," *IEEE International Conference on RFID (IEEE RFID)*, Orlando, FL, April 2014, pp. 60 - 66. DOI: 10.1109/RFID.2014.6810713

[155] J. Fernández-Salmerón, A. Rivadeneyra, M. A. C. Rodríguez, L. F. Capitan-Vallvey and A. J. Palma, "HF RFID Tag as Humidity Sensor: Two Different Approaches," in *IEEE Sensors Journal*, Vol. 15, No. 10, pp. 5726 - 5733, October 2015. DOI: 10.1109/JSEN.2015.2447031

[156] L. R. M. Costa, "UHF RFID Tags In A Controlled Environment: Anechoic Chamber Case," *2015 IEEE Brasil RFID*, Sao Paulo, 2015, pp. 1 - 5. DOI: 10.1109/BrasilRFID.2015.7523836

[157] V. Bhogal, Z. G. Prodanoff, S. P. Ahuja, and K. Martin, "On BFSA Collision Resolution in LF, HF, and UHF RFID Networks," *International Journal of Wireless Networks and Broadband Technologies (IJWNBT),* Vol. 4, pp. 44 - 55, 2015. DOI: 10.4018/IJWNBT.2015040104

[158] T. J. Gallagher, B. Li, A. G. Dempster, and C. Rizos, "Power Efficient Indoor/Outdoor Positioning Handover," *Procs 2nd Int. Conf. on Indoor Positioning & Indoor Navigation*, Guimarães, Portugal, 21-23 September 2011.

[159] M. Aftatah, A. Lahrech and A. Abounada, "Fusion Of GPS/INS/Odometer Measurements For Land Vehicle Navigation With GPS Outage," *2nd International Conference on Cloud Computing Technologies and Applications (CloudTech)*, pp. 48 - 55, 2016. DOI**:** 10.1109/CloudTech.2016.7847724

[160] G. Huang, D. Akopian, and C. L. P. Chen, "Network Delay Modeling For Assisted GPS," *IEEE Transactions on Aerospace and Electronic Systems,* Vol. 51, No. 1, pp. 52 - 64, January 2015. DOI**:** 10.1109/TAES.2014.120686

[161] S. Sand, A. Dammann, and C. Mensing, "*Positioning in Wireless Communications Systems*," John Wiley & Sons, April 2014. ISBN: 978-0-470-77064-1

[162] S. Fischer, "*Observed time difference of arrival (OTDOA) positioning in 3GPP LTE*," Qualcomm White Paper, June 2014.

[163] D. Asghar, M. Zubair, and D. Ahmad, "A Review of Location Technologies for Wireless Mobile Location-Based Services," *Journal of American Science,* Vol. 10, No. 7, pp. 110 - 118, June 2014. (ISSN:1545-1013)

[164] M. N. Borenovic, M. I. Simic, A. M. Neskovic, and M. M. Petrovic, "Enhanced Cell-ID + TA GSM Positioning Technique," *EUROCON 2005 - The International Conference on "Computer as a Tool"*, pp. 1176 - 1179, November 2005. DOI: 10.1109/EURCON.2005.1630164

[165] N. Deblauwe and P. Ruppel, "Combining GPS And GSM Cell-ID Positioning For Proactive Location-Based Services," *Fourth Annual International Conference on Mobile and Ubiquitous Systems: Networking & Services (MobiQuitous)*, pp. 1 - 7, August 2007. DOI**:** 10.1109/MOBIQ.2007.4450985

[166] D. Papadimitriou and I. Vardiambasis, "Hybrid Algorithms For Adaptive Array Systems," *4th International Conference on Telecommunications and Informatics*, TELE-INFO, pp. 1 - 6, 2005.

[167] A. Bensky, "*Wireless positioning technologies and applications*," Artech House, 2nd Edition, 2016. ISBN: 9781608079513

[168] T. Islam, "*System And Method For Hybrid Location In A CDMA 2000 Network*," Google Patents, 2011.

[169] M. Z. Asghar, S. Ahmad, M. R. Yasin, M. Qasim, "A Review of Location Technologies for Wireless Mobile Location-Based Services," *Journal of American Science*, Vol. 10, No. 7, pp. 110 – 118, 2014. (ISSN: 1545-1003)

[170] T. K. Bhattacharya, "*Estimating The Location Of A Wireless Terminal Based On Assisted GPS And Pattern Matching*," Google Patents, November 2007.

[171] A. Havlark, V. Burton, and J. Ahrens, "Wireless Telecommunications Location Based Services Scheme Selection," Google Patents, January 2003.

[172] G. Huang, D. Akopian, and C. P. Chen, "Network Delay Modeling For Assisted GPS," *IEEE Transactions on Aerospace and Electronic Systems,* Vol. 51, No. 1, pp. 52 - 64, January 2015. DOI**:** 10.1109/TAES.2014.120686

[173] J. Joung, Y. K. Chia, and S. Sun, "Energy-Efficient, Large-Scale Distributed-Antenna System (L-DAS) For Multiple Users," *IEEE Journal of Selected Topics in Signal Processing,* Vol. 8, No. 5, pp. 954 - 965, October 2014. DOI**:** 10.1109/JSTSP.2014.2309942

[174] S. Jeong, O. Simeone, A. Haimovich, and J. Kang, "Beamforming Design For Joint Localization And Data Transmission In Distributed Antenna System," *IEEE Transactions on Vehicular Technology,* Vol. 64, No. 1, pp. 62 - 76, January 2015. DOI**:** 10.1109/TVT.2014.2317831

[175] S. V. SV, S. Srikanth, and V. Ramaiyan, "Performance Analysis Of An IEEE 802.11 Ac WLAN With Dynamic Bandwidth Channel Access," *Twenty Second National Conference on Communication (NCC)*, pp. 1 - 6, 2016.

[176] O. Bejarano, E. W. Knightly and M. Park, "IEEE 802.11ac: From Channelization To Multi-User MIMO," *IEEE Communications Magazine*, Vol. 51, No. 10, pp. 84 - 90, October 2013. DOI: 10.1109/MCOM.2013.6619570

[177] Eng Hwee Ong, J. Kneckt, O. Alanen, Z. Chang, T. Huovinen and T. Nihtilä, "IEEE 802.11ac: Enhancements For Very High Throughput WLANS," *IEEE 22nd International Symposium on Personal, Indoor and Mobile Radio Communications*, Toronto, ON, September 2011, pp. 849-853. DOI: 10.1109/PIMRC.2011.6140087

[178] C. Luo, L. Cheng, M. C. Chan, Y. Gu, J. Li and Z. Ming, "Pallas: Self-Bootstrapping Fine-Grained Passive Indoor Localization Using WiFi Monitors," *IEEE Transactions on Mobile Computing*, Vol. 16, No. 2, pp. 466 - 481, February 2017. DOI: 10.1109/TMC.2016.2550452

[179] N. Goga *et al*., "Evaluating Indoor Localization Using Wifi For Patient Tracking," *International Symposium on Fundamentals of Electrical Engineering (ISFEE)*, Bucharest, July 2016, pp. 1-4. DOI: 10.1109/ISFEE.2016.7803173

[180] M. L. Damiani, "Third Party Geolocation Services In LBS: Privacy Requirements And Research Issues," *Transactions on Data Privacy*, Vol. 4, pp. 55 -72, August 2011.

[181] E. Laitinen and E. S. Lohan, "Access Point Topology Evaluation And Optimization Based On Cramér-Rao Lower Bound For WLAN Indoor Positioning," *International Conference on Localization and GNSS (ICL-GNSS)*, Barcelona, August 2016, pp. 1 -5. DOI: 10.1109/ICL-GNSS.2016.7533850

[182] N. Chatzipanagiotis and M. M. Zavlanos, "Distributed Scheduling of Network Connectivity Using Mobile Access Point Robots," in *IEEE Transactions on Robotics*, Vol. 32, No. 6, pp. 1333 - 1346, December 2016. DOI: 10.1109/TRO.2016.2593041

[183] A. Pham, K. Huguenin, I. Bilogrevic, I. Dacosta and J. P. Hubaux, "SecureRun: Cheat-Proof and Private Summaries for Location-Based Activities," in *IEEE Transactions on Mobile Computing*, Vol. 15, No. 8, pp. 2109 - 2123, August 2016. DOI: 10.1109/TMC.2015.2483498

[184] M. Outmesguine, "*Wi-Fi Toys: 15 Cool Wireless Projects For Home, Office, And Entertainment*", Wiley, July 2004. ISBN: 978-0-7645-5894-8

[185] I. F. Akyildiz, W. Wang, and Y.-J. Lee, "Location Management In 3G/4G Wireless Systems," *SPIE - The Convergence of Information Technologies and Communications (ITCom 2001) Conference*, Denver, USA, July 2001. DOI: 10.1117/12.434442

[186] H. Yoon, Y. Ham, M. Golparvar-Fard, and B. F. Spencer, "Forward-Backward Approach for 3D Event Localization Using Commodity Smartphones for Ubiquitous Context-Aware Applications in Civil and Infrastructure Engineering," *Computer-Aided Civil and Infrastructure Engineering*, Vol. 31, pp. 245-260, June 2015. DOI: 10.1111/mice.12154

[187] Z. Zhang, X. Zhou, W. Zhang, Y. Zhang, G. Wang, B. Y. Zhao, et al., "I Am The Antenna: Accurate Outdoor Ap Location Using Smartphones," *17th annual international conference on Mobile computing and networking*, pp. 109-120, September 2011.

[188] N. Krommenacker, Ó. C. Vásquez, M. D. Alfaro and I. Soto, "A Self-Adaptive Cell-ID Positioning System Based On Visible Light Communications In Underground Mines," *IEEE International Conference on Automatica (ICA-ACCA)*, Curico, October 2016, pp. 1 - 7. DOI: 10.1109/ICA-ACCA.2016.7778427

[189] R. Margolies, R. Becker, S. Byers, S. Deb, R. Jana, S. Urbanek, et al., "Can You Find Me Now? Evaluation of Network-based Localization in a 4G LTE Network," *IEEE INFOCOM 2017*, 2017.

[190] K. Abed-Meraim, "Mobile Localization Techniques," *IEEE International Conference on Signal Processing and Communications*, Dubai, November 2007, pp. xlvi - xlvii.DOI: 10.1109/ICSPC.2007.4728235

[191] S. A. Shaukat, K. Munawar, M. Arif, A. I. Bhatti, U. I. Bhatti and U. M. Al-Saggaf, "Robust Vehicle Localization With GPS Dropouts," *6th International Conference on Intelligent and Advanced Systems (ICIAS)*, Kuala Lumpur, August 2016, pp. 1-6. DOI: 10.1109/ICIAS.2016.7824135

[192] J. Racko, P. Brida, A. Perttula, J. Parviainen and J. Collin, "Pedestrian Dead Reckoning with Particle Filter for handheld smartphone," *International Conference on Indoor Positioning and Indoor Navigation (IPIN)*, Alcala de Henares, October 2016, pp. 1 - 7. DOI: 10.1109/IPIN.2016.7743608

[193] S. Qiu, Z. Wang, H. Zhao, K. Qin, Z. Li, and H. Hu, "Inertial/Magnetic Sensors based Pedestrian Dead Reckoning by Means of Multi-sensor Fusion," *Information Fusion*, Vol. 39, pp 108 – 119, January 2018. DOI: https://doi.org/10.1016/j.inffus.2017.04.006

[194] Y. H. Cheng, Q. H. Meng, Y. J. Liu, M. Zeng, L. Xue and S. G. Ma, "Fusing Sound And Dead Reckoning For Multi-Robot Cooperative Localization," *12th World Congress on Intelligent Control and Automation (WCICA)*, Guilin, 2016, pp.1474 - 1478. DOI: 10.1109/WCICA.2016.7578703

[195] P. Xu, B. Yan, and S. Hu, "Angle of arrival (AOA)-based Cross-localization Algorithm using Orientation Angle for Improved Target Estimation in Far-field Environments," *International Journal of Simulation--Systems, Science & Technology*, Vol. 17, pp. 1 – 8, 2016.

[196] Y. Norouzi, E. S. Kashani and A. Ajorloo, "Angle Of Arrival-Based Target Localisation With Low Earth Orbit Satellite Observer," *IET Radar, Sonar & Navigation*, Vol. 10, No. 7, pp. 1186 - 1190, July 2016. DOI: 10.1049/iet-rsn.2015.0437

[197] A. Badawy, T. Khattab, D. Trinchero, T. M. Elfouly and A. Mohamed, "A Simple Cross Correlation Switched Beam System (XSBS) for Angle of Arrival Estimation," *IEEE Access*, Vol. 5, No. , pp. 3340 - 3352, February 2017. DOI: 10.1109/ACCESS.2017.2669202

[198] A. Chamseddine, O. Akhrif, F. Gagnon and D. Couillard, "Communication Relay For Multi-Ground Units Using Unmanned Aircraft," *14th International Conference on Control, Automation, Robotics and Vision (ICARCV)*, Phuket, November 2016, pp. 1 - 6. DOI: 10.1109/ICARCV.2016.7838647

[199] M. Dirix and D. Heberling, "Full-Sphere Angle of Arrival Detection using CMRCLEAN," *IEEE Transactions on Antennas and Propagation*, Vol. 65, No. 5, pp. 2769 - 2772, May 2017. DOI: 10.1109/TAP.2017.2670568.

[200] J. Moghaddasi, T. Djerafi, and K. Wu, "Multiport Interferometer-Enabled 2-D Angle of Arrival (AOA) Estimation System," *IEEE Transactions on Microwave Theory and Techniques*, Vol. 65, No. 5, pp. 1767 - 1779, May 2017. DOI: 10.1109/TMTT.2017.2690869

[201] L. Zimmermann, A. Goetz, G. Fischer, and R. Weigel, "Performance Analysis of Time Difference of Arrival and Angle of Arrival Estimation Methods for GSM Mobile Phone Localization," *Communication, Signal Processing &*

Information Technology: Extended Papers from the Multiconference on Signals, Systems and Devices, p. 17 -34, 2017.

[202] A. Dempster, "Dilution Of Precision In Angle-Of-Arrival Positioning Systems," *Electronics Letters*, Vol. 42, pp. 291 - 292, April 2006. DOI: 10.1049/el:20064410

[203] J. Uren and W. F. Price, "*Surveying for Engineers*," Palgrave Macmillan, 5th Edition, March 2010. ISBN-13**:** 978-0230221574

[204] C. Wong, R. Klukas, and G. Messier, "Using WLAN Infrastructure For Angle-Of-Arrival Indoor User Location," *IEEE 68th Vehicular Technology Conference*, pp. 1 - 5, September 2008. DOI:10.1109/VETECF.2008.146

[205] S. Jeong, J. Kang, K. Pahlavan, and V. Tarokh, "Fundamental Limits of TOA/DOA and Inertial Measurement Unit-Based Wireless Capsule Endoscopy Hybrid Localization," *International Journal of Wireless Information Networks*, pp. 1 - 11, February 2017. DOI: 10.1007/s10776-017-0342-7

[206] X. Wang, L. Gao, S. Mao, and S. Pandey, "CSI-Based Fingerprinting For Indoor Localization: A Deep Learning Approach," *IEEE Transactions on Vehicular Technology*, Vol. 66, pp. 763-776, 2017.

[207] Y. Shu, Y. Huang, J. Zhang, P. Coué, P. Cheng, J. Chen, et al., "Gradient-Based Fingerprinting For Indoor Localization And Tracking," *IEEE Transactions on Industrial Electronics*, Vol. 63, pp. 2424-2433, April 2016. DOI**:** 10.1109/TIE.2015.2509917

[208] J. Yim, "Comparison between RSSI-based and TOF-based Indoor Positioning Methods," International Journal of Multimedia and Ubiquitous Engineering, Vol. 7, No. 2, pp. 221 – 234, April 2012.

[209] C. Steiner and A. Wittneben, "Efficient Training Phase for Ultrawideband-Based Location Fingerprinting Systems," IEEE Transactions on Signal Processing, Vol. 59, No. 12 pp. 6021 - 6032, December 2011. DOI: 10.1109/TSP.2011.2166390

[210] C. M. Bishop, "*Pattern recognition and machine learning*," Springer, 1st Edition, February 2007.

[211] V. Honkavirta, T. Perala, S. Ali-Loytty, and R. Piché, "A Comparative Survey Of WLAN Location Fingerprinting Methods," *6th Workshop on Positioning, Navigation and Communication*, pp. 243 – 251, March 2009. DOI: 10.1109/WPNC.2009.4907834

[212] M. A. Youssef, A. Agrawala, and A. Udaya Shankar, "WLAN Location Determination Via Clustering And Probability Distributions," *1st IEEE International Conference on Pervasive Computing and Communications*, pp. 143 - 150, April 2003. DOI: 10.1109/PERCOM.2003.1192736

[213] L. Koski, R. Piché, V. Kaseva, S. Ali-Löytty and M. Hännikäinen, "Positioning With Coverage Area Estimates Generated From Location Fingerprints," *7th Workshop on Positioning, Navigation and Communication*, Dresden, pp. 99 – 106, March 2010. DOI: 10.1109/WPNC.2010.5653409

[214] S. He and S. H. G. Chan, "Tilejunction: Mitigating Signal Noise for Fingerprint-Based Indoor Localization," *IEEE Transactions on Mobile Computing*, Vol. 15, No. 6, pp. 1554 - 1568, June 2016. DOI: 10.1109/TMC.2015.2463287

[215] T. Xue, X. Dong and Y. Shi, "Resource-Allocation Strategy for Multiuser Cognitive Radio Systems: Location-Aware Spectrum Access," *IEEE Transactions on Vehicular Technology*, Vol. 66, No. 1, pp. 884-889, January 2017. DOI: 10.1109/TVT.2016.2531738

[216] L. Zeng and G. Weber, "Exploration of Location-Aware You-Are-Here Maps on a Pin-Matrix Display," *IEEE Transactions on Human-Machine Systems*, Vol. 46, No. 1, pp. 88 - 100, February 2016. DOI: 10.1109/THMS.2015.2477999

[217] C. Chen, X. Meng, Z. Xu and T. Lukasiewicz, "Location-Aware Personalized News Recommendation With Deep Semantic Analysis," *IEEE Access*, Vol. 5, pp. 1624 - 1638, January 2017. DOI: 10.1109/ACCESS.2017.2655150

[218] Y. Wang, D. Xu and F. Li, "Providing Location-Aware Location Privacy Protection For Mobile Location-Based Services," *Tsinghua Science and Technology*, Vol. 21, No. 3, pp. 243 - 259, June 2016. DOI: 10.1109/TST.2016.7488736

[219] Y. Huang, Z. Liu and P. Nguyen, "Location-Based Event Search In Social Texts," *2015 International Conference on Computing, Networking and Communications (ICNC)*, Garden Grove, CA, 2015, pp. 668-672. DOI: 10.1109/ICCNC.2015.7069425

[220] W. Xu and C. Y. Chow, "A Location- and Diversity-Aware News Feed System for Mobile Users," *IEEE Transactions on Services Computing*, Vol. 9, No. 6, pp. 846 - 861, December 2016. DOI: 10.1109/TSC.2015.2436396

[221] S. Qi, D. Wu and N. Mamoulis, "Location Aware Keyword Query Suggestion Based On Document Proximity," *IEEE 32nd International Conference on Data Engineering (ICDE)*, Helsinki, 2016, pp. 1566 - 1567. DOI: 10.1109/ICDE.2016.7498428

[222] S. Benford, C. Magerkurth, and P. Ljungstrand, "Bridging The Physical And Digital In Pervasive Gaming," *Communications of the ACM*, Vol. 48, pp. 54 - 57, March 2005. DOI: 10.1145/1047671.1047704

[223] H. Ghafghazi, A. Elmougy, H. T. Mouftah, and C. Adams, "Location-Aware Authorization Scheme for Emergency Response," *IEEE Access*, Vol. 4, pp. 4590-4608, August 2016. DOI: 10.1109/ACCESS.2016.2601442

[224] K. Lee, W.-C. Lee, B. Zheng, and J. Xu, "Caching Complementary Space For Location-Based Services," *Advances in Database Technology-EDBT 2006*, pp. 1020 - 1038, 2006.

[225] R. Oorni and A. Goulart, "In-Vehicle Emergency Call Services: eCall and Beyond," *IEEE Communications Magazine*, Vol. 55, pp. 159 - 165, January 2017. DOI: 10.1109/MCOM.2017.1600289CM

[226] C. Evans, "Intelligent Retail Business: Location Based Services for Mobile Customers," *2007 2nd International Conference on Pervasive Computing and Applications*, Birmingham, pp. 354 – 359, July 2007. DOI: 10.1109/ICPCA.2007.4365468

[227] A. LaMarca and Eyal de Lara, "*Location Systems: An Introduction to the Technology Behind Location Awareness*," Morgan & Claypool, 2008. DOI: (https://doi.org/10.2200/S00115ED1V01Y200804MPC004)

[228] F. H. Bruneteau, Thomas; Lumbreras, Cristina ; O'Brien, Tony; Heward, Andy, "Caller Location in Support of Emergency Services," *Europen emergency number association (EENA)*, Vol. 2.0, pp. 1 – 30, November 2014.

[229] A. J. Jara, Y. Bocchi, D. Genoud, I. Thomas and L. Lambrinos, "Enabling Federated Emergencies And Public Safety Answering Points With Wearable And Mobile Internet Of Things Support: An Approach Based On EENA And OMA LWM2M Emerging Standards," *IEEE International Conference on Communications (ICC)*, London, pp. 679-684, June 2015. DOI: 10.1109/ICC.2015.7248400

[230] J. Raper, G. Gartner, H. Karimi, and C. Rizos, "Applications Of Location–Based Services: A Selected Review," *Journal of Location Based Services*, Vol. 1, pp. 89-111, December 2007. DOI: http://dx.doi.org/10.1080/17489720701862184

[231] A. M. Hendawi, M. Khalefa, H. Liu, M. Ali, and J. A. Stankovic, "A Vision For Micro And Macro Location Aware Services," *24th International Conference on Advances in Geographic Information Systems*, 2016. ISBN: 978-1-4503-4589-7

[232] B. Klein and U.-D. Reips, "Innovative Social Location-aware Services for Mobile Phones," *The SAGE Handbook of Social Media Research Methods*, p. 421, 2017.

[233] J. Baus, A. Krüger, and W. Wahlster, "A Resource-Adaptive Mobile Navigation System," *7th International Conference On Intelligent User Interfaces*, pp. 15 - 22, 2002.

[234] M. Pagani and G. Malacarne, "Experiential Engagement and Active vs. Passive Behavior in Mobile Location-based Social Networks: The Moderating Role of Privacy," *Journal of Interactive Marketing*, Vol. 37, pp. 133-148, January 2017. DOI: 10.1016/j.intmar.2016.10.001

[235] A. Krüger, J. Baus, D. Heckmann, M. Kruppa, and R. Wasinger, "*Adaptive Mobile Guides,*" Springer, Vol 4321 pp. 521-549, 2007. DOI: https://doi.org/10.1007/978-3-540-72079-9_17

[236] J. Santa, F. Pereniguez-Garcia, F. Bernal, P. J. Fernandez, R. Marin-Lopez and A. F. Skarmeta, "A Framework for Supporting Network Continuity in Vehicular IPv6 Communications," *IEEE Intelligent Transportation Systems Magazine*, Vol. 6, No. 1, pp. 17 - 34, Spring 2014. DOI: 10.1109/MITS.2013.2274876

[237] M. Birsak, P. Musialski, P. Wonka and M. Wimmer, "Dynamic Path Exploration on Mobile Devices," in *IEEE Transactions on Visualization and Computer Graphics*, Vol. PP, No. 99, pp. 1 - 1. DOI: 10.1109/TVCG.2017.2690294

[238] T. S. Cooner, A. Knowles, and B. Stout, "Creating A Mobile App To Teach Ethical Social Media Practices," *Social Work Education*, Vol. 35, pp. 245 - 259, 2016.

[239] H. Fouchal, E. Bourdy, G. Wilhelm and M. Ayaida, "A Framework for Validation of Cooperative Intelligent Transport Systems," *IEEE Global Communications Conference (GLOBECOM)*, Washington, DC, 2016, pp. 1 - 6. DOI: 10.1109/GLOCOM.2016.7841500

[240] A. Karapantelakis, A. Vulgarakis, L. Mokrushin, R. Inam, C. Azevedo, K. Raizer, et al., "A Framework For Knowledge Management And Automated Reasoning Applied On Intelligent Transport Systems," January 2017.

[241] K. Malone, A. Silla, C. Johanssen, and D. Bell, "Safety, Mobility And Comfort Assessment Methodologies Of Intelligent Transport Systems For Vulnerable Road Users," *European Transport Research Review*, Vol. 9, pp. 21, 2017.

[242] E. Osaba, E. Onieva, A. Moreno, P. Lopez-Garcia, A. Perallos, and P. G. Bringas, "Decentralised Intelligent Transport System With Distributed Intelligence Based On Classification Techniques," *IET Intelligent Transport Systems*, Vol. 10, pp. 674 - 682, 2016.

[243] H. A. Karimi and A. Hammad, "*Telegeoinformatics: Location-Based Computing And Services*," CRC Press, March 2004. ISBN 9780415369763

[244] K. Sjoberg, P. Andres, T. Buburuzan and A. Brakemeier, "Cooperative Intelligent Transport Systems in Europe: Current Deployment Status and Outlook," *IEEE Vehicular Technology Magazine*, Vol. 12, No. 2, pp. 89 - 97, June 2017. DOI: 10.1109/MVT.2017.2670018

[245] D. N. Tien, T. MacDonald and Z. Xu, "TDplanner: Public Transport Planning System with Real-Time Route Updates Based on Service Delays and Location Tracking," *IEEE 73rd Vehicular Technology Conference (VTC Spring)*, Yokohama, 2011, pp. 1 - 5. DOI: 10.1109/VETECS.2011.5956479

[246] V. R. Tomás, M. Pla-Castells, J. J. Martínez and J. Martínez, "Forecasting Adverse Weather Situations in the Road Network," *IEEE Transactions on*

Intelligent Transportation Systems, Vol. 17, No. 8, pp. 2334 - 2343, August 2016. DOI: 10.1109/TITS.2016.2519103

[247] J. Joshi, A. Singh, L. G. Moitra, and M. J. Deka, "DASITS: Driver Assistance System in Intelligent Transport System," *30th International Conference on Advanced Information Networking and Applications Workshops (WAINA)*, pp. 545 – 550, 2016.

[248] K. Siddiqi, A. D. Raza, and S. S. Muhammad, "Visible Light Communication For V2V Intelligent Transport System," *International Conference on Broadband Communications for Next Generation Networks and Multimedia Applications (CoBCom)*, pp. 1 – 4, 2016.

[249] H. KaiSheng, H. Jianye, L. RongSheng, and R. Dakai, "Energy Consumption Optimization Of Vehicle Power System Based On Big Data," *IET International Conference on Intelligent and Connected Vehicles (ICV 2016)*, pp. 1-6, 2016.

[250] C. A. R. L. Brennand, F. D. da Cunha, G. Maia, E. Cerqueira, A. A. F. Loureiro and L. A. Villas, "FOX: A Traffic Management System Of Computer-Based Vehicles FOG," *IEEE Symposium on Computers and Communication (ISCC)*, Messina, pp. 982 – 987, 2016. DOI: 10.1109/ISCC.2016.7543864

[251] K. H. Johansson, "Cyber-Physical Control of Road Freight Transport," *2016 IEEE International Conference on Autonomic Computing (ICAC)*, Wurzburg, pp. 4 – 4, 2016. DOI: 10.1109/ICAC.2016.47

[252] M. Aldibaja, N. Suganuma and K. Yoneda, "Robust Intensity-Based Localization Method for Autonomous Driving on Snow–Wet Road Surface," in *IEEE*

Transactions on Industrial Informatics, Vol. 13, No. 5, pp. 2369 - 2378, October 2017. DOI: 10.1109/TII.2017.2713836

[253] A.-M. Roxin, C. Dumez, M. Wack, and J. Gaber, "Middleware Models For Location-Based Services: A Survey," *2nd international workshop on Agent-oriented software engineering challenges for ubiquitous and pervasive computing*, pp. 35-40, 2008.

[254] F. J. Martinez, C.-K. Toh, J.-C. Cano, C. T. Calafate, and P. Manzoni, "Emergency Services In Future Intelligent Transportation Systems Based On Vehicular Communication Networks," Intelligent Transportation Systems Magazine, IEEE, Vol. 2, pp. 6 - 20, 2010.

[255] J. Huang and P. Uys, "A Location-Based Services System (LBSS) Designed For An Arboretum," *2012 IEEE/ION Position, Location and Navigation Symposium*, Myrtle Beach, SC, 2012, pp. 1008 - 1012. DOI: 10.1109/PLANS.2012.6236842

[256] S. Benford, W. Seager, M. Flintham, R. Anastasi, D. Rowland, J. Humble, et al., "The Error Of Our Ways: The Experience Of Self-Reported Position In A Location-Based Game," *UbiComp 2004: Ubiquitous Computing*, pp. 70 - 87, 2004.

[257] J. Garay-Cortes and A. Uribe-Quevedo, "Location-Based Augmented Reality Game To Engage Students In Discovering Institutional Landmarks," *7th International Conference on Information, Intelligence, Systems & Applications (IISA)*, pp. 1 - 4, 2016.

[258] J. Melero and D. HernÁndez-Leo, "Design and Implementation of Location-Based Learning Games: Four Case Studies with “QuesTInSitu: The Game”,” *IEEE*

Transactions on Emerging Topics in Computing, Vol. 5, No. 1, pp. 84 - 94, March 2017. DOI: 10.1109/TETC.2016.2615861

[259] C. Nolêto, M. Lima, L. F. Maia, W. Viana, and F. Trinta, "An Authoring Tool for Location-Based Mobile Games with Augmented Reality Features," *14th Brazilian Symposium on Computer Games and Digital Entertainment (SBGames)*, pp. 99 – 108, 2015.

[260] J. Shin, J. Kim, and W. Woo, "Narrative Design For Rediscovering Daereungwon: A Location-Based Augmented Reality Game," *IEEE International Conference on Consumer Electronics (ICCE)*, pp. 384 – 387, 2017.

[261] C. Magerkurth, A. D. Cheok, R. L. Mandryk, and T. Nilsen, "Pervasive Games: Bringing Computer Entertainment Back To The Real World," *Computers in Entertainment (CIE)*, Vol. 3, pp. 4 - 4, 2005.

[262] M. Laibowitz, v. samanta, S. Ali and R. Azuma, "Chamber of Mirrors: A Socially Activated Game Exploits Pervasive Technology," *IEEE Pervasive Computing*, Vol. 11, No. 2, pp. 38 - 45, Feb. 2012. DOI: 10.1109/MPRV.2012.18

[263] E. Pasher, G. Bendersky, H. Raz and G. Gabrielli, “Pervasive Games,” *Directory of Open Access Journals*, Vol. 1, pp. 1 – 2, January 2015. DOI: https://doi.org/10.4108/sg.1.4.e1

[264] R. Dörner, S. Göbel, W. Effelsberg, and J. Wiemeyer, “*Serious Games: Foundations, Concepts and Practice*,” Springer, August 2016.

[265] H. Petrie, V. Johnson, T. Strothotte, A. Raab, R. Michel, L. Reichert, et al., "MoBIC: An Aid To Increase The Independent Mobility Of Blind Travellers," *British Journal of Visual Impairment*, Vol. 15, pp. 63 - 66, 1997.

[266] O. Dialameh, D. Miller, C. Blanchard, T. C. Dorcey, and J. M. Sudol, "*Augmented Reality Panorama Supporting Visually Impaired Individuals*," Google Patents, 2016.

[267] K. L. Lim, K. P. Seng, L. S. Yeong, and L.-M. Ang, "*Handbook of Research on Recent Developments in Intelligent Communication Application*," Scopus, 2016. ISBN-13: 9781522517856

[268] S. Gowtham, M. Gokulamanikandan, P. Pavithran, and K. Gopinath, "Interactive Voice & IOT Based Route Navigation System For Visually Impaired People Using Lifi," *International Journal of Scientific Research in Computer Science, Engineering and Information Technology*, Vol. 2, No. 2, 2017. ISSN : 2456-3307

[269] T. Strothotte, S. Fritz, R. Michel, A. Raab, H. Petrie, V. Johnson, et al., "Development Of Dialogue Systems For A Mobility Aid For Blind People: Initial Design And Usability Testing," *2nd Annual ACM conference on Assistive Technologies*, pp. 139 – 144, 1996.

[270] L. Ran, S. Helal, and S. Moore, "Drishti: An Integrated Indoor/Outdoor Blind Navigation System And Service," 2nd *IEEE Annual Conference on Pervasive Computing and Communications, 2004. PerCom 2004,* pp. 23 - 30, 2004.

[271] A. Wattal, A. Ojha, and M. Kumar, "Obstacle Detection for Visually Impaired Using Raspberry Pi and Ultrasonic Sensors," *National Conference on Product Design (NCPD 2016)*, July 2016.

[272] R. L. Mackett, Y. Gong, K. Kitazawa, and J. Paskins, "Children's Local Travel Behaviour: How The Environment Influences, Controls, And Facilitates It," *11th World Conference on Transport Research,* 2007.

[273] Z. Hunaiti, V. Garaj, and W. Balachandran, "A Remote Vision Guidance System For Visually Impaired Pedestrians," *Journal of Navigation*, Vol. 59, pp. 497 - 504, 2006.

[274] M. N. K. Boulos, A. Rocha, A. Martins, et al., "CAALYX: A New Generation Of Location-Based Services In Healthcare," *International Journal of Health Geographics 2007*, March 2007. DOI: https://doi.org/10.1186/1476-072X-6-9

[275] V. Poornima and R. Ganesan, "Implementation Of Health Information System Using Location Based Services," *IEEE International Conference on Advanced Communications, Control and Computing Technologies*, Ramanathapuram, pp. 1692 – 1696, 2014. DOI: 10.1109/ICACCCT.2014.7019397

[276] L. Herdiman, F. Kusumawardani, S. Susmartini, and I. Pryadhitama, "Manual Wheelchair Intervention On Transmission System By Assistive Technology To Increase User Mobility," *International Conference on Industrial, Mechanical, Electrical, and Chemical Engineering (ICIMECE)*, pp. 225 – 230, 2016.

[277] R. Hervás, J. Bravo, and J. Fontecha, "An Assistive Navigation System Based On Augmented Reality And Context Awareness For People With Mild Cognitive Impairments," *IEEE Journal of Biomedical and Health Informatics*, Vol. 18, pp. 368 - 374, 2014.

[278] S. J. Barnes, "Wireless Digital Advertising: Nature And Implications," *International Journal Of Advertising*, Vol. 21, pp. 399 - 420, 2002.

[279] V. Zeimpekis, P. E. Kourouthanassis, and G. M. Giaglis, "Mobile And Wireless Positioning Technologies," *Telecommunication Systems and Technologies,* Vol. 1, 2003.

[280] P. G. Date and N. Patil, "Proximity Based And Security Aware Rewarding System For Mobile Marketing," Advances in Signal Processing (CASP), pp. 350-353, 2016.

[281] I. Trebaljevac and Z. Bojovic, "Business Model For The Internet And Mobile Based Marketing For The Smart Parking Operators," *23rd Telecommunications Forum Telfor (TELFOR)*, pp. 752 – 755, 2015.

[282] K. Hadadi and M. K. Almsafir, "The Relationship between Mobile Marketing and Customer Relationship Management (CRM)," *3rd International Conference on Advanced Computer Science Applications and Technologies (ACSAT)*, pp. 61 - 66, 2014.

[283] R. Ström, M. Vendel, and J. Bredican, "Mobile marketing: A Literature Review On Its Value For Consumers And Retailers," *Journal of Retailing and Consumer Services*, Vol. 21, pp. 1001 - 1012, 2014.

[284] H. Gao and H. Liu, "Data Analysis On Location-Based Social Networks," *Mobile social networking*, *Springer*, pp. 165 - 194, 2014.

[285] N. Limpf and H. A. Voorveld, "Mobile Location-Based Advertising: How Information Privacy Concerns Influence Consumers' Attitude And Acceptance," *Journal of Interactive Advertising*, Vol. 15, pp. 111 - 123, 2015.

[286] A. Bawa-Cavia, "Sensing The Urban: Using Location-Based Social Network Data In Urban Analysis," *Second Workshop on Pervasive Urban Applications (PURBA)*, 2011.

[287] M. Koch, G. Groh, C. Hillebrand and N. Fremuth, "Mobile Support for Lifestyle Communities," *Community Online Services and Mobile Solutions*, pp. 1 – 26, November 2002. ISSN 0942-5098

[288] A. Tasch and O. Brakel, "Location Based Community Services New Services For A New Type Of Web Communities," *IADIS Conference on Web Based Communities*, pp. 294 – 302, 2004. DOI: 10.1.1.96.4798

[289] G. Retscher and Q. Fu, "Integration Of RFID, GNSS And DR For Ubiquitous Positioning In Pedestrian Navigation," *Journal of Global Positioning Systems*, Vol. 6, No. 1, pp. 56 - 64, September 2007.

[290] B. S. Lakmali and D. Dias, "Database Correlation For GSM Location In Outdoor & Indoor Environments," *4th International Conference on Information and Automation for Sustainability (ICIAFS),* pp. 42 – 47, 2008. DOI: 10.1109/ICIAFS.2008.4783992

[291] H. Tootell, "Investigating The Relationship Between Location-Based Services And National Security," *TENCON IEEE Region 10 Conference*, Melbourne, Qld., pp. 1 – 4, 2005. DOI: 10.1109/TENCON.2005.300973

[292] M. Osborne, S. Moran, R. McCreadie, A. Von Lunen, M. D. Sykora, E. Cano, et al., "Real-Time Detection, Tracking, And Monitoring Of Automatically Discovered Events In Social Media," *52nd annual meeting of the Association for Computational Linguistics (ACL)*, pp. 1 – 6, June 2014. ISBN: 978-1-937284-73-2

[293] S. W. Ho, J. Duan, and C. S. Chen, "Location-Based Information Transmission Systems Using Visible Light Communications," *Transactions on Emerging Telecommunications Technologies*, Vol. 28, No. 1, January 2017. DOI: 10.1002/ett.2922

[294] L. E. Halchin, "Electronic government: Government capability and terrorist resource," *Government Information Quarterly*, Vol. 21, No. 4, pp. 406 - 419, 2004. DOI: https://doi.org/10.1016/j.giq.2004.08.002

[295] L. Andreu, I. Ng, R. Maull, and W. Shadbolt, "Reducing The Fear Of Crime In A Community As A Complex Service System: The Case Of London Borough Of Sutton," *European Management Journal*, Vol. 30, p. 410, 2012.

[296] R. Boondao, V. Esichaikul, and N. K. Tripathi, "A Model Of Location Based Services For Crime Control," 37th ASEE/IEEE Frontiers in Education Conference, October 2003.

[297] S. Chanta, M. E. Mayorga and L.A. McLay, “Improving Emergency Service In Rural Areas: A Bi-Objective Covering Location Model For EMS Systems,” *Annals of Operations Research*, Vol. 22, No. 1, pp. 133 – 159, September 2011. DOI: https://doi.org/10.1007/s10479-011-0972-6

[298] M. Ayad, M. Taher and A. Salem, "Real-Time Mobile Cloud Computing: A Case Study in Face Recognition," *28th International Conference on Advanced Information Networking and Applications Workshops*, Victoria, BC, pp. 73 – 78, 2014. DOI: 10.1109/WAINA.2014.22

[299] M. A. Tayebi, M. Ester, U. Glässer, and P. L. Brantingham, "Crimetracer: Activity Space Based Crime Location Prediction," *IEEE/ACM International*

Conference on Advances in Social Networks Analysis and Mining (ASONAM), pp. 472 - 480, 2014. DOI: 10.1109/ASONAM.2014.6921628

[300] F. Luo, L. Ren, and J. S. Zhao, "Location-Based Fear of Crime: A Case Study in Houston, Texas," *Criminal Justice Review*, Vol. 41, No 1, pp. 75 - 97, December 2016. DOI: 10.1177/0734016815623035

[301] J. H. Schiller and A. Voisard, "*Location-based services*," Morgan Kaufmann Publications, May 2004. ISBN-13: 978-1558609297

[302] C.-C. Chen, T.-C. Huang, J. J. Park, and N. Y. Yen, " Real-Time Smartphone Sensing And Recommendations Towards Context-Awareness Shopping," *Multimedia systems*, Vol. 21, No. 1, pp. 61 - 72, February 2013. DOI: 10.1007/s00530-013-0348-7

[303] J. R. Santana, J. Carrasco, J. A. Galache, L. Sanchez, and R. Agüero, "A Solution for Tracking Visitors in Smart Shopping Environments: A Real Platform Implementation Based on Raspberry Pi," *International Conference on Mobile Networks and Management*, Vol. 191, pp. 72-87, 2016. DOI https://doi.org/10.1007/978-3-319-52712-3_6

[304] Y. Zheng, Y. Chen, X. Xie, and W.-Y. Ma, "GeoLife2. 0: A Location-Based Social Networking Service," *Tenth International Conference on Mobile Data Management: Systems, Services and Middleware*, pp. 357 - 358, May 2009. DOI: 10.1109/MDM.2009.50.

[305] J. Lindqvist, J. Cranshaw, J. Wiese, J. Hong, and J. Zimmerman, "I'm The Mayor of My House: Examining Why People Use Foursquare-A Social-Driven

Location Sharing Application," *Annual Conference on Human Factors in Computing Systems*, pp. 2409 - 2418. 2011. DOI=10.1145/1978942.1979295

[306] J. Samsioe, A. Samsioe, "*Introduction to Location Based Services — Markets and Technologies*," R. Reichwald Mobile Kommunikation, 2002, DOI https://doi.org/10.1007/978-3-322-90695-3_25

[307] S. Dhar and U. Varshney, "Challenges and Business Models for Mobile Location-Based Services and Advertising," Communications of the ACM, Vol. 54, No. 5, pp. 121 - 128, May 2011. DOI: 10.1145/1941487.1941515

[308] Q. Zhao, Z. Liao, J. Li, Y. Shi and Q. Tang, "A Split Smart Swap Clustering for Clutter Problem in Web Mapping System," *IEEE/WIC/ACM International Conference on Web Intelligence (WI)*, Omaha, NE, 2016, pp. 439 - 443. DOI: 10.1109/WI.2016.0070

[309] T. Yeh, K. Tollmar, and T. Darrell, "IDeixis: Image-Based Deixis For Finding Location-Based Information," *Human factors in computing systems*, pp. 781 - 782, 2004. DOI: 10.1145/985921.985933.

[310] K. Ogawa, E. Verbree, S. Zlatanova, N. Kohtake, and Y. Ohkami, "Toward Seamless Indoor-Outdoor Applications: Developing Stakeholder-Oriented Location-Based Services," *Geo-spatial Information Science,* Vol. 14, No. 2, pp. 109 - 118, 2011. DOI: https://doi.org/10.1007/s11806-011-0469-0

[311] M. Espeter and M. Raubal, "Location-Based Decision Support For User Groups," *Journal of Location Based Services,* Vol. 3, pp. 165 - 187, September 2009. DOI: 10.1080/17489720903339668

[312] M. Bãdut, "A Perspective Over The Location-Based Applications/Services– Lbs/Lba," 10th EC GI & GIS Workshop, ESDI State of the Art, Warsaw, Poland, 23 – 25, June 2004.

[313] S. Zlatanova and E. Verbree, " Technological Developments Within 3D Location-Based Services," *International Symposium and Exhibition on Geoinformation*, pp. 13-14, October 2003.

[314] S. He and S. H. G. Chan, "Wi-Fi Fingerprint-Based Indoor Positioning: Recent Advances and Comparisons," *IEEE Communications Surveys & Tutorials*, Vol. 18, No. 1, pp. 466 - 490, Firstquarter 2016. DOI: 10.1109/COMST.2015.2464084

[315] U. Rerrer and O. Kao, "Suitability of Positioning Techniques for Location-based Services in Wireless LANs," *International Workshop on Positioning, Navigation and Communication (WPNC)*, pp. 51 - 56, January 2004.

[316] M. N. Borenović and A. M. Nešković, "Positioning In WLAN Environment By Use Of Artificial Neural Networks And Space Partitioning," *Annals of Telecommunications,* Vol. 64, pp. 665 - 676, 2009. DOI: https://doi.org/10.1007/s12243-009-0115-0

[317] M. Borenović and A. NeśNović, "Positioning in Indoor Mobile Systems," *Radio Communications,* pp. 978-953, April 2010. DOI: 10.5772/9466

[318] A. Aloudat, K. Michael, X. Chen, and M. M. Al-Debei, "Social Acceptance Of Location-Based Mobile Government Services For Emergency Management," *Telematics and Informatics,* Vol. 31, No. 1, pp. 153 - 171, February 2014. DOI: https://doi.org/10.1016/j.tele.2013.02.002

[319] P. Khomchuk, I. Stainvas and I. Bilik, "Pedestrian Motion Direction Estimation Using Simulated Automotive MIMO Radar," *IEEE Transactions on Aerospace and Electronic Systems*, Vol. 52, No. 3, pp. 1132 - 1145, June 2016. DOI: 10.1109/TAES.2016.140682

[320] G. Wang, J. Xin, J. Wang, N. Zheng and A. Sano, "Subspace-Based Two-Dimensional Direction Estimation And Tracking Of Multiple Targets," *IEEE Transactions on Aerospace and Electronic Systems*, Vol. 51, No. 2, pp. 1386 - 1402, April 2015. DOI: 10.1109/TAES.2014.130018

[321] Z. Lu, Y. Li and M. Gao, "Direction Estimation For Two Steady Targets In Monopulse Radar," *Journal of Systems Engineering and Electronics*, Vol. 26, No. 1, pp. 61 - 68, February 2015. DOI: 10.1109/JSEE.2015.00009

[322] N. Iliev and I. Paprotny, "Review and Comparison of Spatial Localization Methods for Low-Power Wireless Sensor Networks," *IEEE Sensors Journal*, Vol. 15, No. 10, pp. 5971 - 5987, October 2015. DOI: 10.1109/JSEN.2015.2450742

[323] T. D. Bui, B. H. Nguyen, Q. C. Nguyen, and M. T. Le, "Design Of Beam Steering Antenna For Localization Applications," *International Symposium on Antennas and Propagation (ISAP),* pp. 956-957, 2016.

[324] S.-K. Lin, "*Electronic Warfare Target Location Methods*,"Artech House, 2012, ISBN: 9781608075232

[325] F. Gross, "*Smart antennas with Matlab: Principles and Applications in Wireless Communication*" McGraw-Hill Professional, 2015. ISBN-13: 978-0071822381

[326] W. Y. Yang, Y. S. Cho, and C. Y. Choo, “*MATLAB/SIMULINK for Digital Signal Processing*,” Hongrung Publishing Company, 2012.

[327] C. Siagian, C. K. Chang, and L. Itti, "Autonomous Mobile Robot Localization And Navigation Using A Hierarchical Map Representation Primarily Guided By Vision," *Journal of Field Robotics,* Vol. 31, No. 3, pp. 408 - 440,May/June 2014. DOI: 10.1002/rob.21505

[328] C. H. Lin and K. T. Song, "Probability-Based Location Aware Design and On-Demand Robotic Intrusion Detection System," *IEEE Transactions on Systems*, *Man, and Cybernetics*, Vol. 44, No. 6, pp. 705 - 715, June 2014. DOI: 10.1109/TSMC.2013.2277691

[329] H. Cheng, H. Chen and Y. Liu, "Topological Indoor Localization and Navigation for Autonomous Mobile Robot," *IEEE Transactions on Automation Science and Engineering*, Vol. 12, No. 2, pp. 729 - 738, April 2015. DOI: 10.1109/TASE.2014.2351814

[330] P. J. Costa, N. Moreira, D. Campos, J. Gonçalves, J. Lima and P. L. Costa, "Localization and Navigation of an Omnidirectional Mobile Robot: The Robot@Factory Case Study," IEEE Revista Iberoamericana de Tecnologias del Aprendizaje, Vol. 11, No. 1, pp. 1-9, February 2016. DOI: 10.1109/RITA.2016.2518420

[331] L. Paull, S. Saeedi, M. Seto and H. Li, "AUV Navigation and Localization: A Review," *IEEE Journal of Oceanic Engineering*, Vol. 39, No. 1, pp. 131 - 149, January 2014. DOI: 10.1109/JOE.2013.2278891

[332] M. Dredze, M. J. Paul, S. Bergsma, and H. Tran, "Carmen: A Twitter Geolocation System With Applications To Public Health," *AAAI Workshop On Expanding The Boundaries of Health Informatics Using AI (HIAI)*, pp. 20-24, 2013.

[333] J. He, K. Pahlavan, S. Li and Q. Wang, "A Testbed for Evaluation of the Effects of Multipath on Performance of TOA-Based Indoor Geolocation," *IEEE Transactions on Instrumentation and Measurement*, Vol. 62, No. 8, pp. 2237-2247, August 2013. DOI: 10.1109/TIM.2013.2255976

[334] A. Redondi, M. Chirico, L. Borsani, M. Cesana, and M. Tagliasacchi, "An Integrated System Based On Wireless Sensor Networks For Patient Monitoring, Localization And Tracking," *Ad Hoc Networks,* Vol. 11, No. 1, pp. 39 - 53, January 2013. DOI: https://doi.org/10.1016/j.adhoc.2012.04.006

[335] B. Doshi, E. Gunduzhan, Jay Chang and O. Farrag, "Mobile Geolocation Techniques For Location-Aware Emergency Response Services," *IEEE Military Communications Conference*, Tampa, FL, pp. 1618 - 1623, 2015. DOI: 10.1109/MILCOM.2015.7357676

[336] M. S. Bartlett, "*An introduction to stochastic processes: with special reference to methods and applications*," Cambridge University Press Archive, 3rd Edition 1980. ISBN-13: 978-0521280853

[337] J. Capon, "High-resolution frequency-wavenumber spectrum analysis," *Proceedings of the IEEE*, Vol. 57, No. 8, pp. 1408 - 1418, August 1969. DOI: 10.1109/PROC.1969.7278

[338] Hoi-Shun Lui, H. T. Hui and Mook Seng Leong, "A Note on the Mutual-Coupling Problems in Transmitting and Receiving Antenna Arrays," *IEEE Antennas*

and Propagation Magazine, Vol. 51, No. 5, pp. 171 - 176, October 2009. DOI: 10.1109/MAP.2009.5432083

[339] H. S. Lui and H. T. Hui, "Direction-of-Arrival Estimation: Measurement Using Compact Antenna Arrays Under The Influence Of Mutual Coupling.," *IEEE Antennas and Propagation Magazine*, Vol. 57, No. 6, pp. 62 - 68, December 2015. DOI: 10.1109/MAP.2015.2480072

[340] H. S. Lui and H. T. Hui, "Mutual coupling compensation for direction finding using receiving mutual impedance," *International Symposium on Antennas and Propagation*, Kaohsiung, 2014, pp. 61 - 62. DOI: 10.1109/ISANP.2014.7026530

[341] H. T. Hui, "Decoupling methods for the mutual coupling effect in antenna arrays: A review," *Recent Patents on Engineering,* Vol. 1, No. 2, pp. 187-193, 2007.

[342] Y. Yu, H. S. Lui, C. H. Niow and H. T. Hui, "Improved DOA Estimations Using the Receiving Mutual Impedances for Mutual Coupling Compensation: An Experimental Study," *IEEE Transactions on Wireless Communications*, Vol. 10, No. 7, pp. 2228 - 2233, July 2011. DOI: 10.1109/TWC.2011.041311.101062

[343] W. Du and S. Xie, "Mutual Coupling Analysis of Adcock Watson Watt Direction Finding System Based on the Receiving Mutual Impedance," *10th International Symposium on Antennas, Propagation & EM Theory (ISAPE),* pp. 302 - 305, 2012. DOI: 10.1109/ISAPE.2012.6408769

[344] H. s. Lui and H. T. Hui, "Improved Mutual Coupling Compensation In Compact Antenna Arrays," *IET Microwaves, Antennas & Propagation*, Vol. 4, No. 10, pp. 1506 - 1516, October 2010. DOI: 10.1049/iet-map.2009.0200

[345] S. Henault and Y. M. Antar, "Wideband Analysis Of Mutual Coupling Compensation Methods," *International Journal of Antennas and Propagation,* Vol. 2011, 2011.

[346] M. A. G. Al-Sadoon et al., "The Effects Of Mutual Coupling Within Antenna Arrays On Angle Of Arrival Methods," *Loughborough Antennas & Propagation Conference (LAPC), Loughborough*, pp. 1 – 5, 2016. DOI: 10.1109/LAPC.2016.7807547

[347] I. Gupta and A. Ksienski, "Effect Of Mutual Coupling On The Performance Of Adaptive Arrays," *IEEE Transactions on Antennas and Propagation*, Vol. 31, No. 5, pp. 785 - 791, September 1983. DOI: 10.1109/TAP.1983.1143128

[348] H. T. Hui, H. P. Low, T. T. Zhang and Y. L. Lu, "Antenna Designer's Notebook - Receiving Mutual Impedance Between Two Normal-Mode Helical Antennas (NMHAs)," *IEEE Antennas and Propagation Magazine*, Vol. 48, No. 4, pp. 92 - 96, August 2006. DOI: 10.1109/MAP.2006.1715238

[349] J. S. McLean, "A Re-Examination Of The Fundamental Limits On The Radiation Q Of Electrically Small Antennas," *IEEE Transactions on Antennas and Propagation*, Vol. 44, No. 5, pp. 672 - 676, May 1996. DOI: 10.1109/8.496253

[350] O. S. Kim, "Rapid Prototyping of Electrically Small Spherical Wire Antennas," *IEEE Transactions on Antennas and Propagation*, Vol. 62, No. 7, pp. 3839 - 3842, July 2014. DOI: 10.1109/TAP.2014.2317489

[351] R. W. Ziolkowski, M. C. Tang and N. Zhu, "An Efficient, Electrically Small Antenna With Large Impedance Bandwidth Simultaneously With High Directivity

And Large Front-To-Back Ratio," *International Symposium on Electromagnetic Theory*, Hiroshima, pp. 885-887, 2013.

[352] R. C. Hansen, "Fundamental Limitations In Antennas," *Proceedings of the IEEE*, Vol. 69, No. 2, pp. 170 - 182, February 1981. DOI: 10.1109/PROC.1981.11950

[353] K. Fujimoto and H. Morishita, "*Modern small antennas*," Cambridge University Press, January 2014. DOI: https://doi.org/10.1017/CBO9780511977602

[354] J. Oh and K. Sarabandi, "Low Profile Vertically Polarized Omnidirectional Wideband Antenna With Capacitively Coupled Parasitic Elements," *IEEE Transactions on Antennas and Propagation*, Vol. 62, No. 2, pp. 977 - 982, February 2014. DOI: 10.1109/TAP.2013.2291891

[355] S. Zhu *et al*., "Improved Bandwidth Low-Profile Miniaturized Multi-Arm Logarithmic Spiral Antenna," *The 8th European Conference on Antennas and Propagation (EuCAP 2014)*, The Hague, pp. 1918 - 1920, 2014. DOI: 10.1109/EuCAP.2014.6902174

[356] M. Li and K. M. Luk, "A Low-Profile Wideband Planar Antenna," *IEEE Transactions on Antennas and Propagation*, Vol. 61, No. 9, pp. 4411 - 4418, September 2013. DOI: 10.1109/TAP.2013.2267715

[357] C. A. Balanis, "*Modern Antenna Handbook*" John Wiley & Sons, Inc, September 2008. ISBN: 978-0-470-03634-1

[358] Yuan Zhang and Chang-Ying Wu, "An Approach For Optimizing The Reconfigurable Antenna And Improving Its Reconfigurability," *IEEE International*

Conference on Signal Processing, Communications and Computing (ICSPCC), Hong Kong, pp. 1 – 5, 2016. DOI: 10.1109/ICSPCC.2016.7753587

[359] L. Ke and Z. Wang, "Degrees of Freedom Regions of Two-User MIMO Z and Full Interference Channels: The Benefit of Reconfigurable Antennas," *IEEE Transactions on Information Theory*, Vol. 58, No. 6, pp. 3766 - 3779, June 2012. doi: 10.1109/TIT.2012.2185483

[360] J. M. Hannula, J. Holopainen and V. Viikari, "Concept for Frequency-Reconfigurable Antenna Based on Distributed Transceivers," *IEEE Antennas and Wireless Propagation Letters*, Vol. 16, pp. 764 - 767, 2017. DOI: 10.1109/LAWP.2016.2602006

[361] H. A. Majid, M. K. Abdul Rahim, M. R. Hamid, N. A. Murad and M. F. Ismail, "Frequency-Reconfigurable Microstrip Patch-Slot Antenna," *IEEE Antennas and Wireless Propagation Letters*, Vol. 12, pp. 218 - 220, 2013. DOI: 10.1109/LAWP.2013.2245293

[362] G. Chaabane, C. Guines, M. Chatras, V. Madrangeas and P. Blondy, "Reconfigurable PIFA antenna using RF MEMS switches," *9th European Conference on Antennas and Propagation (EuCAP)*, Lisbon, pp. 1-4, 2015.

[363] B. A. Cetiner, G. Roqueta Crusats, L. Jofre and N. Biyikli, "RF MEMS Integrated Frequency Reconfigurable Annular Slot Antenna," in *IEEE Transactions on Antennas and Propagation*, Vol. 58, No. 3, pp. 626-632, March 2010. DOI: 10.1109/TAP.2009.2039300

[364] R. George, C. R. S. Kumar and S. A. Gangal, "Design Of A Frequency Reconfigurable Pixel Patch Antenna For Cognitive Radio Applications,"

International Conference on Communication and Signal Processing (ICCSP), Melmaruvathur, pp. 1684 - 1688, 2016. DOI: 10.1109/ICCSP.2016.7754451

[365] L. R. Tan, R. X. Wu, C. Y. Wang and Y. Poo, "Ferrite-Loaded SIW Bowtie Slot Antenna With Broadband Frequency Tunability," *IEEE Antennas and Wireless Propagation Letters*, Vol. 13, pp. 325-328, 2014. DOI: 10.1109/LAWP.2014.2305431

[366] G. Chen, X. l. Yang and Y. Wang, "Dual-Band Frequency-Reconfigurable Folded Slot Antenna for Wireless Communications," *IEEE Antennas and Wireless Propagation Letters*, Vol. 11, pp. 1386 - 1389, 2012. DOI: 10.1109/LAWP.2012.2227293

[367] J. Perruisseau-Carrier, P. Pardo-Carrera and P. Miskovsky, "Modeling, Design and Characterization of a Very Wideband Slot Antenna With Reconfigurable Band Rejection," *IEEE Transactions on Antennas and Propagation*, Vol. 58, No. 7, pp. 2218 - 2226, July 2010. DOI: 10.1109/TAP.2010.2048872

[368] Symeon Nikolaou *et al*., "Pattern And Frequency Reconfigurable Annular Slot Antenna Using PIN Diodes," *IEEE Transactions on Antennas and Propagation*, Vol. 54, No. 2, pp. 439 - 448, February 2006. DOI: 10.1109/TAP.2005.863398

[369] S. Lucyszyn and S. Pranonsatit, "RF MEMS For Antenna Applications," *7th European Conference on Antennas and Propagation (EuCAP)*, Gothenburg, pp. 1988 – 1992, 2013.

[370] H. A. Majid, M. K. A. Rahim, R. Dewan and M. F. Ismail, "Frequency Reconfigurable Square Ring Slot Antenna," *IEEE International RF and Microwave*

Conference (RFM), Kuching, pp. 147 – 150, 2015. DOI: 10.1109/RFM.2015.7587732

[371] P. Kułakowski, J. Vales-Alonso, E. Egea-López, W. Ludwin, and J. García-Haro, "Angle-Of-Arrival Localization Based On Antenna Arrays For Wireless Sensor Networks," *Computers & Electrical Engineering,* Vol. 36, No. 6, pp. 1181 - 1186, November 2010. DOI:https://doi.org/10.1016/j.compeleceng.2010.03.007

[372] L. Yang, L. Yang and K. C. Ho, "Moving Target Localization In Multistatic Sonar Using Time Delays, Doppler Shifts And Arrival Angles," *IEEE International Conference on Acoustics, Speech and Signal Processing (ICASSP)*, New Orleans, LA, pp. 3399 - 3403, 2017. DOI: 10.1109/ICASSP.2017.7952787

[373] B. Sklar, "Rayleigh fading channels in mobile digital communication systems .I. Characterization," *IEEE Communications Magazine*, Vol. 35, No. 7, pp. 90 - 100, July 1997. DOI: 10.1109/35.601747

[374] S. Dixit and H. Katiyar, "Performance Analysis Of OFDM Under Frequency Selective Fading In Varying Power Delay Profile," *International Conference on Emerging Trends in Electrical Electronics & Sustainable Energy Systems (ICETEESES)*, Sultanpur, pp. 213 - 215, 2016. DOI: 10.1109/ICETEESES.2016.7581387

AUTHOR PUBLICATIONS

List of Publications

JOURNAL PAPERS

1. **R. Asif**, Raed Abd-alhameed and J M Noras. “MIMO Wavelet Transform Using Optimized Successive Interference Cancellation” International Journal of Computer Applications, vol. 178, Nov. 2017, (Accepted Paper)

2. **R. Asif**, Raed Abd-alhameed and J M Noras. “Effects of Transmit Diversity on a Discrete Wavelet Transform and Wavelet Packet Transform-based Multicarrier Systems” International Journal of Computer Applications, vol. 178, Nov. 2017, (Accepted Paper)

3. A. F. Mirza, **R. Asif** et al., "An Active Microwave Sensor for Near Field Imaging,” IEEE Sensors Journal, vol. 17, no. 9, pp. 2749-2757, May1, 1 2017.doi: 10.1109/JSEN.2017.2673961

4. **R. Asif**, Raed Abd-alhameed and J M Noras, “A Unique Wavelet-based Multicarrier System with and without MIMO over Multipath Channels with AWGN” International Journal of Computer Applications, vol. 117, issue 9, May 2015, pp. 31-40, ISSN: 0975 – 8887, DOI: 10.5120/20585-3015

5. K. Anoh, **R. Asif**, R. Abd-Alhameed, J. Rodriguez, J. M. Noras, S.M.R. Jones, A. S. Hussaini, "Multi-Antenna OFDM System Using Coded Wavelet with Weighted Beamforming", Radio Engineering, vol. 24, no. 1, pp. 356-361, April 2014, pp. 356-361. http://www.radioeng.cz/fulltexts/2014/14_01_0356_0361.pdf

6. **R. Asif**, T.S. Ghazaany, R.A. Abd-Alhameed, J.M. Noras, S.M.R. Jones, J Rodriguez and C.H. See, “MIMO Discrete Wavelet Transform for the Next

Generation Wireless Systems," International Journal of Advanced Research in Electrical, Electronics and Instrumentation Engineering (IJAREEIE), vol. 2, no 10, October 2013, pp. 4791-4800. ISSN: 2278-8875 (online), ISSN: 2320-3765 (Print).

7. C. H. See, R. A. Abd-Alhameed, N. J. McEwan, S. M. R. Jones, **R. Asif**, P. S. Excell, "Design of a Printed MIMO/Diversity Monopole Antenna for Future Generation Handheld Devices," International Journal of RF and Microwave. Computer-Aided Engineering, Published in Wiley Online Library, vol. 24, no. 3, pp. 348-359, May 2014 (wileyonlinelibrary.com); DOI: 10.1002/mmce.20767; ISSN (Print) 1096-4290 - ISSN (Online) 1099-047X

8. **R. Asif**, R. A. Abd-alhameed, O. O. Anoh, Y. A. S. Dama, "Performance Evaluation of DWT-OFDM and FFT-OFDM for Multicarrier Communications Systems using Time Domain Zero Forcing Equalization", International Journal of Computer Applications, vol. 51, no.4, August 2012, pp. 34-38. ISSN: 0975 – 8887; Digital Library URI: http://www.ijcaonline.org/archives/volume51/number4/8032-1314

CONFERENCE PAPERS

1. Imran Ahmed, **R. Asif**, R. A. Abd-Alhameed, et.al, "Current Technologies and location based services", *IEEE Seventh International Conference on Internet Technologies & Applications, Wales, United Kingdom,* pp: 299 - 304, 2017. DOI: 10.1109/ITECHA.2017.8101958

2. **R. Asif**, R. A. Abd-Alhameed, "Angle of Arrival Estimation Using Inverse Difference Maximum Signal Subspace", *Festival of Radio Science,* December 2017.

3. M.A.G. Sadoon, **R. Asif**, R. A. Abd-Alhameed," OFDM Wideband DOA System for Detecting and Tracking Vehicles Applications, " *12th European Conference on Antennas and Propagation (Submitted Paper),* 2018.

4. **R. Asif**, R. A. Abd-Alhameed, O. O. Anoh, "Performance comparison between DWT-OFDM and FFT-OFDM using time domain zero forcing equalization", *International Conference on Telecommunications and Multimedia (TEMU)*, DOI: 10.1109/TEMU.2012.6294712, pp: 175 – 179, 2012.

5. **R. Asif**, A. S. Hussaini, R. A. Abd-Alhameed, et al: "MIMO wavelet multicarrier system using feedback circuit", *Proceeding of the 2013 19th European Wireless Conference (EW)*, Guildford UK, Print ISBN 978-3-8007-3498-6, pp: 1 – 4, 16 – 18 April 2013.

6. **R. Asif**, N.T. Ali, H.S.O. Migdadi, R.A. Abd-Alhameed, A.S. Hussaini, Tahereh S. Ghazaany, S. Naveed, J.M. Noras, P.S. Excell, J. Rodriguez, "Wavelet Based MIMO-Multicarrier System Using Forward Error Correction and Beam

Forming", *Fifth International Conference on Internet Technologies and Applications*, Wrexham, North East Wales, UK, 2013

7. R. A. Abd-Alhameed, **R. Asif**, et. Al: "A Review of Location Based Services: Current Developments, Trends and Issues, *Fifth International Conference on Internet Technologies and Applications*, Wrexham, North East Wales, UK, 2013

8. **R. Asif**, R. A. Abd-Alhameed, et al: " Performance of Different Wavelet Families Using DWT and DWPT- Channel Equalization Using ZF and MMSE ", *7th IEEE International Design and Test Symposium*, Doha, Qatar, 2012

9. **R. Asif**, R. A. Abd-Alhameed, "Evaluation of The Angel of Arrival Based Techniques", *IEEE International design and test symposium*, Marrakech, Morocco, December, 2013

10. **R. Asif**, R. A. Abd-Alhameed, "Performance Evaluation of ZF and MMSE Equalizers for Wavelets V-Blast", *IEEE International design and test symposium*, Marrakech, Morocco, December, 2013

11. A.F. Mirza, **R. Asif**, R. A. Abd-Alhameed, "Breast Cancer Detection Using 1D, 2D, and 3D FDTD Numerical Methods.", IEEE International Conference on Computer and Information Technology; Ubiquitous Computing and Communications; Dependable, Autonomic and Secure Computing; Pervasive Intelligence and Computing, pp. 1042 – 1045, 2015, DOI: 10.1109/CIT/IUCC/DASC/PICOM.2015.158

12. A. Ghani, C.H. See, **R. Asif**, "Reconfigurable neurons - making the most of configurable logic blocks (CLBs), Internet, Technologies and Applications, pp. 475 – 478, 2015.

13. **R. Asif**, R. A. Abd-Alhameed, “Performance analysis of angle of arrival estimation algorithms in a multi-source environment including mutual coupling effects and compensation techniques.”, Loughborough Antennas and Propagation Conference (LAPC), pp. 359 – 362, 2014, DOI: 10.1109/LAPC.2014.6996397

14. **R. Asif**, R. A. Abd-Alhameed, “Study on specific absorption rate”, Loughborough Antennas and Propagation Conference (LAPC), pp. 148 – 150, 2014, DOI: 10.1109/LAPC.2014.6996342

15. S. Adnan; R. A. Abd-Alhameed; **R. Asif**; C. H. See; P. S Excell, “Microwave antennas for near field imaging”, IEEE MTT-S International Microwave Workshop Series on RF and Wireless Technologies for Biomedical and Healthcare Applications, pp. 1 – 3, 2014, DOI: 10.1109/IMWS-BIO.2014.7032405

Evaluation of The Angle of Arrival Based Techniques

R. Asif[1], M. UsmaN[2], T. Ghazaany[1], A.S Hussaini[3,4], Raed A. Abd-Alhameed[1], S.M.R. Jones[1], J.M. Noras[1], J. Rodriguez[3]
[1]Mobile and Satellite Communications Research Centre, University of Bradford UK, BD7 1DP
{r.asif, r.a.a.abd}@bradford.ac.uk
Tahereh.Ghazaany@datong.co.uk
[2]Department of Electrical & Electronics Engineering, University of Hail, Saudi Arabia
m.usman@uoh.edu.sa
[3]Instituto de Telecomunicacoes – Aveiro, Portugal
{ash, jonathan@av.it.pt}
[4]Department of Electrical & Electronics Engineering Modibbo Adama University of Technology, Yola Nigeria

Abstract: **In this work we present the angle of arrival estimation techniques and their comparison at different values of SNR using a 5 element UCA. The techniques that have been considered include phase interferometry, Multiple Signal Classification and covariance. The results show that for very low values of SNR the performance of the covariance matrix based algorithm is the best but for slightly higher values of SNR, MUSIC algorithm outperforms covariance.**

Index Terms- Angle of Arrival, Interferometry, MUSIC, Covariance, Localization

I. INTRODUCTION

The evolution of the wireless sensor networks and the necessity of connectivity to the physical environment in an absolute frame through different localization techniques has found wide spread applications in a variety of fields [1]. The data that is gathered for these applications is useless without the position information of the corresponding node. The position information can be derived either by using the Global Positioning System or by having some reference nodes [2]. However the requirement of LOS between the node and the satellite puts a constraint on the use of GPS signal for localization in harsh urban environments or indoor environments [3].

Due to the limited effectiveness of GPS signal many applications like emergency response, tracking and monitoring require assistance using the hand placed reference nodes or beacons which allow the unknown nodes to localize themselves [4]. There are two existing approaches to localization which can be characterized as range based and range free [5]. Mostly the techniques in practice are range based e.g. received signal strength (RSS) [6], Time of Arrival (TOA), Time Difference of Arrival (TDOA) [7] and the angle of arrival based techniques [8].

The angle of arrival can be determined using different approaches like phase interferometery, covariance, Music and post processing methods like CLEAN [9]. Angle of arrival calculations requires the knowledge of the angle of the inward bound signal in order to resolve the bearing between the receiver and the transmitter. But these algorithms and localization techniques in general raise many challenges from the perspective of DSP they should provide highly resolved parameters under different application specific and propagation channel conditions. In this work we present the comparative study of phase interferometry, Multiple Signal Classfication (MUSIC) and Covariance based algorithms.

978-1-4799-3525-3/13/$31.00 ©2013 IEEE

II. Estimation Techniques

Any algorithm that is to use for the localization

i) Interferometry

This technique makes use of the principal that the incoming plane wave with some angle of arrival will be received first in time by one of the elements as compared to the rest of the elements due to the different path lengths which results in the phase difference between the received signals.

$$\Delta\varphi = \left(\frac{2\pi}{\lambda}\right) d\sin\theta \qquad (1)$$

Where, θ represent the angle of elevation. The phase difference is then compared to the reference phase difference for the localization array at each wavelength and locates the point of maximum correlation which corresponds to the angle of the arriving signal.

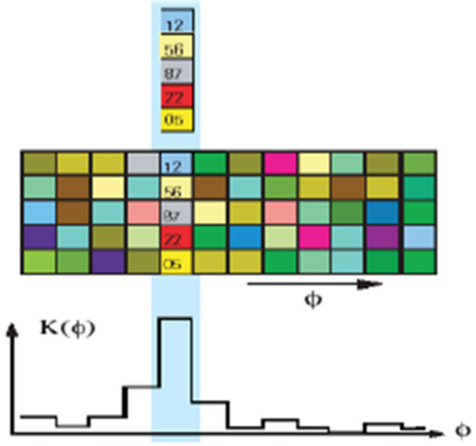

Figure 1: Correlative Interferometry

ii) MUSIC

MUSIC algorithm makes use of the covariance matrix by decomposing it into its corresponding eigenvectors and eigenvalues in order to estimate the direction of arrival based on the orthogonality principle of the noise and signal subspaces. For this purpose the first assumption is that the covariance matrix is invertible (Non-singular). Where we can represent the eigenvectors with large eigenvalues as M and call them signal sub space and eigenvectors with lower eigenvalues can be represented by N and call them the noise subspace. Mathematically;

$$R_{xx} = \sum_{i=1}^{M} \lambda\, e_i\, e_i^* = U_s \Lambda_s U_s^* + U_N \Lambda_N U_s^* \quad (2)$$

By writing the values of EK eigenvectors we can define the MUSIC pseudo spectrum as;

$$P_{music}(\theta) = \frac{1}{a(\theta)^* E_K E_k^* a(\theta)} \quad (3)$$

III. System Design

A uniform circular array of five isotropic antennas spatially distributed at known locations as shown in Figure 2 is used to capture a propagation electromagnetic field and the output of the array elements is used to resolve the field for angle of arrival estimation. It is assumed that the receiving array and the far field transmitter lie in the same plane and the complex Gaussian samples of noise are also considered to be uncorrelated from the incoming signals at each element constituting the receiver array.

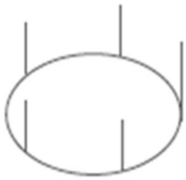

Figure 2: Five element ring array

The elements are evenly distributed 72 degrees apart in the azimuth plane. Inter element spacing is set to Lamda/4 where lambda is the wavelength at the carrier frequency of 400MHz.

Signal is transmitted towards the receiver array from the transmitters at known positions with regular azimuthal and frequency stepping [10]. The stepping size of 4° or less is proposed by [10]. The amplitude and differential phase values from the 5 elements are stored into a calibration table and the columns of the data matrix correspond to the azimuth angle and then form a comparison vector as shown in Figure 1. Column of the reference matrix and the comparison vector are both correlated. The angle that is linked to the comparison matrix with the highest correlation is the bearing angle.

IV. Results and Discussion

All the simulation have been performed using MATLAB and CST.

All the algorithms were tested for different values of SNR and as can be seen from Figure 3 covariance matrix provided the least error as compared to the other algorithms at SNR of -10dB

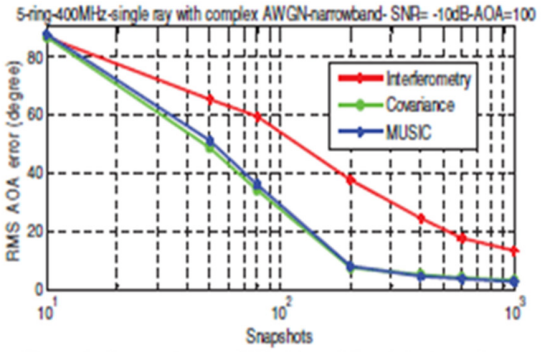

Figure 3: Comparison at SNR -10, and Lambda/4 spacing

Next experiment was performed by increasing the SNR value to -5dB.

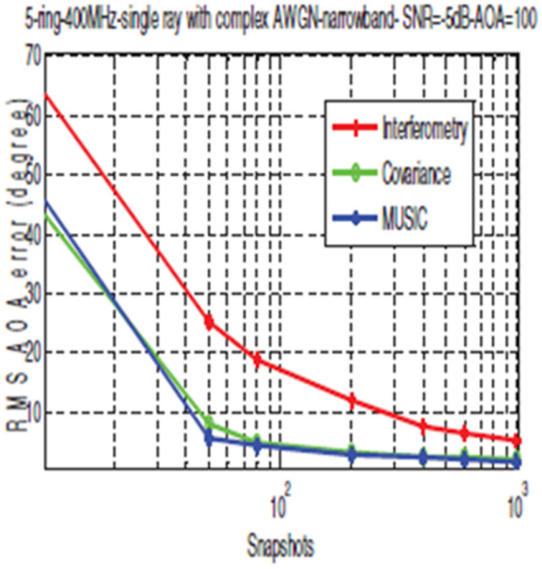

Figure 4: Comparison at SNR -5, and Lambda/4 spacing

In Figure we can clearly see that the performance of both covariance and MUSIC algorithms is about the same and the degree of error for the interferometry has also reduced but it is still comparatively quite high as compared to the other two techniques

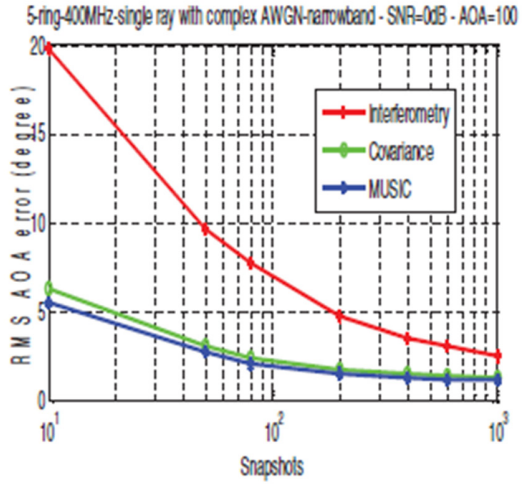

Figure 5: Comparison at SNR 0, and Lambda/4 spacing

Both the graphs obtained in Figure 5 and 6 supports the idea that the MUSIC algorithm can slightly outperform the covariance algorithm at large SNR values for narrow band systems.

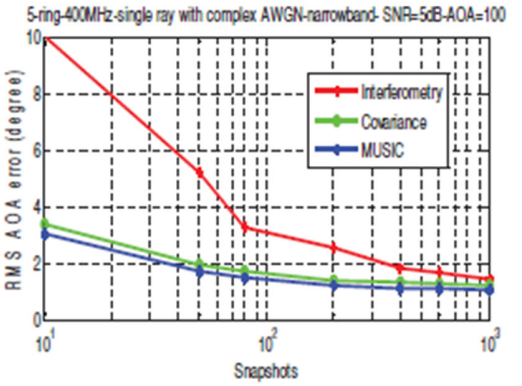

Figure 6: Comparison at SNR 5, and Lambda/4 spacing

V. Conclusion

It was concluded from the above work that for localization in narrowband environments MUSIC and Covariance algorithms can provide a high advantage over interferometry. It was also learnt during the study that an angle of arrival estimation error of 1° leads to an error of about 55m in the actual location of the transmitter. It was also concluded that both covariance and music algorithm are well suited for low SNR systems.

Acknowledgment

This work has been performed in the framework of ARTEMOS project under work programme ENIAC JU 2010 and FCT (Fundação para a Ciência e Tecnologia and Department of Electrical & Electronics Engineering Modibbo Adama University of Technology, Yola Nigeria.

References

1. Shen, Y. and M.Z. Win, *On the accuracy of localization systems using wideband antenna arrays*. Communications, IEEE Transactions on, 2010. **58**(1): p. 270-280.
2. Spilker Jr, J., *GPS signal structure and performance characteristics*. Navigation, 1978. **25**: p. 121-146.
3. Jourdan, D., D. Dardari, and M. Win, *Position error bound for UWB localization in dense cluttered environments*. Aerospace and Electronic Systems, IEEE Transactions on, 2008. **44**(2): p. 613-628.
4. Rong, P. and M.L. Sichitiu. *Angle of arrival localization for wireless sensor networks*. in *Sensor and Ad Hoc Communications and Networks, 2006. SECON'06. 2006 3rd Annual IEEE Communications Society on*. 2006. IEEE.
5. Munoz, D., et al., *Position location techniques and applications*2009: Academic Press.
6. Niculescu, D. and B. Nath, *DV based positioning in ad hoc networks*. Telecommunication Systems, 2003. **22**(1-4): p. 267-280.
7. Priyantha, N.B., A. Chakraborty, and H. Balakrishnan. *The cricket location-support system*. in *Proceedings of the 6th annual international conference on Mobile computing and networking*. 2000. ACM.
8. Amundson, I., et al., *Radio interferometric angle of arrival estimation*, in *Wireless Sensor Networks*2010, Springer. p. 1-16.
9. Hislop, G., N. Sakar, and C. Craeye, *Direction finding with MUSIC and CLEAN*. 2013.
10. Park, C.-S. and D.-Y. Kim. *The fast correlative interferometer direction finder using I/Q demodulator*. in *Communications, 2006. APCC'06. Asia-Pacific Conference on*. 2006. IEEE.

Performance Analysis of Angle of Arrival Estimation Algorithms in a Multi Source Environment including Mutual Coupling Effects and Compensation Techniques

R. Asif, Raed Abd-Alhameed, H. Alhassan, J.M. Noras, S. M. R Jones, H. Jameel, A.F. Mirza
Antennas and Advanced Electromagnetics Research Group, University of Bradford, Bradford, UK
{r.asif1, r.a.a.abd, jmnoras, a.f.mirza}@bradford.ac.uk

***Abstract*— The performances of two different angle of arrival estimation algorithms, phase interferometry and covariance based super resolution, and two different mutual coupling compensation methods, conventional and received mutual impedance, have been compared. Two different scenarios have been explored, firstly with a single source transmitter, and then with dual source transmitters. Different powers levels were used to estimate the performance of these algorithms in a multipath/multisource environment over a perfect ground plane. The results show greater accuracy using the covariance based technique, and also support the use of the received mutual impedance method for coupling compensation.**

***Keywords*—Angle of Arrival, Antenna array, interferometry, covariance**

I. Introduction

Recent advances in the field of digital computing, digital electronics, wireless communications and micro-electro-mechanical systems (MEMS) have led to the development of low cost sensor nodes with short communication ranges [1]. A sensor network consists of the radio path that transmits the data which is then detected by the sensor nodes, with subsequent signal processing for the characterization of the arrived ray. Wireless sensors networks have many uses, including patient monitoring, weather measurements and military applications.

Often the data received at the base station is of less value if the position of the transmitting node is unknown: this localization problem provides a very active research topic. The information is needed for location based services, including inventory tracking at loading docks or warehouses, detection of intruders, providing emergency services and in mining and patient tracking.

Different estimation techniques current in the literature include time of arrival (TOA), time difference of arrival, received signal strength (RSS) and angle of arrival (AOA). Using TOA methods requires a costly and complicated setup with synchronized clocks at both transmitting and receiving nodes, which run transmission protocols to exchange the time information between each other [2]. RSS can also be used to predict the proximity of the transmitted signal but the many variables in a multipath environment make these readings very unpredictable [3]. AOA estimation is most commonly used, with measurements using two different approaches. The first uses interferometry to calculate the time at every element of the antenna array whereas in the second approach, using a covariance algorithm, the RSS ratio between the sensor node and two or more directional antennas is calculated. These methods are explained in more detail below and their comparison forms the main content of this paper. The use of directional rotatable antennas has been suggested in [4, 5].

When a plane wave arrives at an antenna array it will be received by some nodes before others due to the differences in the lengths of the paths between the elements, resulting in phase differences between the rays received. These depend on the geometry of the array. The interferometry algorithm compares the relative phases of the received rays at each node of an antenna array. For a circular array antenna like the one shown in Figure 1, the path length difference can be calculated by using the centre of the array as a reference point.

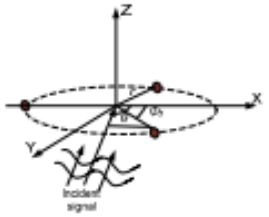

Fig 1. Uniform Circular Array with three elements

For an antenna array of three elements at least two sets of phase differences are required to get an unambiguous AOA estimate.

The covariance estimation algorithm uses eigenvalue analysis. Prior knowledge of the total number of the uncorrelated sources is required for estimation of the ray characteristics, meaning that the number of rays incident at the receiver must be known if the algorithm is to be able to estimate the position of the transmitters. The algorithm

978-1-4799-3662-5/14/$31.00 ©2014 IEEE

computes the eigenvalue decomposition of the covariance matrix, and then the signal sub-space is searched for maxima.

Mutual coupling between the antenna arrays degrades the accuracy of the signal processing algorithms used in the antenna array applications, and can result in enormous error in direction-of-arrival (DOA) estimation. Several studies have examined techniques to compensate the undesired effects of the mutual coupling and several approaches have been developed. Conventionally the mutual coupling was described using the mutual impedances between the array elements in their transmitting mode. However, it has been found that mutual coupling has to be treated differently in transmitting and receiving antenna arrays [6, 7].

II. Simulations and Discussion

All the simulations have been carried out using NEC software, with simple half-wavelength dipoles and quarter wavelengths monopoles mounted on square conducting material of size 1λ × 1λ. The antenna elements in each case were separated by λ/3. A perfect ground plane was used for the simulation model, and no mutual coupling compensation was applied. The antennas were placed at 1.5λ above the ground plane. Vertically polarized antenna arrays were simulated with the transmitter or transmitters (half wavelength dipole/s 0.5λ above the ground plane) placed 5λ from the receiving array. Signal processing was done using MATLAB.

Case 1: Single source transmitter: In the first case the true angle of the transmitter was set at 0° or 45°. The results in Figure 2 suggest that the performance of interferometry is much better with the monopole antenna array than with the dipole case; the covariance matrix gave stable results in both cases but still with better performance using the monopole array antenna.

Case 2: Dual source transmitters: In the second case using dual source transmitters with different power levels the true angle of the transmitters were set at 0° and 90° with 90° being five times dominant, or at 45° and 300°, with 300° being dominant, using a monopole antenna array only. The results obtained from the simulations are shown in Figure 3.

The results obtained in Figure 3 again showed the superior performance of the covariance based technique for both the angles. Interferometry was able to resolve the 90 degree source as the dominant angle but was unable to resolve the 300 degree source as being dominant. Both angles were well resolved by the covariance estimation with low error.

After the selection of the covariance matrix the study progressed to the design of an Inverted F Antenna (IFA) with non-symmetrical pattern of radiation to be used as part of the three element equilateral triangle shaped array simulated using Computer Simulation Technology (CST) software. The elements of the antenna array were spaced 25 cm apart and a single transmitter was set at 3 m away from the center of the antenna array: the setup is shown in Figure 5. A half-wavelength dipole antenna was used to simulate the transmitter antenna with omni-directional radiation in the azimuthal plane. A finite ground plane of 1 m x 1 m was used for the receiver array.

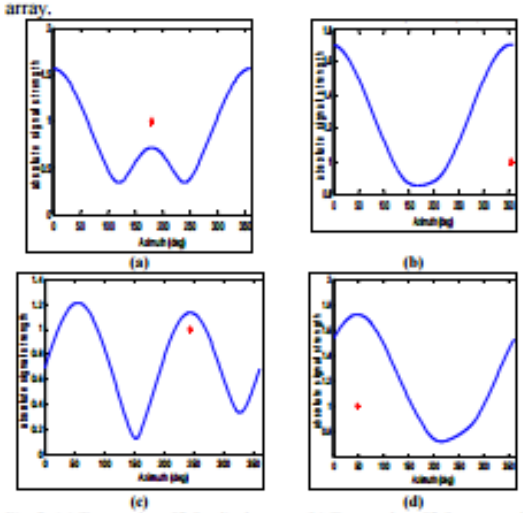

Fig. 2: (a) True angle = 0° for dipole array; (b) True angle = 0° for monopole antenna array; (c) True angle = 45° for dipole array (d) True angle = 45° for monopole antenna array; (solid line: scanning steering vector of the covariance method, asterisk: results of interferometry method).

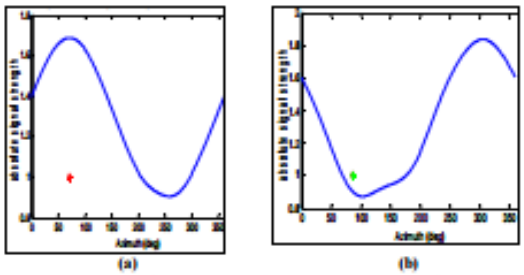

Fig. 3: (a) True angle = (0°, 90° (dominant)), (b) True angle = (45°, 300° (dominant)), solid line: scanning steering vector of the covariance method, asterisk: results of interferometry method).

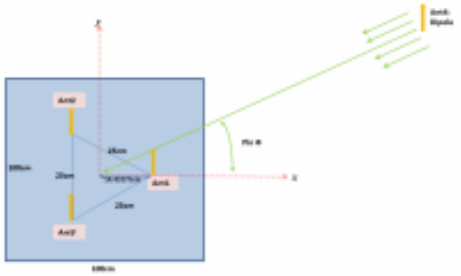

Fig 4. Simulation setup using IFA array

Angle of arrival measurements were based on the azimuthal plane observations as both the transmission and reception antennas were at the same level in the elevation plane. For simulation purposes the transmitter antenna was set to rotate anti-clockwise with a step size of 20° from 0° to 360°. 18 angles in total were used.

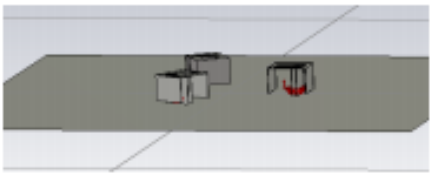

Fig. 5 Receiver antenna geometry for IFA

Table 1 gives the AOA estimation errors due to mutual coupling using a wideband signal over 25 MHz radiations from the transmitter. The simulation step size was 25 kHz.

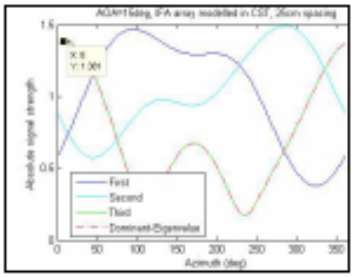

Fig 6. IFA array with mutual coupling

Table 1:
Simulation Results

AOA_REF /degrees	AOA_interferometry /degrees	AOA_Covariance /degrees
0	0	0
20	23.48	22
40	46.13	44
60	60.9	61
80	75.36	78
100	94.82	96
120	116.64	117
140	147.23	145
160	167.67	166
180	180	180
200	194.2	196
220	212.77	215
240	239.53	239
260	267.88	266
280	282.85	280
300	299.39	299
320	313.27	315
340	335.68	337
360	360	360

Simulation results using an array of three IFAs were derived using the covariance estimation algorithm. A decoupling matrix extracted for each angle using the received mutual impedance method as stated in [6] was then used to compensate for mutual coupling. The calculation of the decoupling matrix was done with the assumptions 1) that the antenna array is in the receiving mode and 2) that all the antenna elements have been terminated using matching loads, Z_L, with excitation through an external plane wave.

The current distribution at the resonant frequency of the omni-directional antenna does not change due to the azimuthal angle of the inbound signal thus producing no change in the received mutual impedance. For this reason omni-directional antennas are well suited for AOA applications. However as seen in Figure 3, the decoupling matrix will also depend on the geometry of the ground plane as the inbound ray will travel a varying distance over the ground plane to reach the array, depending upon its bearing.

The results shown in Figures 6 and 7 clearly show the improvement in the angle of arrival estimation when the mutual coupling between the elements is compensated. It can be seen that the angle error for a true angle of 15° has been reduced from 7° to 2° by the decoupling.

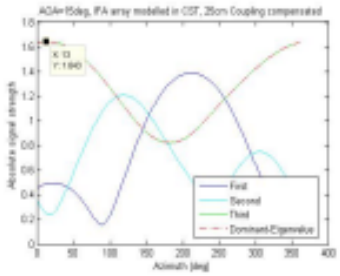

Fig 7. IFA array with mutual coupling compensated

Further simulations were carried out with the same setup, but with fewer observation angles, in order to investigate different mutual coupling compensation methods.

a) Conventional Mutual Impedance

The conventional mutual impedance method was applied to the IFA array. Four different incoming signal angles were studied for this occasion, and three different direction finding algorithms were applied. The decoupling matrices were calculated and applied to obtain the AoA estimation after compensation. From Table 2 we can see that for the IFA array, the transmitting mode decoupling matrix did not improve the estimation error. For some angles, the error even became much worse.

b) Received Mutual Impedance

Next the receiving mode method was used to generate the decoupling matrices for the IFA array. The true angles are calculated using the receiving mode matrices as shown in Table 3. In contrast to the transmitting mode method, the receiving mode method much improved the true angle

estimation. The maximum estimation error after compensation is 1° for all direction-finding algorithms.

Table 2
AOA estimation error before and after transmission mode compensation for the IFA array

AOA-ref (deg)	AOA error - Covariance-phase only		AOA error - Covariance Amplitude & phase		AOA error - Interferometry	
	before	after	before	after	before	after
15	-4	-6	-4	-6	-2.41	-6.3
120	-1	-1	-1	0	-1.38	-0.83
205	-4	-1	-2	-8	-3.77	-0.67
320	-3	7	-1	-6	-3.12	6.92

Table 3
AOA estimation error before and after receiving mode compensation for IFA array

AOA-ref (deg)	AOA error - Covariance-phase only		AOA error - Covariance Amplitude & phase		AOA error - Interferometry	
	before	after	before	after	before	after
15	-2	1	-4	1	-2.4	1.2415
120	-1	-1	-1	-1	-1.38	-0.8
205	-4	1	-2	1	-3.8	0.53
320	-3	0	-1	0	-3.12	-0.23

III. Conclusion

This study serves as a reference for the choice between the angle of arrival techniques of interferometry and covariance and also describes the negative effects that can be caused by the mutual coupling present between the elements of an antenna array.

Results have been given for the performance of both algorithms for different true angles and in a multipath environment with multiple transmission sources. The results support the idea of using covariance based estimation technique in order to increase the accuracy.

The decoupling matrices using these mutual coupling compensation methods were then generated and applied to simulation data. After validating these matrices by various direction-finding algorithms, the receiving mode method has shown its obvious advantages. Compared to other methods, the receiving mode method is easy to apply, requiring the same amount of calculation and memory space as the open-circuit voltage method.

References

[1] I. F. Akyildiz, W. Su, Y. Sankarasubramaniam, and E. Cayirci, "Wireless sensor networks: a survey," *Computer networks*, vol. 38, pp. 393-422, 2002.

[2] N. Patwari, A. O. Hero, M. Perkins, N. S. Correal, and R. J. O'dea, "Relative location estimation in wireless sensor networks," *Signal Processing, IEEE Transactions on*, vol. 51, pp. 2137-2148, 2003.

[3] I. F. Akyildiz, W. Su, Y. Sankarasubramaniam, and E. Cayirci, "SENSOR NETWORKS," *Y, et al. A survey on IEEE Communications Magazine*, vol. 40, pp. 102-114, 2002.

[4] B. N. Hood and P. Barooah, "Estimating DoA from radio-frequency RSSI measurements using an actuated reflector," *Sensors Journal, IEEE*, vol. 11, pp. 413-417, 2011.

[5] M. Abusultan, S. Harkness, B. J. LaMeres, and Y. Huang, "FPGA implementation of a Bartlett direction of arrival algorithm for a 5.8 ghz circular antenna array," in *Aerospace Conference, 2010 IEEE*, 2010, pp. 1-10.

[6] Hema Singh, H. L. Sneha, and R. M. Jha, "Mutual Coupling in Phased Arrays: A Review," *International Journal of Antennas and Propagation*, vol. 2013, Article ID 348123, http://dx.doi.org/10.1155/2013/348123

[7] Hoi Shun Lui and Hon Tat Hui, "Mutual Coupling Compensation for Direction-of-Arrival Estimations Using the Receiving-Mutual-Impedance Method," *International Journal of Antennas and Propagation*, vol. 2010, Article ID 373061, doi:10.1155/2010/373061

OFDM Wideband DOA System for Detecting and Tracking Vehicles Applications

M.A.G. Al-Sadoon[1,4], R. Asif[1], N.T. Ali[1,2], I.T.E. Elfergani[3], J. Rodriguez[3], S.M.R. Jones[1], J.M. Noras[1], R.A. Abd-Alhameed[1], and A. Zuid[4]
[1]School of Electrical Engineering and Computer Science, University of Bradford, Bradford, BD7 1DP, UK
[2]ECE Dept., Khalifa University, Abu Dhabi, UAE
[3]Instituto de Telecomunicações, Portugal
[4]Basra University College of Science and Technology, Basra, 61004, Iraq

Abstract— **This work proposes a new angle of arrival method for tracking applications using compact omni-directional spiral antenna arrays. The impact of mutual coupling is considered within the covariance matrix calculation and then a suitable decoupling method is used to remove such effect. An urban area consisting of many buildings with different heights and characterized by various materials was modelled using Wireless In-Site Software to extract the impulse response of the channel between non-stationary locations of the transmitted target and the receiver antenna array. Orthogonal Frequency Division Multiplexing (OFDM) scheme based on wideband spectrum is integrated with the proposed angle of arrival to improve the estimation accuracy. MATLAB code is developed to simulate the above conditions and the experiment results are presented and discussed.**

Index Terms— **antenna array, tracking systems, propagation, multipath channel, OFDM, DOA and location estimation, localisation, wireless communication.**

I. INTRODUCTION

Position-awareness is currently an active research topic playing a fundamental role in many applications including tracking systems [1], rescue-and-search operations [2] and localisation services in fifth generation (5G) cellular networks [3]. Although the Global Positioning System (GPS) is efficient technology that can provide accurate position-awareness around the world through a constellation of at least twenty four satellites [4], the efficiency of GPS drops in harsh environments, for example, in urban canyons, in caves and buildings and under tree canopies [5], since most GPS signals are not able to penetrate obstacles. Therefore, new and more accurate localisation techniques are needed for use in such environments. A wideband wireless network can provide precise localisation in GPS-denied environments [6]. In particular, wide bandwidth signals can provide reliable and accurate range measurements due to their fine delay precision and robustness in harsh environments [7]. In general, position-aware networks consist of two categories of nodes: anchors and agents. The location of anchors can be known through system design or GPS, whereas the agent's positions are initially unknown and attempt to find their locations. In order to determine its position and/or directions, each node needs to be equipped with a wideband transceiver, and localisation can be achieved through radio signaling between users and their neighbouring anchors. Localising a target needs a number of signals sent from the anchors, and the relative location of the target can be inferred from these incoming signals using a variety of waveforms metrics. Due to possible physical obstructions in the direct path, non-line-of-sight (NLOS) conditions can result, together with multiple paths, resulting in fading and interference issues.

Angle of Arrival (AOA) is a popular approach in which the arrival angles of the agents, which arrive to the base stations are used to estimate a target's location [8]. Wideband AOA systems can estimate not only the LOS direction of emitters but also the direction of multipath components, which provide extra spatial information. However, since the received signals are affected by random phenomena, for instance fading, scattering, shadowing, NLOS and multipath propagation, the estimation of an agent's location can be uncertain. In the state of the art, comparatively few works have investigated the impact of NLOS and multipath propagations on localisation resolution. Other studies utilize narrowband signal models, which use averaging of the received path and are not applicable for wideband networks. In contrast, wideband AOA models utilize the directions of all the multiple paths, which have different directions, timings and signal strengths.

The size of an antenna array is crucial in several applications and should be as small as is practical. Typically, it is most desirable for localization and tracking systems to combine an efficient angle of arrival technique with small compact omni-directional antenna arrays. The contribution of this work is to integrate the compact omni-directional spiral antenna that proposed in [9] with a new, efficient AOA algorithm for tracking applications in urban areas. This system is intended to work on top of cars, so that the smallest antenna height is desirable. An urban area is modelled in Wireless-Insite software where NLOS and multipath propagations are produced and then used to track and localise the agent's position. The mutual coupling matrix is calculated as in [10] and then inserted in the covariance matrix, when an appropriate decoupling algorithm eliminates the effect of mutual coupling. The OFDM scheme is used in this study to combat multipath phenomenon, with the received signals split into many small narrowband sub-carriers to improve the estimation accuracy. Several estimation strategies are investigated such as exploiting the strongest signal path, the path with least time of arrival, and the averaging of all or some of the arrival path.

The rest of this paper is organized as following. Section II provides the mathematical model for the antenna array and the OFDM scheme to be used. In section III, the principles and mathematical model of a new algorithm we call "Inverse of Subtracting" (IOS) are presented. The computer simulation,

experimental results and discussions appear in section IV. Section V summarizes the results and gives brief conclusions.

II. ANTENNA ARRAY AND SIGNAL MODELLING WITH OFDM

A circular array of spiral antennas is a common geometry which can be used to increase gain. It is suitable in scenarios where 360 degrees of coverage or both elevation and azimuth for specific coverage area are required. For a resonant frequency of 400 MHz, the geometry of the antenna array used in this work is shown in Fig.1. The radius (r) of the ring array is calculated based on ($d = \lambda/2 = 37.5$ cm), then $r = r = \frac{d}{2\sin\left(\frac{\pi}{M}\right)} = 31.9$ cm, where M is the number of antenna elements.

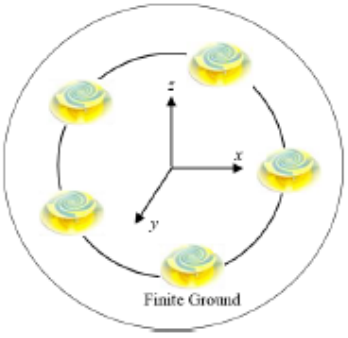

Fig. 1: Basic geometry of 5 element spiral antenna array on finite ground plane.

After the antenna array receives all signals from different directions of arrival (DOA)s, the OFDM scheme is applied to divide the active transmission bandwidth into narrow band carriers which are suitable for wideband AOA estimation. The broadband impulse channel response is given by:

$$h(\tau) = \sum_{k=1}^{n} a_k e^{j\phi_k}\delta(\tau-\tau_k) \quad (1)$$

Apply an input signal:

$$f(t,\omega) = e^{j\omega t} \quad (2)$$

Then the output can be simplified to the following:

$$s(t,\omega) = \sum_{k=1}^{n} a_k e^{j\phi_k} e^{j\omega(t-\tau_k)} \quad (3)$$

This alternatively can be given by:

$$s(t,\omega) = e^{j\omega t}\sum_{k=1}^{n} a_k e^{j\phi_k} e^{-j\omega\tau_k} = e^{j\omega t}U(\omega) \quad (4)$$

Extending U(ω) over baseband bandwidth B (as shown in Fig.2) for N frequency samples, then the i^{th} frequency sample can be expressed by:

$$f_i = -\frac{B}{2} + (i-1)n\Delta f \quad (5)$$

$$f_i = -\frac{B}{2} + (i-1)n\frac{B}{N} = \frac{B}{2}\left(-1 + (i-1)\frac{2n}{N}\right)$$

where

$$N\Delta f = B \quad (6)$$

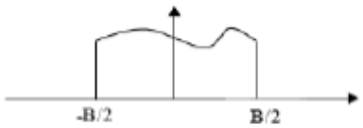

Fig. 2: Assumed bandwidth range

The sampling time can be stated as follows:

$$\frac{1}{2\Delta t} = \frac{B}{2}, \text{ hence } \Delta t = \frac{1}{B} \quad (7)$$

Thus, the minimum sampling frequency is:

$$f_s \geq 2\frac{B}{2} = B \quad (8)$$

The i^{th} uniform frequency sample of U(ω) can be given by:

$$U(2\pi f_i) = \sum_{k=1}^{n} a_k e^{j\phi_k} e^{-j\omega\tau_k} e^{-j2\pi f_i\tau_k} \quad (9)$$

Then, the covariance matrix is computed as follows:

$$R_{xx} = U\,U^H \quad (10)$$

III. THE MAXIMUM SIGNAL SUBSPACE (MSS) AOA METHOD

After the covariance matrix is obtained, an AOA is applied method to estimate DOAs. The proposed algorithm is based on the orthogonality between manifold array vector and the eigenvector associated with the largest eigenvalue with regraded less to the number of received signals. Therefore, the new method does not require previous knowledge of the number of arrival signals in comparison with Multiple Signal Classification (MUSIC) [11] and Estimation of Signal Parameters via Rotational Invariance Technique (ESPRIT) [12]. To summarise the proposed algorithm, first we construct the covariance matrix(R_{xx}), secondly apply eigenvalue decomposition (EVD) on R_{xx} to yield:

$$R_{xx} = Q\,\Sigma Q^H \quad (11)$$

Q is the (M×M) eigenvectors matrix and is given as follows:

$$Q = [q_1, \quad q_2, \ldots\ldots\ldots q_M] \quad (12)$$

and Σ are the eigenvalues that corresponding to every eigenvector, given by:

$$\Sigma = [\lambda_1, \lambda_2, \quad \ldots\ldots, \lambda_M] \quad (13)$$

Next sort the eigenvalues in descending order (i.e. $\lambda_1 > \lambda_2 > \lambda_3 > \cdots\cdots > \lambda_M$) and choose the eigenvector associated with the largest eigenvalue (λ_1). Once this eigenvector is obtained, the spatial spectrum can be constructed by using the following equation:

$$P_1(\theta) = q_1\, a(\theta) \tag{14}$$

Then, normalise the pseudospectrum of the above equation using the maximum value:

$$P_{Norm}(\theta) = P_1(\theta)/max(P_1(\theta)) \tag{15}$$

Next subtract $P_{Norm}(\theta)$ from unity in order to obtain narrower peaks and also to minimize side-lobe levels, as described below:

$$P_S(\theta) = 1 - P_{Norm} \tag{16}$$

Once this condition is achieved, we will obtain nulls in the direction of received signals, to obtain peaks in the DOA signals, the inverse of subtracting (IOS) is computed as follows:

$$P_{IOS}(\theta) = \frac{1}{P_S(\theta) + \varepsilon} \tag{17}$$

where ε is a small scalar value added in order to avoid possible singularities. The last step is find the locations of the peaks to determine the direction of the transmitters or targets.

Fig. 3. Showing scenario of tracking process for an outdoor urban area.

IV. EXPERIMENTAL RESULTS AND DISCUSSION

In this section, we simulate the proposed system for tracking scenario such as rescue-and-search operations and /or public security applications. A 5-element spiral antenna array is located on top of a vehicle at 2 m height. These sensors are spatially distributed in the azimuthal plane with angular separation of 72 degrees and inter-element spacing set to $\lambda/2$. The wireless propagation simulation software Wireless Insite is used in this study since it can provide the most realistic simulation model for wireless propagation. It is an electromagnetic simulation tool that helps predict the propagation behaviour of electromagnetic waves in the presence of objects with different electrical properties. The tracking scenario used in this work is an urban environment (1000 m × 650 m): part of this area is shown in Fig. 3. An omni-directional transmitter antenna located at a height of 1.5 m was considered for the evaluation process.

The urban area consists of many buildings with different heights, with a maximum height of 50 m. There are various materials - concrete, brick and wet earth. The loudest received path is only shown in Fig. 3 to avoid ambiguity in the presence of so much multipath. As can be seen in Fig.3, the tracking process is started by taking the first measurement at point Rx1-1 and then at point Rx2-1, … until the last point at Rx8-1. The sequence and location of the receiver at these points and of the transmitter are given in Table 1.

Table 1. Showing the sequence and location of the receiver at each point in the tracking process.

Tracking steps sequences	Location of receiver in x(m)	Location of receiver in y (m)
a. Rx1-1	994	297
b. Rx2-1	928	292
c. Rx3-1	859	290
d. Rx4-1	849	250
e. Rx5-1	847	180
f. Rx6-1	767	172
g. Rx7-1	765	131
h. Rx8-1	753	89
i. Tx1	720	59

At each point of the tracking process, the antenna array receives ten multipath at each element with different power, TOA and phase. The impulse response from all received channels between non-stationary locations of the transmitted target and the receiver antenna is processed via the wideband OFDM scheme: the bandwidth here is 10 MHz, split over 64 sub-carriers. The IFFT was applied to the received channel transfer function to acquire the impulse response with 10 multipaths. Based on the suggested bandwidth the tracking process was applied over several options such as loudest signal strength, least time of arrival and the average of all / or small number of arrival paths.

The covariance matrix is calculated and the effect of the mutual coupling is taken into account, and an appropriate decoupling method is exploited to reduce the coupling effects. Then the data are passed to the IOS angle of arrival method to estimate DOAs and track the location of the agent. This process is repeated at each measurement point in Table 1 and the estimated direction at each point is shown in Fig.4. The performance estimation of the proposed system can be presented based on the locations of receiver at all the measurement points and the estimated directions at these points as shown in Fig.5. As can be seen from this graph, the proposed system works efficiently and it is useful for such applications. Another advantages has been obtained in the IOS algorithm is by removing the false peaks and/or the side lobe issues completely, which otherwise could create uncertainty for selecting the correct direction.

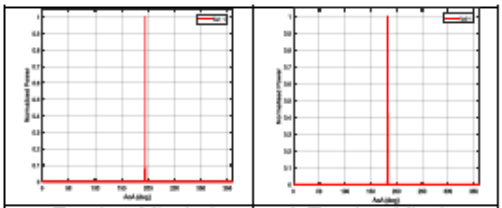

a. The estimated direction is 194.2°.

b. The estimated direction is182.8°.

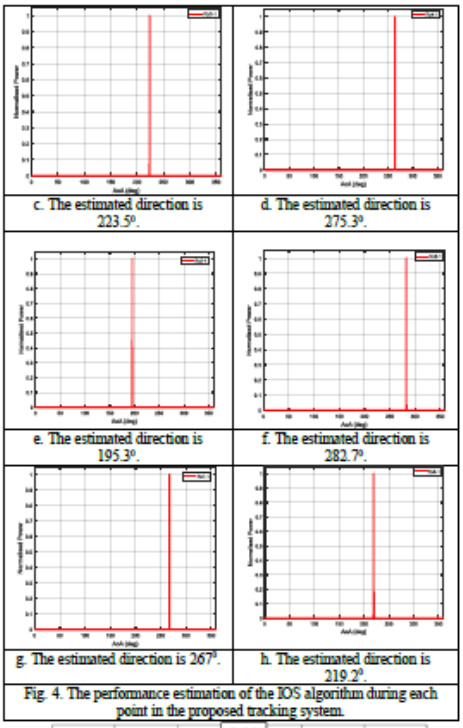

c. The estimated direction is 223.5°.

d. The estimated direction is 275.3°.

e. The estimated direction is 195.3°.

f. The estimated direction is 282.7°.

g. The estimated direction is 267°.

h. The estimated direction is 219.2°.

Fig. 4. The performance estimation of the IOS algorithm during each point in the proposed tracking system.

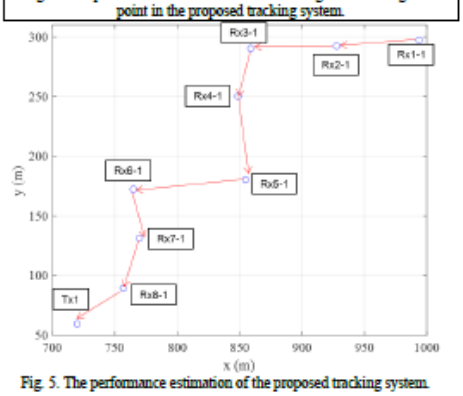

Fig. 5. The performance estimation of the proposed tracking system.

V. CONCLUSION

In this paper, a new and efficient angle of arrival method has been presented based on the received signals from a 5-element ring array for outdoor tracking, using small omni-directional spiral antennas for possible integration on top of cars. OFDM over a wideband spectrum was considered and found to be suitable modulation candidate for a such tracking system. The mutual coupling effect was included and an efficient decoupling method was utilized to eliminate the negative effects from the covariance matrix. An example was implemented to simulate the scenario of tracking in an urban area under multipath conditions and the results confirmed that the proposed tracking system works efficiently.

REFERENCES

[1] L. Wan, G. Han, L. Shu, S. Chan, and T. Zhu, "The Application of DOA Estimation Approach in Patient Tracking Systems with High Patient Density," *IEEE Tran. on Industrial Informatics*, vol. PP, pp. 1-1, 2016.

[2] S. S. Anjum, R. M. Noor, and M. H. Anisi, "Survey on MANET based communication scenarios for search and rescue operations," 5th Int. Conf. in *IT Convergence and Security. 2015*, pp. 1-5.

[3] M. A. Khan, N. Saeed, A. W. Ahmad, and C. Lee, "Location Awareness in 5G Networks using RSS Measurements for Public Safety Applications," *IEEE Access*, 2017.

[4] L. M. Kaplan, "Global node selection for localization in a distributed sensor network," *IEEE Transactions on Aerospace and Electronic systems*, vol. 42, pp. 113-135, 2006.

[5] D. B. Jourdan, D. Dardari, and M. Z. Win, "Position error bound for UWB localization in dense cluttered environments," *IEEE transactions on aerospace and electronic systems*, vol. 44, 2008.

[6] S. Gezici, Z. Tian, G. B. Giannakis, H. Kobayashi, A. F. Molisch, H. V. Poor, *et al.*, "Localization via ultra-wideband radios: a look at positioning aspects for future sensor networks," *IEEE signal processing magazine*, vol. 22, pp. 70-84, 2005.

[7] Y. Shen and M. Z. Win, "On the accuracy of localization systems using wideband antenna arrays," *IEEE Transactions on Communications*, vol. 58, 2010.

[8] A. H. Sayed, A. Tarighat, and N. Khajehnouri, "Network-based wireless location: challenges faced in developing techniques for accurate wireless location information," *Signal Processing Magazine, IEEE*, vol. 22, pp. 24-40, 2005.

[9] T. S. Ghazaany, S. Zhu, R. A. Alhameed, J. M. Noras, S. M. Jones, T. V. Buren, *et al.*, "Experimental Study of Coupling Compensation of Low Profile Spiral Antenna Arrays Response for Direction-finding Applications," *Applied Computational Electromagnetics Society Journal*, vol. 31, pp. 744-749, 2016.

[10] H. T. Hui, "A new definition of mutual impedance for application in dipole receiving antenna arrays," *IEEE Antennas and Wireless Propagation Letters*, vol. vol. 3, no. 1, pp. 364-367, 2004.

[11] R. Schmidt, "Multiple emitter location and signal parameter estimation," *IEEE Transactions on Antennas and Propagation*, vol. 34, pp. 276-280, 1986.

[12] R. Roy, and T. Kailath, ", "ESPRIT-Estimation of Signal Parameters via Rotational Invariance Techniques " *IEEE Transactions on ASSP*, vol. 37, pp. 984–995, July 1989.

Current Technologies and Location Based Services

I. Ahmad, R. Asif, R.A. Abd-Alhameed, H. Alhassan, F. Elmegri, J.M. Noras, CH See, H. Obidat, W. Shuaieb, J.C. Riberio, K. Hameed, A. Alabdullah, A. Ali, M Bin melha, M. Al Khambashi, H. Migdadi, M.B. Child, M.A.G. Al-Sadoon, F.M. Abdussalam, I.M. Dunjuma, A. Saleh, G. Oguntala, N. Eya, M. Buhari, N. Abduljabbar, Geili T.A. El Sanousi, J. Kosha, SJ Shepherd, A. Mirza, S.M.R. Jones, ITE Elfergani, J Roderguez, AS Hussaini, R. Qahwaji, PS Excell, NJ McEwan

Radio Frequency and Sensor Design Research Group, School of Electrical Engineering and Computer Science, University of Bradford, Bradford BD71DP, UK, Email: r.a.a.abd@bradford.ac.uk

Abstract — **This paper examines the benefits and drawbacks of these services, reviewing differences in infrastructure, power requirements, sensing devices, and other factors. Technologies covered include Radio Frequency Identification, GSM, GPS, A-GPS, Smart Antennas, Distributed Antenna Systems, Localization by Cell-ID, Localization by Prediction (Dead Reckoning method), Angle of Arrival (AOA), Localization by Finger Printing, Localization by Time of Arrival (TOA), Localization by Observed Time Difference of Arrival (TDOA), and Hybrid Localization-based AOA-TOA.**

Keywords— Localization Based Services LBS; Benefits of LBS; Drawbacks of LBS; Advantages of LBS; Disadvantages of LBS; GPS; GSM; RFID Systems.

I. INTRODUCTION

Location Based Services (LBS) comprise business and consumer services that rely on the position of the users, in order to provide services (both information and entertainment) to their users [1, 2]. LBS functions on three different levels [3, 4]:

- position level, based on the present position of the user;
- tracking level requiring both the present and the past position of the user;
- planning level, requiring the present, past and future positioning of the user.

LBS technologies may also be characterized as Itinerant (serving moving users), Distributed (services via a computer network) and Ubiquitous (providing services to any location within the network) [5].

II. CATEGORIZATION OF LBS

Kemper and Linde introduced a passive infrared technique using the thermal radiation of humans for localization. It is useful in health sector to take care of old and special persons. It does not require a hardware tag, so it is very convenient [6]. LBS use other localization techniques such as radio-based systems, ultrasonic-based systems, active infrared-based systems, camera-based systems and Smart Floor systems. The drawback of radio-based systems is they need special hardware. Hybrid systems use ultrasonic-based systems, e.g. Active Bat [7]. Active infrared-based systems also require hardware and its precision is limited to a room only. The Active Badge System is an active infrared-based system [8]. The benefit of camera-based systems is the non-dependency on hardware. An example is the Easy-Living-Tracker, but the need for computing power and the violation of privacy is a drawback [9]. The Smart Floor system uses foot fall on load cells within the floor [10]. LBS utilize components such as wireless networks, user devices, position technologies, geographical data servers and application servers [11]. The network congestion in LBS can be decreased by using distributed architecture. Zhi-xiang Fang and Qing-quan Li proposed a "layered spatial service architecture" in which there is a localization of a geographical database on a distributed network [12]. This architecture diminishes the load on central servers. Ching-Sheng Wang and Ching-Yang Hong proposed the use of P2P procedure in order to deliver data related to the location [13]. The data is utilized in combination with the virtual navigation scheme that receives the positioning of the users in the real environment and then shows the position of the user in a virtual model facing the same environment. In order to optimize the sharing of P2P file, groups of users are formed depending upon the location and the concerns. There are different approaches for determining the positions of objects in LBS such as Terminal-based Approaches and Network-based Approaches. Terminal-based Approaches include Global Positioning System (GPS), Assisted Global Positioning System (A-GPS) and Enhanced Observed Time Distance (E-OTD). Network-based Approached includes Cell Global Identity (CGI) and Time of Arrival (TOA). There are different positioning systems for mobile terminals in LBS that differ in reliability, accuracy and calculations. These positioning systems include satellite positioning systems, network-based positioning systems and local positioning systems [14]. Positioning technologies greatly affects the reliability, efficiency and performance of the LBS [15]. Positioning Systems can be indoor, outdoor or mixed. High precision and signal strength is needed for indoor localization. Flora, Ficco, Russo and Vecchio proposed a software architecture that was based upon both indoor and outdoor location sensing techniques. They introduced a generic API at the top of the architecture that could support hybrid applications. Bluetooth and Global Positioning System devices were utilized as location sensors. This architecture was based upon client side mechanism and zoning location sensing method. It is in accordance to JSR-179 provisions [16]. The information about the location is kept on the mobile for personal usage. There are various privacy issues that need to be addressed in future for this architecture. The advantages and disadvantages of different Outdoor Systems Localization are discussed below:

III. RADIO FREQUENCY IDENTIFICATION (RFID)

Radio Frequency Identification (RFID) technology commenced in the 1970s. Initially this technology was just used for tracking animals. Today, Radio Frequency Identification has various applications, ranging from tracking luggage on airports to storing university student's details.

Radio Frequency Identification beacons are minute and light weight. They operate by propagating small radio packets at small wavelengths [17]. Radio Frequency Identification beacons just have a range of up to 1 or 2 meters. Furthermore, it is not necessary that the receivers and the transmitters are in the Line of Sight for the completion of a transmission. Radio Frequency Identification tags also store huge quantity of data, as well as instructions. They can pinpoint locations to approximately exact coordinates.

978-1-5090-4815-1/17/$31.00 ©2017 IEEE

RFID uses Automatic Identification ID, that is; biometric, voice recognition, smart cards, optical character recognition, magnetic inks, bar codes, touch memory, etc. These technologies are good for huge production networks. It makes use of electromagnetic waves or inductive coupling for gathering data related to some item [18]. The data carrier comprises of a microchip which is connected to an antenna which enables the microchip to propagate information to the user. For security purpose, data can be encrypted and anti-collision algorithms can be used for the tags if numerous of them are read by the users simultaneously.

The significant feature of RFID for tracking items is that it provides unique identification. Electronic Product Code (EPC) is used for the identification of an item. This code provides a standard number to the item in the EPC global network. The Object Name Service (ONS) provides internet addresses to access the data. The use of ONS is relatively expensive, so it cannot be always used in the global networking [19].

IV. Different Applications of RFID

RFID technology is utilized in different fields of life. Some of the applications are explained in Table I.

Table I: Applications of RFID.

A. Transportation
In Transportation, it can be used for safety management, distribution management and material processing management. Radio Frequency tags on the trucks are used for the verification of the truck drivers, trucks and the company to which the trucks belong. The Commercial Driving License with the tags verifies that they have come for business at the terminals. This system also enables determining the contents of the containers in the trucks [20]. This fleet management system is good for safety purpose and for reducing congestion.
B. Retailing
In Retailing, RFID technology can be used for checkout management, shelf-stock management and inventory management, smart fitting rooms, smart checkout and product location tools [21].
C. Agriculture
In Agriculture, it can be used for crop identification, animal tracking and animal diagnostics. This technology is used in the whole process of seed quality management such as in the cultivation of seeds, storage of seeds and transportation of seeds to the supervision, seed quality confirmation and supply of seeds to the farmers [22].
D. Ticketing and Traffic Management
In ticketing and traffic management, it can used for public transport ticket, automatic vehicle location, toll collection and smart car key. In toll payment it is used in pre-paid access cards which comprises of embedded microchip. RFID technology is used in Automated Parking Management System. In this system, The Integrated Recognition and Identification System (IRIS) links Automatic Number Plate Recognition (ANPR) technology with the Radio Frequency Identification [23]. The plate number of a vehicle is automatically captured, stored and is checked with the database comprising of registered vehicles. The matching of the plate number with the database results in the automatic opening of barrier.
E. Healthcare System
In healthcare system, it can be used for elderly care [24], pharmaceutics, hospital equipment and personnel management, implants, prostheses and for tracing patient medical history. Stanford Children's Health Clinic is using real time location system for the identification of the patients, personnel, medical equipment, etc. The clinic installed active 433 MHz. Radio Frequency Identification (RFID) and Infrared (IR) tags in the form of badges. The badges are used for the transmission of the unique identifier to the receivers (V-Direct – with cable or power connection or V-link – wireless battery powered connection). The sensors on the ceilings receive the unique IDs transmitted by the badges. The badge includes a button which the patient or the staff member presses for getting assistance. Versus Asset tags have also being attached to the medical equipment (e.g. for measuring Blood Pressure) and for the interpretation of the language. Current surveys conducted in 2016 have revealed that the introduction of the RFID technology has greatly improved the performance of the clinic [25].
F. Human Identification Management
In human identification management, it can be used for digital ID, electronic passport, getting access to facilities and for punishment system management. By using RFID technology for human identification management, crime rate can be reduced as there will be fewer chances of fraud or theft cases.
G. Internal Location-based Services for Mobile Users
RFID also provides internal LBS for mobile users. Siadat and Selamat proposed a system combining wireless J2ME and RFID technology for locating the users accurately inside a building and sending information to them according to their interests. The mobile phone reads RFID tags, sends the request to the server via the wireless network. The server searches the relevant information and sends it back to the user. A client side application named Java 2 Micro Edition (J2ME) was used for this purpose [26].
H. Education and Research Purpose
Miniature RFID tags are used for education and research purpose, such as, in the year 2009, researchers of Bristol University used Radio Frequency Identification micro transponders for studying the behaviour of ants [27]. The dust size micro RFID chips are 0.05 mm in size and utilize Silicon-on-Insulator (SOI) technique. Hence, RFID technology is quite useful for studying the life patterns, habitat and behaviour of animals and birds. In birds, it can be used to study their migration range and habits. The major limitation is the need of antennas which limits the range to just millimetres. Apart from these applications, RFID can be used in military logistics, dispensing control systems of fuels and chemicals, luggage handling, library inventory management, digital signature and parcel and mailbag tracking system.

V. Global Positioning systems (GPS)

The Global Positioning System (GPS) is an operational system comprising of earth orbiting satellite built routing system. It provides it users all around the world with 24 hour a day accurate positioning and time observable to the standard global time in the three dimensions. It comprises of three "segments" namely, the Control Segment, the Space Segment and the User Segment. Correct functioning of these three segments leads to the precise and consistent working of the whole system. The Control Segment is also known as the main control center as it is involved in the transmission to the satellites. The Space Segment is composed of a collection of satellites that orbits about 20,000 km beyond the Earth. The User Segment is composed of the receivers that listen to the satellites at any given time. The User Segment involves the receiver that is currently functioning and its linked antenna. GPS does not work efficiently in indoor environment as GPS satellites possess weak signals which cannot cross the walls of buildings. Hence, GPS is not effective for indoor localization. Indoor localization requires high None Line of Sight (NLOS) and efficient positioning system.

VI. Applications of GPS

GPS technology is used in variant field of life. Some of the applications are discussed in Table II.

Table II: GPS technology and its applications.

A. Satellite Navigation
The foremost application of GPS is satellite navigation in ships, aircraft or vehicles. It enables a GPS receiver to locate their position or pinpoint their speed with accuracy whether on land, air or sea. It does not only provide a route to drivers to follow but also provides alert regarding traffic issues.
B. Emergency Situations
GPS can serve as an important purpose in emergency situations. It aids rescue teams at sea or land to pinpoint the desired location of the accident immediately.
C. Adventurous Trips
Hikers use various maps and compasses to reach their desired locations but now GPS can provide all the essential information for adventure seekers. It provides the correct route, alternative routes and directions to reach back to the original point. GPS can also pin point the clearest location in case if hikers forget their tracks or get into some trouble [28].
D. Mapping and Surveying
GPS provides a high accuracy data related to mapping and surveying. The collection of data is way too faster - less than a single day as compared to other techniques used for mapping and surveying. From heights of mountain to the depth of rivers, GPS supports the precise mapping around the globe.
E. Driving and Locating Routes
Keeping in view the mobile applications, Glimpse is an application through which one can share the mobile location by text messaging and through the social media applications. The application locates stores and public places around the users if they have arrived at any unknown place. This application also informs about the routes, traffic alerts and the alternate routes. Ulysse speedometer provides the users with information such as altitudes, directions and warnings in case of fast driving [29].
F. Military Purpose
GPS has its significant application in jamming properties of military navigation. The location information of forces in military procedures and operations are vital. It aids in monitoring and tracking of potential targets. These

tracking procedures can use other techniques as well, e.g. photo reconnaissance in order to enhance awareness and information to bombing missions. In the modern era, Unmanned Aerial Vehicles (UAVs) are used in military actions around the globe. The GPS tracking systems are quite affective in providing guidance to high altitude UAVs, especially in those areas where camera instalment fails due to environmental factors. The emergence of GPS in jamming devices is of prime importance. A signal jamming is a major thread in military operations. GPS uses satellite navigation to broadcast signal, as a result of which, required information is obtained. One of the military applications is GPS Jammer Location (JLOC). It is designed to monitor GPS interference threats as well as to provide alerts for the threats in the detected area. Apart from it, GPS also serves civil purposes in aircraft navigation and maritime navigation [30].

G. Assisted GPS (A-GPS or a-GPS)

A-GPS uses a server from an external device and the satellite system. The advantage of A-GPS is that the signals are always complete and there are no fragments in it. Secondly, it is faster and uses the surrounding cell towers which give a vivid picture of the position. A-GPS comes along with negative externalities. To use A-GPS a subscription is required, so it is costly. Other A-GPS require Wi-Fi or other wireless internet connection which may not be available universally but if available they will once agnin increase the cost. There are also some privacy concerns as the third party knows the location of the user which is dangerous. Most of the A-GPS devices are dependent on the outside server, so they might not function properly without it [31].

VII. Outdoor Systems Using Terrestrial Base Station

The Outdoor system using Terrestrial BSs comprises of Global System for Mobile Communications GSM (with E-OTD), GSM (with CELL-ID), CDMA/GPRS (with A-GPS), CDMA/GPRS (with A-GPS) - AFLT+AGPS, Wireless Assisted GPS and AFLT: GPS One A Hybrid Solution, WCDMA (with IPDL, TA-IPDL and OTDOA-PE), Systems with Smart Antennas and Distributed Antenna Systems (DAS). The merits and demerits of these systems are illustrated in Table III.

Table III: Merits and demerits of the localized outdoor systems.

A. Global System for Mobile Communication (GSM)

Global System for Mobile Communication is the modern cellular tech used to voice and data throughout the world. GSM has become the industry standard when it comes to mobile communication. Moreover, due to the extensive coverage, GSM users can travel in over 218 countries without changing their mobile phone number. Although, different countries use variant frequency bands, it comes down to the handset of the user, whether it can support those frequencies or not and how much the user's original carrier charges for roaming [32].

On the other hand, GSM suffers from the issue of bandwidth lag. This is a major setback as when many users share a bandwidth, interference can be created easily. That is why faster technologies like 3G are being built upon CDMA, a different type network, to avoid such limitations. Another very crucial drawback for GSM is that it has the tendency to interfere with certain electronic equipment. Due to its pulse transmission technology it can affect a pacemaker or radio communications of an airport.

B. GSM (with E-OTD)

Enhanced Observed Time Difference (E-OTD) is a positioning technique used by GSM mobile operators to locate their users, by multilateration [33]. The procedure is very much similar to the technique Time Difference of Arrival, except the fact that the positioning algorithm and all other calculations are performed in the user's device or handset rather than the base station or server. In order to facilitate the equations a lot of data is required, including different time measurements, called Location Measurement Unit (LMU) [34]. The Location Measurement Unit provides the mobile user with a real time difference which is required by the handset to calculate the geometric time difference and the location consecutively. Placing Location measurement units throughout the coverage region is very expensive and so is equipping the user's handset with special software. This localizing method increases expense more than others and whilst under consideration, Localization by Time Difference of arrival is seen as a better alternative.

C. GSM (with CELL-ID)

To have the most coverage, network providers divided areas and assigned base transceiver stations. Then, further divided the regions and assigned to each a Cell ID and a radio tower through which every user was to connect to. Now, GSM providers could use different localization algorithms to position a user, as a fix to the Cell ID would narrow down the position to some extent [35]. Algorithms like ToA (Time of Arrival), TDoA (Time Difference of Arrival), AoA (Angle of Arrival), etc. are although not as accurate as GPS as the user can be anywhere in a Cell ID, but positioning is fast as there is no searching for satellites available [36]. Moreover, seamless integration to Google maps has made this technique quite popular.

D. CDMA/GPRS (with A-GPS)

One of the most popular GPS location trackers in the market today, is the GSM GPRS tracker. GPS tracker but with one that has access to a GSM SIM card. The GSM sim card allows the tracker to transmit wireless data to an APN or a wireless access point. Next, the APN transmits the received data to a GPS service provider via internet, so that the end user can access the tracking data. This method overcomes the flaws of the older system which involved data transmission through SMS messages, that being expensive and unreliable. Thus, it makes the GPRS tracker cost effective, reliable and efficient.

The key difference among the GSM and GPRS techniques is that former is based on circuit switching while the later one is based on packet switching just like internet protocols in addition to this TDMA user can also be embedded in existing GPRS techniques. The connection speed in GPRS is far more than wired connections, as this system utilizes packet data network just like the internet [37]. This simple radio principle is adopted by GPRS to transfer data packets. These packets are later on directly routed over the packet switched either for accessing the internet or making the calls and sending SMS. The key feature associated with GPRS are always online capability, easy upgrade of the existing GSM connection and the foundations created for further enhancements in this arena which leads to the introduction of 3G, EDGE, LTE and similar other connections [38]. There are also some key characteristics associated with a GPRS which includes Mobility (online while roaming around), immediate connection and getting the exact co-ordinates. All these advantages greatly outshine the second generation cellular system GSM.

The CDMA GPS trackers differ from the former ones such that they use a GPSOne chipset, which is not as accurate as the GPRS tracker. The CDMA tracker, functions using Assisted GPS. A-GPS uses data stored on a network server with fragmented data to localize an object [39]. Using a separate server storage is costly that makes the CDMA tracker much more expensive than the GPRS tracker.

E. CDMA/GPRS (with A-GPS) - AFLT+AGPS

When positioning outdoors, the Hybrid system of Assisted Global Positioning Satellite system and Advanced Forward Link Trilateration system is considered the best and most accurate of all. Obtaining fixes include the use of both GPS pseudo ranges and the CDMA or GSM pilot measurements. The pilot measurements are used in the same trilateration technique when there are insufficient pseudo ranges for a GPS-only localization. This hybrid system provides the most accurate position even when a GPS only solution is not available. Although, there is a slight set back to acknowledge that if a GPS-only solution is not available, and a direct Line of Sight to three (trilateration requires three beacons) cellular tower is also not available than there is a risk of inaccuracy or vague positioning [40]. This case is highly unlikely to take place. To sum up, users can enjoy the accuracy of Assisted GPS, cellular positioning and advanced forward link trilateration. Moreover, AFLT itself gives nearly a 99% yield indoors too.

F. Wireless Assisted GPS and AFLT: GPS One A Hybrid Solution

The Hybrid localization solution GPSOne performs positioning using the cellular network and the GPS constellation. The hybrid was designed to combine the benefits of both single systems while covering their drawbacks. Its gains include more accurate localizations even indoors and in places where less than 4 satellites are visible and enhanced GPS receiver sensitivity. Moreover, GPSOne is faster as the GPS receiver is provided a search window as to which satellites might be visible by the cellular network via Cell ID or other technique [41]. Furthermore, this system cost less financially and in terms of battery usage as well. There is also a reduced interference in the mobile network, hence, no hindrance in calls during localization. Moreover, it offers continuous tracking automatically once a fix is obtained which reduces the time to get an accurate fix upon user request. The only downside is that is has its own hardware and software and an installed chipset is required for its use.

G. Systems with Smart Antenna

Smart Antennas use adaptive array antennas to increase efficiency in wireless communications systems. Special Antenna arrays can use signal processing algorithms to locate or track a mobile user [42]. Using smart antennas gives the service provider many benefits such as much higher number of users can be catered concurrently. The antennas with gained foci can cover a much larger region, hence being cost effective. Moreover, they provide higher security and reduced interference, due to their directionality, than the old-fashioned Omni-directional antennas. Furthermore, in Smart Antennas the broadcasted frequencies are re-usable and multiple paths are available for data packets to travel. Hence, there is an increased bandwidth as well [43].

H. Distributed Antenna Systems (DAS)

Distributed Antenna System is a structure of spatially alienated antenna nodes linked to a common source through a transport mode that gives wireless service inside a geographic area. A Distributed Antenna System utilizes coaxial cable, fibre optic cable and antennas in order to increase cellular, public safety and other

signals inside a building environment [44]. Distributed Antenna System (DAS) has appeared as a potential technology for future wireless communications as a result of its merits of increasing the capacity of the system, enhancing the quality of the signals and decreasing the power [45-46].

VII. APPLICATIONS OF DAS

In the past few years, Indoor Positioning Systems (IPS) has gained an extensive significance as commercially available satellite positioning systems. Active radio frequency identification systems can provide accuracy up to centimetre range, but due to complexity of digital signal processing, these systems are too costly. Therefore, several power levels at the access points can be combined with the previous knowledge about the properties of antenna system into an estimator for the positioning of the client's terminals. However, this could be difficult because amplitude detection is sensitive regarding intrinsic amplitude fading affects. In any case, a large number of access points are required to reach the accuracy. It can be achieved by placing Distributed Antenna System between the access points. Secondly, use of leaky wave cable is also challenging due to difficulty in allocation of radiating pattern to a radiating slot. Furthermore, to enhance the functionality of the cable requires a modification that can result in a complete change of design of the whole cable structure. Therefore, a Distributed Antenna System is perfectly suited due to the possibility of changing single components with well-known properties individually [47].

Distributed Antenna System is now a common feature of current underwater networks as well. It includes secondary communication link, centralized processing and multiple acoustic nodes at various locations. Due to current acoustic OFDM modem technology, any message can be sent, no matter what the content of the message is. In case of stationary network such as Distributed Antenna System, the Doppler speed of any mobile node can be accurately measured. Apart from this position and instantaneous velocity can also be estimated [48]. In the past few years, widely distributed stations have been introduced in the radar architectures including multiple input multiple out, multi static radar systems and radar systems with widely spread antennas. These systems are serving significant advantages as compared to monostatic radar system. Therefore, Multiple Input Multiple Output (MIMO) along with widely distributed antenna network provides an enhanced target localization capability by exploiting increased spatial speed. Localization functionality can be improved as well by increasing the number of participating radars or the transmission power.

DAS system is of critical importance in radar applications including the surveillance radars that are on vehicles and anti-missile defence radar systems with limited energy sources [49]. Usually wireless devices are not reliable for huge buildings. They might not be available for the person standing on the 75th floor or in the basement. Secondly, these buildings are made up of metals and concrete. Therefore, it is nearly impossible to maintain reliable link. Here, Distributed Antenna Systems eliminates the poor wireless reception in these environments and provides increased coverage, highly data throughput and improved call clarity. Installation of Distributed Antenna System replaces the need of additional base stations or tower locations that can solve capacity issues. It allows macro cells to address other network issues and allows for reduced power levels thereby reducing interference and increasing bandwidth. It does not disrupt the surrounding macro network and thus can be utilized more effectively with less expense. The cost associated with providing service in buildings and to other RF resistant environments is shared among the number of carriers in a Neutral Host DAS model, hence enabling medium and smaller venues to become economically feasible. It also provides speed to market for service provision [50]. Localization by Distributed Antenna System can deliberately serve for public safety. For critical communications, public agencies require wireless coverage. Public safety for TE's DAS ensures for distortion free transmission along with the distribution of critical communication information whether wireless voice or data. DAS solution supports primary public safety as well as the critical first responder frequencies in the bands on a single system. It provides high reliability coverage for public safety services both indoors and outdoors. This is a proven solution for making buildings safer. Apart from this, it can also be used by the government, first responder, transit, commercial enterprises, security personnel, education and also in military.

Digital Distributed Antenna Systems provide unmatched benefits such as a common hub for indoor and outdoor Distributed Antenna Systems. It enables the mixed match of high and low power remotes. The system allows the use of existing fibre, flowing expansion and remotes to achieve the highest access. It is easy to install and manage and unified by 2G, 3G and 4G support. It permits low loss fibre transport and TE digital DAS offers an IP connection for Wi-Fi or security. Flex wave prism is multi band high power DAS that can support up to four frequencies per node and deliver high performance coverage. It effectively enhances wireless coverage in outdoor large venues and it is also very cost effective. It is best suited to outdoor coverage including urban or sub urban shadow areas, along roadways, coastal, and canyon areas, subways, tunnels, corporate or university campuses, stadiums, malls and conventional centres. Another one is flex wave spectrum which is an advanced multi band in-building DAS along with distributed amplifiers. It is used to extend the wireless services throughout a building, multi buildings or campus. It provides multi band flexibility and edge to edge bandwidth.

XI. TECHNIQUES FOR THE EXISTING LOCALIZATION

The techniques for the existing localization comprises of Localization by Cell-ID, Localization by Prediction (Dead - Reckoning Method), Localization by Angle of Arrival (AOA), Localization by Time of Arrival (TOA) and Observed Time Difference of Arrival (OTD), Hybrid Localization AOA-TOA-based and Localization by Finger Printing. The merits and demerits of these technologies are explained in Table IV.

Table IV: Merits and demerits of the localized systems of Section XI techniques.

A. Localization by Cell-ID
Cell ID Positioning requires an already established cellular network to localize a mobile user. The base transceiver station communicates with a user handset, while covering many cells and smaller areas of the region under coverage by a BTS [51]. Every cell has a specific signal transmitter and Cell ID, through which the BTS communicates with the user's device. Whilst positioning, the network server checks the Cell ID of the user that has requested localization. The BTS then approximates the position of the user by using its location and the Cell ID which are known exactly, by using any of the techniques, i.e. Time of Arrival (ToA), Time Difference of Arrival (TDoA), etc. This method consumes lower power than many of its competitors and can cover a range from a radius of a few hundred meters to several kilometers.
B. Localization by Prediction (Dead -Reckoning Method)

During navigation, Dead Reckoning or prediction is the technique used to calculate a user's current position by using previously calculated position, and advancing it on the basis of estimated speeds over an elapsed time and distance. Same technique has been used in wild life sciences for the monitoring of patterns of the migration of animals. It is known as path integration. This technology was very popular until it was discovered that Dead Reckoning was subject to error accumulation. Its biggest flaw is the fact that once a wrong fix or location is obtained the deviation continues to grow over the course of time, due to the fact that every new position is based on a previous fix [52].

C. Localization by Angle of Arrival (AOA)

Localization by Angle of Arrival is done by estimating the angle at which signals are received at multiple receivers on a base station, then by using simple geometric equations, node locations are calculated. Generally, Angle of Arrival (AOA) methods delivers more precise localization outcome than Received Signal Strength Indicator-based techniques but the cost of hardware is very high in this methodology. The flaw in this technique is that for a quickly moving object, localization by Angle of Arrival is very inaccurate, and time consuming due to the fact that the multiple receivers at the base station do not account for the time difference in between and fail to predict motion [53].

D. Localization by Time of Arrival (TOA) and Observed Time Difference of Arrival (TDOA)

Localization by Time of Arrival (TOA) is an iteration method that is used to calculate the location of a mobile user [54]. The TOA system, calculates the position of the user by determining the distance of the user to signal receiving beacons. After multiple beacons have registered a time stamped signal, the system calculates the distance by the transmission time delay and the signal progression speed, then a little geometry is required to complete the algorithm. Another plus point is this system is that it can be applied to other types of signals as well, e.g. RF, acoustic, infrared, ultrasound, etc. This system is very accurate if the user is in Line of Sight. This is a major drawback of this system, as it requires the user to be in Line of Sight of the signal receiving beacons, which is not always possible for a mobile user. Another flaw is the fact that the wave progression in air differs with weather conditions such as temperature and humidity. This introduces inaccuracy in localization via distance estimation [55].

E. Hybrid Localization AOA-TOA-based

Hybrid systems are a merger of different single localization techniques which overcomes the flaws present in the solo implementation of single positioning methods, e.g. TOA, AOA, Time Difference of Arrival, etc. The Hybrid of Time of Arrival and Angle of Arrival, solves the issue of Line of Sight between the receiving beacon and the mobile source. As the technique Angle of Arrival cannot distinguish between Line of Sight and reflected signals, the system deploys many efficient algorithms to overcome it. The benefits are clear, accurate localization and reliability. New and much more complex algorithms are used to speed up the localization [56]. Moreover, special hardware could be more robust and expensive [57]. For TOA-AOA, both the receiving towers and the mobile user need to be time synchronized.

F. Localization by Finger Printing

Fingerprinting refers to identifying a specified location by relying on the data representing it. In fingerprinting, a database is created that stores location signatures. Signatures are data of position markers spread out evenly through the region in consideration. Fingerprinting techniques are very effective in locating a mobile user in an indoor environment and in complex environments also, where common localization techniques based on Time of Arrival or triangulation are prone to serious errors such as canyons, tunnels, etc. Furthermore, this technique does not require any network access to a central server, and hence is a standalone localization solution [58].

X. Conclusion

The indoor and outdoor localization techniques of LBS have several merits and demerits. Advancement in RFID has led to optimization of resources, enhanced efficiency of business transactions, increased health care systems and improved customer support. On the other hand, the drawback is that RFID takes a lot of time to be programmed for the specific needs. The GPS system is very cost effective relative to other navigation systems, and the receiver is not affected by weather or climate changes. The drawback of GPS technology is that it does not work efficiently indoors as GPS satellites possess weak signals which cannot cross the walls of buildings. The merit of A-GPS technology is that the signals are always complete and there are no fragments in it. GSM Technology provides worldwide coverage for communication and data exchange but the drawback is the bandwidth lag. Smart Antennas provide the advantage of connection to a larger number of users concurrently, re-usable frequencies, multiple paths, increased bandwidth and cost effectiveness. The drawback of smart antennas is that managing their large size and location needs a lot of planning. Distributed Antenna Systems (DAS) prevents shadowing and penetration data losses, provides better coverage, lower power configuration and fewer coverage holes. The demerit of Distributed Antenna Systems is that there is high infrastructural expense and maintaining the system is complicated. Localization by Cell-ID consumes low power but it does not cover a long distance. Localization by Prediction (Dead Reckoning method) uses path integration and is useful for monitoring patterns of migration of wildlife but the demerit is that it is subject to error accumulation as new position is based upon the previously calculated position. Angle of Arrival (AOA) methods provides more precise localization outcome but the hardware cost is very high.

Localization by Time of Arrival (TOA) can be applied to different signals such as RF, infrared, ultrasound, etc. but the demerit is that it requires the user to be in Line of Sight of the signal receiving beacons, which is not always possible for a mobile user. Observed Time Difference of Arrival (TDOA) localizes a user by using time synchronized receivers. This technology is more cost effective and faster but it does not address the drawback of the need to be in Line of Sight of the receiving beacons. Hybrid Localization AOA-TOA-based solves the issue of Line of Sight between the receiving beacon and the mobile source as it is a merger of different single localization techniques. Its demerit is increased computational cost. Localization by Finger Printing is very effective in locating a mobile user in an indoor environment and in complex environments. It is precise and accurate but the drawback is that the database needs to be updated every time there is a change in the environment and it is very expensive.

Researchers have proposed various solutions for enhancing the existing LBS technology and services. The future prospects of LBS are very high as with further research, the existing technologies can be improved and new ones can be created.

References

[1] P. Bellavista, A. Küpper and S. Helal, "Location-Based Services: Back to the Future. Standards & Emerging Technologies," University of Florida. Pervasive Computing, *IEEE*, vol. 7, no. 2, 2008, pp. 85-89.

[2] Kushwaha & Kushwaha, "Location Based Services using Android Mobile Operating System," *Int. Journal of Advances in Engg. & Technology*, 2011.

[3] N.J. Mazzarella, "Location-Based Services System (LBSS)," 3rd Generation Partnership Project 2, 2000, http://www.3gpp2.org/public_html/specs/S.R0019__LBSS_Stage_1_v1.0.0.pdf (current March 2017).

[4] T. Abulleif and A. Al-Dossary, Location Based Services (LBS), Surveying Services Division, Saudi Aramco, Dhahran, Saudi Arabia, 2008.

[5] H. M. Khoury and V. R. Kamat, "Evaluation of Position Tracking Technologies for User Localization in Indoor Construction Environments," *Automation in Construction*, vol. 18, no.4, 2009, pp. 444-457.

[6] J. Kamper and H. Linde, "Challenges of Passive Infrared Indoor Localization", Proc. 5th Workshop on Positioning, Navigation and Communication, 2008.

[7] A. Ward, A. Jones, and A. Hopper, "A New Location Technique for the Active Office," *IEEE Personal Comms.*, vol. 4, no. 5, 1997, pp. 42-47.

[8] R. Want, A. Hopper, V. Falcao, and J. Gibbons, "The Active Badge Location System," Olivetti Research Ltd. (ORL), Tech. Rep. 92.1, 1992.

[9] B. Brumitt, B. Meyers, et.al., "Easy Living Technologies for Intelligent Environments," in *Handheld and Ubiquitous Computing*, 2000.

[10] R. J. Orr and G. D. Abowd, "The Smart Floor: A Mechanism for Natural User Identification and Tracking," Proc. Conference on Human Factors in Computing Systems, ACM Press, 2000, pp. 275-276.

[11] I. K. Adusei, and F. E. Kyamakya, Location Based Services: Advances and Challenges, master's dissertation, Institute of Communication Engineering, University of Hannover, 2005.

[12] Z. Fang, and Q. Li, "Mobile Agent Based Layered Spatial Service Architecture for Mobile GIS," Proc. International Conference on Service Operations Logistics and Informatics. IEEE, Shanghai, China, 2006.
[13] C. Wang, and C. Hong, "A Location and Interest Based Peer to Peer virtual Navigation System," 2nd Int. Conf. on the Applications of Digital Information and Web Technologies, London, U.K., 2009.
[14] A. Tsalgatidou et al., "Mobile E-Commerce and Location-Based Services: Technology and Requirements," The University of Athens, 2003 http://www.scangis.org/scangis2003/papers/27.pdf (current March 2017)
[15] D. Mohaptra, and S.B. Suma, "Survey of Location Based Wireless Services," Proc. 7th International Conference on Personal Wireless Communications. (ICPWC), IEEE, 2005, pp. 358-362.
[16] C. Flora, M. Ficco, S. Russo and V. Vecchio, "Indoor and Outdoor Location Based Services for Portable Wireless Devices," 25th Int. Conf. on Distributed Computing Systems Workshop (ICDCSW'05), 2005.
[17] R. Want, "An Introduction to RFID Technology", *IEEE Pervasive Computing*, vol. 5, no. 1, 2006, pp. 25-33.
[18] S.A. Weis, RFID (Radio Frequency Identification): Principles and Applications, master's dissertation, CSAIL, 2007.
[19] K. Ahsan, H. Shah, and P. Kingston, "RFID Applications: An Introductory and Exploratory Study," Faculty of Computing, Engineering and Technology. Staffordshire University, Stafford, U.K., *International Journal of Computer Science Issues*, vol. 7, no. 3. Issue 1. 2010.
[20] T. Nguyen," Port trucks get RFID," Fleet Owner, vol. 101, no. 2, 2006.
[21] ZIH Corp. Zebra, "Traceability in Retail: Reducing RFID Media Costs for Best Value," 2013.
[22] H. Li, "Application of RFID in Agricultural Seed Quality Tracking System," Proc. 8th World Congress on Intelligent Control and Automation (WCICA), IEEE, Jinan, China, 2010, pp. 3073-3077.
[23] J. Gitford, RFID Application in Transportation Operations, George Mason University, San Diego, 2006.
[24] L. Ho, M. Moh, Z. Walker, T. Hamada, and C. F. Su, "A Prototype on RFID and Sensor Networks for Elder Healthcare: Progress Report," Proc. ACM SIGCOMM Workshop on Experimental Approaches to Wireless Network Design and Analysis, ACM, Pennsylvania, USA, 2005, pp. 70-75.
[25] C. Swedberg, "Satisfaction and Efficiency at Stanford Children's Health," *RFID J.*, http://rfidjournal.com/articles/view?14661 (current March 2017).
[26] S.H. Siadat, and A. Selamat, "Location-Based System for Mobile Devices Using RFID," Proc. 2nd Asia International Conference on Modeling and Simulation, Malaysia, 2008, pp. 293-296.
[27] TFOT, "Hitachi Develops World's Smallest RFID Chips," 2007.
[28] Ergen, et al., "Application of GPS to Mobile IP and Routing in Wireless Networks," University of California Berkeley, 2002, http://research.microsoft.com/en-us/um/people/padmanab/temp/tmc-8-022002.pdf (current March 2017).
[29] L. Cassavoy, "21 Awesome GPS And Location-Aware Apps For Android," PCWorld, 2016, http://www.pcworld.com/article/260112/21_awesome_gps_and_location_aware_apps_for_android.html
[30] B. Patil, R. Patil, and A. Pittet, "Energy Saving Techniques for GPS Based Tracking Applications," Proc. Integrated Communications, Navigation and Surveillance Conference (ICNS), 2011, pp. 8-10.
[31] M. Yongwei, A Study of Localization Methods on Mobile Platform and WIFI-Based User Movement Detection, University of Delaware, UMI. ProQuest LLC, 2015.
[32] Y. Zhang et al., "Localization Algorithm for GSM Mobiles Based on RSSI and Pearson's Correlation Coefficient," Proc. International Conference on Consumer Electronics (ICCE), *IEEE*, 10-13 Jan. 2014.
[33] R. Oscar, E.I. Martin and A. Francisco, "A Field Study on Satellite and Cellular Signals as Sources for Location," Proc. 2nd Int. Conf. Computer Engineering and Applications, Bali Island, Indonesia, 2010, pp. 474-478.
[34] S. Charitanetra and S. Noppanakeepong, "Mobile Positioning Location using E-OTD Method for GSM Network," Proc. Student Conf. Research and Development, 2003, pp. 319 -324.
[35] F. Nazarpour, "A New Method for Cell Id Assignment for Distance Based Location Management in Cellular Communication Systems," 3rd Int. Conf. on Information and Comm. Technologies: From Theory to Applications (ICTTA), 2008, pp. 1–5.
[36] M.A. Yongwei, Study of Localization Methods on Mobile Platform and WIFI-Based User Movement Detection, Faculty of the University of Delaware, UMI 1585167, ProQuest LLC, 2014.
[37] W. Jing, L. Jianxin, and X. Tong, "The Study on Implementing GPRS Intelligent Network and its Services," *International Conference on Communication Technology Proceedings (ICCT)*, 2003.
[38] Y. Zhang, and Z. Gao, "An Adaptive Resource Allocation Scheme for GPRS/EDGE Towards 3G," *5th International Conference on Wireless Communications, Networking and Mobile Computing*, 2009.
[39] B. Patil, R. Patil, and A. Pittet, "Energy Saving Techniques for GPS Based Tracking Applications," Proc. Integrated Communications, Navigation and Surveillance Conference (ICNS), 2011.
[40] S. Chia-Yenand and P.J Marron, "COLA: Complexity-Reduced Trilateration Approach for 3D Localization in Wireless Sensor Networks," Proc. 4th International Conference on Sensor Technologies and Applications (SENSORCOMM), 2010, pp. 24-32.
[41] S. Soliman et al., "GPSOne: A Hybrid Position Location System," Proc. 6th International Symposium on Spread Spectrum Techniques and Applications (ISSSTA), IEEE, 2000, pp. 1.
[42] X. Zhu, Y. Wang, and H. Zhu, "A Precise 2-D Wireless Localization Technique Using Smart Antenna," Int. Conf. on Cyber-Enabled Distributed Computing and Knowledge Discovery, CyberC, 2010, pp. 59-63
[43] S. Gao and Qi Luo, "Low-cost Smart Antennas for Advanced Wireless Systems," Proc. International Workshop on Antenna Technology: Small Antennas, Novel EM Structures and Materials, and Applications, iWAT, 2014, pp. 132 – 135.
[44] D. H. Hoglund, "Distributed Antenna Systems for Healthcare," IT horizons. Inc., 2010, http://www.hyperioninc.com/wp-content/uploads/DAS-Behind-the-Technology.pdf (current March 2017).
[45] Y. Wang, Y. U. Xiangbin, et.al., "Energy Efficient Power Allocation for Distributed Antenna System over Shadowed Nakagami Fading Channel," Radio Engineering, vol. 24, no. 4, 2015, (current March 2017). http://www.radioeng.cz/fulltexts/2015/15_04_1077_1083.pdf
[46] R.W. Heath, T. Wu, and et.al., "Multiuser MIMO in Distributed Antenna Systems with Outdoor Interference," IEEE Trans. on Signal Proc., 59:10, 2011, http://ieeexplore.ieee.org/document/5953530/ (current March 2017).
[47] J. Joung, Y.K. Chia and S. Sun, "Energy Efficient Large Scale Distributed Antenna System (L-DAS) for Multiple Users," IEEE Journal of Selected Topics in Signal Processing, vol. 8, no. 5, 2014, pp. 954-965.
[48] P. Carroll, K. Domrese, H. Zhou and P. Wilett, "Localization of Mobile Nodes in an Underwater Distributed Antenna System," Procs. 9th Int. Conf. on Underwater Networks and Systems, Rome, Italy, November 12-14, 2014.
[49] H. Godrich, H. Petropulu and H.V Poor, "Resource Allocation Schemes for Target Localization in Distributed Multiple Radar Architectures," Procs. 18th European Signal Processing Conference, 2010.
[50] H. Dahrouj and W. Yu, "Coordinated Beamforming for the Multicell Multi-Antenna Wireless System," IEEE Transactions on Wireless Communications, vol. 9, no. 5, 2010, pp. 1784-1759.
[51] E. Trevisani and A. Vitaletti, "Cell-id Location Technique, Limits and Benefits: An Experimental Study," Proc. 6th International Workshop on Mobile Computing Systems and Applications (WMCSA), IEEE, Dec 2004, pp. 51–60.
[52] H. Samuel et al., "Indoor localization Using Pedestrian Dead Reckoning Updated with RFID-based Fiducials," Proc. 33rd Annual Int. Conf. on Engineering in Medicine and Biology Society, IEEE, 2011, pp. 7598–7601.
[53] A. Mesmoudi, M. Feham, and N. Labraoui, "Wireless Sensor Networks Localization Algorithms: A Comprehensive Survey," *Int. J. of Computer Networks and Communications (IJCNC)*, vol.5, no.6, 2013.
[54] D. Zhang, F. Xia, Z. Yang, L. Yao and W. Zhao, "Localization Technologies for Indoor Human Tracking," Proc. 5th International Conference on Future Information Technology (FutureTech 10), May 2010.
[55] V. Walia and S. Kaur, "Survey of Different Localization Techniques of Wireless Sensor Networks," *IJEEE*, vol. 1, issue 4, 2014.
[56] M.W. Khan, N. Salman and A.H. Kemp, "Enhanced Hybrid Positioning in Wireless Networks 1: AoA-ToA," Proc. International Conference on Telecommunications and Multimedia, TEMU, 2014.
[57] A.D. Gantea and M. Sillera, "A Survey of Hybrid Schemes for Location Estimation in Wireless Sensor Networks," Proc. Iberoamerican Conf. on Elec. Engg. and Computer Science. Procedia Technology, 2013, pp. 377 – 383.
[58] L. Yu, M. Laaraiedh, S. Avrillon, and B. Uguen, "Fingerprinting Localization Based on Neural Networks and Ultra-Wideband Signals," Proc. International Symposium on Signal Processing and Information Technology (ISSPIT), IEEE, Bilbao, Spain, Dec 2011, pp. 184 -189.

International Journal of Computer Applications (0975 – 8887)
Volume 177 – No.5, November 2017

MIMO Wavelet Transform using Optimized Successive Interference Cancellation

Rameez Asif
Faculty of Engineering and Informatics, University of Bradford
Bradford, West Yorkshire BD7 1DP, U.K.

M. S. Binmelha
Faculty of Engineering and Informatics, University of Bradford
Bradford, West Yorkshire BD7 1DP, U.K.

Raed Abd-Alhameed
Faculty of Engineering and Informatics, University of Bradford
Bradford, West Yorkshire BD7 1DP, U.K.

J. M. Noras
Faculty of Engineering and Informatics, University of Bradford
Bradford, West Yorkshire BD7 1DP, U.K.

ABSTRACT
This research introduces a physical layer technique to enhance the capability of MIMO wavelet systems by using successive interference cancellation which enables the receiver to decode simultaneous data packets. The received power of the data packet was introduced to further optimize the receiver's decision capability. Results show that a Discrete Wavelet Transform-based MIMO system with interference cancellation provides a performance gain as compared to a theoretical 2x2 MIMO channel in terms of BER vs. SNR performance. The performances of two different techniques have been evaluated in this work using interference cancellation both with and without consideration of received signal power.

Keywords
OFDM, Wavelets, DWT, WPT, Zero-Forcing, Minimum Mean Squared Error.

1. INTRODUCTION
Wavelet transforms provide an alternative to the Discrete Fourier Transform (DFT) used in Orthogonal Frequency Division Multiplex (OFDM) multicarrier transmission. When compared to conventional single-carrier systems, multicarrier systems have the well-known advantage that they reduce inter-symbol interference (ISI) caused by the channel delay spread in high data-rate transmission. In a multicarrier system, multiple high data-rate serial streams are divided into a number of lower rate parallel streams [1]. With a fixed overall bandwidth, an increased number of sub-channels means lower bandwidth and hence lower data-rate in each sub-channel, resulting in longer symbol periods with reduced susceptibility to channel delay spread and related ISI. Alternatively, this can be viewed as making the sub-channel bandwidth small compared to the coherence bandwidth of the channel [2].

Wavelet-based systems can provide all the conventional advantages of OFDM systems and can help improve the PAPR, sensitivity to carrier frequency timing offset and overall Bit Error Rate (BER) performance of the system [3]. The ISI produced in the wavelet-based multi carrier system (MCS) can be divided among different wavelet symbols, thus becoming easily correctible at the receiver. Insertion of a cyclic prefix (CP) or a guard band is not required in such systems as they maintain orthogonality using perfect reconstruction quadrature mirror filter banks (PRQMF). Due to the energy containment in the main lobe of the wavelet symbol, these symbols have strongly suppressed side lobes providing them with high spectral density and reducing inter-carrier interference (ICI). Moreover, the sub-channel in this transform is compact which increases the probability of correct bit decoding. Basis sets of this transform use time-frequency partitioning, which in turn provides SNR performance gain [4].

To make more reliable and efficient systems with higher data-rate and increased coverage, Multiple Input Multiple Output (MIMO) has been used to create multiple channels in space (spatial multiplexing) without requiring additional bandwidth. MIMO-based systems are superior to Single Input Single Output (SISO) systems in terms of their spectral efficiency and they require less transmission energy to match a given throughput for any given BER.

The three main contributions of this work are 1) to enhance the capabilities of wavelet MIMO systems, optimizing their potential use in next generation wireless communication systems, which will require about 1 Gb/s transfer rates, and 2) to permit efficient use of the frequency spectrum without the bandwidth wastage due to the CP insertion. Depending on the system design, the CP can waste up to a quarter of the total bandwidth.

The final main contribution is to propose the best equalization and data recovery technique for wavelet-based systems, since without a CP these symbols go through time domain convolution with the channel introducing an irreducible error. It was said in [9] that if the coefficients from the noisy wavelet signal are used for channel equalization rather than the original transmitted signal they can produce large estimation errors since longer wavelet filter sequences are required. No previous published work has contributed to the study of this problem in wavelet-based systems.

Successive interference cancellation (SIC) and optimized successive interference cancellation (OSIC) physical layer techniques use zero-forcing (ZF) and minimum mean squared error (MMSE) equalization algorithms to increase the accuracy of equalization at the receiver, using the received signal strength at the receiver. Both techniques provide a marginal gain in terms of BER performance when compared to a theoretical 2x2 MIMO channel and can provide much bigger performance difference than practical systems.

This paper has been organized as follows; the basics of wavelet transforms are described in Section 2, followed by the DWT baseband architecture in section 3, system model in section 4, channel equalization methods in section 5, simulation results in 6, followed by the conclusions.

2. WAVELET TRANSFORM BASICS
The wavelet-based transform is a technique of signal manipulation for multi-resolution analysis, which allows a signal x[n] to be decomposed and analysed using shifting and

scaling into approximate $G_{L,n}$ and detailed $H_{m,n}$ coefficients. This relies on the concept of embedded vector spaces

$$\cdots \subset V_3 \subset V_2 \subset V_1 \subset V_0 \subset V_{-1} \subset \cdots \quad (1)$$

If a vector space V_T consists of subspaces V_{T-r} these subspaces can be referred to as decomposed signal spaces, so the multiply-resolved components of our total original vector space can be shown as in Fig. 1.

In [5] V_{T-r} is being mathematically defined using a dilation equation as;

$$\varphi(t) = \sqrt{2}\sum_n g(n)\varphi(2t-n) \quad (2)$$

Once this dilation takes place the original vector space of the signal gets divided, and by using Equation 2 the low frequency component can be extracted through a half-band low-pass filter g(n) which will have half the bandwidth as compared to the original signal as implied by the dilation factor 2 used in Equation 2. The same can be done for the high frequency component, using a half-band high-pass filter h(n), which can be mathematically stated as:

$$\psi(t) = \sqrt{2}\sum_n h(n)\psi(2t-n) \quad (3)$$

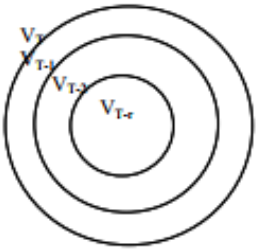

Fig 1: Multiply-resolved vector spaces

Equations 2 and 3 can be further solved to determine one of the infinite sets of wavelet basis functions. Once the low-pass filter coefficients are extracted the relation in Equation 4 can be used to extract the high-pass filter coefficients to construct the PRQMF filter bank:

$$h(n) = (-1)^n g(L-n+1) \quad (4)$$

where L stands for the filter length and n is the filter coefficient. The continuous wavelet transform of a signal x[n] over the vector space T can be written as;

$$X_{CWT}(\alpha,\tau) = \int_T x(n)\psi_{\alpha,\tau}(t)dt \quad (5)$$

where α is the scale and τ is the shift. The transform in its continuous form requires extensive analytical solution and no viable practical inverse exists so it is important to discretize it which also produces an error when an infinite sequence is squeezed to finite length and can be mathematically written as [6]:

$$\psi_{m,n} = 2^{-\frac{m}{2}}\psi(2^{-m}t-n) \quad (6)$$

where m represents the scale and n represents the shift. The discretized signal composed of its constituent approximation and detail parts can be written as [7];

$$x(t) = \sum_{n=-\infty}^{\infty} G_{L,n}2^{-\frac{L}{2}}\varphi(2^{-L}t-n) + \sum_{m=1}^{L}\sum_{n=-\infty}^{\infty} H_{m,n}2^{-\frac{m}{2}}\psi(2^{-m}t-n) \quad (7)$$

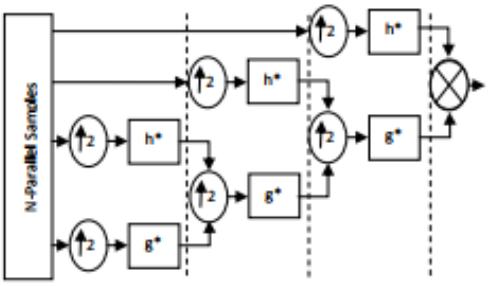

Fig 2: 3-level inverse discrete wavelet transform

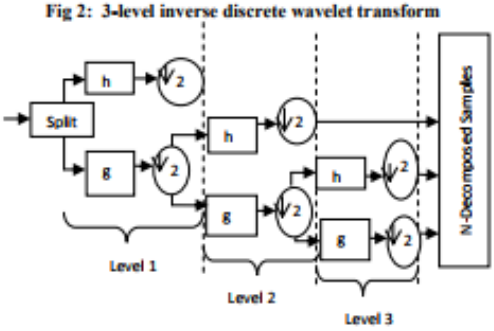

Fig 3: 3-level discrete wavelet transform

3. THE DWT BASEBAND ARCHITECTURE

Once the data is discretised the input signal can be analysed in different frequency bands by decomposing it into an approximation part, $G_{L,n}$, and a detail part $H_{m,n}$. This decomposition takes place for every shift and scale. It is to be noted that when the DWT is employed $G_{L,n}$ is the only part that gets iteratively decomposed which means that the second half of Equation 4 is absent and the total number of sub-channels that can be considered for multiplexing will equal M = $\log_2(K)$ + 2. K stands for the number of decomposition levels and M represents the resultant sub-channels in each level.

4. SYSTEM MODEL

A two transmit- and two receive-antenna based MIMO system was formed, which will be used to model the transmission of the data stream. The data stream is divided and arranged as two sets of symbols in each time slot for both the antennas, which enables to double the data-rate by reducing the total number of time slots by half, when compared to a one-transmit-antenna system.

4.1 Multipath Propagation Environment

The channel environments used was Rayleigh multipath with Additive White Gaussian Noise (AWGN) and each transmitted stream encounters an independent multipath. When a multipath environment is present there will be a train of impulses received at the receiver for every transmitted impulse. The band-pass signal can be written mathematically as [8]:

$$x(t) = \Re\{x_{bs}(t).e^{j2\pi f_c t}\} \quad (8)$$

where $x_{bs}(t)$ denotes the baseband signal, $\Re$ represents the real part, f_c is the carrier frequency and time is t. The received signal after travelling through the multiple path channel where the attenuation of the k^{th} path is $\alpha_k(t)$ and time delay is $\tau_k(t)$, can be mathematically described as:

$$y(t) = \sum_k \alpha_k(t)x[t - \tau_k(t)]. \quad (9)$$

Substituting Eq. (8) into Eq. (9) yields

$$y(t) = \Re\left\{\sum_k \alpha_k(t)x_{bs}[t - \tau_k(t)]e^{j2\pi f_c[t-\tau_k(t)}\right\} \quad (10)$$

The baseband equivalent of the received signal has a mathematical form:

$$y_{bs}(t) = \sum_k \alpha_k(t)e^{-j\theta_k(t)}x_{bs}[t - \tau_k(t)] \quad (11)$$

where $\theta_k(t) = 2\pi f_c\tau_k(t)$ represents the phase of the k^{th} path and the impulse response is written as:

$$h_{bs}(t) = \sum_k \alpha_k(t)e^{-j\theta_k(t)} \quad (12)$$

4.2 Rayleigh Fading Environment

Assuming a total of k paths, the central limit theorem can be applied and each path can be modelled as circularly symmetric complex Gaussian random variable:

$$Z = X + jY \quad (13)$$

Time is the variable quantity. Equation 13 shows that both the real and imaginary parts are zero-mean independent and identically distributed random Gaussian variables. For Z

$$E[Z] = E[e^{j\theta}Z] = e^{j\theta}E[Z] \quad (14)$$

the statistics of Z can be satisfied by the variance as:

$$\sigma^2 = E[Z^2] \quad (15)$$

The quantity |Z| represents the Rayleigh random variable. This is the most practical dynamically changing channel model.

5. CHANNEL EQUALIZATION METHOD

A transmitted signal convolved in the time domain with a channel with no cyclic prefix gives rise to an irreducible ISI error. Thus, it is important to note that the signal will not only be corrupted by the channel impairments and noise but will also be corrupted by the ISI.

5.1 Zero Forcing, SIC and Optimization

When transmitting using a 2×2 MIMO scheme the total number of channels that exist between the transmitter and receiver are four, where channel h_1 exists between tx_1 and rx_1, h_2 exists between tx_1 and rx_2, h_3 exists between tx_2 and rx_1 and h_4 exists between tx_2 and rx_2. x_1 and x_2 are the transmitted symbols in time slot 1 for each antenna. This means that h_1 and h_2 will convolve with x_1 and x_2 with the addition of noise and ISI resulting in y_1 and same is true for h_3 and h_4 which will result in y_2.

$$y_1 = h_1x_1 + h_2x_2 + n_1 \quad (16)$$

$$y_2 = h_3x_1 + h_4x_2 + n_2 \quad (17)$$

$$\begin{bmatrix}y_1\\y_2\end{bmatrix} = \begin{bmatrix}h_1h_2\\h_3h_4\end{bmatrix}\begin{bmatrix}x_1\\x_2\end{bmatrix} + \begin{bmatrix}n_1\\n_2\end{bmatrix} \quad (18)$$

So, in the zero forcing linear detector, $\in$, can be modelled as:

$$\in = (H^HH)^{-1}H^H \quad (19)$$

Multiplying Equation 18 with received signal matrix $\begin{bmatrix}y_1\\y_2\end{bmatrix}$ will provide the estimated transmitted signal.

$$\begin{bmatrix}x_{est1}\\x_{est2}\end{bmatrix} = (H^HH)^{-1}H^H\begin{bmatrix}y_1\\y_2\end{bmatrix} \quad (20)$$

Now, the receiver can arbitrarily choose one symbol, in this case x_{est1}, and subtract its effect from the received signal vectors y_1 and y_2 i.e.

$$\begin{bmatrix}\bar{r}_1\\\bar{r}_1\end{bmatrix} = \begin{bmatrix}y_1 - h_1x_{est1}\\y_1 - h_2x_{est1}\end{bmatrix} = \begin{bmatrix}h_1x_{est2}\\h_2x_{est2}\end{bmatrix} + \begin{bmatrix}n_1\\n_1\end{bmatrix} \quad (21)$$

The same procedure as in Equation 20 can be done for $\bar{r}_2$.

$$\begin{bmatrix}\bar{r}_2\\\bar{r}_2\end{bmatrix} = \begin{bmatrix}y_2 - h_3x_{est1}\\y_2 - h_4x_{est1}\end{bmatrix} = \begin{bmatrix}h_3x_{est2}\\h_4x_{est2}\end{bmatrix} + \begin{bmatrix}n_2\\n_2\end{bmatrix} \quad (22)$$

Once r is successfully extracted, it can be combined using Maximum Ratio Combining (MRC) as the system is now similar to one transmit two receive antennas and the receiver diversity can be used to combine the information.
For optimization, signal power can be used which can be calculated as:

$$Px_1 = |h_1|^2 + |h_2|^2 \quad (23)$$

and

$$Px_2 = |h_3|^2 + |h_4|^2 \quad (24)$$

5.2 MMSE Equalization

In MMSE equalization the main step is to derive the equalization coefficients k[i] for each sampling instant [i] which can be used to reduce the error between the original transmitted signal and the estimated received signal k[1]×r[1]. Mathematically it can be shown [9];

$$E(err(i))^2 = E(s(i) - k(i) * r(i))^2 \quad (25)$$

$$= E(s(i) - k^Tr)(s(i) - k^Tr)^T \quad (26)$$

$$= E(s(i))^2 - E(k^T rs(i)) - E(s(i)r^T k) + E(k^T rr^T c) \quad (27)$$

$$= E(s(i))^2 - k^T R_{rs} - R_{sr}k + k^T R_{ii}k \quad (28)$$

where at any sampling point the error introduced (i) is err(i), k represents the equalization coefficients and the received samples are denoted as r. R shows the cross- and auto-correlations between the sequences. To decipher for MMSE, k is required that will reduce $E(err(i))^2$ to a negligible value. Differentiating Equation 28 with respect to k and setting the result equal to zero will provide the minimal error rate coefficients:

$$\frac{d}{dk}[E(s(i))^2 - k^T R_{rs} - R_{sr}k + k^T R_{ii}k] = 0 \quad (19)$$

After solving the above equation

$$-R_{si} + R_{ii}k = 0 \quad (20)$$

adding R_{si} to both sides of the equation and then dividing by R_{ii} provides the required equalization coefficients k as;

$$k = R_{ii}^{-1} R_{si} \quad (21)$$

6. SIMULATION RESULTS.

All the simulations have been performed using Monte Carlo simulations with following parameters as in Table I:

6.1 Successive Interference Cancellation

In the first simulation only the ZF-SIC technique has been used where the receiver can choose any symbol it likes and ignore the other one which in turn makes the whole system exactly like one transmit two receive antennas. Maximal ratio combining was then employed to efficiently combine the information. Results produced by such a system are shown in Figure 4.

NOTE: The results are compared to theoretical results for accuracy

The SIC provides a marginal performance gain of about 0.2 dB at low SNR compared with theoretical values which is not significant enough but if real life practical systems are considered it will be a great performance improvement, but still to optimize the algorithm further the signal power in addition to SIC was employed to see the performance gain after optimization.

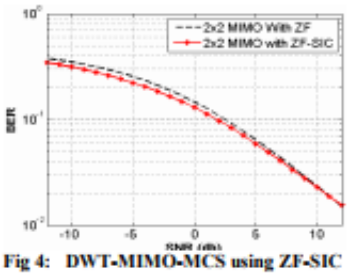

Fig 4: DWT-MIMO-MCS using ZF-SIC

6.2 Optimized Successive Interference Cancellation

In this method, the power of the received signal has been considered for more accurate prediction of which symbol to keep. The results for the study are shown in Figure 5. Comparing both Figure 4 and Figure 5 it is evident that even though it is assumed that the channel is known at the receiver, the ZF equalizations gives rise to extra noise which makes it hard to predict the correct symbol. Thus, this technique with ZF equalization does not provide satisfying results.

TABLE 1: Simulation Parameters

Transform	DWT
Symbol Length	10^4 x 2^k
Modulation	BPSK
Channel	Rayleigh Flat Fading Multipath With AWGN
Wavelet Family and Filter Order	Daubechies 8
Combining Technique	MRC

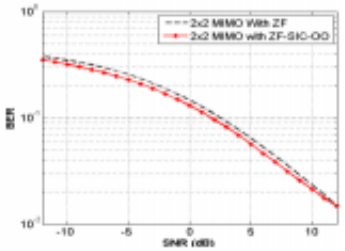

Fig 5: DWT-MIMO-MCS using ZF-Optimized-SIC

6.3 MMSE Equalization using SIC and OSIC

To further study and differentiate between the performances of Zero forcing equalization that gives rise to added noise also MMSE was implemented both with and without OSIC and the results are shown in Figure 6.

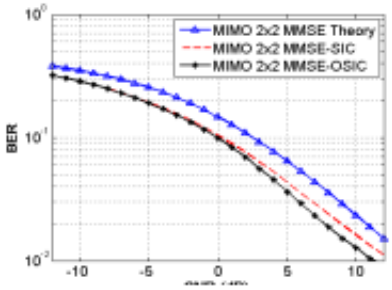

Fig 6: DWT-MIMO using MMSE with successive interference cancellation and optimized successive interference cancellation

This equalization method when employed gives a considerable gain of about 3 dB at BER of 10^{-1} for both techniques steady gain of 3 dB around BER close to 10^{-3} whereas the optimized system yields 2 dB extra gain.

6.4 MMSE VS. ZF in SISO DWT-MCS

In the simulation results shown below it can be seen that the performances of both equalization techniques match each other. This is because the noise term addition in the ZF algorithm, even though the channel is known, reduces the BER performance. So, the MMSE equalization which conventional OFDM theory suggests should perform better than ZF does not. This is due to ISI produced by the channel signal linear convolution which increases the error in the equalization coefficients for MMSE.

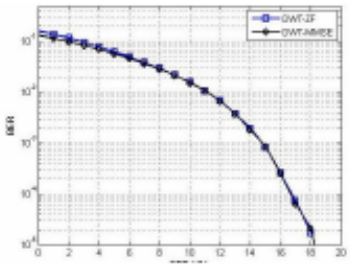

Figure 7: ZF and MMSE in SISO-DWT

7. CONCLUSIONS

In this work, a wavelet-based multicarrier system using a MIMO 2x2 scheme was proposed to optimize the performance of wavelet-based systems and to increase the overall system reliability, data-rate, spectral efficiency and optimized use of the bandwidth provided. These systems do not have the constraints of guard time insertion because even though the signal is distorted when passed through the channel this does not affect the orthogonality which is maintained using the PRQMF bank. Wavelets are more appealing because of their improved SNR performance as compared to the conventional FFT OFDM system because the signal energy containment in the main lobe and suppressed side lobes. The MIMO scheme allows the data-rate to be doubled as the timing slots required for the transmission of a given sequence are reduced by half because the symbols can be transmitted in pairs.

Equalization of wavelet symbols, removal of noise and correct symbol prediction is also a problem: it is shown that OSIC when employed with MMSE equalization will produce the best results. A comparison of MMSE and ZF has also been presented to show that both equalization algorithms show equal performance in SISO wavelet-based MCS but when the MIMO-OSIC and MIMO-SIC is employed MMSE outperforms ZF because no added noise is produced which makes it easy to predict the correct signal.

8. REFERENCES

[1] H. Hosseini, S. K. B. S. Yusof, N. Fisal and A. Farzamnia, "Wavelet Packet-Based Transceiver for Cognitive UWB," in *Canadian Journal of Electrical and Computer Engineering*, vol. 37, no. 2, pp. 59-64, Spring 2014. doi: 10.1109/CJECE.2014.2312451

[2] Andrea Goldsmith, *Wireless Communications*, Cambridge University Press, (2005).

[3] R Asif, Raed Abd-alhameed and J M Noras, "A Unique Wavelet-based Multicarrier System with and without MIMO over Multipath Channels with AWGN" International Journal of Computer Applications, vol. 117, issue 9, May 2015, pp. 31-40, ISSN: 0975 – 8887, DOI: 10.5120/20585-3015

[4] R. Asif, R. A. Abd-alhameed, "Performance Evaluation of DWT-OFDM and FFT-OFDM for Multicarrier Communications Systems using Time Domain Zero Forcing Equalization", International Journal of Computer Applications, vol. 51, no.4, August 2012, pp. 34-38. ISSN: 0975 – 8887.

[5] M. Vetterli and C. Herley, "Wavelets and Filter Banks: Theory and Design." *IEEE Transaction on Signal Processing*, Vol.40, N0.9, pp.2207 – 2231, Sept. 1992.

[6] I. Daubechies, "*Ten lectures on wavelets*," Society for Industrial Mathematics, Vol. 61, 1992.

[7] E. Vlachos, A. S. Lalos and K. Berberidis, "Low-Complexity OSIC Equalization for OFDM-Based Vehicular Communications," in *IEEE Transactions on Vehicular Technology*, vol. 66, no. 5, pp. 3765-3776, May 2017. doi: 10.1109/TVT.2016.2598185

[8] D. Tse and P. Viswanath, "*Fundamentals of Wireless Communication*." Cambridge University Press, 2005.

[9] Yong Soo Cho, et al., Mimo-OFDM wireless communication with Matlab, John-Wiley and Sons, Ltd., October 2010.

International Journal of Computer Applications (0975 – 8887)
Volume 178 – No.6, November 2017

Effects of Transmit Diversity on a Discrete Wavelet Transform and Wavelet Packet Transform-based Multicarrier Systems

Rameez Asif
Faculty of Engineering and Informatics, University of Bradford
Bradford, West Yorkshire, BD7 1DP, U.K

M. S. Binmelha
Faculty of Engineering and Informatics, University of Bradford
Bradford, West Yorkshire, BD7 1DP, U.K

Asmaa Hameed
Department of Laser and Optoelectronic Engineering, College of Engineering, Al-Nahrain University Baghdad, Iraq

Raed Abd-Alhameed
Faculty of Engineering and Informatics, University of Bradford
Bradford, West Yorkshire, BD7 1DP, U.K

J. M. Noras
Faculty of Engineering and Informatics, University of Bradford
Bradford, West Yorkshire, BD7 1DP, U.K

ABSTRACT
This paper proposes a MIMO-WPT-based multicarrier system with feedback from the receiver to the transmitter carrying the channel state information (CSI), whereby a steering matrix can be defined to enhance robust performance against multipath fading effects at the receiver. This relies on the time-scale localization of wavelet bases, and is demonstrated in terms of bit error rate performance. In contrast to sinusoidal carriers WP have very narrow side lobes, with most energy contained in the main lobe; this makes the proposed system less susceptible to inter-carrier interference. The main contribution of this work is the evaluation of system parameters using different wavelet families, order of filters and number of elements to balance overall performance and cost of the system, and to provide a reliable system with a high data-rate.

Keywords
MIMO, Wavelet, Transmit Diversity, Beam-forming, Multicarrier System

1. INTRODUCTION
The fundamental issue in communication theory is to transmit information through an unreliable multipath channel with minimum distortion. Most researchers divide their approaches into two, treating source coding or channel coding, although these are strongly interrelated in real world problems. However, by using Shannon's source channel theorem these problems can be handled as two independent entities and can be addressed without much loss in the overall system performance, although for particular channel classes only [1].

Source coding techniques are implemented to reduce redundancy in data, minimizing the amount of data to be transmitted. Usually a discrete digital representation is preferred such as a discrete binary bit stream. Much research has focused on using source coding to enhance multi-rate signal processing [2 - 4].

Channel coding then adds additional information to the minimized source-coded data to combat the effects of the channel. Optimal performance can be achieved if this can be based on the specific channel characteristics. Channel coding, modulation schemes and use of different waveforms are still less explored areas in the field digital communications and can play a vital role in the advancement of wireless systems.

Currently Orthogonal Frequency Division Multiplexing (OFDM) systems using the fast Fourier transform lead the market because of their ability to increase the symbol period of the transmitted symbol and so counter the degrading effects of multipath environments. However, the orthogonality of the OFDM subcarrier is highly sensitive to frequency errors and signal phase offsets. Also, the truncation of windowing in OFDM causes production of subcarrier side lobes with a frequency spectrum which is not band-limited [5]. The first side lobe generated by the FFT processing is only 13 dB less than the main lobe, generating inter-carrier interference when the sub-carriers lose their orthogonality. In mitigation, a guard interval is added, equivalent to the channel delay response, but this results in less efficient transmission.

Some blind methods have been proposed for both CDMA and OFDM-based systems [6-7]. In [6] the authors have implicitly made use of time diversity, and proposed a filter design to convert the stationary transmitted signal to a cyclo-stationary form so that a second order method can be derived.

The radio frequency channels for wireless communications usually contain multiple paths because of reflections and diffraction due to obstacles and the resultant multiple signals are then superimposed at the receiver. If the received signals combine destructively the signal can suffer attenuation. A typical figure would be around 35 dB. Depending upon the total system bandwidth, fading can be flat or frequency selective. When dealing with mobile systems it will be time-varying [8].

Diversity techniques are used to mitigate the negative effects of fading, classified into different techniques as spectral diversity, spatial diversity, or time diversity.

This paper sets out a multi-rate filter bank-based system employing a wavelet representation of the data and channel coding to achieve highly reliable multipath transmission: this is proposed as a novel strategy to provide diversity for an unreliable channel.

Wavelet-based systems use wavelet pulses which have discrete time and frequency localization as compared to the discrete time rectangular pulses with ideal unlimited response in the frequency domain. The use of wavelets for signaling was also proposed as a bandwidth efficient modulation in [11-12]. In [13] the authors proposed using wavelets for user signature waveforms to improve the cross correlation of the pseudo-random codes. In [14] another wavelet-based CDMA system was proposed, and in [15] the authors applied a wavelet packet-based CDMA system to design an optimal joint detector. In [16] authors found significant performance improvement of quadrature amplitude modulation using wavelet packets, and in [17] an optimized wavelet packet multiplexing algorithm was proposed after the study of the timing error effects. The idea of

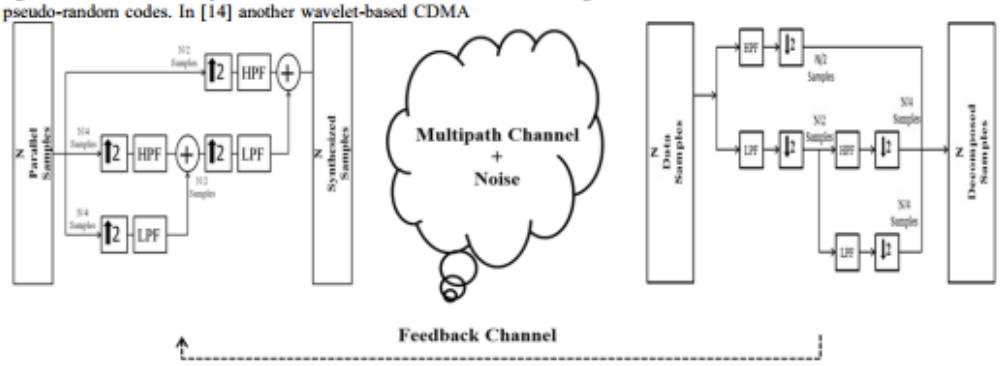

Fig 1a: 1-level wavelet reconstruction (Synthesis) **Fig 1b: Multi-path Channel** **Fig 1c: 2-level wavelet decomposition (Analysis)**

forward error correction (FEC) and wavelet packet multiplexing was introduced in [18] for MC-CDMA channel equalization methods in section 5, simulation results in 6, followed by the conclusions.

None of the work cited above utilized the time localization properties of wavelets. Firstly, the research proposes a new wavelet-based multi-rate modulation scheme and its system model for multi user communication over a Rayleigh fading channel which proved to be a great tool in successfully mitigating the fading effects in multipath environments. The proposed system can be implemented for both forward and reverse links. The proposed treatment does not consider interference types such as shadowing, hostile jamming, military applications, or co-channel interference.

Secondly, MIMO and beam-forming are employed using an antenna array at the transmitter with two elements to provide temporal diversity to the multi-user system. A complete parametric study has been carried out to find the best communication system architecture. The research considers the behavior of different wavelet transforms, families, and filters, and suggest one that has the best reconstruction properties for use in a multicarrier (MC) system. The proposed system consists of three aspects: 1) using wavelets to reduce ICI and multipath fading and to reduce bandwidth usage, 2) using MIMO to ensure high data-rates and 3) beam-forming for good link reliability. Most of the processing burden is kept at the Base-Station (BS) with less cost and power constraints.

The paper is divided as follows. Section II provides a background in wavelet analysis, sub-band coding and perfect reconstruction of filter banks, Section III will describe the system model, Section IV deals with the error probability and transmit beam-forming, followed by the simulation and results in Section V, with conclusions in Section VI.

2. WAVELET ANALYSIS

Wavelets transform decomposes a signal into its constituent components corresponding to different scales, covering different frequency ranges. There are three different transform methods namely: a) the dyadic wavelet transform [19] in which logarithmic band division is achieved using a two band wavelet transform, b) using wavelet packets by employing the full dyadic tree decomposition [19], and c) n-band wavelet analysis [8], which divides the spectrum into equal-sized bands. Wavelets are quickly decaying oscillations deriving from a basis function, the mother wavelet, with translated and scaled replicas known as daughter wavelets [20]. Signal analysis can use any of an infinite number of basis functions to isolate the information required, in contrast to other signal analysis methods.

The continuous wavelet transform can be mathematically defined as [20]:

$$\psi_{x,z}(t) = \frac{1}{\sqrt{a}}\psi\left(\frac{t-z}{x}\right) \quad (1)$$

Here "x" stands for the scaling factor, "z" for the shifting parameter and "$\psi_{x,z}(t)$" is the mother wavelet. In its continuous form the transform requires extensive analytical calculations due to data redundancy and no practicable inverse exists for this transform other than in theory, so is restricted to discrete valued data. In order to accomplish this we choose $x = x_0^{-(m/2)}$ and $z = mz_0x_0^l$ where l and m are integers with fixed values of $x_0 > 1$ and $z_0 > 0$. Then we have:

$$\psi_{l,m}(t) = x_0^{-\frac{l}{2}}\psi\left(\frac{t - mz_0x^l}{x_0^l}\right) \quad (2)$$

$$= x^{-\frac{l}{2}}\psi\left(a_0^{-l}t - mz_0\right) \quad (3)$$

$$s(t) = \sum\sum \alpha(s, \psi_{x,z}), \psi_{x,z}(t). \quad (4)$$

The mother wavelet in (2) can be written in its discretized form as:

$$DWT(l,m) = 2^{-l/2}\sum\sum s(m)\psi\left(\frac{t-m2^l}{2^l}\right) \quad (5)$$

Any signal with a finite amount of energy can be successfully reconstructed by using (4). The k^{th} coefficient of the wavelet transform is linked to a fastidious scale for fastidious number of times, orthonormal transform. We can define the DWT of any random signal s[n] as its product with the scaling and wavelet function [20] as:

$$\left.\begin{aligned}\varphi_{a,b}(t) &= 2^{\frac{a}{2}}\varphi(2^a t-b)\\ \psi_{a,b}(t) &= 2^{\frac{a}{2}}\psi(2^a t-b)\end{aligned}\right\} \quad (6)$$

where $\varphi(t)$ is the scaling function and $\psi(t)$ is called the wavelet function. These functions are discretized at a (a = 1,2 …., m) and at translation b (1,2 …., t). The DWT is implemented in a MCM system using a Perfect Reconstruction Quadrature Mirror Filter Bank (PR-QMF) with a half-band high-pass filter g(b) and a half-band low-pass filter h(b). These filters values can be calculated as:

$$h(b) = (-1)^b g(L+1-m) \quad (7)$$

The filters satisfy the conditions:

$$\left.\begin{aligned}\varphi_{a+1,o}(t) &= \textstyle\sum_b h[b]\,.\,\varphi_{a,b}\\ \psi_{a+1,o}(t) &= \textstyle\sum_b g[b].\psi_{a,b}\end{aligned}\right\} \quad (8)$$

The resulting DWT can be written to express the approximation and detailed coefficients in a mathematical form as;

$$\left.\begin{aligned}A_{b+1,m} &= \textstyle\sum_b A_{a,b}\,.\,h_a[b-2m]\\ D_{b+1,m} &= \textstyle\sum_b A_{a,b}\,.\,g_a[b-2m]\end{aligned}\right\} \quad (9)$$

Due to shifting and translation of the wavelet signal, each of the composite symbols suffer a delay by a factor 'α' according to the z-transform relation $(X(z) = \sum_n x(m)\,z^{-\alpha}$, where $z^{-\alpha} = e^{-j\omega w})$ for which adjacent matched filters are required to perfectly reconstruct the signal. This condition can be written as:

$$h(z)h^*(z) + g(z)g^*(z) = 2z^{-\alpha} \quad (10a)$$

$$h(z)h^*(-z) + g(z)g^*(-z) = 0 \quad (10b)$$

2.1 Sub-Band Coding and Perfect Reconstruction

Sub-band coding is very useful in signal, audio and video coding applications. The input signal s(m) is decomposed into N different frequency sub-bands, using the analysis filter bank as shown in Figure (1c). These are down-sampled to get $y_i(n) = s_i(Nn)$ and then quantized. The quantized outputs $\overline{y_i}(n)$are then up-sampled to $\overline{s_i}(m)$ (with $(\overline{s_i}nN) = \overline{y_i}(n)$ and $\overline{s_i}(nN+1)$ summed to get an output signal $\overline{s}_m$ using the synthesis filter bank as shown in Figure (1a).

Now for such a filter bank to be employed in a MCM it must be nearly perfect reconstruction filter bank in practical life, when no quantization is performed (in theory (perfect reconstruction)) can be defined as;

The conditions that the filters need to follow have been shown in (10a) and (10b).

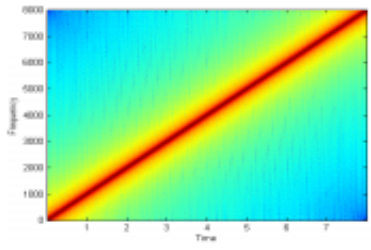

Fig 2: Chirp signal

In Figure 2 - 3 it has been shown that how the signal gets replicated when it is directly up-sampled or down-sampled by 2 without the filters being present. In Figure 4 down-sampled and up-sampled signal using low pass synthesis filter is shown and lastly in Figure 5-6 a signal that has been down-sampled and up-sampled using the low-pass (analysis and synthesis filter) and high-pass (analysis and synthesis filter) is shown and Figure 7 shows the reconstructed signal of two channel filter bank.

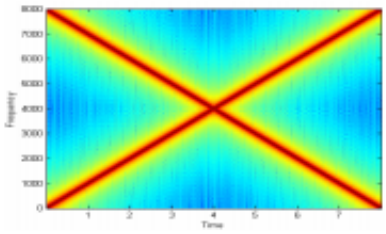

Fig 3: Replicated chirp signal due to up-sampling and down-sampling without filter bank employment

3. SYSTEM DESIGN

The system that is considered is for a wireless cellular network with many users connected to the same base station even though it can be used for several other applications. The communication between the base station and the mobile user which is the forward link and mobile user to base station or reverse link is essential and requires non-interfering channels [21]. A general system model is shown in Figure (1 and 9). At the transmitter, the incoming bit stream with a bit rate of (K/LM) is represented as (12);

$$s_n(t) = \sum_{z=-\infty}^{\infty} s_n^z\,\Pi_{K/(LM)}\left(t - z\left(K/LM\right)\right) \quad (12)$$

This stream is then serial to parallel converted to yield (13)

$$s_{nl}(t) = \sum_{z=-\infty}^{\infty} s_{nl}^z\,\Pi_{K/(M)}\left(t - z\left(K/M\right)\right) \quad (13)$$

where K represents the bit duration of this super stream, and $\Pi_i(\cdot)$ is the rectangular pulse of duration I and M is the total number of super-streams. These parallel streams are then modulated using a suitable modulation technique and then passed through the synthesis filter bank.

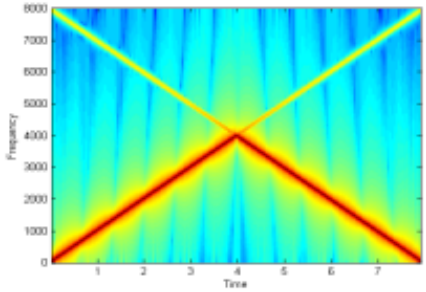

Fig 4: Output of a low-pass filter in a synthesis filter part

To implement wavelet transform in a MCM system the inverse transform needs to be implemented at the transmitter as shown in Figure 1. Using the PRQMF the parallel symbols are first up-converted by a factor of two and then passed through the high pass filter (HPF) and low pass filter (LPF). This convolution between the symbols and the filters can be mathematically described as;

$$\left.\begin{aligned} s_{low}(b) &= s(b) * h(b) \\ s_{high}(b) &= s(b) * g(b) \end{aligned}\right\} \quad (13)$$

These resultant approximate coefficients from the LPF and detailed coefficients from the HPF are then summed to constitute a wavelet symbol. The process of IDWT is also referred to as a Synthesis Process. This synthesized signal then propagates through the Rayleigh multipath fading channel in the presence of noise. For greater understanding of the process of convolution with the filters and channel please refer to authors [12].

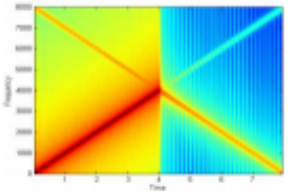

Fig 5: Up-sampled and down-sampled output of filter bank with LPF.

3.1 WMCM signal in Rayleigh Multipath Channel and AWGN

T The signal when propagated through the Rayleigh fading channel suffers phase and amplitude changes, time delay and the mathematical Equation in (12) can very well summarize this effect.

$$h(t,\tau) = \sum_{r=1}^{R} a_r(t,\tau)\, e^{-j\theta_r}\delta\left(t-\tau_r(t)\right) \quad (12)$$

where $a_r(t,\tau)$, represents the amplitude and the time delay is represented by and τ_r, phase shift for any r^{th} multipath at time instance t can be described as θ_r ($\theta_r = 2\pi f_c \tau_i(t)$). Multipath summation limits are from r = 1 to R, where R stands for the total number of multipaths with the Dirac delta $\delta(\bullet)$. The resultant received signal at the receiver can be given as [22].

$$s[n] = \sum_{k=0}^{K-1}\sum_{m} a_k[n;m]y_k[n-m] + \omega[n] \quad (13)$$

The effects of the multipath propagation caused by the media fluctuations and the transmitter and receiver motion are captured at time instance of n for the m^{th} sample for the unit time sample n-m in $a_k[n;m]$. Noise and any other type of interferences present in the system are captured by the $\omega[n]$. If the kernels in (13) are zero mean and Gaussian the resultant channel will be the Rayleigh fading channel [22].

For frequency selective channels the magnitude of the time variant frequency response varies for every n as a function of ω and is independent of ω for flat fading channels and can be mathematically written as (14):

$$A_k[\omega;n] = \sum_{m} a_k[n;m]e^{-j\omega m} \quad (14)$$

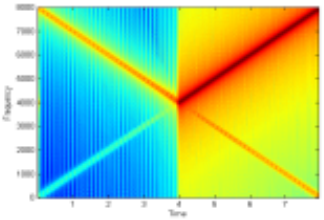

Fig 6: Up-sampled and down-sampled output of filter bank with HPF.

3.2 Implementation WMCM in Receiver

When the signal is received at the receiver it is passed through the conjugate LPF $h^*(-b)$ and HPF $g^*(-b)$. The signal is decomposed into its approximate and detailed coefficients and then down-sampled by a factor of 2. This process is repeated until the desired N data streams are successfully recovered. A parallel to serial conversion is applied next which is followed by a suitable de-mapping scheme.

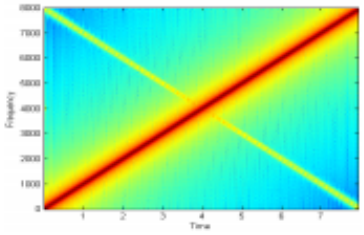

Fig 7: Resultant signal from 2-channel filter bank

3.3 Implementation of WPMCM

This transform follows the concept of DWT very closely other than the fact that both the detailed and approximated parts of the signal are again passed through the LPF and HPF at the transmitter and through their conjugate filters at the receiver which means more processing is required at each node as shown in Figure (9).

Fig 8: Transmit beam-forming 2Tx 1Rx

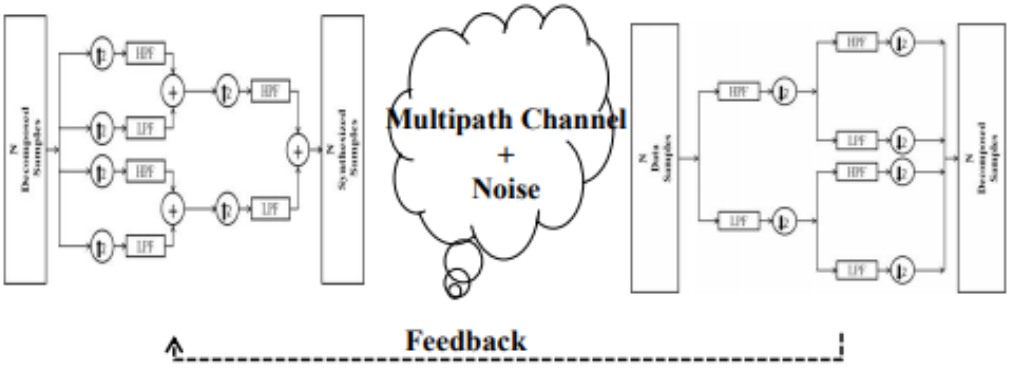

Fig 9a: 2 Level WPT- Synthesis Process Fig 9b: Rayleigh Multipath Channel + AWGN Fig 9c: 2 level WPT- Analysis Process

However, now this error probability will change if the beam forming is applied and can be given as;

$$\bar{P}_e = \int_0^\infty z_\gamma(\gamma) P_e(\gamma) d\gamma \tag{16}$$

where the probability density function (PDF) of the output signal is represented by $z_\gamma(\gamma)$, however this value will depend on the PDF of the input signal.

To implement transmit beam-forming system two or more antennas are required at the transmitter. This technique is then applied to every subcarrier of the WMCM system at the baseband level. A steering matrix is computed which is used to steer the transmitted signal in the direction required. The transmitter weights that are applied in the steering matrix are derived using the channel state information (CSI) which is provided by the receiver in the closed loop systems.

Unless the phases of the signals from two different antennas align at the receiver no diversity gain can be achieved because of each transmitted signal will traverse through a different Rayleigh multipath channel so the overall system performance will be equal to a SISO system.

Mathematically the implementation of this technique can be realized as;

If 's' is the transmitted symbol and 'h' is the channel impulse response then;

$$y = hs + n \tag{17}$$

where n is AWGN. When two different transmitters are employed then (17) can be modified to add another independent channel and can be written as;

$$y = [h_1 h_2] \begin{bmatrix} s \\ s \end{bmatrix} + noise \tag{18}$$

4. ERROR PROBABILITY AND TRANSMIT BEAM-FORMING

The instantaneous probability of error in the presence of AWGN for lucid detection can be mathematically written as:

$$P_e(\gamma) = \frac{1}{2} erfc(\sqrt{\gamma}) \tag{15}$$

If the channels have phases $e^{j\varphi_1}$ and $e^{j\varphi_2}$ respectively. As there is a closed loop between the receiver and the transmitter and CSI is known Equation (18) can be further modified using steering matrix to;

$$y = [h_1 h_2] \begin{bmatrix} -e^{j\varphi_1} \\ -e^{j\varphi_2} \end{bmatrix} s + noise \tag{19}$$

The received signal 'y' is then passed through the DWT and Equalized.

5. SIMULATION RESULTS AND DISCUSSION

This section presents the performance of the proposed system and the parametric studies that were done. The performance of different wavelet families, impact of filter order, diversity order and the performance of DWT and WPT have been considered. For simplicity, BPSK modulation was used for the proposed final system and the parameters used for each simulation have been described in the corresponding tables. All the results presented in this paper are through computer simulations using MATLAB and are solely based on numerical integration.

5.1 Performance Comparison of Wavelet Families

Figure 10 and Figure 11 show the performance of two initial systems employing two different transform methods, i.e. DWT and WPT. From the results, it can be seen that when DWT is employed orthogonal, biorthogonal and reverse biorthogonal wavelets perform alike. If the order of filter is increased, the performance degrades in the case of biorthogonal and reverse biorthogonal wavelets because these wavelets don't have good reconstruction properties, while orthogonal wavelets have been applauded for their reconstruction properties, so even the signal is decomposed more rigorously and many more coefficients need to be

recovered to construct the original transmitted signal, orthogonal wavelets were shown to do that with ease.

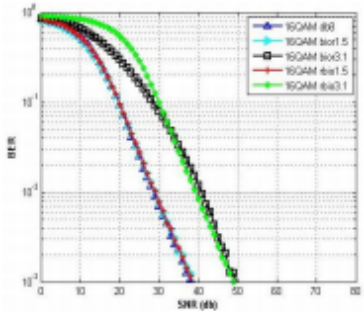

Fig 10: DWT-based MCM system with different wavelet family filters

Table I Modulation Parameter for Comparison of WP and DW using Orthogonal, Biorthogonal and reverse biorthogonal wavelets

	DWT	WPT
Modulation	16-QAM	16-QAM
Symbol length	2^6 * 10^4	2^6 * 10^4
Channel	Rayleigh Multipath Fading	Rayleigh Multipath Fading
Noise	AWGN	AWGN
Decomposition Levels	Log2(n), n = 64;	Log2(n), n = 64;
Antennas	1 Transmit, 1 Receive	1 Transmit, 1 Receive

In Figure 11 however even the lower order biorthogonal and reverse biorthogonal wavelets cannot compare to the orthogonal Daubechies wavelets; reason being the decomposition at every node of the wavelet packet which will require a wavelet that has good reconstruction properties to recover the signal correctly. Daubechies wavelets however performed alike regardless of the transform employed. Any orthogonal wavelets (e.g. Daubechies, Symlet, Coiflet) will show the same performance in AWGN and Rayleigh channels [23]. The answer to the question of the effect of filter order in orthogonal wavelets is addressed later in the discussion. The reason for selecting a higher order modulation technique for this simulation was to study the performance of these wavelets for high data-rate systems and complex mapping.

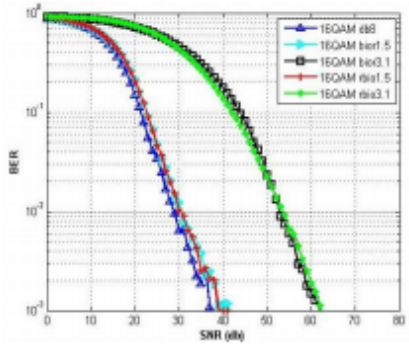

Fig 11: WPT-based MCM system with different wavelet family filters

5.2 BER performance of orthogonal wavelet families

Figure 12 shows a comparison between three different orthogonal wavelet families. It has been suggested in [23] that all orthogonal wavelets perform alike which is true in the case of BER performance both with and without beam-forming but the system processing time considerably varies between them. In this study, it was noticed that the processing time of the Daubechies wavelet filters of order 8 had the fastest processing followed by the Symlet filters of order 8 and the Coiflet filters of order 5 had the slowest processing. The reasoning behind this is how the coefficients of these wavelets behave which is out of the context of this paper but the reader is referred to [24] for a general idea of the difference. This difference is important in the case of digital image processing but for effective communication system purposes Daubechies 8 is better suited.

TABLE II Modulation Parameter for Comparison of WP and DW using Orthogonal, Biorthogonal and reverse biorthogonal wavelets

	DWT
Modulation	BPSK
Symbol length	2^6 * 10^4
Channel	Rayleigh Multipath Fading
Noise	AWGN
Decomposition Levels	Log2(n), n = 64;
Wavelet Families	Symlet 8 Coiflet 5 Daubechies 8
Antennas	2 Transmit 1 Receive

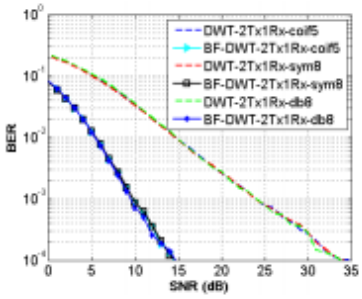

Fig 12: Comparison of different orthogonal wavelet families using DWT

5.3 BER performance of DWT with beam-forming and effect of the order of diversity

This part of the study studies the behavior of different wavelet families, performance comparison between a low order Daubechies filters and high order Daubechies filters, and the effect of order of diversity on the total system performance, to understand other tradeoffs that are required in the systems parameters to achieve a specific diversity gain.

TABLE III Modulation Parameter for Comparison of WP and DW using Orthogonal, Biorthogonal and reverse biorthogonal wavelets

	DWT
Modulation	BPSK
Symbol length	2^6 * 10^4
Channel	Rayleigh Multipath Fading
Noise	AWGN
Decomposition	Log2(n), n = 64;

Levels	
Daubechies Filter Order	Daubechies 2 Daubechies 8 Daubechies 16
Antennas	2 Transmit, 1 Receive 3 Transmit, 1 Receive

Figure 13 shows that the implementation of Transmit beam-forming considerably improves the system performance due to the prior knowledge of the channel at the transmitter with the help of the feedback loop from the equalizer, through which decision can be made on the phase of the channel and the phases of both transmitted data streams can be constructively combined at the receiver using a steering matrix. The increase in the order of filter marginally improves the system performance due to higher filter coefficients but that also increases the system latency quite a bit. Between the three different filter orders that were used the performance of Daubechies family filter with 8 coefficients can be regarded the best overall when the tradeoff is made based on performance and latency.

The system does not show any performance gain by just increasing the wavelet filter order if the beam-forming is not applied. Each data stream encounters an independent channel which makes the equalization at the receiver a challenge and will require more effective techniques which will increase the total receiver cost and power requirements.

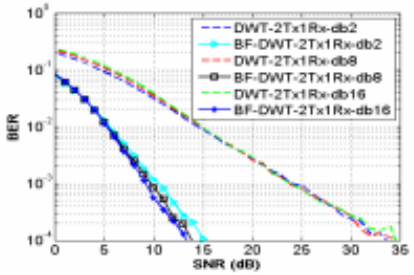

Fig 13 Effects of beam-forming and wavelet filter order with 2 transmit elements using DWT

In Figure 14 effects on the system performance have been studied by increasing the number of transmitting elements by 1, i.e. from 2 transmit antennas to three antennas which will increase the system implementation cost at the Base Station, power is not a constraint at the Base Station, so it is just the tradeoff between the cost of hardware implementation and maintenance and the performance. It is evident from the results produces that the system gain increases about 5 dB at BER of 10^{-4} but the overall system gain has decreased to the quarter between the addition of one extra transmit element and two extra transmit elements.

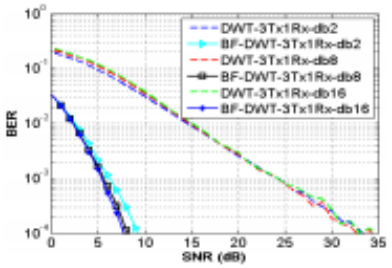

Fig 14: Effects of beam-forming and wavelet filter order with 3 transmit elements using DWT

5.4 BER performance of WPT with beam-forming and effect of the order of diversity

Figure 15 shows the system performance of WPT with beam-forming and the effect of the order of wavelet filters used. In WPT more super channels are created within parallel sub channels as can be seen in Figure 9 which at the end of the filtering process are combined to obtain a wavelet packet. This type of decomposition results in detailed decomposition of signal which results in more number of coefficients. This type of system requires more processing time and can suffer badly from the effects of ISI that is created when the convolution between the channel and the wavelet packet occurs as explained in [12].

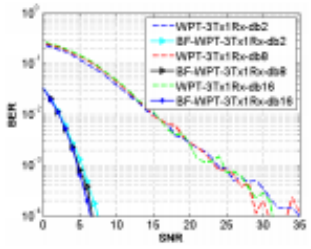

Fig 15: Effects of beam-forming and wavelet filter order with 3 transmit elements using WPT

This interference is then distributed in different wavelet domain to make the degradation effect minimal. But if the channel response is known and the steering matrix is applied then as can be seen the constructive interference of two signals at the receiver can provide high gain as compared to the three independent streams travelling through a multipath channel.

TABLE IV Modulation Parameter for Comparison of WP and DW using Orthogonal, Biorthogonal and reverse biorthogonal wavelets

	WPT
Modulation	BPSK
Symbol length	2^6 * 10^4
Channel	Rayleigh Multipath Fading
Noise	AWGN
Decomposition Levels	Log2(n), n = 64;
Daubechies Filter Order	Daubechies 2 Daubechies 8 Daubechies 16
Antennas	3 Transmit, 1 Receive

It was also noted that the performance of separate streams degrades when the WPT is applied because the coefficients are badly affected by the multipath and the ISI that it makes it impossible to predict the arriving signal to successfully

equalize the channel effects and retrieve the original transmitted data. But on the other hand, same system outperforms the DWT-based system when beam-forming is applied for the reasons.

5.5 Proposed System compared with DWT

Figure 16 shows the performance of the DWT and WPT using beam-forming with two transmit and one receive antennas. The WPT-based system provides the best BER performance.

TABLE V Modulation Parameter for Comparison of WP and DW using Orthogonal, Biorthogonal and reverse biorthogonal wavelets

	DWT	WPT
Modulation	BPSK	BPSK
Symbol length	2^6 * 10^4	2^6 * 10^4
Channel	Rayleigh Multipath Fading	Rayleigh Multipath Fading
Noise	AWGN	AWGN
Decomposition Levels	Log2(n), n = 64;	Log2(n), n = 64;
Antennas	2 Transmit, 1 Receive	2 Transmit, 1 Receive
Wavelet Family and Order	Daubechies 8	Daubechies 8

The WPT-based system provides a higher gain at the cost of extra processing time when compared to DWT with two transmit antennas, but the performance is the same as a 3 element DWT which also takes additional processing time and includes extra hardware cost to implement the third transmit antenna

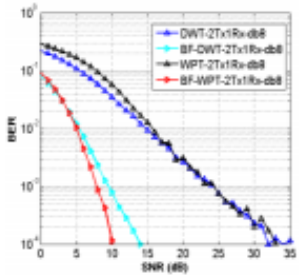

Fig 16: Comparison of DWT and WPT

6. CONCLUSION

From the above study, it can be concluded Wavelet Packet Transform-based MCS using Daubechies 8 filters can give the best BER vs. SNR performance using two elements which can reduce the overall system cost, Increase the coverage and reliability of the system, Power burden is all on the transmitter so the receivers can save power. Processing time is slightly increased when WPM is employed but 3 dB to 4 dB is sufficient gain with one less element at the transmitter for this system to be acceptable. An addition of an extra element with DWT-based system will also increase the processing time and the hardware cost. It is also concluded from the results above that for the communication system orthogonal wavelets of Daubechies family show the best overall performance and orthogonal wavelets perform alike in terms of BER but differ in processing time. From the results it is also evident that even though 2x1 transmitters are employed they perform just like a SISO system because of the independent channels and the sudden changes are due to the small symbol length while when the CSI is known and the signal adds constructively at the receiver the error is minimized.

7. REFERENCES

[1] R. G. Gallager, Information theory and reliable communication, New York: Wiley, 1968.

[2] T. Berger, Rate Distortion Theory: A mathematical basis for data compression, Englewood Cliffs, NJ: Prentice-Hall, 1971.

[3] H. S. Malvar, Signal processing with lapped transforms, Norwood, MA: Artech, 1992.

[4] M. Vetterli and J. Kovacevic, Wavelets and sub-band coding, Englewood Cliffs, NJ: Prentice-Hall, 1995.

[5] S. B. Weinstein and P. M. Ebert, Data transmission by frequency division multiplexing using the discrete Fourier transform, IEEE transaction on communication technology, Vol. 19, pp. 628 – 634, Oct 1971.

[6] H. Bolcskei, P. Duhamel, and R. Hleiss, "A subspace-based approach to blind channel identification in pulse shaping OFDM/OQAM systems,"IEEE Transaction on Signal Processing, Vol. 49, pp. 1594–1598, Jul. 2001.

[7] Y. Sun and L. Tong, "Channel equalization using one-tap DFE for wireless OFDM systems with ICI and ISI," in Proc. IEEE SPAWC'99, Annapolis, MD, pp. 146–149 May 1999.

[8] G. W. Wornell, Emerging applications of multi-rate signal processing and wavelets in digital communications, Proceedings of the IEEE, Vol. 84, No. 4, pp. 586 – 603, April 1996.

[9] G. W. Wornell and A. V. Oppenheim, "Wavelet-based representations for a class of self-similar signals with applications to fractal modulation", IEEE transaction on information theory, Vol. 38, pp. 785 – 800, 1992.

[10] G. W. Wornell, Signal Processing with fractals: A wavelet-based approach, Upper Saddle River, NJ: Prentice-Hall, 1995.

[11] F. Daneshgaran and M. Mondin: 'Bandwidth efficient Modulation with wavelets', Electronic Letters, Vol. 30, No.1, pp. 1200–1202, July 1994

[12] R. Asif, R.A. Abd-Alhameed, "Performance Evaluation Of FFT-OFDM and DWT-OFDM for multicarrier communications systems using time domain zero forcing equalization", International journal of Computer Applications, Foundation of Computer Science, NY, USA, Vol. 51, No. 4, pp- 34-38, August 2012.

[13] K. Hetling, G. Saulnier, and P. Das, "Spreading codes for wireless spread spectrum communications," Proceedings of IEEE, Vol. 1, pp. 68–72, 1996.

[14] A. Muayyadi and M. A. Abu-Rgheff , "Wavelet-based multicarrier CDMA system and its corresponding multi-user detection", IEE Communication Proceedings, Vol 150, No. 6, Dec 2003.

[15] R. E. Learned, A. S.Willsky, and D. M. Boroson, "Low complexity optimal joint detection for oversaturated multiple access communications," IEEE Transactions on Signal Processing, Vol. 45, pp. 113–123, Jan. 1997.

[16] A. R. Lindsey, "Wavelet packet modulation for orthogonally multiplexed communications," IEEE Transaction on Signal Processing, Vol. 45, pp. 1336–1339, May 1997.

[17] K. M. Wong, J. Wu, T. N. Davidson, and Q. Jin, "Wavelet packet division multiplexing and wavelet packet design under timing error effects," IEEE Transactions on Signal Processing, Vol. 45, pp. 2877–2890, Dec. 1997.

[18] R. Asif, R. A. Abd-alhameed, "Performance Evaluation of DWT-OFDM and FFT-OFDM for Multicarrier Communications Systems using Time Domain Zero Forcing Equalization", International Journal of Computer Applications, vol. 51, no.4, August 2012, pp. 34-38. ISSN: 0975 – 8887..

[19] M. Vetterli and C. Herley, "Wavelets And Filter Banks: Theory And Design," IEEE Transactions on Signal Processing, Vol. 40, No. 9, pp. 2207 – 2231, Sept.1992.

[20] I. Daubechies, Ten Lectures on Wavelets, 2nd Edition. Philadelphia, PA, USA. CBMS-NSF-Regional Conference Series on Applied Mathematics, 1992.

[21] K. Abdullah, A. Z. Sadik, and Zahir M. Hussain, "On the DWT and WPT- OFDM versus FFT-OFDM", 5th IEEE GCC Conference and Exhibition, Kuwait City, 17-19, pp 1 – 5, March 2009,

[22] W. C. Jakes, Ed., Microwave Mobile Communications. New York: Wiley, 1974.

[23] R. Asif, "A Unique Wavelet-based Multicarrier System with and without MIMO over Multipath Channels with AWGN." International Journal of Computer Applications, Vol 17, No. 9, 2015.

[24] M. Srivastava, Y. Yashu, S. Singh, P. Panigrahi, "Multi-segmentation through wavelets: Comparing the efficacy of Daubechies vs. Coiflets", International Conference on Signal Processing and Real Time Operating System (SPRTOS), March 2011.

International Journal of Computer Applications (0975 – 8887)
Volume 117 – No. 9, May 2015

A Unique Wavelet-based Multicarrier System with and without MIMO over Multipath Channels with AWGN

Rameez Asif
MIEEE, MIET
University of Bradford
United Kingdom

Raed Abd-Alhameed
FIEEE, FIET
University of Bradford
United Kingdom

J. M. Noras
University of Bradford
United Kingdom

ABSTRACT
Recent studies suggest that multicarrier systems using wavelets outperform conventional OFDM systems using the FFT, in that they have well-contained side lobes, improved spectral efficiency and BER performance, and they do not require a cyclic prefix. Here we study the wavelet packet and discrete wavelet transforms, comparing the BER performance of wavelet transform-based multicarrier systems and Fourier based OFDM systems, for multipath Rayleigh channels with AWGN. In the proposed system zero-forcing channel estimation in the frequency domain has been used. Results confirm that discrete wavelet-based systems using Daubechies wavelets outperform both wavelet packet transform- based systems and FFT-OFDM systems in terms of BER. Finally, Alamouti coding and maximal ratio combining schemes were employed in MIMO environments, where results show that the effects of multipath fading were greatly reduced by the antenna diversity.

Keywords
OFDM, BER, Multipath, Discrete Wavelet Transform (DWT), Wavelet Packet Transform (WPT), Multiple Input Multiple Output (MIMO)..

1. INTRODUCTION
Contemporary communication systems employ a number of different techniques for signal transmission, reception and processing [1]. High level methodologies such as multiplexing in frequency [2], [3], in time [4] and spatially [5], which are now in common use, are undergoing extensive research in the search for highest quality of service.

Orthogonal Frequency Division Multiplexing (OFDM) is the main contender for the communication systems of the next generation. In this multicarrier modulation technique, the total channel bandwidth is divided into different sub-bands and the data symbols are then transmitted over these sub-bands. This division of the channel bandwidth provides high tolerance against multipath fading [6]. OFDM is now accepted as a standard in asymmetric digital subscriber line (ADSL) and digital video broadcasting (DVB), and in WiMAX and IEEE 802.11 [7].

However OFDM does have major disadvantages, namely strong side lobes, high peak to average power ratio (PAPR), and sensitivity to carrier timing offset [8].

In consideration of the above OFDM limitations, recent studies have suggested wavelet-based multicarrier systems [9]-[12] as an alternative to conventional FFT-OFDM, using the Discrete Wavelet Transform (DWT), or the Wavelet Packet Transform (WPT). This may provide all the advantages of conventional OFDM, but also mitigate the problems of PAPR and carrier timing offset [13]-[15].

In fast Fourier analysis a signal is decomposed into its constituent individual sinusoids, whereas a wavelet transform decomposes signal into different bands of the frequency spectrum, with the same computational complexity of order $O(N\log_2 N)$ [16] for discrete cosine while many other types of wavelet transforms in which FFT is approximated using wavelets can be effectively computed with the time complexity of O(N) [17]. Inter-symbol interference (ISI) and inter-carrier interference (ICI) arising from the loss of orthogonality of transmitted symbols in OFDM can be countered by the use of wavelets and in [18], the effect of narrowband interference has been shown to be more pronounced in OFDM using the FFT rather than the DWT.

The wavelet-based system achieves orthogonality through the use of orthogonal wavelet filters, also referred to as filter banks [19]. The DWT produces narrow side lobes with large power spectral density. No cyclic prefix insertion is required, which can save up to 25% of the bandwidth making wavelet-based multicarrier systems more bandwidth efficient [20]-[24] and enabling improved BER performance. The wavelet transform represents signals jointly in the time and frequency domains, using multi-resolution analysis. This property of wavelets also makes them suitable for treating signals with exotic spectral properties, for example signals that have time-dependent spectral properties.

More recently, the present authors in R. Asif et al [25] have proposed DWT for multi-carrier modulations using time domain equalization. In this study we present a new way of channel equalization when working with wavelets. We examine the ISI, and compare the performance of different wavelet families in terms of signal reconstruction. DWT and WPT methods are studied in terms of processing time and performance. Another major contribution of this study is the extension of the DWT technique into the MIMO environment where the performance of the system has been evaluated using both receive and transmit diversity techniques.

Section II of this paper illustrates the baseband architecture and implementation of the proposed system. The simulation results are discussed in Section III and Section IV contains the conclusions.

2. DWT BASEBAND ARCHITECTURE AND IMPLEMENTATION
The continuous-time wavelet transform (CWT) can be written [26]:

$$CWT\,x(\tau,a) = \langle x(t), \psi_{a,\tau} \rangle = \frac{1}{\sqrt{|a|}} \int_{-\infty}^{\infty} x(t)\psi^*\left(\frac{t-\tau}{a}\right) dt \qquad (1)$$

In this equation the parameter 'a' is a scaling factor which controls the scaling of the signal in frequency and τ is the shift parameter which controls the signal dilation or contraction in

time, while ψ^* is the function which defines the CWT, known as the mother wavelet from which all daughter wavelets that are used in transformation are derived. '*' denotes the complex conjugate.

The mother wavelet is designed such that it can be inverted and the original signal can be retrieved, so that in theory we can write the inverse of the CWT as [27]:

$$x(t) = \frac{1}{C_\psi} \int_a \int_\tau \frac{1}{a^2} x(a,\tau)\psi\left(\frac{t-\tau}{a}\right) dt da \quad (2)$$

However, in its continuous form the transform is extremely redundant, involves extensive analytical calculation, and, cannot easily be inverted in practice. To avoid these difficulties, the wavelets are made discrete using scaling and translation parameters $a = 2^{-j/2}$ and $\tau = 2^j k$ respectively, so that the DWT transformed signal can be written as [27]:

$$DWTx(j,k) = \langle x, \psi_{j,k} \rangle = 2^{\frac{-j}{2}} \sum_{n=-\infty}^{\infty} x(n)\psi(2^{-j} n - k) \quad (3)$$

In this study, we have constrained *'n'* into a positive finite region only, since the length of a signal cannot be infinite. This transform can be readily inverted to retrieve the original signal as follows,

$$x(n) = \sum_{k=0}^{\infty} \sum_{j=-\infty}^{\infty} DWTx(j,k)\psi\left(2^{-j} n - k\right) \quad (4)$$

With the above baseband architecture, a Multiple Input and Multiple Output (MIMO) front-end is then appended to the DWT-OFDM whereby data is both transmitted and received by multiple antennas. MIMO systems can provide significant increases in data throughput and link reliability without any additional bandwidth usage. This form of baseband and front-end formulation is known to achieve high spectral efficiency and throughput [28]-[30].

2.1 Proposed Wavelet based Multicarrier System

The proposed implementation has similarities to FFT-OFDM. On the transmitter side data bits are modulated, for example using BPSK or higher level modulation, mapping the data into symbols, which then pass through a serial to parallel converter to reform as *N* parallel streams, where *N* is the number of sub-channels. Next, orthogonal wavelet division multiplexing is applied: a pair of data streams $x_i(n)$ are up-sampled by a factor of two and then passed through a Quadrature Mirror Filter (QMF) bank that consists of two half-band filters. These are a lowpass filter (LPF), with impulse response *h*, and a highpass filter (HPF) with impulse response *g*. These convolve with the signal, such that $x_{low}[n] = h[n]*x[n]$ *and* $x_{high}[n] = g[n]*x[n]$, where $x[n]$ is the original signal.

The coefficients output from the two filters constitute a wavelet symbol. The combined process of up-conversion and filtering is known as synthesis, and is repeated successively to complete the translation-scaling process. Fig. 1 shows a two level wavelet synthesis process, also called the Inverse Discrete Wavelet Transform (IDWT).

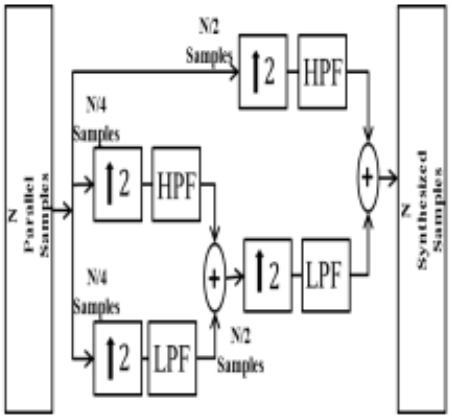

Fig. 1. 2-Level Wavelet Synthesis

The synthesized data is then passed through the channel in the presence of AWGN as shown in Fig. 2.

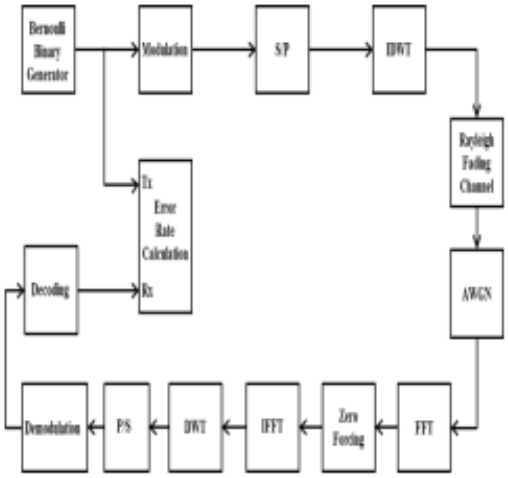

Fig. 2. Proposed DWT multicarrier system.

The convolution between the channel and the signal is linear and the effects are discussed in Part (C).

On the receiver side, the received signal is converted to the frequency domain using FFT and then equalized using zero forcing (ZF) equalization algorithm. Once the received signal is successfully equalized in the frequency domain it is converted back to time domain using IFFT and then analyzed using discrete wavelet transform process. This involves conjugate high pass $h^*(-n)$ and low pass filters $g^*(-n)$ followed by down-sampling by a factor of 2. This process is repeated until the initial *N* parallel streams are obtained, which are passed through a parallel to serial convertor and demodulated. Fig. 3 shows two levels of the DWT.

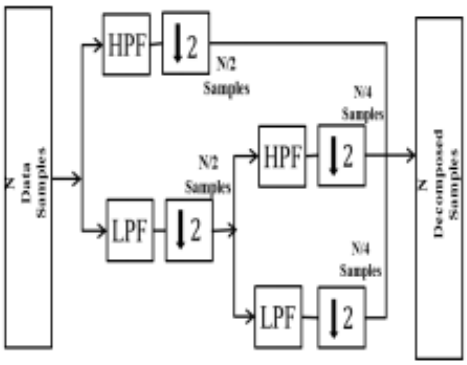

Fig. 3. 2-Level Wavelet Decomposition.

Consider an input sequence, *x(n)*, which is to be transformed by a scaling filter *g(n)* with coefficients [g(0), g(1), g(2), g(3)] and wavelet filters *h(n)* with coefficients [h(0), h(1), h(2), h(3)]. These will be convolved with *x(n)* according to the following [31], [32];

$$\begin{bmatrix} p(0) \\ p(1) \\ p(2) \\ p(3) \\ p(4) \\ p(5) \\ M \\ p(n-1) \end{bmatrix} = \begin{bmatrix} h(3) & h(2) & h(1) & h(0) & 0 & \Lambda & 0 & 0 \\ g(3) & g(2) & g(1) & g(0) & 0 & \Lambda & 0 & 0 \\ 0 & 0 & h(3) & h(2) & h(1) & h(0) & \Lambda & 0 \\ 0 & 0 & g(3) & g(2) & g(1) & g(0) & \Lambda & 0 \\ M & & & O & & & & M \\ h(1) & h(0) & 0 & \Lambda & 0 & 0 & h(3) & h(2) \\ g(1) & g(0) & 0 & \Lambda & 0 & 0 & g(3) & g(2) \\ h(2) & h(1) & h(0) & 0 & \Lambda & 0 & 0 & h(3) \\ g(2) & g(1) & g(0) & 0 & \Lambda & 0 & 0 & g(3) \end{bmatrix} \begin{bmatrix} x(0) \\ x(1) \\ x(2) \\ x(3) \\ x(4) \\ x(5) \\ M \\ x(n-1) \end{bmatrix} \quad (5)$$

By a lifting scheme [32]-[35] the LPF and the HPF can form a single function p(n), and we can express the relation above in a compact form as;

$$y(n) = p(n) * x(n) \quad (6)$$

p(n) in the relation above has been shown in M. Vetterli et al [31] to be a Toeplitz matrix. The shifting by 2 (looking from the left-hand-side) in the matrix equation is produced by the up-sampling (or down-sampling, as the case may be) in the wavelet configuration [32]. The matrix for the filter impulse response must be resized according to the length of the input signal.

As the signal *y(n)* traverses the multipath channel, the orthogonality of the symbols will be lost but if delays are not longer than the shifts during the scaling and translations, by applying equivalent matching filters, the signals will be correctly reconstructed [36].

The relationship between the high-pass and low-pass filters of QMF banks can be expressed mathematically as:

$$h(n) = (-1)^n g(l+1-n) \quad (7)$$

Where, *l* is the length of *g(n)*.

2.2 Multi-resolution Analysis and Sub-Band Coding

Various techniques of multi-resolution analysis enable signals to be analyzed into multiple frequency bands. The approach employed in this investigation is called sub-band coding in which signals are divided into several independent sub-bands.

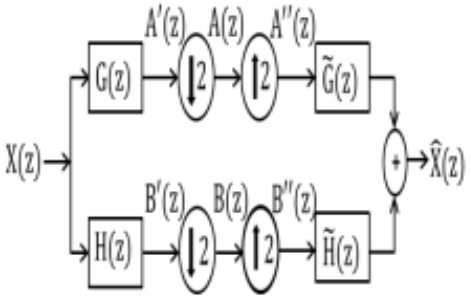

Fig. 4. Two channel sub-band coding analysis and synthesis.

The block diagram in Fig. 4 shows one stage of analysis and synthesis. Two parallel streams are created by de-multiplexing the input signal stream, one of which is analyzed using the low pass filter and the other using the high pass filter.

Meanwhile, the input signal and the filter follow the z-transform tradition as follows;

$$X(z) = \sum_n x(n) z^{-n} \quad (8a)$$

Where,

$$z^{-n} = e^{-jnw} \quad (9)$$

The intermediate signals *A'(z)* and *B'(z)* that are obtained after the filtering process of *X(z)* are as follows:

$$A'(z) = X(z)G(z) \quad (10)$$

And,

$$B'(z) = X(z)H(z) \quad (11)$$

A'(z) and *B'(z)* are then down-sampled by a factor of 2, to give:

$$A(z) = \frac{1}{2}\left[A'\left(z^{\frac{1}{2}}\right) + A'\left(-z^{\frac{1}{2}}\right)\right] \quad (12)$$

And,

$$B(z) = \frac{1}{2}\left[B'\left(z^{\frac{1}{2}}\right) + B'\left(-z^{\frac{1}{2}}\right)\right] \quad (13)$$

Following the signal path on Fig. 4, these signals are then up-sampled by a factor of 2 to give two intermediate signals as follows:

$$A^*(z) = A(z^2) \quad (14)$$

And,

$$B^*(z) = B(z^2) \quad (15)$$

Now, substituting (10) in (12) and (11) in (13) yields:

$$A''(z) = \frac{1}{2}[A'(z) + A'(-z)] \tag{16}$$

And,

$$B''(z) = \frac{1}{2}[B'(z) + B'(-z)] \tag{17}$$

Hence the output produced by the filter bank can be expressed by the following:

$$\hat{X}(z) = A''(z)\tilde{G}(z) + B(z)\tilde{H}(z) \tag{18}$$

Substituting (16) and (17) into (18), $\hat{X}(z)$ is given by:

$$\hat{X}(z) = \frac{1}{2}[A'(z) + A'(-z)]\tilde{G}(z) + \frac{1}{2}[B'(z) + B'(-z)]\tilde{H}(z) \tag{19}$$

It follows that the synthesized output can be given in terms of the original signal, $X(z)$ by substituting the values of (10) and (11) into (19),

$$\hat{X}(z) = \frac{1}{2}[X(z)G(z) + X(-z)G(-z)]\tilde{G}(z) + \frac{1}{2}[X(z)H(z) + X(-z)H(-z)]\tilde{H}(z) \tag{20}$$

Simplifying (20), results in:

$$\hat{X}(z) = \frac{1}{2}[G(z)\tilde{G}(z) + H(z)\tilde{H}(z)]X(z) + \frac{1}{2}[G(-z)\tilde{G}(z) + H(-z)\tilde{H}(z)]X(-z) \tag{21}$$

It is worth noting that the estimated signal $\hat{X}(z)$ in (21) contains both the original transmitted signal (first term) and an associated alias part in the second term.

In order to remove the aliasing part, the second term is set to zero, i.e.

$$G(-z)\tilde{G}(z) + H(-z)\tilde{H}(z) = 0 \tag{22}$$

To extract a realizable solution for (20), $H(z)$ is taken as a Finite Impulse Response (FIR) filter of order $(N+1)$, where N is always an odd number. Then the following two conditions are applied to compensate the anti-aliasing in (22):

$$\tilde{G}(z) = -H(z) \tag{23a}$$

And,

$$G(z) = \tilde{H}(z) \tag{23b}$$

With anti-aliasing imposed, the output produced by the filter bank ($\hat{X}(z)$), in (21) reduces to:

$$\hat{X}(z) = \frac{1}{2}[G(z)\tilde{G}(z) + H(z)\tilde{H}(z)]X(z) \tag{24}$$

We now need the following well known definitions [30]:

$$\tilde{H}(z) \triangleq z^{-N}H(z^{-1}) \tag{25a}$$

$$\tilde{h}(n) \triangleq h(N-n) \tag{25b}$$

$$\tilde{G}(z) \triangleq z^{-N}G(z^{-1}) \tag{26a}$$

And

$$\tilde{g}(n) \triangleq g(N-n) \tag{26b}$$

If (23b) and (25a) are combined, $G(z)$ can be expressed in terms of $H(z^{-1})$ thus:

$$G(z) = \tilde{H}(-z) = -(z^{-N})H(-z^{-1}) \tag{27}$$

The above equation can also be rewritten in the following format:

$$G(z) = -z^{-N}H(-z^{-1}) \tag{28}$$

Now substituting (23a), (25a) and (28) into (24), $\hat{X}(z)$ can be written in terms of $H(z)$ as follows:

$$\hat{X}(z) = \frac{1}{2}[-z^{-N}H(-z^{-1})(-H(-z)) + H(z)z^{-N}H(z^{-1})]X(z) \tag{29}$$

The simplified form of (29) is given by:

$$\hat{X}(z) = \frac{1}{2}[H(-z)H(-z^{-1}) + H(z)H(z^{-1})]z^{-N}X(z) \tag{30}$$

Setting the inner elements within the two brackets of (30), equal to the value 2:

$$H(-z)H(-z^{-1}) + H(z)H(-z^{-1}) = 2 \tag{31}$$

It follows that the estimated signal $\hat{X}(z)$ will be precisely equal to the transmitted signal $X(z)$ with an N sample delay. If (9), is used in (31), this gives:

$$|H(e^{j\omega})|^2 + |H(e^{j(\omega+\pi)})|^2 = 2 \tag{32}$$

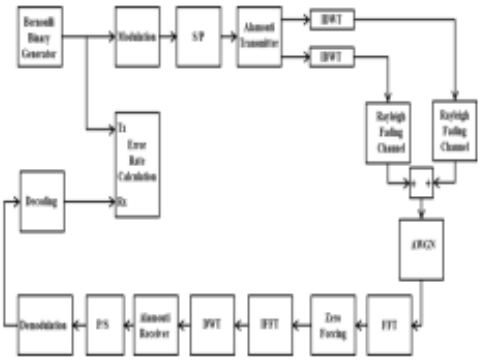

Fig. 5. Proposed Alamouti Coded 2x1 DWT-MIMO Multi-Carrier System

Thus the criterion for perfect reconstruction is expressed by (32) or equivalently by (31). $H(z)$ and $G(z)$ are quadrature mirror filters. If $H(z)$ is known, the three required filters given in (23a), (25a) and (28) can be easily derived to form the perfect reconstruction filter bank.

2.3 Zero Forcing Equalization

Channel estimation in wavelet-based multicarrier systems is a challenge, and finite impulse response (FIR) based zero-forcing was proposed in Farrukh et al [22] for a time domain equalization. In this work, we implement frequency-domain equalization. An FFT operation has been performed on the

wavelet signal at the receiver (see Fig. 2, 5 and 6) according to the following;

$$S(f) \overset{FFT}{\Longleftrightarrow} X(\tau, a) \tag{33}$$

Where, $X(\tau, a)$ is the wavelet-domain signal scaled by "a" and shifted by "τ" and $S(f)$ is the transformed signal which will pass the equalizer.

In conventional OFDM systems where a cyclic prefix is included, linear convolution in the time domain with channel impulse response $h(t)$ is equivalent to cyclic convolution. As a result, there is no ISI and frequency domain equalization can be implemented exactly by dividing by the frequency response of the channel, H. This is estimated, e.g. by transmitting known training data. If the received signal in the frequency domain is

$$R = HS + N, \tag{34}$$

Where, S is the signal spectrum and N is the noise spectrum, then

$$R/H = S + N/H. \tag{35}$$

Note that noise will be increased in sub-channels in which H is faded. Where there is no cyclic prefix, then the convolution is not cyclic and the convolution theorem does not apply exactly. Then

$$R' = S + X + N, \tag{36}$$

Where, X represents the ISI in the frequency domain, introducing an error. It follows that

$$R'/H = S + (X+N)/H. \tag{37}$$

In conventional OFDM, symbols transmitted in sub channels where H is faded will experience increased probability of error due to X as well as to N. In the proposed system, the ISI is spread by the wavelet transform across a number of wavelet domain symbols. The deleterious effect on error probability is offset by having more symbol power, since none is wasted in transmitting the cyclic prefix.

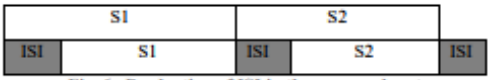

Fig. 6. Production of ISI in the proposed system

2.4 Maximal Ratio Combining

The above mentioned technique is now extended to include a receive diversity scheme, using maximal ratio combining to obtain optimal performance, although at the cost of increased complexity. The benefits of using receive diversity, with a number K of different antennas, is to improve the effective (E_b/N_o) K times as compared to that of a single receive antenna [32]:

$$\gamma = \sum_{k=1}^{K} \frac{|h_k|^2 E_b}{N_o} \tag{38}$$

Where, K is the number of the receive antenna, and γ is the signal to noise power ratio (SNR) gain as the K increases.

2.5 Alamouti Coded Wavelet based System

Next, space-time block coding is introduced, which is also a MIMO technique. Fig. 5 below shows an Alamouti coded wavelet-based OFDM system with two transmitting and one receiving antennas.

At the transmitter the binary data were BPSK modulated and then reformed into parallel data by a serial to parallel converter. After the IDWT process, the data were coded using the Alamouti scheme before transmission over a multipath Rayleigh channel with AWGN. The particular Alamouti code is as follows [37]:

$$S = \begin{bmatrix} s_1 & s_2^* \\ s_2 & -s_1^* \end{bmatrix} \tag{39}$$

Symbols s_1 and s_2 were transmitted in the first time slot (t) over the two channels and $-s^*_1$ and $-s^*_2$ (where * again denotes the complex conjugate) were transmitted in the second time slot ($t+T$). The symbols received can be written as:

$$R = \begin{bmatrix} h_1 & h_2 \end{bmatrix} \begin{bmatrix} s_1 & s_2^* \\ s_2 & -s_1^* \end{bmatrix} \tag{40a}$$

Or,

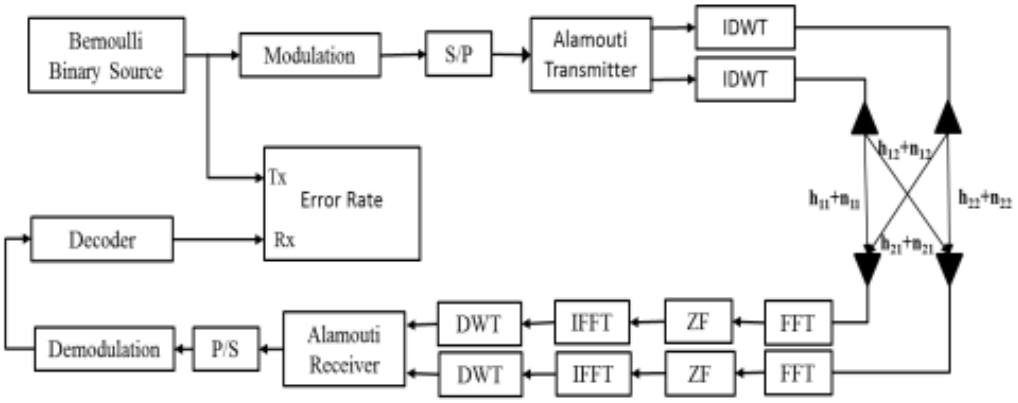

Fig. 7. Proposed Alamouti Coded 2-Transmitter 2-Receiver-based Wavelet Multi Carrier System

$$R = \begin{bmatrix} h_1 s_1 + h_2 s_2 & h_2 s_2^* - h_2 s_1^* \end{bmatrix} \quad (40b)$$

Where, h_k represents the channel. AWGN has been added to each element of R.

Now, $R * S^H$, where, $(.)^H$ stands for the Hermitian transpose, gives:

$$RS^H = h.S.S^H = \begin{bmatrix} h_1 & h_2 \end{bmatrix} (|s_1|^2 + |s_2|^2) \quad (41)$$

Since,

$$S.S^H = (|s_1|^2 + |s_2|^2)[I] \quad (42)$$

Where, $[I]$ is the identity matrix.

Once R is known, for the subsequent unknown symbols, a matrix Q is constructed as:

$$H = \begin{bmatrix} h_1 & h_2 \\ h_2^* & -h_1^* \end{bmatrix} \quad (43)$$

Then

$$Q = Hs = \begin{bmatrix} R(1) \\ -R(2)^* \end{bmatrix} \quad (44)$$

Therefore

$$H^H Q = \left(|h_1|^2 + |h_2|^2 \right) \begin{bmatrix} s_1 \\ s_2 \end{bmatrix} \quad (45)$$

Where, HH^H is a diagonal matrix.

Once the symbols are separated they can be decoded in the detector, the serial data passing through the DWT, and the N parallel streams then reformed via the parallel to serial convertor, prior to demodulation.

In Fig. 7 we now show a discrete wavelet transform-based Alamouti-coded two transmitter and two receiver-based system. The transmitter part of the 2×2 Alamouti coded wavelet-based OFDM is the same as that of 2×1 but we now have two receive antennas, so that there are four channels involved:

$$\begin{bmatrix} y_1^1 \\ y_2^1 \\ y_1^{2*} \\ y_2^{2*} \end{bmatrix} = \begin{bmatrix} h_{11} & h_{12} \\ h_{21} & h_{22} \\ h_{12}^* & -h_{11}^* \\ h_{22}^* & -h_{21}^* \end{bmatrix} \begin{bmatrix} x_1 \\ x_2 \end{bmatrix} + \begin{bmatrix} n_1^1 \\ n_2^1 \\ n_1^{2*} \\ n_2^{2*} \end{bmatrix} \quad (46)$$

Where, h_{ij} (for i=1,2 and j=1,2) is one of the four independent Rayleigh fading channels. Then after equalization the estimated transmitted symbols can be written as:

$$\begin{bmatrix} \hat{x}_1 \\ \hat{x}_2^* \end{bmatrix} = \left(HH^H \right)^{-1} H^H \begin{bmatrix} y_1^1 \\ y_2^1 \\ y_1^{2*} \\ y_2^{2*} \end{bmatrix} \quad (47)$$

In this case, equalized serial symbols then pass through three levels of DWT, the parallel to serial convertor and are then demodulated.

3. SIMULATION AND RESULTS

In this section the results from the systems described above are discussed. These were obtained through Monte-Carlo simulations.

The first study was to compare the performances of different wavelet families: not all wavelet families perform alike because they all involve different filters.

The results support the theory that the Daubechies family works best for reconstruction and can provide the best results in multicarrier systems, and Fig. 8 depicts an (E_b/N_o) gain of approximately 2 dB for a BER of 10^{-3} in a multipath Rayleigh channel with AWGN.

The simulation was repeated under the same conditions as shown in Table I for Daubechies, Biorthogonal and Reverse Biorthogonal wavelets.

TABLE I

DWT SIMULATION PARAMETERS

Parameter	Parameter Value
Modulation scheme	BPSK
FFT size	Nil
Cyclic prefix	Nil
Wavelet families	db8, bior1.3, rbior1.3
Propagation	Rayleigh fading + AWGN
Decomposition stages	$K = \log_2(N)$, $N = 64$
Symbol length	$2^6 \times M$, $M = 10^5$

After selecting the Daubechies wavelet family, a filter length of 8 was found, after several trials, to give the best balance between overall system performance and acceptable processing speed. We next compared the BER performances of the wavelet packet transform-based system and the discrete wavelet-based system. Simulation parameters used for both the DWT and WPT are described in Table II below.

TABLE II

SIMULATION PARAMETERS DWT AND WPT

Parameter	DWT	WPT
Modulation scheme	16-QAM, 64-QAM	16-QAM, 64-QAM
Wavelet family	db8	db8
Propagation	Rayleigh fading + AWGN	Rayleigh fading + AWGN
Decomposition stages	$K = \log_2(N)$, $N = 64$	$K = \log_2(N)$, $N = 64$
Symbol length	$2^6 \times M$, $M = 10^5$	$2^6 \times M$, $M = 10^5$

Monte-Carlo simulation results obtained are shown below in Fig. 9.

It was observed through simulations as shown in Fig. 9 that the DWT outperforms the WPT by an (E_b/N_o) margin of about 5 dB for the same BER of 10^{-1}. The performance of wavelet packet transform based system marginally improves at high (E_b/N_o) values, but the discrete wavelet transform still performs better. Thus we selected the DWT for our system.

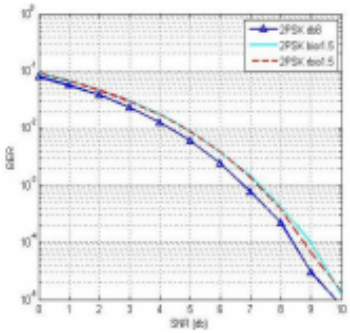

Fig. 8. Performance Comparison of Different Wavelet Families

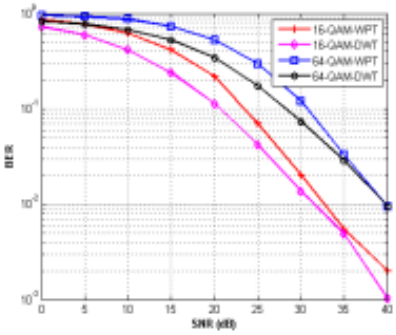

Fig. 9. Performance Comparison OF DWT and WPT in MCS

The final choice is what type of modulation scheme to use. Simulations were performed in which we choose four different types of modulations and kept the rest of the simulation parameters the same as in Table I.

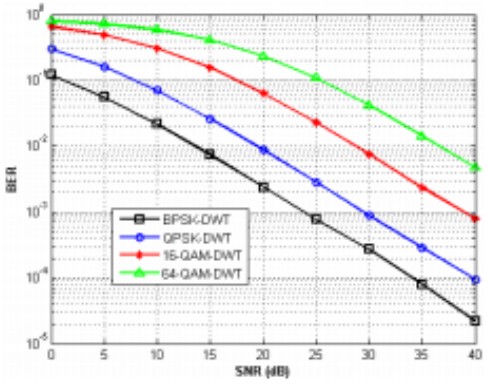

Fig. 10. DWT-based MCS using different modulation schemes

For simplicity and best BER performance BPSK was selected as the modulation scheme for the rest of this study.

TABLE III

SIMULATION PARAMETERS DWT AND FFT

Parameter	DWT	WPT
Modulation scheme	BPSK	BPSK
FFT size	Nil	64
Wavelet family	db8	db8
Propagation	Rayleigh fading + AWGN	Rayleigh fading + AWGN
Decomposition stages	K = $\log_2$(N), N = 64	K = $\log_2$(N), N = 64
Symbol length	2^6×M, M = 10^5	2^6×M, M = 10^5

Next we compared the conventional FFT-OFDM and DWT-based multicarrier systems. The results produced in the Fig. 11 and Fig. 12 clearly suggest that the DWT-based MCS performs better than the conventional Fourier-based OFDM system by a margin in (E_b/N_o) of about 6 dB at a BER of 10^{-4} in a multipath fading environment.

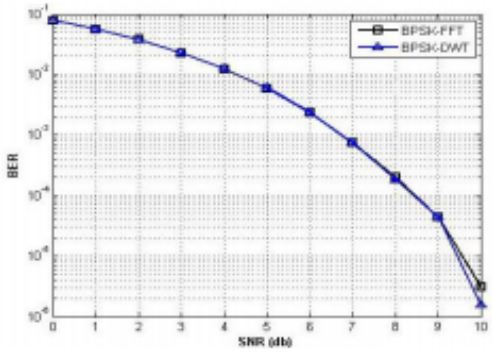

Fig. 11. Comparison of DWT-OFDM and FFT-OFDM in AWGN

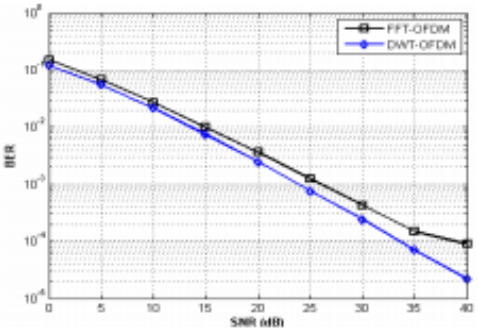

Fig. 12. Performance comparison of DWT-based MCS and FFT-OFDM

The model was then extended to use Maximal Ratio Combining receive diversity.

The results obtained are depicted in Fig. 13 and they show that as the number of antennas on the receiver is increased the performance approaches that of line-of-sight systems. Also, it can be seen that wavelet-based MCS complies with the law of diminishing returns. Thus, the antenna gain decreases with increasing number of antennas.

The Alamouti-based transmit diversity technique was then applied and compared with MRC which showed that two antennas on the transmitter side and one antenna on the receiver side has the same diversity order as that of one transmit and two receive antennas as suggested by Sivash Alamouti [38]. Fig. 14 shows these results.

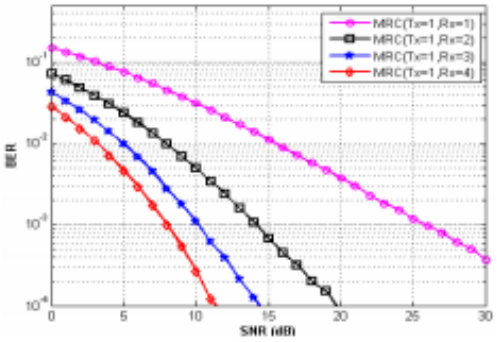

Fig. 13. DWT-MIMO-MCS using Maximal Ratio Combining

4. CONCLUSION

In this work, an alternative technique to FFT-OFDM has been presented and investigated, and made comparisons between different wavelet families and different wavelet transforms a frequency-domain channel equalization method using zero-forcing equalization was introduced which showed better performance than conventional FFT-OFDM frequency-domain equalization. The proposed system exploits the special property of wavelet transforms such that filter distortions and signal aliasing is completely cancelled using the analysis and synthesis filters. This resulted in the perfect reconstruction of the original input data signal and perfect extraction of the multiplexed input signals. The aliasing cancellation condition that is imposed in the filter banks ensures no cross talk in the corresponding transmultiplexer. Meanwhile, the proposed wavelet transform multicarrier modulation scheme brought increased spectral efficiency, consequent on the non-inclusion of cyclic prefixing which needs up to 25% of the transmit bandwidth in the conventional FFT-based OFDM. Comparison between two different types of wavelet-based modulations was also presented which showed that the DWT performs better than WPT both in terms of BER performance, and in terms of processing times as WPT decomposition is performed at each node. Diversity techniques were then studied using the proposed DWT-OFDM with frequency domain equalization. Overall discrete wavelet transform-based MC system performed better than the conventional OFDM system in terms of BER performance with savings of 8% to 25% bandwidth.

5. REFERENCES

[1] P. H. Young, Electronic Communications Techniques, *Prentice Hall*, Englewood Cliffs, NJ, 1994.

[2] J. G. Proakis, Digital Communications, *McGraw-Hill, 1995*.

[3] J. G. Proakis, M. Salehi, and G. Bauch, Contemporary communication systems using MATLAB, *Brooks/Cole*, 2000.

[4] E. Telatar, "Capacity of Multiple antenna Gaussian Channels," *European transactions on telecommunications*, vol. 10, no. 6, pp. 585-595, 1999.

[5] Z. Hong, et al., "Spatial multiplexing in correlated fading via the virtual channel representation," *IEEE Journal on Selected Areas in Communications*, vol. 21, no. 5, pp. 856-866, 2003.

[6] S. Hara, and R. Prasad, Multicarrier techniques for 4G mobile communications, *Artech House Publishers*, 2003.

[7] K. Abdullah, N. Al-Hinai, A. Z. Sadik and Z. M. Hussain, "Circular 16-QAM modulation scheme for wavelet and Fourier based OFDM systems," *5th IEEE GCC Conference and Exhibition*, pp. 1 – 5, 2009.

[8] V. Kumbasarand O. Kucur, "Better wavelet packet tree structures for PAPR reduction in WOFDM systems," *Digital Signal Processing*, vol. 18, no. 6, pp. 885-891, 2008.

[9] B. G. Negash, H. Nikookar, "Wavelet based OFDM for wireless channels," *Vehicular Technology Conference, IEEE VTS 53rd*, vol. 1, pp. 688-691, 2001.

[10] I. Widad, "Implementation of WiMAX (IEEE802. 16. d) OFDM Baseband Transceiver-Based Multi wavelet OFDM on a Multi-Core Software-Defined Radio Platform," *ISRN Signal Processing*, 2011.

[11] H. J. Taha, M. F. M. Salleh, "Performance analysis of QAM modulation parameters on wavelet packet transform (WPT) and FFT- OFDM system," *IEEE 9th Malaysia International Conference on Communications (MICC)*, pp. 1 – 5, 2009.

[12] M. Gautier, M. Arndt, J. Lienard, "Efficient Wavelet Packet Modulation for Wireless Communication," *The Third Advanced International Conference on Telecommunications (AICT)*, pp. 19 - 24, 2007.

[13] B. G. Negash and H. Nikookar, "Wavelet-based multicarrier transmission over multipath wireless channels," *Electronics Letters*, vol. 36, no. 21, pp. 1787-1788, 2000.

[14] M. Gautier, C. Lereau, M. Arndt, J. Lienard, "PAPR analysis in wavelet packet modulation," *3rd International Symposium on Communications, Control and Signal Processing (ISCCSP)*, pp 799 – 803, 2008.

[15] L. Zbydniewski, T. Zielinski, "OFDM vs. Wavelet OFDM and Circular Wavelet-OFDM in high speed communication over power lines," *Signal Processing Algorithms, Architectures, Arrangements and Applications Conference Proceedings (SPA)*, pp. 76 – 81, 2009.

[16] A. K. Jain, Fundamentals of Digital Image Processing, *Prentice-Hall of*

India, New Delhi, 1995.

[17] C. S. Burrus, R. A. Gopinath and H. Guo, "Introduction to Wavelets and Wavelet Transforms-A Primer, *Prentice-Hall*, New Jersey, USA, 1998.

[18] U. Khan, S. Baig and M. J. Mughal, "Performance Comparison of Wavelet Packet Modulation and OFDM over Multipath Wireless Channel with Narrowband Interference," *International Journal of Electrical Engineering and Computer Sciences*, IJECS, Spet. 2009 vol.9, no.9, pp.431-434.

[19] V. Kumbasar, et al., "Optimization of wavelet based OFDM for multipath powerline channel by genetic algorithm", *Wireless Communications and Mobile Computing*, vol. 9, no. 9, pp. 1243-1250, 2009.

[20] G. Strang and T. Nguyen, Wavelets and filter banks, *Cambridge University Press*, 1996.

[21] M. K. Gupta, S. Shrivastava, A. S. Raghuvanshi, S. Tiwari, "Channel Estimation for Wavelet Based OFDM Systems," *International Conference on Devices and Communications (ICDeCom)*, pp. 1 - 4, 2011.

[22] F. Farrukh, S. Baig, M. J. Mughal, "Performance Comparison of DFT-OFDM and Wavelet-OFDM with Zero Forcing Equalizer for FIR Channel Equalization," *International Conference on Electrical Engineering (ICEE)*, pp 1 – 5, 2007.

[23] A. Jaminand P. Mahonen, "Wavelet packet modulation for wireless communications," *Wireless Communications and Mobile Computing*, vol. 5, no. 2, pp. 123-137, March 2005.

[24] T. Nawaz and S. Baig, "Wavelet OFDM- A solution for reliable communication in a frequency selective Rayleigh fading channel," *9th International Bhurban Conference on Applied Sciences and Technology (IBCAST)*, pp. 413 – 417, 2012.

[25] R. Asif, R. A. Abd-alhameed, O. O. Anoh, Y. A. S. Dama, "Performance Evaluation of DWT-OFDM and FFT-OFDM for Multicarrier Communications Systems using Time Domain Zero Forcing Equalization," *International Journal of Computer Applications*, vol. 51– no. 4, pp. 34-38, August 2012.

[26] J. Sadowsky, "Investigation of signal characteristics using the continuous wavelet transform," *Johns Hopkins applied technical digest*, vol. 17, no. 3, pp. 258-269, 1996.

[27] I. Daubechies, Ten lectures on wavelets, *Society for Industrial Mathematics*, vol. 61, 1992.

[28] N. M. Shafik, "Wavelet Transform Effect on MIMO-OFDM System Performance," *Cyber Journals: Multidisciplinary Journals in Science and Technology, Journal of Selected Areas in Telecommunications (JSAT)*, pp. 46 – 50, September Edition, 2011.

[29] D. Gesbert, et al., "From theory to practice: an overview of MIMO space-time coded wireless systems," *IEEE Journal on Selected Areas in Communications*, vol. 21, no. 2, pp. 281-302.

[30] S. L. Linfoot, M.K. Ibrahim, and M.M. Al-Akaidi, "Orthogonal wavelet division multiplex: an alternative to OFDM," *IEEE Transactions on Consumer Electronics*, vol. 53, no. 2, pp. 278-284, May 2007.

[31] M. Vetterli and C. Herley, "Wavelets and Filter Banks: Theory and Design," *IEEE Transaction on Signal Processing*, vol.40, no.9, pp.2207 – 2231, Sept. 1992,

[32] M. Weeks, Digital Signal Processing Using MATLAB and Wavelets, Second Edition, *Jones and Bartlett Publishers*, London, 2011.

[33] W. Sweldens, "The Lifting Scheme: A New Philosophy in Biorthogonal Wavelet Constructions," *Wavelet Applications in Signal and Image Processing III*, vol.2569, pp.68 – 79

[34] W. Sweldens, "The Lifting Scheme: A Custom-Design Construction of Biorthogonal Wavelets," *Applied and Computational Harmonic Analysis*, vol.3, no. 0015, pp.186 – 200, 1996.

[35] W. Sweldens, "The Lifting Scheme: A Construction of Second Generation Wavelets," *SIAM Journal on Mathematical Analysis*, vol. 29, no. 2, pp.511-546, 1997.

[36] D. Daly, C. Heneghan, A. Fagan and M. Vetterli, "Optimal Wavelet Packet Modulation under Finite Complexity Constraint," *IEEE International Conference on Acoustics, Speech, and Signal Processing (ICASSP)*, pp. III-2789 - III-2792, May 2002.

[37] S. Gracias, V. U. Reddy, "An equalization algorithm for wavelet packet based modulation schemes," *IEEE Transactions on Signal Processing*, vol. 46, no. 11, pp. 3082-3087, 1998.

[38] S. M. Alamouti, "A simple Transmit Diversity Technique for wireless communications," *IEEE Journal on Selected Areas in Communications*, vol. 16, no. 8, pp. 1451 – 1458, 1998.

International Journal of Computer Applications (0975 – 8887)
Volume 51– No.4, August 2012

Performance Evaluation of DWT-FDM and FFT-OFDM for Multicarrier Communications Systems using Time Domain Zero Forcing Equalization

R. Asif, R. A. Abd-Alhameed, O.O. Anoh and Y.A.S. Dama
School of Engineering, Design and Technology,
Bradford University,
Bradford, West Yorkshire, BD7 1DP, UK

ABSTRACT

Other than the conventional fast Fourier transform (FFT) for multicarrier modulation, a new approach for multicarrier modulation (MCM) has been known. Meanwhile, multicarrier modulation involves dividing the broadband channel into many orthogonal but overlapping narrowband carriers. In an OFDM modulation based multicarrier system using the FFT, a cyclic prefix (CP) is inserted after each symbol frame to combat the effects of inter symbol interference (ISI). By inserting the CP, which results in spectral inefficiency OFDM schemes trades up to 25% of the transmit bandwidth. A new MCM approach that is void of the expense is the wavelet transform-based systems. These systems also have very suppressed side-lobes and exhibit improved BER performance. In wavelet based systems, the latest challenge in its implementation is in the channel estimation. In this work we have studied the performance of the FFT based OFDM system against wavelet transform (WT) based multicarrier system using a simple zero forcing (ZF) equalization in time domain. The studied system shows some improved BER performance.

General Terms

Equalization, Algorithm, Performance

Keywords

Orthogonal Frequency Division Multiplexing (OFDM), Bit error ratio (BER), Wavelet Transform (WT), Multicarrier Modulation (MCM)

1. INTRODUCTION

There is an ever-growing need for the communication systems that can provide high data rates. Modulation schemes characterized by theses high data rate transmissions can in turn incur ISI which is usually caused by the channel delay spread and as a result, high performance equalizers are required. Solution to this problem involves using multicarrier modulations (MCM), which divides the high data rate serial streams into a number of parallel streams with low data rates [1]. The number of sub-channels is selected so as to increase the symbol time as compared to the channel delay spread, and also to reduce the sub-stream bandwidth size than the size of the channel coherence bandwidth so the ISI can be bearable [2]. An instance of such MCM is the OFDM which is an FFT-based multicarrier modulation (MCM) scheme. OFDM modulation is the main contender for the communication systems required for the next generation. This method of multiplexing is rather expanded by the large side-lobes intrinsic in the fixed rectangular shaped FFT-window. This scheme also required a cyclic prefix insertion in order to compensate for the inter-symbol interference (ISI) which wastes up to 25% of the scarce bandwidth [3, 4]. Also, the OFDM signals are characterized by high peak-to-average power ratio (PAPR) which drives the high power amplifiers to operate near the saturation limits.

Wavelet Transform based multicarrier modulation is seriously being investigated as an alternative to the conventional Fast Fourier Transform for use in OFDM systems due to the fact that they can provide all the same benefits as of the FFT-OFDM with an added benefit of PAPR combat and carrier frequency timing offset [5]. Unlike the conventional FFT-OFDM system wavelet scheme satisfies the condition for orthogonality and achieves perfect reconstruction (PR) using the orthogonal filters of the Quadrature mirror filter (QMF) banks [6]. Discrete wavelet transform has large power spectral density as compared to FFT-OFDM due to the fact that DWT produce well contained side lobes with the narrower side lobe having the contained energy with reduced out-of-band emissions. Since there is no CP, the equivalent copied noise during cyclic prefixing is saved so that the BER performance of the WT-based systems is improved. Besides all these benefits wavelets also use multi-resolution analysis of the signal in which by the applied basis functions, the signal is well localized both in time and frequency domain and their resolution [7]. This multi-resolution- time-frequency signal representation is achieved by some shifting (translation) and scaling. Digital signal processing has played a very vital role in the advancement of the communication systems. By the filtering scheme in wavelets studies, the multirate filter banks have been in use in many fields such as digital communications, image processing and digital signal processing [8]. If we use the wavelet filters that allow the decomposition of the studied signals into equal high band and low band components of equal filter length, like the db2, and with the frequency components scaled in time, a simple zero-forcing (ZF) can achieve a fair equalization wherein the channel state is known to the receiver.

The rest of this paper is divided as follows. Section II describes the implementation of the OFDM scheme, Section III covers wavelets as multicarrier modulation, simulation and results are presented in Section IV and Section V gives the conclusion.

2. OFDM MODULATION

2.1 OFDM Transmitter

Let us assume that we have an OFDM system that has N number of subcarriers. The subcarriers that will be used for transmission can be written as Nu + 1 which lie at the central

spectrum and the subcarriers at the edges will form the guard bands. The transmission subcarriers are then modulated using a data symbol $X_{a,n}$ where 'a' is the number of the OFDM symbol and 'n' stands for the subcarrier number. Inverse fast Fourier transform (IFFT) of size N is then applied. The subcarriers in the guard band are not utilized in order to keep the size of the transmit signal less than the bandwidth size of 1/T where T represents the sampling time of the OFDM signal. The addition of a guard band helps determine the best analog transmission filter to be employed in order to restrict the periodic spectrum at the output of the IFFT produced by the time signal (discrete). A guard interval also helps combat the inter symbol interference in a multipath fading channel environment. The resultant signal at the output of the transmitter can be mathematically written as [9]

$$s(t) = \sum_{a=-\infty}^{\infty} \sum_{n=-N_u/2}^{N_u/2} X_{a,n} \Psi_{a,n}(t) \otimes g_T(t) \qquad (1)$$

Where, $\otimes$ represents the convolution, impulse response of the analog filter used in the transmission is given by $g_T(t)$ and $\Psi_{a,n}(t)$ stands for the subcarrier pulse and is defined as [9]

$$\Psi_{a,n}(t) = \begin{cases} e^{j2\pi \frac{n}{T_u}(t-\Delta-aT_s)}, & aT_s \le t \le (a+1)T_s \\ 0 & otherwise \end{cases} \qquad (2)$$

The total time of the OFDM symbol including the guard band will be equal to $T_s = T_u + \Delta$, OFDM subcarrier spacing will be equal to $1/T_u$ and Δ is the length of the guard interval.

2.2 Multipath Rayleigh Channel

The signal was then transmitted over the Rayleigh fading channel which causes a change in phase, amplitude and the angle of arrival of the received signal and can be characterized by

$$h(t,\tau) = \sum_{r=1}^{R} a_r(t,\tau)\, e^{-j\theta_r} \delta\big(t - \tau_r(t)\big) \qquad (3)$$

where, $a_r(t,\tau)$, and τ_r represent the amplitude and the time delay respectively and $\theta_r = 2\pi f_c \tau_i(t)$ is the phase shift for the n^{th} multipath at a time t. R stands for the maximum number of multipath possible with $\delta(*)$ as the Dirac delta. Thus, a Rayleigh fading channel is modeled as a complex-valued Gaussian process with zero mean.

2.3 OFDM Receiver

At the receiver it is assumed that the guard interval is longer than the channel delay spread, with perfect synchronization, and then the n^{th} subcarrier output during the a^{th} OFDM symbol can be written as [11]

$$Y_{a,n} = X_{a,n}.H_{a,n}.G_T(n)G_R(n) + n_{a,n}, \quad -\frac{N_u}{2} \le n \le \frac{N_u}{2} \qquad (4)$$

Where, $n_{a,n}$ represents the additive white Gaussian noise, $G_T(n)$ stands for the frequency response of the analog transmission filter and $G_R(n)$ denotes the frequency response of the receiver filter at the nth subcarrier frequency $f_n = \frac{n}{T_u}$, channel response in the frequency domain is denoted as $H_{a,n}$ and can be mathematically explained as [11]

$$H_{a,n} = \sum_{r=1}^{R} h_n(aT_s).\, e^{-j2\pi \frac{nT_g}{NT}} \qquad (5)$$

The channels r^{th} path gain during the a^{th} number of the OFDM symbol is represented by $h_n(aT_s)$ in Equation (5). Now if we assume that our transmission subcarriers lie in the flat region of the analog filters both at the transmitter and the receiver then we can rewrite the Equation (4) as [11]

$$Y_{a,n} = X_{a,n}.H_{a,n} + n_{a,n} \qquad (6)$$

Which mean we have assumed $G_T(n)$ and $G_R(n)$ to be equal to one in their flat region. Another way to eliminate $G_T(n)$ and $G_R(n)$from Equation (4) will be to use the *a priori* knowledge of the transmitter and receiver filters. We have assumed Equation (6) to be correct for this study.

3. MULTICARRIER MODULATION WITH WAVELETS

3.1 Wavelets Background

Wavelet Transform (WT) is a mathematical function which can be used to decompose a continuous time signal at different scales and different times using the multi-resolution analysis [12].The continuous wavelet transform of a signal x(t) can be mathematically written as [12];

$$CWTx(\tau,a) = \langle x(t), \psi_{a,\tau} \rangle = \frac{1}{\sqrt{|a|}} \int_{-\infty}^{\infty} x(t) \psi^* \left(\frac{t-\tau}{a}\right) dt \qquad (7)$$

Where ' ψ ' represents the mother wavelet, parameter ' τ ' is the translation which corresponds to the time information present in the signal and 'a' is the scaling parameter which corresponds to the frequency information contained in the signal and '*' represents the complex conjugate, which will not be required if 'ψ' is assumed to be real [13].

When a mother wavelet is designed it is designed in such a way that it can be inverted to retrieve the original transmitted signal. For continuous wavelet transform there exist no viable inverse in practice due to the redundancy in the information which will require extensive analytical calculation, but in theory (only mathematically) the inverse for this transform can be written as [6]:

$$x(t) = \frac{1}{C_\psi} \int_a \int_\tau \frac{1}{a^2} x(a,\tau) \psi \left(\frac{t-\tau}{a}\right) d\tau da \qquad (8)$$

Now to circumvent the above mentioned data redundancy issue we discretize the scaling and in addition the translation variables. Now using the Equation (7) as a reference if we discretize the translation parameter ' τ ' by 2^k, and scaling parameter 'a' by 2^j, then we can rewrite Equation (7) as:

$$DWTx(j,k) = \langle x, \psi_{j,k} \rangle = 2^{\frac{-j}{2}} \sum_{n=-\infty}^{\infty} x(n) \psi(2^{-j} n - k) \qquad (9)$$

And thus the Equation (9) will be our discrete wavelet transform of signal x(t).This transform can also be referred to

as a form of sub-band coding because in order to analyze a signal it has to pass through a string of filter banks [14].

3.2 DWT scheme and Perfect Reconstruction

The process involved in implementing the wavelet based MCM is quite similar to that of the conventional FFT-OFDM as follows;

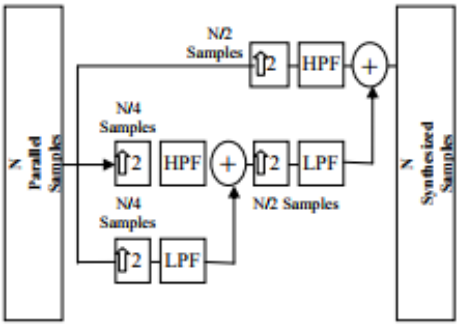

Figure 1: 2-Level Wavelet reconstruction (synthesis)

Wavelet transform based multicarrier modulated systems consist of perfect reconstruction quadrature mirror filter bank that employ half band low pass filter (LPF) whose impulse response can be written as 'h' and half band high pass filter (HPF) whose impulse response can be written as 'g' which convolve with the input signal $x[n]$. Two sequential parallel data streams are created in wavelet transform multiplexing at each scale and translation i.e. $x_{low}(n)$ and $x_{high}(n)$ as shown in Figure (1) which are then upsampled by a factor of 2 and passed through the LPF and HPF of QMF bank. The input signal to each filter convolves with the impulse response of the filter to yield $x_{low}[n] = h[n] * x[n]$ for the low pass filter, which gives us our approximate coefficient and $x_{high}[n] = g[n] * x[n]$ for the high pass filter which produces the detail coefficient at the filter output. Anti-imaging filter is required in order to filter out the image frequencies that are produced during the upsampling operation within each channel. These filtered streams are then summed and constitute a wavelet symbol. This just explained process emphasizes synthesis (inverse DWT-IDWT) process. This synthesized data is then passed through the channel in the presence of AWGN.

When the signal is received on the receiver side it is then again passed through the Quadrature mirror filter bank which consists of a pair of conjugate LPF h*(-n) and conjugate HPF g*(-n) on the receiver end. Two such pairs constitute a two-channel QMF bank as shown in Figure (2). The received signal is first decomposed into its respective detailed and approximate coefficients and then downsampled by a factor of 2 which is also apparent from the Figure (2). This process continues until the N parallel streams of data are recovered. The recovered data is then converted into a serial stream using a parallel to serial converter and then demodulated using a suitable scheme. In this study we have used BPSK and 16-QAM.

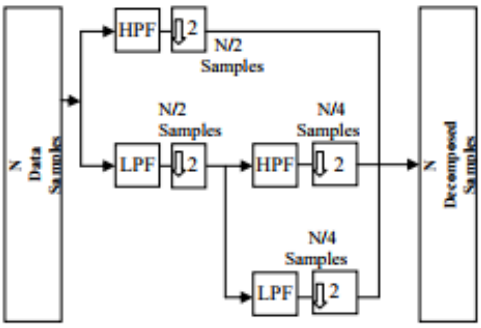

Figure 2: 2-Level Wavelet Decomposition (Analysis)

The HPF and LPF of the QMF bank can be expressed mathematically as:

$$h(n) = (-1)^n g(L + 1 - n) \quad (10)$$

Where, L describes the sequence of length of g (n).
Because of the shift and translation of the wavelet transformed signals, each of the composite symbols is rather delayed by a factor 'α' according to the z-transform relation ($X(z) = \sum_n x(n) z^{-\alpha}$, where $z^{-\alpha} = e^{-jaw}$) which requires adjacent matched filters to perfectly reconstruct the signals. This perfect reconstruction can only hold if the matched filters respect the following.

$$h(z)h^*(z) + g(z)g^*(z) = 2z^{-\alpha} \quad (11a)$$

$$h(z)h^*(-z) + g(z)g^*(-z) = 0 \quad (11b)$$

4. Zero Forcing Equalization Algorithm

One of the challenges faced when implementing a wavelet transform based multicarrier system is of the channel equalization. The use of zero-forcing channel equalization algorithm for wavelet transform based multicarrier systems using some finite response filters (FIR) was suggested in [15]. Meanwhile, ZF is adopted for channel equalization wherein the channel state is known to the receiver.

Table 1: Simulation Parameters for DWT and FFT in the presence of AWGN

	DWT	FFT
Modulation Scheme	BPSK, 16-QAM	BPSK, and 16-QAM
FFT size	Nil	64
Cyclic Prefix	Nil	1/4
DWT Family	Db2	Nil
Decompositio n Stages	K = log2(N), N = 2^6	Nil
Propagation Environment	AWGN	AWGN
Symbol Length	2^6×M, M = 10^4	2^6×M, M = 10^4

Without the ZF-with FIR approach, we can achieve a fair equalization in WT-transmissions since there are equal lengths of wavelet filters in both the receiver as of the transmitter for the wavelet family considered, db2. So, the zero forcing equalization algorithm is performed for WT and compared with that of the conventional FFT-OFDM over Rayleigh fading channel with some additive white Gaussian noise (AWGN).

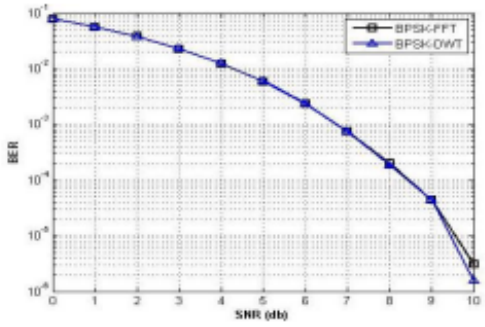

Figure 3: Performance comparison of DWT-OFDM and FFT-OFDM

The signal that reaches the receiver after the convolution with the channel and addition of noise can be mathematically written as $s_{rec} = hs + n$, where h is the channel impulse response and n is the AWGN. In zero forcing equalization we need to find the filter coefficients c[t] that can make $h[t] \otimes c[t] = \delta[t]$. By ZF, we proceed as follows;

$$\hat{y}_{ZF}[t] = c[t] \otimes y[t] \quad 12(a)$$

$$= c[t](s[t] \otimes h[t] + n) \quad 12(b)$$

$$= s[t] + c[t] \otimes n \quad 12(c)$$

This $c[t] \otimes n$ causes noise amplification in zero forcing channel equalization. The equalized signal was then further processed for onward bit error ratio (BER) estimation.

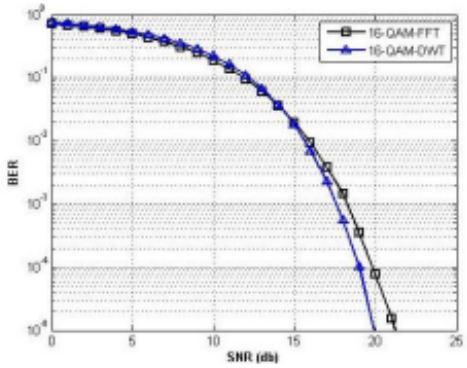

Figure 4: Performance comparison of DWT-OFDM and FFT-OFDM in AWGN using 16-QAM

5. Simulation And Results

In this section the results of the above mentioned system are discussed. Table 1 outlines the parameters that were used to carry out these simulations. The performance was studied using different modulation schemes in the presence of AWGN channel only as shown in Figures (3) and (4).

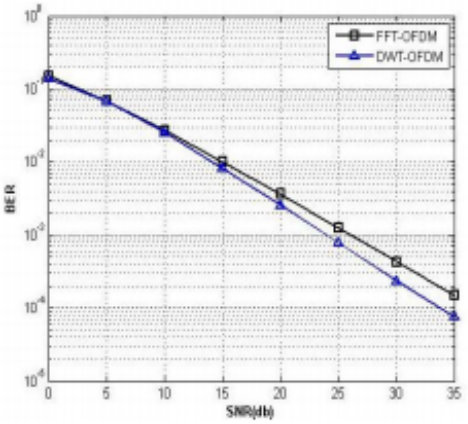

Figure 5: Performance comparison of DWT-OFDM and FFT-OFDM in Rayleigh Fading + AWGN using BPSK

It was noticed that the performance of the DWT was meritoriously marginal although with about 1db better at BER of 10^{-5} in the case of BPSK system in Figure (3) as compared to the conventional FFT-OFDM system. This performance can be better at some longer symbol length than the investigated. For higher data rate investigation, e.g. the 16-QAM in Figure (4), the performance advantage of the DWT-scheme becomes more pronounced with up to 2dB gain at 10^{-4} BER in favor of the DWT modulation. The performance merit can be explained on the premise of cyclic prefixing required in the FFT-OFDM which is not required in the DWT-OFDM modulations since by copying 25 percent of each of the transmit symbol length, proportionate amount of noise is also copied. This would lower the likelihood of decoding the transmitted bits correctly.

Over the multipath, more disorientation are imposed on the transmit signal by the impulse response of the channel. But the signals processed by the DWT scheme posses some sturdy flexibility in time and frequency coupled the filtering mechanisms used in the wavelet. The filters of the wavelet used (db2) decompose the signal into equal lengths of low-band and high-band and reconstructs them likewise. Since the channel state is known to the receiver, the effect of the channel can be removed with some bearable error introduced by the system noise. Comparing the performance of the DWT-OFDM and FFT-OFDM in Figure (5), the results obtained from the simulation using discussed time domain equalization shows an improved BER performance and a gain of up to 3db at BER close to 10^{-4} in favor of DWT modulation when propagated through a multipath channel environment in the presence of AWGN using BPSK.

6. CONCLUSION

In this study we implemented a wavelet transform based multicarrier system which comprised of perfect reconstruction Quadrature mirror filter banks and compared its performance against the conventional Fast Fourier transform based multicarrier system in the Rayleigh multipath fading environment with additive white Gaussian noise using zero forcing channel equalization algorithm which was implemented in time domain just before the DWT process. Results obtained showed slightly better BER performance in favor of the wavelet transform modulation. As no cyclic prefix or guard band was inserted spectral efficiency was improved in DWT as compared to the conventional FFT-OFDM system where in order to counter the degrading effects of ISI cyclic prefixing is required. Consequently, further multicarrier modulation studies can be possible using the DWT-OFDM.

7. REFERENCES

[1] J. A. C. Bingham, "*Multicarrier modulation for data transmission: An Idea Whose Time Has Come*", IEEE Communications Magazine, vol. 28, no.5, pp. 5-14, 1990.

[2] Andrea Goldsmith, *Wireless Communications*, Cambridge University Press, (2005).

[3] G. Li and G.L. Stuber, *Orthogonal frequency division multiplexing for wireless communications*, Springer, 2006.

[4] Van De Beek, et al, *Orthogonal frequency division multiplexing (OFDM)*, Review of Radio Science 1996-99, Intern. Union of Radio Science (URSI), 1999.

[5] V. Kumbasar and O. Kucur, "Better wavelet packet tree structures for PAPR reduction in WOFDM systems," *Digital Signal Processing*, 2008, Vol. 18, No. 6, pp. 885-891.

[6] V. Kumbasar, et al., "Optimization of wavelet based OFDM for multipath powerline channel by genetic algorithm," *Wireless Communications and Mobile Computing*, 2009, Vol. 9, No. 9, pp. 1243-1250.

[7] Michael Weeks, *Digital Signal Processing Using MATLAB and Wavelets*, Georgia State University, 2007.

[8] Khan, U., Baig, S.: and Mughal, J. *Performance Comparison of Wavelet Packet Modulation and OFDM for Multipath Wireless Channel with Narrowband Interference*, 2nd International Conference on Computer, Control and Communication, pp1-4, (2009)

[9] Baoguo Yang; Letaief, K.B.; Cheng, R.S.; Zhigang Cao, *Channel estimation for OFDM transmission in multipath fading channels based on parametric channel modeling*, IEEE Transactions on Communications, Vol. 49, No. 3, 2001, pp. 467- 479.

[10] T.S. Rappaport, *Wireless communications: principles and practice*.Vol. 2, 1996: Prentice Hall PTR Upper Saddle River (New Jersey).

[11] Ye Li, G.L. Stuber, *Orthogonal Frequency Division Multiplexing*, Springer science + business media inc., 2006.

[12] N. Akansu and Richard A. Haddad, *Multiresolution Signal Decomposition Transforms, Subbands, and Wavelets*, Academic Press,(2001).

[13] I. Daubechies, *Ten lectures on wavelets*, Society for Industrial Mathematics, Vol. 61, 1992.

[14] M. K. Lakshmanan, and H. Nikookar, *A Review of Wavelets for Digital Wireless Communication*, Wireless Personal Communications, Vol.37, (2006), pp. 387-420.

[15] F. Farrukh, S. Baig, Mughal, M.J., "Performance comparison of DFT-OFDM and wavelet-OFDM with zero-Forcing equalizer For FIR Channel Equalization," *International Conference on Electrical Engineering (ICEE)*,2007,pp.1–5.

Performance evaluation of ZF and MMSE Equalizers for Wavelets V-Blast

R. Asif[1], M. S. BinMilha[1], A.S Hussaini[2,3], Raed A. Abd-Alhameed[1], S.M.R. Jones[1], J.M. Noras[1], J. Rodriguez[2]
[1]Mobile and Satellite Communications Research Centre, University of Bradford UK, BD7 1DP
{r.asif, r.a.a.abd}@bradford.ac.uk
[2]Instituto de Telecomunicacoes – Aveiro, Portugal
{ash, jonathan@av.it.pt}
[3]Department of Electrical & Electronics Engineering Modibbo Adama University of Technology, Yola Nigeria

Abstract- **In this work we present the work on the equalization algorithms to be used in future orthogonally multiplexed wavelets based multi signaling communication systems. The performance of ZF and MMSE algorithms has been analyzed using SISO and MIMO communication models. The transmitted electromagnetic waves were subjected through Rayleigh multipath fading channel with AWGN. The results showed that the performance of both of the above mentioned algorithms is the same in SISO channel but in MIMO environment MMSE has better performance.**

Keywords- Wavelets, DWT, MIMO, Zero-Forcing, Minimum Mean Squared Error, V-Blast.

I. INTRODUCTION

In the context of NGWS world is expecting a lot of changes after the failure of 3G systems due to their poor performance and high deployment cost out of which some physical layer weaknesses are still expected to be present within the 4G networks. It is predicted that the 5G service will open a new world of opportunities for the users, with high data rates and VOIP enabled phones [1]. With such high expectations industry giants are looking for the best available systems that can optimally use the resources some of which are scarce like frequency spectrum. In order to combat the ISI caused by the channel delay spread in a high data rate transmission system multicarrier systems have played a vital role. These multicarrier systems divide the high data rate serial stream into a larger number of parallel streams with low data rate [2]. As a result increasing the on air time of the symbol but reducing the bandwidth size of the sub stream in comparison to the channel coherence bandwidth by choosing the right number of sub-channels which in turn helps avoid ISI. Both multicarrier systems like orthogonal frequency division multiplexing and MIMO antenna techniques have earned their reputation to provide high spectral efficiency[3, 4]. OFDM systems provides for a way to transmit processed signals from the same source at different frequencies but at the cost of bandwidth wastage due to guard bands [4] and high PAPR [5]. The main success of OFDM systems is due to the fact that they provide robust transmission against multipath environment by making using of the cyclic prefix but at the cost of bandwidth [6].

Wavelet based transmission scheme has been proposed for the next generation wireless systems by the authors in [6, 7]. It has also been shown that the wavelets can provide all the same performance advantages as of the OFDM systems and does not require the addition of the cyclic prefix and has improved PAPR and BER performance.

978-1-4799-3525-3/13/$31.00 ©2013 IEEE

The advantage of wavelet based multicarrier modulation technique is that all the benefits of conventional OFDM system can be achieved with some additional benefits namely improved PAPR and BER [8, 9], and also carrier frequency timing offset. Wavelet transforms spreads the ISI over different wavelet symbols thus reducing it to a negligible error which can be easily corrected at the receiver. Another advantage of wavelet transform is that the side lobes are greatly reduced as the main energy is contained in the main lobe thus in turn reducing the error probability that one bit will be decoded as another. The basis sets of wavelets has increased time – frequency partitioning resulting in an improved SNR performance [10]. This transform satisfies the condition of orthogonality by employing a perfect reconstruction Quadrature mirror filter bank which allows for the decomposition of the signal into its constituent approximate and detailed parts and the reconstruction of the signal. This perfect reconstruction is achieved using conjugate filters on the transmitter end.

The goal of this work is to study and evaluate the performance of most critical component within the receiver i.e. the channel equalizer in order to optimize the performance of proposed wavelet based multicarrier system. ZF and MMSE techniques work in the time domain on de-convolution of wavelet symbols in channel impulse response estimation, as channel estimation in wavelet transform is challenging due to the linear convolution between the channel and the wavelet symbols which results in severe inter symbol interference.

No previous published work has signified the importance of this important factor of irreducible inter symbol interference between symbols. We have used two different equalization techniques to show how this affects the wavelet based multicarrier system in terms of equalization. MMSE equalization algorithm in the conventional OFDM systems is well known for its better performance as compared to the ZF algorithm, but in this simulation we will show that even though MMSE starts of better at low SNR's but as the SNR is increased the performance of MMSE algorithm decreases so as to a point where it matches the ZF for the SISO environments but when the MIMO environment is employed MMSE again starts to show better performance confirming the theory that the ISI is evenly distributed among wavelet symbols.

This paper has been divided as follows; Basics of wavelet transform have been described in Section II, followed by the DWT baseband architecture in Section III, Channel

equalizations methods in Section IV, Simulation results in section V followed by the conclusion in Section VI.

II. WAVELET TRANSFORM BASICS

Wavelets are a mathematical tool for the multiresolution study of a signal x[n] i.e. the signal can be analysed at different resolutions through the process of shifting and scaling by decomposing the signal into its constituent approximate $G_{L,n}$ and detailed $H_{m,n}$ coefficients at each shift and scale. This is achieved by using embedded vector spaces.

$$\cdots \subset V_3 \subset V_2 \subset V_1 \subset V_0 \subset V_{-1} \subset \cdots \quad (1)$$

Let us consider a signal within a vector space V_T and within this vector space lays other spaces which we can identify as V_{T-i} i.e. the decomposed part of the signal space. This means that the space constitutes of multiply resolved components of the total vector space V_T as shown in Figure 1.

Using a dilation equation we can mathematically write $V_{T-i} = \varphi(t)$, and $\varphi(t)$ is defined as [11];

$$\varphi(t) = \sqrt{2}\sum_n g(n)\varphi(2t-n) \quad (2)$$

After establishing that the total vector space occupied by the original signal is now divided. Equation (2) will provide the low frequency information using a half-band low-pass filter g(n), the length of the original signal is also halved as implied by the dilation factor 2 used in Equation (2). Now repeating the same idea of multiple vector space resolution using a half-band high-pass filter g(n), the high frequency information can be retrieved and mathematically described as in Equation (3);

$$\psi(t) = \sqrt{2}\sum_n h(n)\psi(2t-n) \quad (3)$$

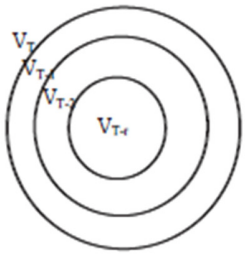

Figure 1: Multiply Resolved Vector Spaces

Equations (2) and (3) can be resolved determine the basis functions.

If the impulse response of one of the filters is known the coefficients required for the other filter can be easily calculated by using the relationship

$$h(n) = (-1)^n g(L-n+1),$$

Where, L stands for the filter length and n is the filter coefficient. Mathematically the continuous wavelet transform of a signal x[n] over the vector space T can be given as;

$$X_{CWT}(\alpha,\tau) = \int_T x(n)\psi_{\alpha,\tau}(t)dt \quad (4)$$

Where, α represents the scale and τ represents the shift. The transform in its continuous form contains redundant information and requires a lot of analytical calculations and also no viable inverse exist in practice so it is discretized and can be written as [6]

$$\psi_{m,n} = 2^{-\frac{m}{2}}\psi(2^{-m}t-n)$$

Where, m is the scale and n is the shift. The discretized signal consisting of its constituent approximation and detail can be described as;

$$x(t) = \sum_{n=-\infty}^{\infty} G_{L,n}2^{-\frac{L}{2}}\varphi(2^{-L}t-n) + \sum_{m=1}^{L}\sum_{n=-\infty}^{\infty} H_{m,n}2^{-\frac{m}{2}}\psi(2^{-m}t-n) \quad (5)$$

Due to the implementation of the strings of filter banks required to perform this transform it is also referred to as sub-band coding.

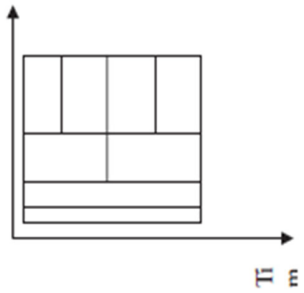

Figure 2: DWT Tiling on T-F plane

III. THE DWT BASEBAND ARCHITECTURE

Once the transform is discretized the DWT can be employed to decompose the signal into an approximation $G_{L,n}$ and detail $H_{m,n}$ for every shift and scale to analyse at different resolutions and at different frequency bands so in order to process the signal's useful information and drop out the rest. The point to note here is that when the DWT is employed we only de-compose the $G_{L,n}$ or the approximate information part which will mean that the second part of Equation (5) is absent and that there will be M = log2(K) + 2 number of total sub-

channels which can be used for signal multiplexing, K represents the total number of decomposition levels and M will be the resultant sub-channels in each level.

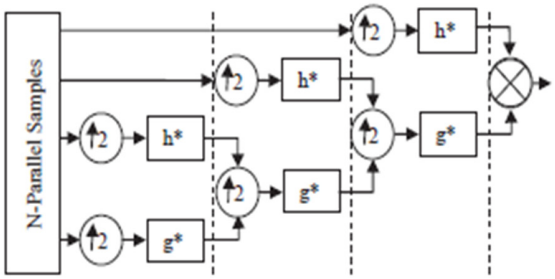

Figure 3: 3-Level Inverse Discrete Wavelet Transform

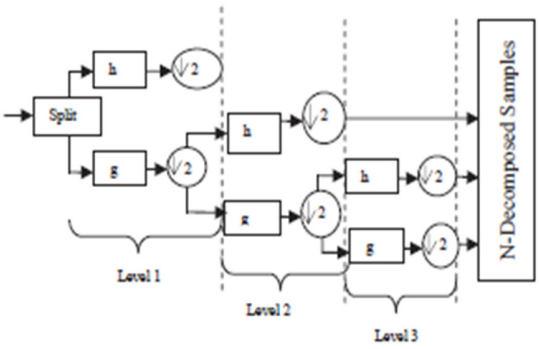

Figure 4: 3-Level Discrete Wavelet Transform

IV. CHANNEL EQUALIZATION METHOD

Channel estimation in wavelets is a tricky subject Authors in [9] said that if the coefficients that are used for channel equalization are of noisy wavelet signals rather than the original transmitted signal they can lead to large estimation errors due to the longer wavelet filter sequences required. Another challenge when working with wavelets is that the transmitted signals when in the time domain linearly convolve with the channel, so that they give rise to the ISI. Thus it is necessary to keep in mind when modeling the channel that the received signal at the receiver end will not only be corrupted due to the addition of AWGN but also by the ISI. In this work we presented the performance comparison between the MMSE and ZF equalization techniques using time domain equalization of DWT coefficients of the original signal that have been corrupted with noise as well as by ISI. In our simulation we have designed a frequency selective multipath channel and corrupted it with noise and ISI. The type of transform is the DWT employing orthogonal Daubechies8 wavelet family filters, and the receiver is only capable of demodulating BPSK symbols.

V. SIMULATION RESULTS

All the results have been produced using the Monte Carlo simulations. Simulation parameters are summarized in Table I and Table II.

TABLE I
Modulation Parameter

	DWT
Modulation	BPSK
Symbol length	2^6 * 10^4
Channel	Rayleigh Multipath Fading
Noise	AWGN
Decomposition Levels	Log2(n), n = 64;
Number of Elements	1Tx – 1Rx

From the results obtained in Figure 5 it can be seen that how both the equalization schemes show the same performance. In zero forcing even though the channel is considered to be known perfectly but still ZF algorithm has a disadvantage of addition of noise term, in OFDM systems MMSE has shown to perform better because there is CP in those systems which reduces the ISI but when the wavelet transform spreads that ISI over a range of wavelet symbols MMSE fail to perform better. Just to establish the fact, it has been proved in [6] that wavelet transform has better performance regardless of the equalization algorithm in comparison to the conventional FFT-OFDM.

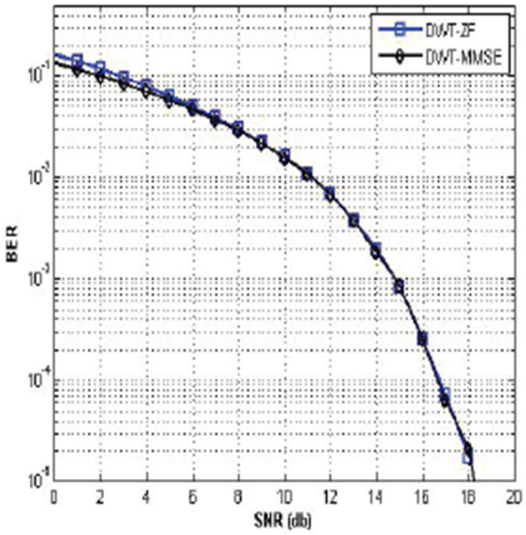

Figure 5: Comparison of ZF and MMSE

TABLE I
Modulation Parameter

	DWT
Modulation	BPSK
Symbol length	2^6 * 10^4
Channel	Rayleigh Multipath Fading
Noise	AWGN
Decomposition Levels	Log2(n), n = 64;
Number of Elements	1Tx – 1Rx

The above stated results led us to perform the same experiment using MIMO V-Blast and the results shown in Figure 6 confirmed the theory that indeed the ISI caused by the linear convolution between the wavelet symbols and the channel impulse response is being distributed evenly over all the symbols and when extra elements were added and antenna gain was achieved which started to suppress the negative effects caused by the ISI distribution MMSE started to show improved performance.

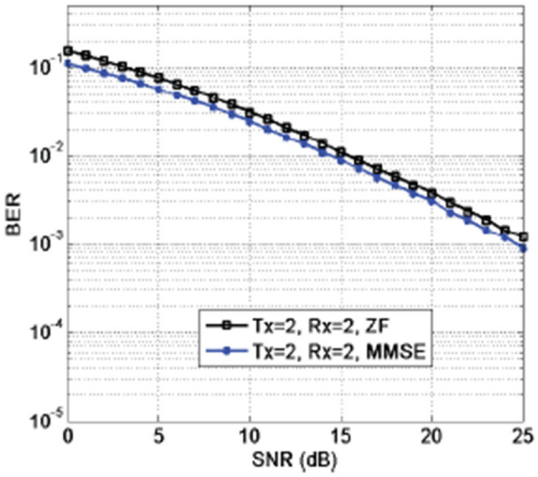

Figure 6: Comparison of ZF and MMSE using MIMO V-Blast

VI. CONCLUSION

From the results obtained through the Monte Carlo simulations it was concluded that the wavelet based multicarrier systems are indeed a better choice for the next generation wireless systems as they are more spectrally efficient, they can combat the degrading effects of the multipath channel without the insertion of the CP. Another important conclusion is that if the channel measurements are made carefully both ZF and MMSE channel equalization methods provide almost the same performance in SISO systems due to the fact that how wavelets transform mitigates the effects of ISI.

Acknowledgment

This work has been performed in the framework of ARTEMOS project under work programme ENIAC JU 2010 and FCT (Fundação para a Ciência e Tecnologia and Department of Electrical & Electronics Engineering Modibbo Adama University of Technology, Yola Nigeria.

REFERENCES

1. Patil, S., V. Patil, and P. Bhat, A Review on 5G Technology.
2. Bingham, J.A., Multicarrier modulation for data transmission: An idea whose time has come. Communications Magazine, IEEE, 1990. **28**(5): p. 5-14.
3. Sharma, P., Evolution of Mobile Wireless Communication Networks-1G to 5G as well as Future Prospective of Next Generation Communication Network. 2013.
4. Abdullah, K. and Z.M. Hussain. Performance of fourier-based and wavelet-based OFDM for DVB-T systems. in Telecommunication Networks and Applications Conference, 2007. ATNAC 2007. Australasian. 2007. IEEE.
5. Li, C.-P., S.-H. Wang, and C.-L. Wang, Novel low-complexity SLM schemes for PAPR reduction in OFDM systems. Signal Processing, IEEE Transactions on, 2010. **58**(5): p. 2916-2921.
6. Asif, R., et al., ``Performance Evaluation of DWT-FDM and FFT-OFDM for Multicarrier Communications Systems using Time Domain Zero Forcing Equalization,". Proc International Journal of Computer Applications (0975–8887) Volume, 2012.
7. Asif, R., et al., MIMO Discrete Wavelet Transform for the Next Generation Wireless Systems.
8. Abdullah, K., A.Z. Sadik, and Z.M. Hussain. On the DWT- and WPT-OFDM versus FFT-OFDM. in GCC Conference & Exhibition, 2009 5th IEEE. 2009. IEEE.
9. Asif, R., et al. Performance comparison between DWT-OFDM and FFT-OFDM using time domain zero forcing equalization. in Telecommunications and Multimedia (TEMU), 2012 International Conference on. 2012. IEEE.
10. Baig, S. and M. Mughal. Performance comparison of DFT, discrete wavelet packet and wavelet transforms, in an OFDM transceiver for multipath fading channel. in 9th International Multitopic Conference, IEEE INMIC 2005. 2005. IEEE.
11. Strang, G., Wavelets and filter banks1996: Wellesley Cambridge Press.

Multi-Antenna OFDM System Using Coded Wavelet and Weighted Beamforming

Kelvin O. O. ANOH[1], Rameez ASIF[1], Raed A. Abd-ALHAMEED[1], Jonathan RODRIGUEZ[1,2], James M. NORAS[1], Steve M. R. JONES[1], Abubakar S. HUSSAINI[2]

[1] Mobile and Satellite Communications Research Centre, University of Bradford, Bradford, United Kingdom
[2]Instituto de Telecomunicacoes, Aveiro, Portugal

r.a.a.abd@bradford.ac.uk

Abstract. *A major drawback in deploying beamforming scheme in orthogonal frequency division multiplexing (OFDM) is to obtain the optimal weights that are associated with information beams. Two beam weighting methods, namely co-phasing and singular vector decomposition (SVD), are considered to maximize the signal beams for such beamforming scheme. Initially the system performance with and without interleaving is investigated using coded fast Fourier transform (FFT)-OFDM and wavelet-based OFDM. The two beamforming schemes are applied to the wavelet-based OFDM as confirmed to perform better than the FFT-OFDM. It is found that the beam-weight by SVD improves the performance of the system by about 2 dB at the expense of the co-phasing method. The capacity performances of the weighting methods are also compared and discussed.*

Keywords

Beamforming, steering, MIMO, wavelet, OFDM, ISI, FFT, LTE, beam-weight.

1. Introduction

The wavelet transform (WT) has been introduced in the design of multicarrier communications systems in quite similar way to the well-known OFDM systems using the FFT [1-3], in which the FFT divides the selected wide-bandwidth into many narrow-bands and then provides many subcarriers for multiplexing input symbols. Meanwhile, WT contributes well suppressed side-lobes with low inter-symbol interference (ISI) and inter-carrier interference (ICI) index than there are in FFT-OFDM [1-4]. WT is also a windowed transform [5] with improved BER performance and can operate without a cyclic prefix (CP).

OFDM symbols can be coded, for instance using convolutional coding, against channel impairments with interleaving [6]. This provides the symbols with improved BER statistics at the expense of effective information rate since redundant bits are required. When decoded, the Viterbi algorithm [7] is used in the receiver with, either early signal quantization (hard-decision) or later quantization (soft-decision). While convolutional coding dominates multicarrier signaling in noisy channels, interleaving is remarked over impulsive distortions due to time variation of the channel response.

Hereafter consider the channel using co-phasing method [8], the degree of correlation of one multipath channel to another is increased thereby reducing the level of impulsive fading experienced by the transmitted symbols. This scheme is usually discussed as beamforming, for which the transmitted symbols may be weighted. It has been shown in [8] that, by harnessing the eigenvectors from the SVD of the channel as beam-weights, the system performance can be improved. It follows that, instead of co-phasing the transmit beams whose weights could represent the power with a number of transmitted antennas; each signal beam might be steered by some respective weight vector from the SVD to maximize the beam over some propagation media. Then, using WT-OFDM, one can observe this can do better than the FFT-OFDM when it is coded. Hence, different beamforming weights in a multi-antenna transmission are compared to establish the best operational performance.

The code structure used is described in Section 2 while the OFDM for different kernels are discussed in Sections 3 and 4. In Section 5, the beamforming scheme is described and simulation results are shown and discussed in Section 6 and then followed by summarized conclusions.

2. Convolutional Coding

The convolutional code structure discussed is similar to the INMARSAT standard-C earlier reported in [6]. It has ½ code rate and two polynomial generators G1 and G2 each defined by 1011011 and 1111001 (in binary form) respectively as in Fig. 1.

Like the name implied, there exist a convolution between the impulse response of the polynomial generator, G_n, $n = 1,2$, and the input bit. Hence, for d_i input bits occupying the prevailing memory register, then the output of the convolution of the i^{th} bit with k^{th} impulse response of the G_n^k polynomial generator (as shown in Fig. 1) becomes;

$$C_i = \sum_{i=0}^{L-1} d_i * G_n^k, \quad \forall \quad n = 1, \ 2 \tag{1}$$

where '*' is the convolution operator, n represents the index of the polynomial generator and C_i represents the output coded bit. The resulted coded bits are mapped using QPSK or BPSK, for example, before OFDM modulation.

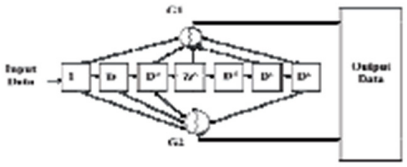

Fig. 1. Convolutional encoder.

3. Orthogonal Frequency Division Multiplexing

WT used in multicarrier signaling follows from the traditional OFDM systems which are designed using the FFT. Wavelets provide as many narrow-bands as the FFT. So, a WT-OFDM system divides a wide bandwidth into many smaller narrow-bands. If there are N-wavelet points, there will be N-narrow-bands. Meanwhile, an N-point FFT-OFDM system sampled at $t = nT$ can be represented as:

$$s[n] = \frac{1}{\sqrt{N}} \sum_{k=0}^{N-1} S_k e^{-j2\pi nk/N}, n = -N_g, \cdots, -1, 0, 1, \ldots, N-1 \tag{2}$$

where $\sqrt{N}$ is a scaling factor with N as number of the sub-channels, T is the signal period, N_g is length of the CP and n is the index of the prevailing subcarrier. S_k represents the complex PSK or QAM modulated input symbols. The sub-channels are spaced equally from another by $\Delta f = 1/T$ such that $N\Delta f = N/T$. So, the individual available narrow-band sub-channel is modulated by the input bits, say, using QPSK.

4. Wavelet-OFDM

In WT, the multicarrier process can be expressed to contain the basis function of the scaling function as [9]:

$$x[n] = \sum_{k} \sum_{m=0}^{M-1} X_{k,n} \varphi_{m,n}(t) \tag{3}$$

where $X_{k,n}$ represents the n^{th} symbol that modulates m^{th}-waveform of the k^{th}-constellation. $\varphi_{m,n}(t)$ is the complex orthogonal basis function like in the traditional OFDM:

$$\varphi_{m,n} = \begin{cases} 1 & n = m \\ 0 & elsewhere \end{cases} \tag{4}$$

where m and n are scales and shifts respectively.

5. Information Beamforming

The beamforming technique was applied to achieve improved diversity gain instead of capacity gain [10] and in addition simplify the system implementation than other MIMO techniques. The beamforming requires that the received signal must be highly correlated and as such the antenna separation must be as close as possible [11]. In outdoor environments, the beamforming technique achieves better performance than in an indoor environment because the beamforming technique depends on the angle of arrival (AoA) spread of the received signal [12]. Consequently, the spatial correlation between the received symbols is high since the angular spread of an outdoor environment is lower than the angular spread of the received symbols in an indoor environment due to the degree effects of multipath.

5.1 Maximizing the Signal Beams (Weight Computation)

The beams of the input signal are usually weighted in beamforming scheme subject to specified constraint as example the power level. In the receiver, a maximum ratio combining (MRC) is applied. With MRC, these weights (w) have been discussed early by [13]; for which if w maximizes λ such that the probability of error is minimum [14], then the SNR due to MRC becomes;

$$SNR_{MRC} = \frac{\left(\sum_{i=0}^{k-1} |h_i|^2\right)\lambda}{\sigma_z^2} = \frac{\sum_{i=0}^{k-1} \alpha_i \lambda}{\sigma_z^2}. \tag{5}$$

Consequently, if the average SNR of a SISO system is defined by $SNR_{SISO} = |h_1|^2\lambda/\sigma_z^2$, then the diversity order of a MIMO system with k antennas by beamforming scheme gives:

$$SNR_{MRC} = \left(k|h_i|^2 \lambda\right)/\sigma_z^2 = k.SNR_{SISO} \tag{6}$$

Since there are usually one-power amplifier per antenna, then each antenna is power constrained such that the weight must not be greater than a threshold, say λ_T, as

$$|w_i|^2 \le \lambda_T, \quad \forall i = 0, 1, \cdots, k-1. \tag{7}$$

In most cases, λ_T is set as unity [14] for short-term power constraint or different for each branch for long-term power constraint [10].

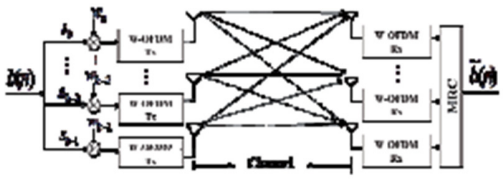

Fig. 2. MIMO-wavelet-OFDM with beamforming

Examples of these weights in MRC can be determined by eigen-filter approach and they could be the same irrespective of the signal branch correlation [15] or equivalently, the complex-valued (conjugate) channel gains [13], [16]. In this case, the optimal transmit beamforming weights can be obtained as;

$$w_i = \sqrt{\lambda_T / k} \cdot e^{-j\theta_i}, \quad \forall i = 0,1,\cdots,k-1 \tag{8}$$

λ_T can be set to 1 [13]. Equation 8 can be written as;

$$w_i = conj(\beta_i e^{-j\theta_i}), \quad \forall i = 0,1,\cdots,k-1 \tag{9}$$

where $\beta_i = \sqrt{\lambda_T / k}$ in (8). Fig. 2 is typical of an OFDM system with beamforming. The input symbols, at each antenna branch, are weighted by $W = [w_1 \quad w_2 \quad \cdots \quad w_k]^T$. $w_i \in C^{N_T \times N_T}, \forall i = 1,2,\cdots,N_T$ where $C^{N_T \times N_T}$ is a complex vector of $N_T \times N_T$ dimension, k is the maximum number of transmit antennas and $[.]^T$ is a transposition operation.

5.2 Weight Computation using SVD

The method for computing the weights for systems with beamforming whose channel state information (CSI) is known to the transmitter is shown in Fig. 3 [7].

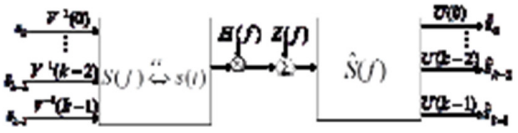

Fig. 3. Basic representation of beamforming weights and channel.

The beam-weights can be obtained from SVD property by letting the channel discussed from the SVD as [7];

$$H = U \zeta V^* . \tag{10}$$

U and V are eigenvectors of dimensions $N_T \times N_T$ and are $C^{N_T \times N_T}$. ζ is the diagonal containing eigenvalues. As shown in Fig. 3, the vectors that are characteristically given by $C^{N_T \times N_T}$, are used to weight the beam of each antenna branch.

5.3 Beamforming by Co-Phasing

Consider a multipath channel of the Rayleigh model with complex envelope as:

$$H = \sqrt{a^2 + b^2} \cdot e^{j\theta} \tag{11}$$

where a and b are *i.i.d* Gaussian variables from $h = a + jb$ and $\theta = \tan^{-1}(b/a)$. The signal beams can then be co-phased in the following way; if the transmit branches have signals with phases θ_i in $x_i = S \cdot e^{-j\theta_i}, \quad \forall i = 1,2,\cdots,k$ where k is the maximum number of antenna elements, then the received symbols from different branches combine at the receiver can be given by:

$$X = [h_1 \quad h_2 \quad h_3] \begin{bmatrix} x_1 \\ x_2 \\ x_3 \end{bmatrix} + Z \tag{12}$$

where Z is the circular symmetry noise term with zero mean and unity variance. The weight factor in this case can be obtained from (10) as $\sqrt{\lambda_T / k}$. Thus, the beams are weighted respective to the number of transmitted elements. In this study, only 3 transmit branches are considered.

6. Simulation Results and Discussion

A typical multi-antenna scenario is presented for up to three transmit antennas. Input symbols are randomly generated and coded using the convolutional encoding structure described in Section 2 and then interleaved using a matrix interleaver. Its trace-back length is 32 to reduce computation time. There are 128 input symbols randomly generated and averaged 10^4 times, mapped using the BPSK and QPSK. In the first case, OFDM was constructed using the FFT and then the wavelet transforms. The DWT and WPT are also investigated. Over each transmission branch for CSI condition, the OFDM is performed and the signals convolved with the channel.

6.1 Coded Wavelet and OFDM Systems

The results for coded and uncoded OFDM systems constructed with three different kerneles, corresponding to single-input single-output system are shown in Fig. 4.

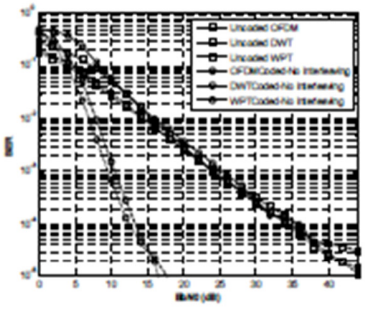

Fig. 4. Coded and uncoded wavelet with traditional OFDM compared.

In [6], it has been shown that the wavelet-based OFDM outperform the FFT-based OFDM. In WT the impulsive distortion effects of the multipath environment can be minimized.

The summarized results shown in Figs. 4 and 5, suggest the use of coded WPT rather than coded DWT or

COFDM in terms of BER performance as a proof of concept. Therefore, it is recommended to adopt the coded WPT for the SVD and Co-Phasing beamforming schemes.

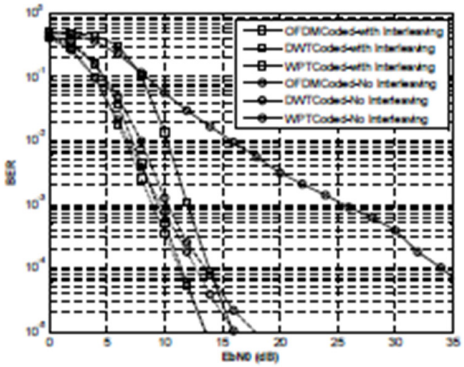

Fig. 5. Comparison of coded and uncoded wavelet with OFDM.

6.2 Beamforming with SVD and Co-Phasing for Uncoded Wavelet-OFDM

The co-phasing beam-steering technique is compared with the method for WPT multi-antenna system (3×1) using BPSK and QPSK in terms of BER and Capacity. Recall that the co-phasing is weighted as discussed in Section 5.3. "*BeamSteer*" is used for SVD and "*cof*" for traditional co-phasing in Figs. 6 and 7.

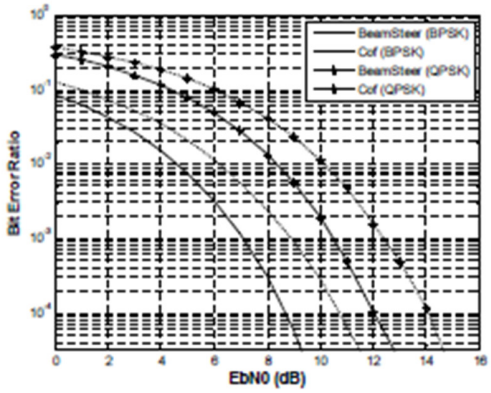

Fig. 6. Comparison of information weighted beam-steering and information beam co-phasing for uncoded WPT OFDM systems (3x1).

The co-phasing method improves the degree of correlation among the sub-channels in which the fading is reduced. However, the fading cannot be similar for all cases and using the steering weight improves the concentration of each received beam for every transmit branch. For BPSK and QPSK systems shown in Fig. 6, the SVD-based weights contribute about 2 dB gain for an uncoded WPT-OFDM system.

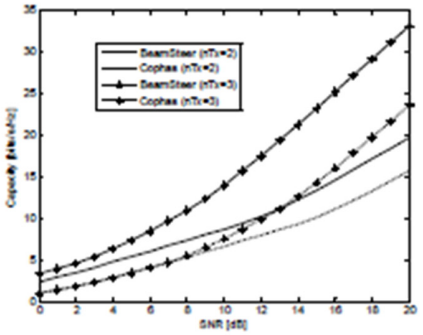

Fig. 7. Capacity performances for SVD weighted beamforming and co-phasing for uncoded WPT-OFDM systems (BPSK).

From the performance metrics of Figs. 6 and 7, the technology can be further extended for coded wavelet-OFDM for any mapping scheme. It can be conjectured based on the performances shown that coding will extend the performance of wavelet-beam weighted OFDM systems using SVD approach at the expense of the traditional co-phased. It is needless, therefore, to emphasize the case of the traditional OFDM. The side-effect in beamforming technology is the computation index since a full block of information is transmitted over different antenna spaces unlike in space-time block coding (STBC) wherein the information is coded in smaller number of bits (respective to the number of antenna spaces) for different time slots. Perhaps the propagation link severed the information beams (in beamforming), the likelihood of correctly decoding transmitted data will be reduced than in STBC.

7. Conclusion

A multi-antenna system based on beamforming with WT and FFT as the baseband kernels have been presented and discussed. It was found that WT-OFDM is sturdier over impulsive channel when coded than FFT-OFDM. Selected for further examination, WT-OFDM in multi-antenna design was shown for beamforming with two different weighting schemes. Although the co-phasing method has been used in discussing beamforming, the use of SVD beam-weights is now shown to outperform the traditional co-phasing beamforming method in terms of capacity and BER. Capacity plots confirmed the performance advantage of the SVD-weighted beamforming compared to the traditional co-phasing technique. It is conjectured that by combining the SVD weighted beamforming technique with coded WT-OFDM for multi-antenna design, it is possible that scheme can show greater improvement, than uncoded scheme.

Acknowledgements

The authors would like to thank the support from

Datong Plc. UK, under the KTP project No. 008734 with Bradford University. In addition to the framework of ARTEMOS project under work programme ENIAC JU 2010 and FCT (Fundação para a Ciência e Tecnologia), and has been supported by the Ebonyi State Government, Nigeria.

References

[1] NEGASH, B., NIKOOKAR, H. Wavelet-based multicarrier transmission over multipath wireless channels. *Electronics Letters*, 2000, vol. 36, p. 1787-1788.

[2] ZHANG, Y., S. CHENG, S. A novel multicarrier signal transmission system over multipath channel of low-voltage power line. *IEEE Transactions on Power Delivery*, 2004, vol. 19, p. 1668-1672.

[3] ASIF, R., GHAZAANY, T. S., ABD-ALHAMEED, R. A., et al. MIMO discrete wavelet transform for the next generation wireless systems. *International Journal of Advanced Research in Electrical, Electronics and Instrumentation Engineering (IJAREEIE)*, Oct. 2013, vol. 2, no. 10.

[4] NEGASH, B., NIKOOKAR, H Wavelet based OFDM for wireless channels. In *IEEE VTS 53rd Vehicular Technology Conference, 2001. VTC 2001 Spring*. 2001, p. 688-691.

[5] HUANG, Y., SUTER, B. The fractional wave packet transform. In *Recent Developments in Time-Frequency Analysis*, Ed: Springer, 1998, p. 67-70.

[6] ANOH, K. O. O., ABD-ALHAMEED, R. A., GHAZAANY, T., HUSSAINI, A. S., JONES, S., RODRIGUEZ, J. An evaluation of coded wavelet for multicarrier modulation with OFDM. *International Journal on Communications Antenna and Propagation (IRECAP)*, 2013, vol. 3., No. 9, p. 83 - 89.

[7] VITERBI, A. Convolutional codes and their performance in communication systems. *IEEE Transactions on Communication Technology*, 1971, vol. 19, p. 751-772.

[8] ANOH, K., ELKAZMI, E., ABD-ALHAMEED, R., MADUBUKO, O., BIN-MELHA, M., JONES, S., GHAZAANY, T. Improved multi-antenna system capacity using beamformer weights. In *2013 8th International Design and Test Symposium (IDT)*. 2013, p. 1-4.

[9] JAMIN, A., MÄHÖNEN, P. Wavelet packet modulation for wireless communications. *Wireless Communications and Mobile Computing*, 2005, vol. 5, p. 123-137.

[10] GOLDSMITH, A. *Wireless Communications*. Cambridge University Press, 2005.

[11] W. MENG, W., GU, L., LI, C. The combined beamforming and space-time block coding technique for downlink transmission. In *2005 International Conference on Wireless Networks, Communications and Mobile Computing*. 2005, p. 481-486.

[12] FIGUEIREDO, D. V., RAHMAN, M. I., MARCHETTI, N., FITZEK, F. H., KATZ, M. D., CHO, Y., PRASAD, R. Transmit diversity vs beamforming for multi-user OFDM systems. *Wireless Personal Mobile Communications*, 2004.

[13] PROAKIS, J., SALEHI, M. *Digital Communications*. Fifth ed. Asia: McGraw-Hill, 2008.

[14] McKAY, M. R., COLLINGS, I. B., SMITH, P. J. Capacity and SER analysis of MIMO beamforming with MRC. In *IEEE International Conference on Communications, 2006. ICC'06*. 2006, p. 1326-1330.

[15] HOLTER, B., ØIEN, G. E. The optimal weights of a maximum ratio combiner using an eigenfilter approach. In *Proc. 5th IEEE Nordic Signal Processing Symposium (NORSIG-2002)*. Hurtigruten (Norway), 2002.

[16] SHAH, A., HAIMOVICH, A. Performance analysis of maximal ratio combining and comparison with optimum combining for mobile radio communications with cochannel interference. *IEEE Transactions on Vehicular Technology*, 2000, vol. 49, p. 1454-1463.

About Authors…

Kelvin O. O. ANOH is from Ohaozara, in Ebonyi State, Nigeria. He received his MSc degree in Data Telecommunications and Networks from the University of Salford-Manchester, UK, in 2010. Since 2011 to present, Kelvin pursues a PhD in Telecommunications Engineering at the School of Engineering, Design and Technology, University of Bradford, UK. He does well in mathematical modeling, system modeling, multicarrier communication systems - where he has published many papers – and cross-disciplinary research, and signal processing. He is a member of IEEE and (IET) since 2011.

Rameez ASIF was born in Lahore, Pakistan. He received the B.Eng. degree in Electronics and Computer Engineering from the University of Delaware, Newark, DE., U.S.A. in 2010 and M.Sc. (With Distinction) in Electrical and Computer Engineering from the University of Bradford, West Yorkshire, U.K., in 2012 and is currently a Ph.D. student at the University of Bradford, West Yorkshire, U.K. His main research interests are digital signal processing, ray tracing, wireless sensor networks and image processing. He has published several journal and conference papers. He became a student member for both IEEE and IET in 2011.

Raed A. Abd-ALHAMEED received the B.Sc. and M.Sc. degrees from Basrah University, Basrah, Iraq, in 1982 and 1985, respectively, and the Ph.D. degree from the University of Bradford, West Yorkshire, U.K., in 1997, all in Electrical Engineering. He is a Professor of electromagnetic and radio frequency engineering at the University of Bradford. He is the senior academic responsible for electromagnetics research in the Mobile and Satellite Communications Research Center, University of Bradford. Currently, he is the leader of the Communication Research Group and head of RF, antenna design and electromagnetics research in the School of Engineering, Design and Technology, Bradford University. He is Principal Investigator for the EPSRC-funded project "Multi-Band Balanced Antennas with Enhanced Stability and Performance for Mobile Handsets". He has also been a named co-investigator in several funded research projects. He is the leader for several successful knowledge transfer programmes such as Pace PLC, YW PLC, Datong PLC, WiMAC and ITEG Ltd. He is also a Research Visitor for Wrexham University, Wales, since September 2009, covering the wireless and communications research areas. He has pub

lished over 400 academic journal and conference papers and is coauthor of two books and several book chapters. He was awarded the certificate of excellence with grade "Outstanding" on 8th Feb. 2011, and the Business Innovation award on 13th April 2011, for the knowledge Transfer Partnerships with Pace Company for the period Jan. 2009 to March 2011, Certificate No. KTP007277, titled: Design, develop test a novel MIMO antenna system for wireless device communications. He is the Chair of several successful workshops on energy efficient and reconfigurable transceivers (EERT) approach towards energy conservation and reduction that addresses the biggest challenges for the future wireless systems. He was invited as keynote speaker for several international conferences such as, ICST, ITA and EPC; in addition to chairing many research sessions. He was appointed as Guest Editor for the *IET Science, Measurements and Technology Journal* in 2009. Prof. Abd-Alhameed is a Fellow of the Institution of Engineering and Technology, Fellow of Higher Education Academy, and a Chartered Engineer in the U.K.

Jonathan RODRIGUEZ received his Masters degree in Electronic and Electrical Engineering and Ph.D from the University of Surrey (UK), in 1998 and 2004 respectively. In 2002, he became a Research Fellow at the Centre for Communication Systems Research and was responsible for coordinating Surrey involvement in European research projects under framework 5 and 6. Since 2005, he is a Senior Researcher at the Instituto de Telecomunicações (Portugal), and founded the 4TELL Wireless Communication Research Group in 2008. He is currently the project coordinator for the Seventh Framework C2POWER project, and technical manager for COGEU. He is author of more than 170 scientific publications, served as general chair for several prestigious conferences and workshops, and has carried out consultancy for major manufacturers participating in DVB-T/H and HS-UPA standardization. His research interests include green communications, network coding, cognitive radio, cooperative networking, radio resource management, and cross-layer design. Dr Rodriguez has appointed as a research visitor to Bradford University since early 2013.

James M. NORAS is a Senior Lecturer in the School of Engineering, Design and Technology at the University of Bradford, UK. He has published 50 journal papers and 85 conference papers, in fundamental semiconductor physics, analog and digital circuit design, digital signal processing and RF system design and evaluation. He is the director of five internationally franchised BEng and MSc Courses in Electrical and Electronic Engineering, has successfully supervised 18 PhD students, and is currently supervising the research of 3 PhD students. His main research interests are now in digital system design and implementation, DSP and coding for communication systems, and localization algorithms for mobile systems. He is a Member of the Institute of Physics and a Chartered Physicist.

Steve M. R. JONES is a lecturer in Telecommunications and is a Director of Studies for programmes in Electronics and Telecommunications in the School of Engineering, Design and Technology at the University of Bradford. Since joining the University in 1987, he has worked on a wide variety of projects in the area of satellite slant-path propagation (e.g. 10 GHz bistatic-scatter, 11/14 GHz scintillation and ice depolarization with Olympus) and mobile radio propagation (notably Mobile VCE and TEAMS projects). He served as an Associate Editor for the IEEE Transactions on Antennas and Propagation 2004-8. Recently, he has worked on multiple-antenna technologies, signal processing and propagation modeling for broadband wireless access systems.

Abubakar S. HUSSAINI received his Diploma in Electrical/Electronic Engineering from the Bayero University (Nigeria) in 2003 with a specialization in Microwave/RF power amplifiers design and Tunable Filters; his MSc in Radio Frequency Communication Engineering and his PhD in Telecommunications Engineering from the University of Bradford in 2007 and 2012, respectively. He is a member of IEEE, IET, Optical Society of America; has contributed to numerous publications and is involved in European and CELTIC research projects. His research interests include radio frequency system design and high-performance RF-MEMS tunable filters with specific emphasis on energy efficiency and linearity and his achievements comprise the participation in the process to produce energy efficient power amplifier at 3.5 GHz (Mobile WiMAX frequency); the design and development of a "Radio over Fiber" optical transmitter and an optical receiver (1550 nm wavelength) in which the frequency limitations of quantum well lasers in direct RF to light transponding was investigated.

An Active Microwave Sensor for Near Field Imaging

Ahmed Faraz Mirza, Chan Hwang See, *Senior Member, IEEE*, Isah Musa Danjuma, Rameez Asif, Raed A. Abd-Alhameed, *Senior Member, IEEE*, James M. Noras, Roger W. Clarke, *Member, IEEE*, and Peter S. Excell, *Life Senior Member, IEEE*

***Abstract*— Near-field imaging using microwaves in medical applications is of great current interest for its capability and accuracy in identifying features of interest, in comparison with other known screening tools. This paper documents microwave imaging experiments on breast cancer detection, using active antenna tuning to obtain matching over a wide bandwidth. A simple phantom consisting of a plastic container with a low dielectric material emulating fatty tissue and a high dielectric constant object emulating a tumor is scanned between 4 and 8 GHz with a ultra-wideband microstrip antenna. Measurements indicate that this prototype microwave sensor is a good candidate for such imaging applications.**

***Index Terms*— Cancer detection, near field imaging, ultra-wideband, microstrip antenna, microwave imaging.**

I. Introduction

BREAST CANCER is the most common non-skin related malignancy and the second most common cause in the world of cancer deaths among women, causing many thousands of deaths every year [1]. Until research finds a way to prevent breast cancer, early detection must be looked upon as the best hope for reducing mortality from this disease.

Fifty years ago, there was no established method for detection of breast cancer at an early stage but advances in technology have very much changed the situation. The use of X-ray imaging for detection of breast cancer was proposed in the early days; however, mammography did not become an acceptable technology until the 1960s. Over the past decade, investment in breast cancer research, including early detection, has increased significantly, with new and improved technologies rapidly emerging.

X-ray mammography has proved to be the most effective tool and plays a major role in early breast cancer detection. Despite providing a high percentage of successful detection compared with other screening tools, X-ray mammography also has its limitations. The uncomfortable breast compression associated with this diagnosis method militates against patients undergoing early stage examination and both false positive and false negative rates have been reported [2]–[4], which suggests a need for screening alternatives. Exposure to ionizing radiation from X-rays is also a concern.

Recently, other sensors such as Electrical Impedance Tomography Sensor [5], Isotopically Etched Silicon Microarrays [6], Acoustic Biosensor [7] and SiNW-FET in-Air Biosensors [8] have been proposed for better detection of breast cancer. One alternative under investigation is ultra-wideband (UWB) microwave sensors. Based on the variations in the dielectric properties of tissue, this technique permits non-destructive evaluation of the biological tissue, and creates images related to the electrical properties of the breast tissue. The tissue of a malignant tumor has a high water content and hence dielectric properties which are distinct from those of normal breast tissue, which has a lower water content [9]. As a result, strong scattering takes place when microwaves hit the tissue of a malignant tumor.

Microwave imaging of breast tissue can be categorized into three types; passive, hybrid and active methods [3].

- The passive method is based on differentiating malignant and healthy tissue by sensing the inherently increased temperature of the tumor by means of microwave radiometry [9]. Temperature measurements then map out an image of the inspected region of the breast for further diagnosis and verification.
- The hybrid method combines microwave and ultrasonic sensors to determine the presence of a tumor. A tumor has higher conductivity than the normal tissue, so microwave energy is preferentially absorbed by the tumor, heating and expanding it. Using ultrasonic transducers, the pressure wave created by an expanded tumor can be detected and transformed into an image to locate the tumor [10], [11].
- The active method uses microwave radiation into the breast to detect the presence of a tumor and is the most widely adopted method. There are significant differences between the dielectric properties of normal and malignant tissue which alter the reflected signal response [12]–[17]. A fully mapped image is generated by controlling and reconstructing the backscattered energy.

In this present work, we propose an active microwave method using surface mounting of microwave sensors for breast cancer detection. Specifically, a microstrip sensor is placed on a finite ground plane to eliminate as far as possible the back-scattered waves in the near field zone and thus to direct most of the radiated power into the breast.

II. Antenna Design

The case for active microwave imaging as a diagnostic tool for breast cancer detection has been strengthened in recent

Manuscript received December 24, 2016; accepted February 16, 2017. Date of publication February 23, 2017; date of current version April 10, 2017. This work was supported in part by the Yorkshire Innovation Fund, in Research Development Project from 2014 to 2016, in part by the TSB-KTP Project under Grant 009734, and in part by the Research Council under Grant EP/E022936/1, all from the United Kingdom. The associate editor coordinating the review of this paper and approving it for publication was Dr. Lorenzo Lo Monte.

A. F. Mirza, R. Asif, R. A. Abd-Alhameed, I. M. Danjuma, J. M. Noras, and R. W. Clarke are with the School of Engineering and Informatics, University of Bradford, BD7 1DP, U.K. (e-mail: r.a.a.abd@bradford.ac.uk).

C. H. See is with the School of Engineering, University of Bolton, Bolton, BL3 5AB U.K. (e-mail: chs1@bolton.ac.uk).

P. S. Excell is with Glyndwr University, Wrexham, LL11 2AW, U.K.

Digital Object Identifier 10.1109/JSEN.2017.2673961

TABLE I
BREAST TISSUE ELECTRICAL PROPERTIES

LAYERS	SKIN	BREAST
Thickness / mm	2	100
Relative permittivity	36	9
Equivalent conductivity / Sm^{-1}	4.0	0.4

years due to its improved tissue characterization capability as compared with existing mammography: several prototypes have been constructed and tested [18]–[20]. Performance is assessed using test "phantoms", targets which closely emulate the actual dielectric mixture of normal and abnormal cancerous tissues. For a feasibility study, it is sufficient to use a uniform block as the phantom, but more sophisticated electromagnetic models for the tissue-sensor interaction can be built up, for example with a two-layer model to represent the breast. The first layer represents the skin, and the second layer the breast tissue, which extends to a width of 10 cm [21], [22]. The electrical properties are summarized in Table 1.

A dual element sensor, for transmission and reception, is investigated in our modelling, and in the subsequent experimental investigations. Mutual coupling between the elements must be taken into consideration within the design and different configurations are investigated through simulation and measurement.

Good electrical matching may be obtained without the addition of a further matching medium or lumped load when the antenna shown in Fig. 1 is in contact with tissue [23]–[27]. This antenna was fabricated in microstrip, with an air dielectric. The antenna is placed on a ground plane of dimension L = W = 40 mm and thickness 0.5 mm. The antenna is fed via a vertical plate of maximum height of 5 mm and a width of 15 mm, which is connected to the feeding probe through an aperture in the ground plane of 4 mm diameter. Another vertical plate with similar dimension was used to short the antenna to the ground as shown in Fig. 1a. The antenna was modelled and optimized using a high frequency structure simulator (HFSS).

A parametric simulation was carried out to optimize the performance of the antenna of Fig. 1a before the antenna was manufactured and tested experimentally. Different antenna parameters were considered for optimization of the operating bandwidth, subject to suitable radiated power gain. Relevant parameters include the total size of the ground, feed length, dimensions of the disc, and gap between the vertical plates. To check the influence of these parameters on the impedance bandwidth, in successive tests one parameter was varied while the other parameters remained fixed. Simulation results showed that the effect of changing these antenna dimensions appreciably changed the resonant frequency and return loss. The results can be found in [23], from which the optimum dimensions can be summarized as follows: radius of the circular disc, gap between the vertical plates, ground size and height of the antenna from ground are 12 mm, 5 mm, 40 mm × 40 mm and 5.5 mm, respectively. The antenna is designed to be placed directly on the breast so the interaction of the antenna with the tissue was investigated.

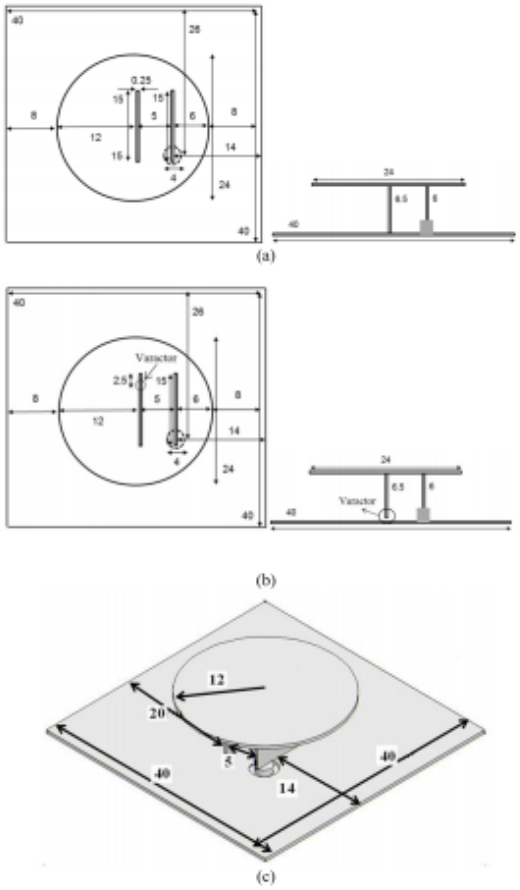

Fig. 1. Antenna geometry (all units in mm). (a) Proposed antenna. (b) Loaded proposed antenna. (c) 3D view.

A homogenous block of tissue characterized by conductivity $\sigma = 0.4$ S/m and a relative permittivity $\varepsilon_r = 9$ in the form of a cubical box of 15 cm side length, has been used as an equivalent model of the interior breast tissue. The antenna geometry including the tissue model is shown in Fig. 2. By observing the resultant reflection coefficient when the antenna is in free space and in contact with the tissue, it is seen that the antenna matching from lower frequencies up to 6.8 GHz was adversely affected by the presence of the tissue. Therefore, the antenna parameters were further optimized with the antenna in contact with the tissue.

After several attempts, good matching was achieved by reducing the height of the antenna from 5.5 mm to 3.5 mm when in contact with the tissue, keeping the remaining dimensions of the antenna fixed. Fig. 3 summarizes the variations of the reflection coefficients of the antenna before optimization with the tissue, after the optimization in free space and in contact with the tissue. As can be seen, the antenna exhibits

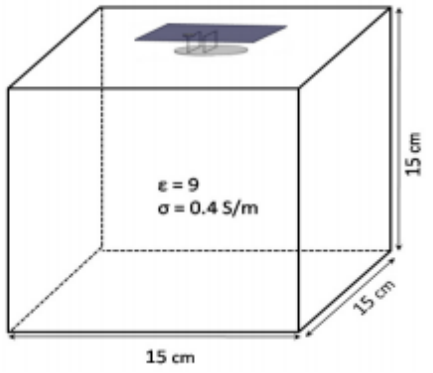

Fig. 2. The geometric model of the antenna with the tissue model.

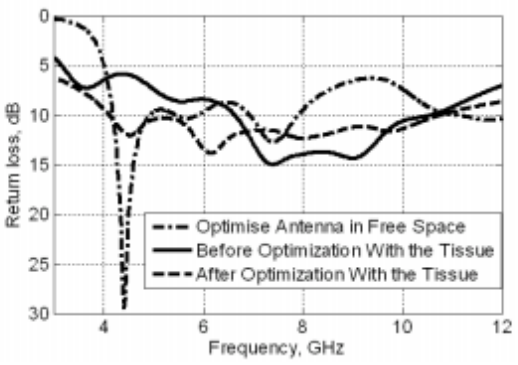

Fig. 3. Antenna input return loss before optimization with the tissue, after optimization in free space and with the tissue.

return loss less than 10 dB in the required frequency band of interest (4 GHz to 8 GHz) proposed for this application.

Two antenna prototypes, i.e. with and without varactor, were fabricated from a copper sheet of thickness 0.25 mm for practical realization, as shown in Fig. 4. The GaAs Hyper-abrupt Varactor diode, model MGV125-08H20 from Aeroflex was used in the prototype. It has a capacitance tunable from 0.1 to 10.5pF over a 1–16 V reverse bias voltage range. A bias tee circuit was integrated at the input port of the antenna. The required decoupling high-Q (>40) capacitor and RF choke inductors were set at 22pF and 1.2nH, respectively but are not shown here. An HP 8510C network analyzer was used for measurements. The experimental results in terms of the input return loss of the antenna without the varactor showed reasonable agreement with the results of the simulation, as illustrated in Fig. 5. The impedance bandwidth of the proposed antenna, determined at −10 dB $|S_{11}|$, is 4.4 GHz or about 73.3% with respect to the 6 GHz centre frequency, which fully covers the frequency spectrum required. The slight differences in the return loss curves can be attributed to fabrication inaccuracies.

As previously remarked, a breast phantom should ideally closely emulate the actual dielectric mixture of the tissue,

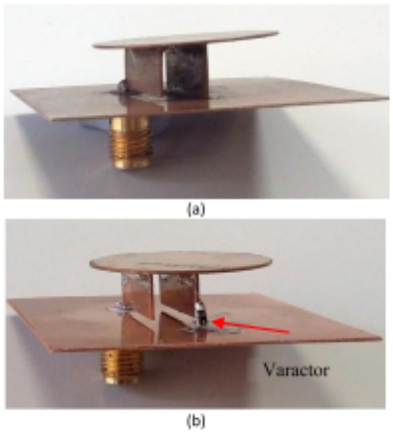

Fig. 4. Physical antenna prototypes: (a) without varactor and (b) with varactor.

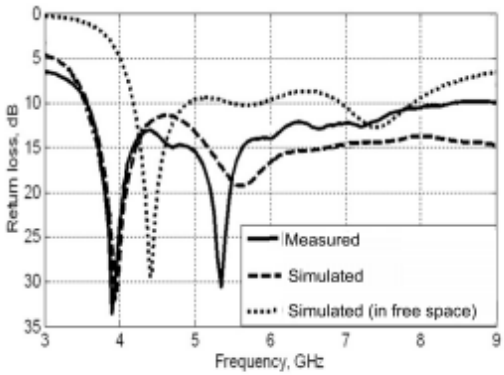

Fig. 5. Measured and simulated input return losses.

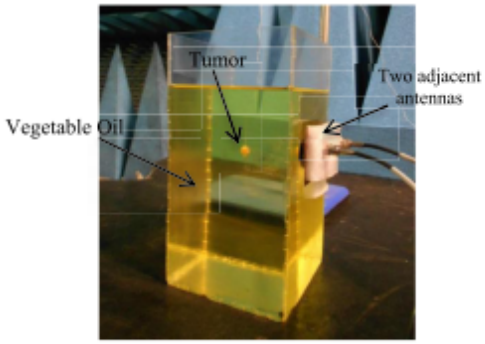

Fig. 6. Experimental set up.

and have an equivalent skin barrier. However, a simplified model is used here, to provide a basic proof of concept. The approximated breast phantom used for experiments is shown in Fig. 6. It comprises a rectangular tube with dimensions 10.0 cm × 10.0 cm × 20.0 cm, and was initially filled

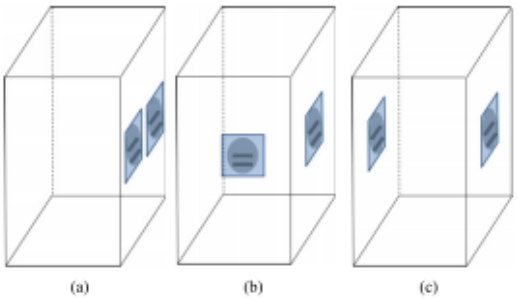

Fig. 7. Investigated locations of the two antennas on the phantom: (a) case 1 (antennas adjacent), (b) case 2 (antennas 90° apart), and (c) case 3 (antennas 180° apart).

with vegetable oil, the skin being replaced by a Plexiglas barrier of 2 mm thickness. Vegetable oil was used as the dielectric filler for cost and safety reasons, as has been chosen by others [28]–[32]. The dielectric constant of the Plexiglas varies from 2.39 to 2.59, with an equivalent conductivity of 0.009–0.007 S/m over the range of 3 GHz to 12 GHz [33]: this obviously differs substantially from skin and thus it was decided that skin would be omitted from the proof-of-concept model.

The performance of the pair of antennas was assessed using different locations on the phantom wall to gain physical insight into the relationship between antenna performance and system performance. Three distinct cases were examined as shown in Fig. 7. In case 1, the transmit antenna (TX) and receive antenna (RX) were positioned side by side. In case 2 they are located 90° apart, and 180° apart in case 3.

The analysis began as a simulation exercise, comparing the antenna return loss in air, and adjacent to the oil phantom. Since the final design of the scanner will employ a multiple array around the breast, it is important to investigate the effects of mutual coupling. Initially two identical antennas were analyzed for different separation distances in air, for a range of frequencies. This process was repeated adjacent to the oil phantom. According to a study [34], a coupling level of −20 dB should be used as the target for imaging in the 4 GHz to 8 GHz range.

III. Experimental Setup

For experimental verification of the simulation model, S_{11} and S_{21} were monitored for each of the above configurations using a network analyzer, both with the phantom empty and also with it filled with oil. The antennas were in contact with the outer container, and connected to the vector network analyzer (VNA) by coaxial cables.

The scattering material used to represent tumors consisted of 10 g of wheat flour mixed with 5.5 g of water. This mixture has a relative permittivity of 23 and a conductivity of 2.57 S/m at a frequency of 4.7 GHz [35]. It is used to represent tumors of various sizes and placed within the breast phantom oil for experimental detection. In order to compare the performances of the three antenna configurations, several experiments were conducted.

IV. Results and Discussions

The specific goal here is to measure and analyze the scattered waves due to the transmitted UWB microwave signal travelling through a phantom containing a simulated tumor as described above. In order to evaluate the two-antenna array system, we examine S_{11}, S_{21}, the envelope correlation (ρ_e), and the Total Active Reflection Coefficient (TARC). The last two parameters are critical for the evaluation of the antenna system; they complement the simple reflection coefficients as they take mutual coupling effects into accounts. They are given by [36]:

$$\rho_e = \frac{\left|S_{11}^{*}S_{12}+S_{21}^{*}S_{22}\right|^2}{\left\{1-\left(|S_{11}|^2+|S_{21}|^2\right)\right\}\left\{1-\left(|S_{22}|^2+|S_{12}|^2\right)\right\}} \quad (1)$$

$$TARC = \Gamma_a' = \sqrt{\frac{\left|S_{11}+S_{12}e^{j\theta}\right|^2+\left|S_{21}+S_{22}e^{j\theta}\right|}{2}} \quad (2)$$

where θ is a random variable with uniform probability density over 0° to 360°.

The variations of the simulated and the measured scattering parameters for the three test cases shown in Fig. 7 are presented in Fig. 8. These results are obtained with the two antenna elements mounted on the surface of the oil-filled phantom, and show that the antenna array system is working effectively in all three cases over the desired bandwidth, from 4 to 8 GHz. The UWB performance was well confirmed, with the reflection coefficient $|S_{11}| < -10$ dB over the frequency range, for all test cases. The S_{21} values confirmed the same bandwidth was acceptable for all test cases, ranging between 20 and 30 dB. The S_{21} values are better than the results achieved in our previous work [37] by around 10 dB, because of reduced backscattered radiation achieved here by improved antenna geometry.

The envelope correlation and the TARC for case 1 are shown in Figs 9 and 10, both when the phantom is with and without oil. It is noted that, for the chosen bandwidth, the curves lie below 20 dB and 10 dB respectively for envelope correlation and TARC. The TARC values retain the original behavior of a single antenna, as shown in Fig. 10. However, bandwidth and return loss are changed because TARC is sensitive to the effect of mutual coupling and the phase of the incident wave. Thus, we conclude that the TARC can be interpreted as the return loss of the complete two-antenna array. The results for cases 2 and 3 are quite similar to those for case 1, and thus are not shown here.

In one practical example of the case 1 two-element array, a 4 mm tumor was placed at different distances from the antenna plane (10 mm, 15 mm, 30 mm and 40 mm separation) to test sensitivity to reflected signals. The S_{21} transmission parameter was first measured with no scattering object present in the medium and then with the object present. The frequency data was then transferred to reconstruct the time domain pulses with and without the target, as shown in Fig. 11. The normalized back-scattered time responses after subtracting the impressed pulses of these three locations are shown in Fig. 12, showing the sensitivity of the imaging system to this small object: the reflections indicate the magnitude of the signals reflected from the tumor, varying with its depth inside the liquid.

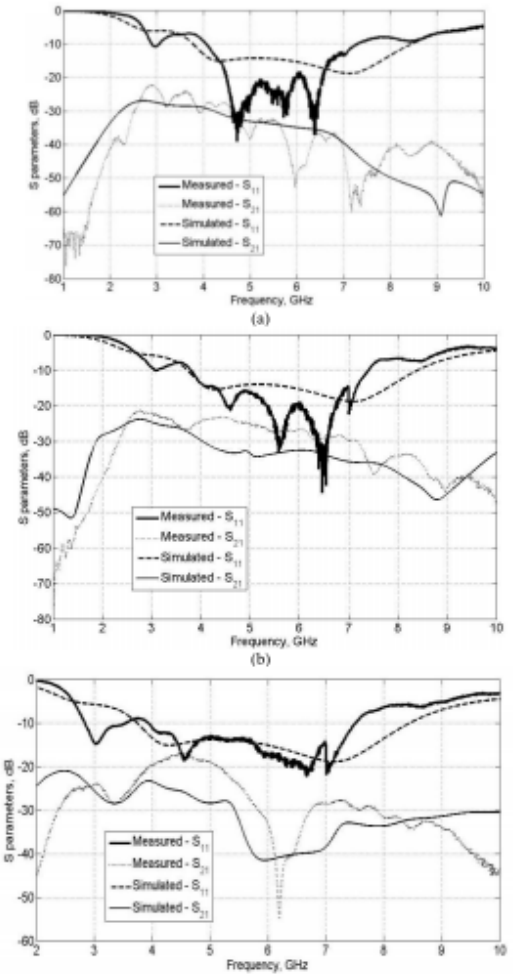

Fig. 8. S_{11} and S_{21} for the antennas with oil-filled phantom: (a) case 1, (b) case 2, and (c) case 3 (see Fig. 7).

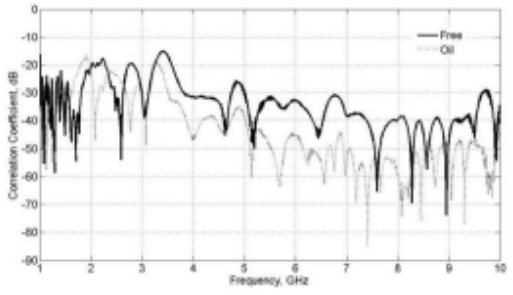

Fig. 9. Measured envelope correlation coefficient for case 1.

To improve the matching of the antenna with the tissue, a varactor diode was added at the base of the second plate, as shown in Fig. 1b and Fig. 4b. The objective was to achieve active frequency tuning over the total bandwidth with maximum return loss. Fig. 13 shows three tuned frequency spectra with three different varactor capacitances when the antenna was mounted on the second phantom representing a generic breast as shown in Fig. 14. More values could have been tested, but the values used (0.1, 1 and 5 pF) were found quite adequate to cover the entire intended bandwidth. In the measurement, these three capacitance values are corresponding to 16V, 12.5V and 1.4V applied voltage of the varactor. Both computed and experimental results are in a good agreement.

Collected data were processed with sinusoidal Gaussian pulse shaping to return the reflected magnitude and delay time variations. Several attempts were performed and optimized to

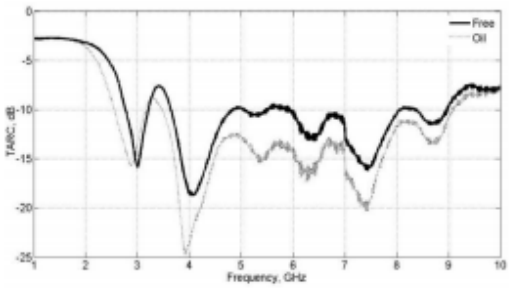

Fig. 10. Measured TARC coefficient for case 1.

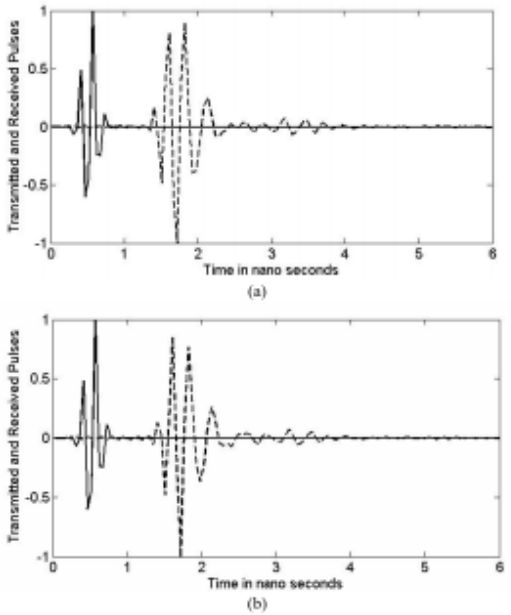

Fig. 11. Measured transmitted and received pulses: (a) with no tumor object and (b) with tumor object. (Solid line: Transmitted signal, Dotted line: Reflected signal).

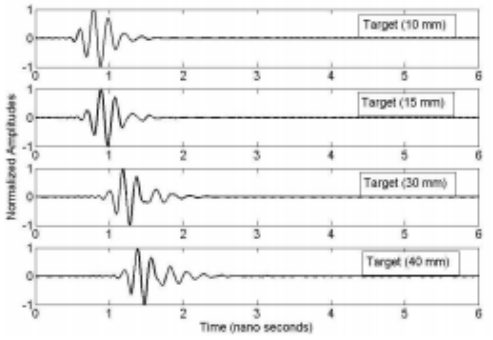

Fig. 12. Comparison of the backscattered responses from various positions.

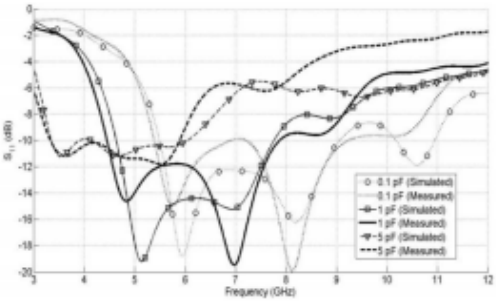

Fig. 13. Simulated and measured S_{11} of the proposed varactor-loaded antenna adjacent to the phantom in Fig. 14, for three values of varactor capacitance.

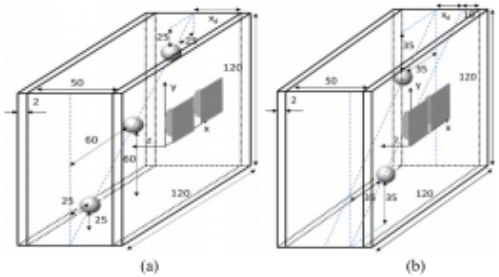

Fig. 14. The tissue model with antenna arrangement including the simulated tumor locations. (a) Three sphere tumor model at the same distances from the skin. (b) Two sphere tumor model: one at 10 mm fixed distance and other at variable distance x_d. (all units in mm).

reduce the overlap between pairs of these spectra, smoothing the response over ±3 dB of the crossing point.

A single antenna was tested with the phantom structure shown in Fig. 14, but with only one simulated tumor sphere present at two locations 10 mm and 30 mm distant from the skin plane. The normalized reflected magnitude is shown in Fig. 15 and clearly indicates the recovery of the scattered

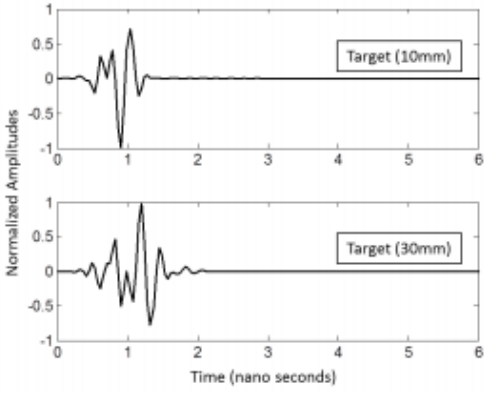

Fig. 15. The normalized magnitude of the reflected signal for tumor locations 10 mm (upper trace), and 30 mm (lower trace).

waves in such active operation giving confidence that small antennas in array configurations will be able to detect tumor locations and their expected sizes.

V. Imaging Model Set-Up and Results

More detailed examples as shown in Fig. 14a and b were next investigated to demonstrate the capability of the system. The tissue was of width 50 mm with 2 mm plexiglass containment thickness in both cases. In Fig. 14a three 5mm diameter spheres representing tumors were placed in a plane whose normal distance x_d from the larger face of the container varied between 10 mm and 30 mm with 10 mm steps. In Fig. 14b there are two similar spheres at different distances from the surface: the first is kept fixed at 10 mm while the second was located at variable distances from the surface and 20 mm lower than the first, fixed tumor model. The two-element arrangement of case 1 in Fig. 7a was applied here, with mutual coupling compensated by subtracting the reflection responses without a "tumor" present from those with one or more.

Fig. 16 shows the magnitude and the time delay of the reflections for the three sphere tumor model of Fig. 14a. In this example the maximum magnitude was normalized to 0dB, and then a dB scale was used in the figures. In the case of the time delay, the values were normalized to 1 nanosecond, and again a logarithmic scale was used. This procedure gives clear images that show the location and the resolution of the tumor plots from these models. The metric of the image performance adopted here is to measure the peak to peak value of the difference in the backscattered reflections with and without the spherical tumor models for each increment move. The corresponding time delay was measured at the absolute maximum of the difference in backscattered reflections. Figs 16: a2, b2 and c2 are extended versions of the magnitudes given in Figs 16: a1, b1 and c1, respectively. The data was interpolated using the piecewise bilinear Gouraud method. The results are encouraging in terms of the feasibility of discriminating and localizing the tumors, at least with a positional resolution of

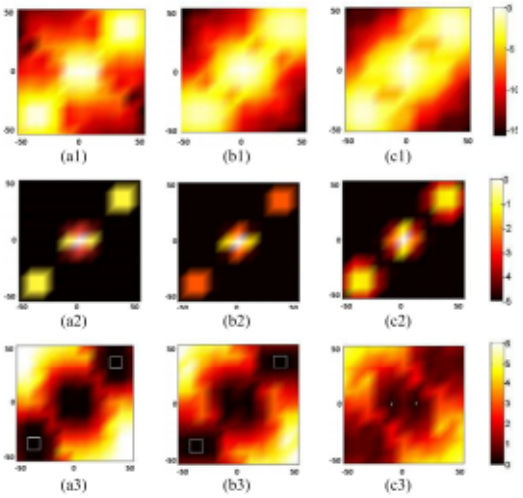

Fig. 16. The magnitude (a1, a2, b1, b2, c1, c2) and the time delay (a3, b3, c3) of the reflected signals for the case in Figure 14a, for various distances x_d: 10 mm (a1, b1, c1), 20 mm (a2, b2, c2), 30 mm (a3, b3, c3).

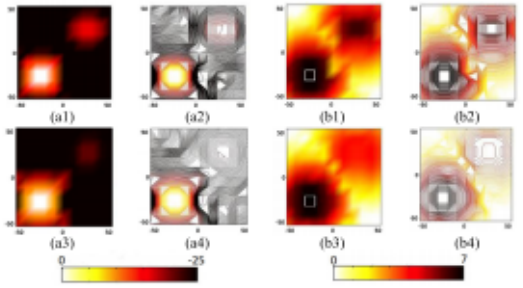

Fig. 17. The magnitude (a1, a2, a3, a4) and the time delay (b1, b2, b3, b4) of the reflected signals of Figure 14b for two distances of x_d: 10 mm (a1, a2, b1 ,b2), 20 mm (a3, a4, b3, b4).

10 mm or better. The depths of the spheres could be found from Figs 16:a3, b3 and c3. It is clear that even with spheres at 30 mm depth the measurements can yield the approximate distances.

Fig. 17 also shows the similar analysis as discussed for Fig. 16, but with the setup shown in Fig. 14b. Contour plots have been added to justify the correct locations of the spherical tumor models since the magnitude data was normalized once subject to the total reflections. The magnitude contour plots shown in Figs 17: a2 and a4 clearly identify the locations of both spheres. In addition the time contour plots were also used as evidence of the depths of cancer models. These contour plots were generated subject to the code provided by Pawlowicz [38] that handles parametric surfaces with inline contour labels.

VI. Conclusions

An experimental investigation was made using small UWB antennas, a breast phantom and simulated tumor targets, and a VNA. The measurements demonstrate that this system is capable of detecting small targets with dimensions comparable to those required for the early detection of breast cancer. Irregularly shaped objects were not tested: however it is anticipated that scattering from such objects will be more pronounced than from a spherical target. A lower limit on size was not determined, but the contrast in the images for 10 mm diameter targets shows that it is likely that smaller target sizes may be detectable under the conditions described in this paper. This confirms the basic design concept, and the choice of antenna elements. The proof of the concept of applying active frequency tuning of the antennas using a varactor diode in order to improve matching performance over the total bandwidth has been demonstrated.

The measurements and the imaging techniques presented in this paper can be used as the basis for investigating a 3D inversion algorithm approach, and further experimental investigation of the super-resolution concept.

References

[1] R. G. Blanks, S. M. Moss, C. E. McGahan, M. J. Quinn, and P. J. Babb, "Effect of NHS breast screening programme on mortality from breast cancer in England and Wales, 1990–8: Comparison of observed with predicted mortality," *BMJ*, vol. 321, pp. 665–669, Apr. 2000.

[2] X. Yun, E. C. Fear, and R. H. Johnston, "Compact antenna for radar-based breast cancer detection," *IEEE Trans. Antennas Propag.*, vol. 53, no. 8, pp. 2374–2380, Aug. 2005.

[3] E. C. Fear, S. C. Hagness, P. M. Meaney, M. Okoniewsk, and M. A. Stuchly, "Enhancing breast tumor detection with near-field imaging," *IEEE Microw. Mag.*, vol. 3, no. 1, pp. 48–56, Mar. 2002.

[4] S. P. Singh, S. Urooj, A. Lay-Ekuakille, "Breast cancer detection using PCPCET and ADEWNN: A geometric invariant approach to medical X-ray image sensors," *IEEE Sensors J.*, vol. 16, no. 12, pp. 4847–4855, Dec. 2016.

[5] Y. Yang, J. Jia, S. Mith, N. Jamil, W. Gamal, and P.-O. Bagnaninchi, "A miniature electrical impedance tomography sensor and 3-D image reconstruction for cell imaging," *IEEE Sensors J.*, vol. 17, no. 2, pp. 514–523, Feb. 2017.

[6] M. Nikkah, J. S. Strobl, V. Srinivasaraghavan, and M. Agah, "Isotopically etched silicon microarrays for rapid breast cancer cell capture," *IEEE Sensors J.*, vol. 13, no. 3, pp. 1125–1132, Apr. 2013.

[7] F. J. Gruhl and K. Lange, "Influence of surface preparation parameters on the signal response of an acoustic biosensor for the detection of a breast cancer marker," *IEEE Sensors J.*, vol. 12, no. 6, pp. 1647–1648, Jun. 2012.

[8] F. Puppo *et al.*, "SiNW-FET in-air biosensors for high sensitive and specific detection in breast tumor extract," *IEEE Sensors J.*, vol. 16, no. 10, pp. 3374–3381, Sep. 2016.

[9] B. Bocquest, J. C. V. D. Velde, A. Mamouni, G. G. Y. Leroy, J. Delannoy, and D. D. Valee, "Microwave radiometric imaging at 3 GHz for the exploration of breast tumors," *IEEE Trans. Microw. Theory Techn.*, vol. 38, no. 6, pp. 791–793, Jun. 1990.

[10] G. Ku and L. V. Wang, "Scanning thermoacoustic tomography in biological tissue," *Med. Phys.*, vol. 27, pp. 1195–1202, Sep. 2000.

[11] E. C. Fear, "Microwave imaging of the breast," *Technol. Cancer Res. Treatment*, vol. 4, pp. 69–82, Feb. 2005.

[12] X. Li and S. C. Hagness, "A confocal microwave imaging algorithm for breast cancer detection," *IEEE Microw. Wireless Compon. Lett.*, vol. 11, no. 3, pp. 130–132, Mar. 2001.

[13] E. C. Fear, X. Li, S. C. Hagness, and M. A. Stuchly, "Confocal microwave imaging for breast cancer detection: Localization of tumors in three dimensions," *IEEE Trans. Biomed. Eng.*, vol. 49, no. 8, pp. 812–822, Aug. 2002.

[14] E. C. Fear and M. A. Stuchly, "Microwave detection of breast cancer," *IEEE Trans. Microw. Theory Techn.*, vol. 48, no. 11, pp. 1854–1863, Nov. 2000.

[15] D. Gibbins *et al.*, "A comparison of a wide-slot and a stacked patch antenna for the purpose of breast cancer detection," *IEEE Trans. Antennas Propag.*, vol. 58, no. 3, pp. 665–674, Mar. 2010.

2015 IEEE International Conference on Computer and Information Technology; Ubiquitous Computing and Communications; Dependable, Autonomic and Secure Computing; Pervasive Intelligence and Computing

Breast Cancer Detection using 1D, 2D and 3D FDTD Numerical Methods

A.F. Mirza, F. Abdulsalam, R. Asif, Y.A.S. Dama, M. M. Abusitta, F. Elmegri, R.A. Abd-Alhameed, J.M. Noras, R. Qahwaji
[1]School of Engineering and Informatics, University of Bradford, UK
{a.f.mirza, r.asif1, r.a.a.abd}@bradford.ac.uk

Abstract - **Early detection of breast cancer using a radio frequency application is technically challenging, but potentially of great importance since it would be fast and cheap to implement. This paper explores an ideal ultra-wideband application for detecting tumour cancer within breast tissues using an FDTD numerical method. 1D, 2D and 3D FDTD models are investigated experimentally and the best ways of identifying the existence of cancerous tissue are discussed. Pulses with a narrow bandwidth of 4 GHz, centred at 6 GHz, were used for excitation, and their reflections from tumour equivalents of various positions and sizes were recorded and plotted. Results of analysis suggest the scheme is a suitable candidate for cancer detection.**

Index Term– **Cancer detection; FDTD; Ultra-wideband; Reflection; Scattering;**

I. Introduction

The present work discusses the Finite-Difference Time-Domain (FDTD) technique for early detection of breast cancers using RF signals of wide bandwidth. The FDTD numerical technique is robust and accurate tool for the analysis of problems in electromagnetics, arguably the simplest method, both conceptually and in implementation. It has been successfully applied in a number of electromagnetic research areas including bio-electromagnetic, micro-strip antennas, integrated optics and ultra-high-speed electronic circuits. FDTD gives direct solutions of Maxwell's fundamental curl differential equations on space grids in the time domain. It allows modelling of complex geometrical configurations comprising different materials and can provide wide frequency response from a single calculation [1, 2].

Breast cancer is the second most common cause of death among women [3]. Use of X-rays for detecting breast cancers was proposed very early, however mammography was not an acceptable technology until the 1960s. Despite being a useful tool it has its drawbacks; the associated uncomfortable breast compression and significant rates of false positive and negative results have been reported, which suggest a need for alternative screening. Moreover, exposure from X-rays is also a concern.

Ultra-wideband (UWB) microwave imaging is currently under investigation as such an alternative. Based on variations in the dielectric properties of tissue, this technique permits non-destructive evaluations and creates images related to the electrical properties of breast tissue [4].

Recently the present authors demonstrated the potential of UWB antennas in identifying features of interest in near-field imaging and other medical applications compared to well-known screening tool. [5]. The work entailed experiments with a simple phantom consisting of a plastic container with a low dielectric material imitating fatty tissue and a high dielectric constant object emulating tumour. This "phantom" was scanned with a UWB microstrip antenna between 4 to 8 GHz. The present work explores the advantages of the UWB approach employing three simulation modes. Several examples illustrate optimum operational performances in detecting the existence of cancer tissue within the breast model. The breast model is modelled through layers of skin and fat that spread over a grid model. For excitation, a Gaussian pulse is used, covering a 4 GHz bandwidth, centred at 6 GHz.

II. Formulation Model

The FDTD method solves Maxwell's curl equations for electric and magnetic vector fields within a finite computational domain truncated by proper boundary conditions. In the presence of electric and magnetic losses, these equations in differential form for a source and isotropic medium are:

$$\nabla\times\mathbf{E} = -\mu\frac{\partial\mathbf{H}}{\partial t} - \sigma^{*}\mathbf{H} \quad (1)$$

$$\nabla\times\mathbf{H} = \varepsilon\frac{\partial\mathbf{E}}{\partial t} + \sigma\,\mathbf{E} \quad (2)$$

where σ is the electric conductivity in S/m and σ^{*} is the magnetic resistivity in Ω/m. Thus, σ**E** and σ^{*}**H** are the electric and magnetic losses respectively inside the medium. Assuming cubical FDTD cells are used, the finite difference updating equations for one magnetic and one electric field components (others can be obtained in similar way) can be derived in the following form [6]:

$$E_{x_{i,j,k}}^{n+1} = C_{a,E_x}\Big|_{i,j,k} E_{x_{i,j,k}}^{n} + C_{b,E_x}\Big|_{i,j,k}\left(H_{z_{i,j+1/2,k}}^{n+1/2} - H_{z_{i,j-1/2,k}}^{n+1/2} + H_{y_{i,j,k-1/2}}^{n+1/2} - H_{y_{i,j,k+1/2}}^{n+1/2}\right) \quad (3)$$

$$H_{y_{i,j,k}}^{n+1/2} = D_{a,H_y}\Big|_{i,j,k} H_{y_{i,j,k}}^{n-1/2} + D_{b,H_y}\Big|_{i,j,k}\left(E_{z_{i+1/2,j,k}}^{n} - E_{z_{i-1/2,j,k}}^{n} + E_{x_{i,j,k-1/2}}^{n} - E_{x_{i,j,k+1/2}}^{n}\right) \quad (4)$$

where the electric updating coefficients are:

$$C_a\Big|_{i,j,k} = \left(1 - \frac{\sigma_{i,j,k}\Delta t}{2\varepsilon_{i,j,k}}\right) \Big/ \left(1 + \frac{\sigma_{i,j,k}\Delta t}{2\varepsilon_{i,j,k}}\right)$$

978-1-5090-0154-5/15 $31.00 © 2015 IEEE
DOI 10.1109/CIT/IUCC/DASC/PICOM.2015.158

$$C_{b_{ee}}\Big|_{i,j,k} = \left(\frac{\Delta t}{\varepsilon_{i,j,k}\Delta_{ee}}\right) \Big/ \left(1+\frac{\sigma_{i,j,k}\Delta t}{2\varepsilon_{i,j,k}}\right)$$

and the magnetic updating coefficients are:

$$D_a\Big|_{i,j,k} = \left(1-\frac{\sigma_{i,j,k}\Delta t}{2\mu_{i,j,k}}\right) \Big/ \left(1+\frac{\sigma^*_{i,j,k}\Delta t}{2\mu_{i,j,k}}\right)$$

$$D_{b_{ee}}\Big|_{i,j,k} = \left(\frac{\Delta t}{\mu_{i,j,k}\Delta_{ee}}\right) \Big/ \left(1+\frac{\sigma^*_{i,j,k}\Delta t}{2\mu_{i,j,k}}\right)$$

The computational domain is truncated using perfectly matched layer (PML) absorbing boundary conditions. The formulation used in these codes is based on the original split-field Beranger PML. The configuration of the fields enables the realisation of a discretised version of Maxwell's equations. After determining the spatial resolution based on the geometrical features and the operating frequency, a suitable step time is chosen to ensure stability. A leapfrog arrangement between E and H components is used to implement the time-stepping FDTD algorithm. The half-cell displacement between the E and H grids reflects the physical reality that the computer must work through them alternately. To ensure the accuracy of the computed results, the spatial increment Δ must be small compared to the wavelength (usually $\Delta \leq \lambda/10$) and the minimum dimension of the scatterer (whichever is smaller). Stability requires that the numerical solution of the differential equation should not grow in future time-steps in an uncontrollable manner. Once the proper spatial increments are chosen, stability is achieved by using the *Courant stability condition*, which sets the relation between the time step and cell size for three-dimensional FDTD as follows:

$$v_{\max}\Delta t \leq \frac{1}{\sqrt{\frac{1}{\Delta x^2}+\frac{1}{\Delta y^2}+\frac{1}{\Delta z^2}}} \qquad (7)$$

where v_{max} is the maximum wave phase velocity within the model. For a cubic cell of size Δ, in a d-dimensional spatially homogeneous FDTD grid (d=1, 2 or 3), equation (7) becomes:

$$\Delta t \leq \frac{\Delta}{v_{\max}\sqrt{d}} \qquad (8)$$

To minimise the computer run-time requirement, the time step should be chosen as large as possible yet satisfying equation (8). Smaller time-steps give more accuracy but with longer simulation run times. Stability also depends upon the algorithm used to model the Absorbing Boundary Conditions to simulate the domain extension to infinity.

The source of excitation for these models comprises a differentiated Gaussian pulse with the following time and frequency properties:

$$v(t) = v_o \sin(2\pi f_o(t-t_o))e^{-((t-t_o)/\tau)^2} \qquad (5)$$

$$V(j\omega) = -jv_o\tau\sqrt{\pi}e^{-j\omega t_o}e^{-\tau^2\left(\pi^2 f_o^2+0.25\omega^2\right)}\sinh\left(\pi\tau f_o\tau^2\right) \qquad (6)$$

where f = 6 GHz, τ = 0.133 ns, to = 4τ and v_o is the voltage amplitude. The pulse has a temporal width of 0.22 ns with an amplitude spectral width of 4 GHz and zero dc content. The excitation spectrum is a band-pass Gaussian function (centred at 6 GHz).

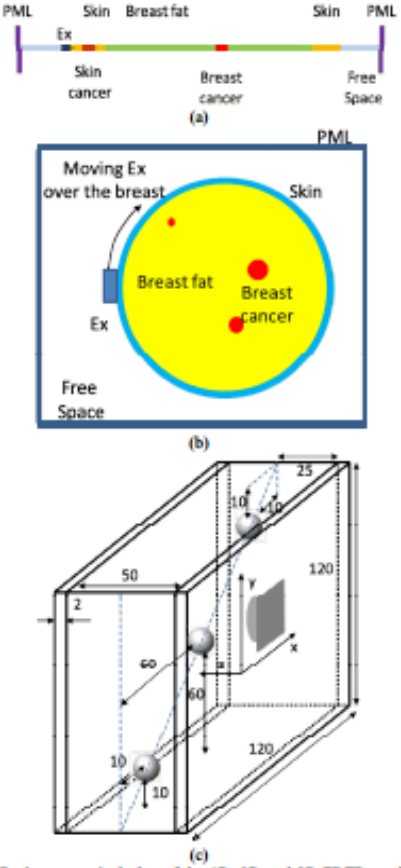

Figure 1: Basic geometrical plan of the 1D, 2D and 3D FDTD models of the proposed work; (a) 1D, (b) 2D, (c) 3D. (dimensions in mm)

Table 1: Electrical properties of Breast Tissue

Tissue	ε	σ[S/m]
Skin	36	1.247
Fat	9	0.4
Tumour	50	2.57

III. Simulation and Results

The three FDTD 1D, 2D and 3D geometrical models used in this work are shown in Figure 1. Beranger PML was applied for 2D and 3D models whereas Mur's Absorbing Boundary Condition was used with the 1D model. For all models the excitation voltage given in Equation (5) was used to model the wide 4 GHz bandwidth. The thickness of the skin is 2 mm for all models. The electrical properties of the layers used in these

models are shown in Table 1. More layers could be added for all three models; however, the idea here is to find the optimum performance of the detection technique and its feasibility including the limitations that possibly compromise accuracy.

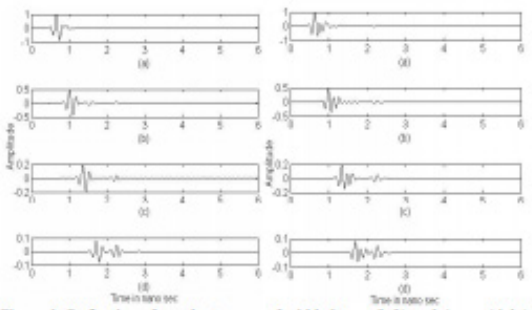

Figure 2: Reflections from the tumour of width 2 mm (left) and 4 mm (right) for various depth distances from the centre of the problem space; a) 140 cells left, b) 70 cells left, c) at the centre d) 70 cells right.

a) The 1D FDTD model shown in Fig. 1a was run without a tumour and reflections were recorded, after which a tumour was placed at various distances from the source and the reflections were recorded again. 2 mm and 4 mm tumour sizes were considered, and the computed FDTD cell adopted here is 0.25 mm. This was selected to see detailed reflection and scattering field effects caused by the skin surrounding the fat tissue. The fat length is 80 mm, equal to the diameter of the cylindrical tissue applied later in the 2D FDTD model. The detected tumour image was computed with the help of the differences of the reflections collected at the source of the excitation port. Figure 3 shows the resultant differences of the reflection amplitudes form both 2 mm and 4 mm tumour sizes. We have normalized the data to the maximum reflection computed from the nearest position of the tumour from the skin and the excitation source. The amplitudes of the reflections for both tumour sizes were comparable to each other. The maximum difference over the range of 210 cells is around 20 dB, clearly shown in Figure 2, which is a workable figure for detection purposes. The reflections from nearest and closest tumour targets could be easily identified for both tumour sizes even with double reflection caused by these small scales tumours.

b) For the 2D model shown in Figure 1b, the field distribution components for 3000 and 6000 time-steps are presented in Figure 3. The cell size here is 0.5 mm. The position of the reflection from the small size tumour (4 mm cylindrical diameter) is clearly found even when the excitation pulse vanishing. (Re-state this last bit – vanishing excitation would be a neat trick) The tumour reflections shown in Figure 4 for various depth distances from the excitation source are again normalized to the nearest tumour position from the source. The difference in magnitude over 120 cell widths is around 34 dB as easily calculated from Figure 4.

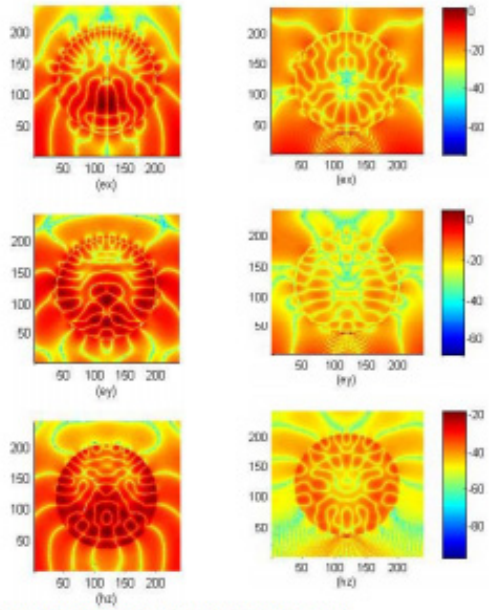

Figure 3: Field distributions at 3000 and 6000 time-steps; (left) 3000 time-steps, (right) 6000 time-steps

c) The last example is the 3D model shown in Figure 1c. A tissue model of 50 mm width with 2 mm skin thickness was considered, with the width of the tissue chosen to be greater than some data previously published in [7, 8, 9] to enhance and match practical realization of such an application. In Figure 1c spheres to model three tumours were placed in one plane whose normal distance from the skin was 10 mm, then 20 mm and then 30 mm. The mutual coupling was compensated by subtracting the reflection responses with no tumour present from those with the three spheres in place. The data were recorded on the basis of a 10 mm increment of one element movement from the centre (located at 60 mm × 60 mm) covering a total surface area of 50 mm × 50 mm. The diameter of each sphere for both examples was 4 mm. Fig. 15 shows the magnitude and the time delay of the reflections for the three sphere model of Fig. 1c. In this example the magnitude was normalized to unity and then dB scaling was performed. In the case of the time delay plots, the values were normalized to 1 nano-second before dB scaling was applied. These procedures were used since we found that the results were quite meaningful in terms of the locations and the resolution of the cancer plots.

The metric of image performance adopted here is peak-to-peak value of the difference of the backscattered reflections with and without the spheres for each increment move. The corresponding time delay was measured at the absolute maximum of the backscattered reflections.

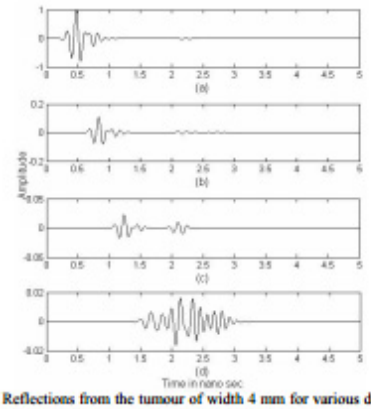

Figure 4: Reflections from the tumour of width 4 mm for various depths from the centre of the problem space; a) 75 cells left, b) 40 cells left, c) at the centre, d) 40 cells right.

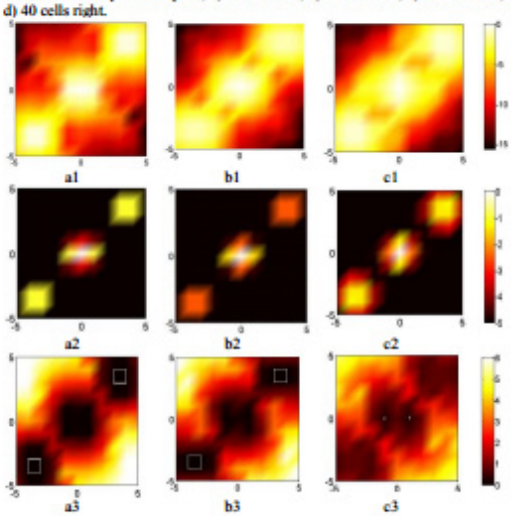

Fig. 5: The magnitude (a1,a2,b1,b2,c1,c2) and the time (a3, b3, c3) delay of the reflected signals of Figure 14a for various distances x_c: 10 mm (a1, b1,c1), 20 mm (a2, b2, c2), 30 mm (a3, b3, c3)

Figs 5 (a2, b2 and c2) are extended versions of the magnitudes given in Figs 5 (a1, b1 and c1) respectively. The data was interpolated using the piecewise bilinear Gouraud method. The results are quite encouraging in terms of the 10 mm resolution applied here that show the actual positions of the cancer locations. The depths of sphere models could be studied from Figs 5 (a3, b3 and c3). It is clearly shown that even at 30 mm depth the data can be useful in identifying the approximated distances.

IV. Conclusion

A computational investigation using 1D, 2D and 3D FDTD with wide spectrum source excitation has been tested for breast cancer detection. The results show that this system is capable of detecting small tumours with dimensions comparable with those required for the early detection of breast cancer. This study has shown the range of the scattering signal magnitudes from such objects for various depth distances of tumours.

References

[1] D. Gedney, "Introduction to the finite-difference time-domain (FDTD) method for electromagnetics," Synthesis Lectures on Computational Electromagnetics, vol. 6, pp. 1-250, 2011

[2] D. M. Sullivan, Electromagnetic simulation using the FDTD method: John Wiley & Sons, 2013.

[3] R. G. Blanks, S. M. Moss, C. E. McGahan, M. J. Quinn, and P. J. Babb, "Effect of NHS breast screening programme on mortality from breast cancer in England and Wales, 1990-8: comparison of observed with predicted mortality," Bmj, vol. 321, pp. 665-9, Sep 16 2000.

[4] B. Bocquet, J. C. van de Velde, A. Mamouni, Y. Leroy, G. Giaux, J. Delannoy, et al., "Microwave radiometric imaging at 3 GHz for the exploration of breast tumours," IEEE Transactions on Microwave Theory and Techniques , vol. 38, pp. 791-793, 1990.

[5] S. Adnan, R. A. Abd-Alhameed, M. Al Khambashi, Q. Yousuf, R. Asif, C. H. See, P. S. Excell, A. F. Mirza, Microwave Antennas for Near Field Imaging, IEEE MTT-S IMWS-Bio 2014, 8-10 Dec London, UK, Paper number: MPos1-9; pp. 1-3

[6] A. Taflove, "Review of the formulation and applications of the finite-difference time-domain method for numerical modeling of electromagnetic wave interactions with arbitrary structures," Wave Motion, vol. 10, pp. 547-582, 1988.

[7] C.H. See, R.A. Abd-Alhameed, S.W.J. Chung, D. Zhou, H. Al-Ahmad, and P.S. Excell, "The Design of a Resistively Loaded Bowtie Antenna for Applications in Breast Cancer Detection Systems", IEEE Trans. Antennas and Propagation, vol. 60, no. 5, pp. 2526 - 2530, May 2012.

[8] J.Bourqui and E. C. Fear, "Shielded UWB Sensor for Biomedical Applications," IEEE AWPL, vol.11, pp.1614-1617, 2012.

[9] R.K. Amineh, M.Ravan, A. Trehan and N.K. Nikolova, "Near-Field Microwave Imaging Based on Aperture Raster Scanning with TEM Horn Antennas," IEEE Trans. Antenna Propagat. ,vol.59, no.3, pp.928-940, March 2011

Reconfigurable Neurons – Making the Most of Configurable Logic Blocks (CLBs)

Arfan Ghani, Chan H. See
Engineering, Sports, and Sciences Academic Group
University of Bolton
Bolton, UK
A.Ghani@bolton.ac.uk

Hassan Migdadi, Rameez Asif, Raed A. A. Abd-Alhameed, James M Noras
School of Electrical Engineering and Computer Science
University of Bradford,
Bradford, UK
r.a.a.abd@bradford.ac.uk

***Abstract*—An area-efficient hardware architecture is used to map fully parallel cortical columns on Field Programmable Gate Arrays (FPGA) is presented in this paper. To demonstrate the concept of this work, the proposed architecture is shown at the system level and benchmarked with image and speech recognition applications. Due to the spatio-temporal nature of spiking neurons, this has allowed such architectures to map on FPGAs in which communication can be performed through the use of spikes and signal can be represented in binary form. The process and viability of designing and implementing the multiple recurrent neural reservoirs with a novel multiplier-less reconfigurable architectures is described.**

Keywords—recurrent neural networks; reservior computing; reconfigurable computing; FPGAs; neural signal processing

I. Introduction

The idea of reservoir computing was initially introduced by Maass [1] and Jaeger [2]. In their works in [1-2], the network activity is regarded as 'reservoir' where a memory-less readout device was used and trained to classify information from an untrained recurrent neural reservoir. Jaeger used analogue sigmoidal neurons as network units and called the model Echo State Network (ESN) [1], while Maass called it Liquid State Machine (LSM) and focused on networks of spiking neurons [2]. Both ESNs and LSMs are generally called reservoir computing (RC) [3] and it has been widely used in range of applications [2. 4-7], i.e. speech recognition, human action recognition and object tracking. There have been several studies in the past to investigate the paradigm of reservoir computing [3, 8-9] but none of them provide any guidelines as how to implement and analyse a stable reservoir on hardware/software (HW/SW) platforms. In order to address this deficiency, authors in [10-11] demonstrated the viability of implementing neural reservoirs on software platforms. The key objective of this work was to analyze and examine the impact of the input connectivity and to understand the parameters that affect the stability of neural reservoirs. Software implementation of small scale reservoirs is not a serious bottleneck, however to exploit the inherent parallelism of cortical columns, hardware implementations are essential. Implementing neural based applications on programmable hardware is challenging because the maximum size of a network that can be implemented on a target FPGA is restricted by the logic and arithmetic operators available on a single device. Therefore, a HW/SW co-design strategy has to be devised for implementation of neuro inspired systems on reconfigurable platforms. The limited number of embedded multipliers available on a single device when implementing large scale artificial neurons on reconfigurable platform is a specific bottleneck in this work. The square of the number of neurons is direct proportional to the number of multi pliers grows. According to [12-14], a two layer network with size of 10 neurons requires 100 multipliers and if this network is further expanded to 100 neurons, then, it will then require 10,000 embedded multipliers.

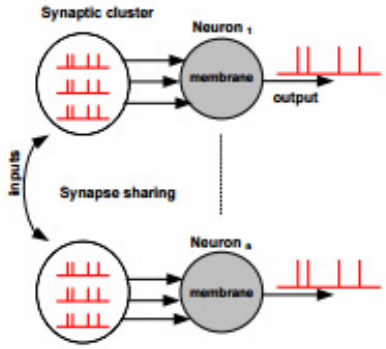

Fig.1: Overview of synaptic interaction amongst different neurons

This paper is a continuation of the work published in [12, 16] where authors' outlined a framework for possible implementation on reconfigurable platforms. It utilizes area efficient multiplier-less architecture [13-14] which significantly reduce the burden of multipliers required for synaptic multiplications. In order to investigate the viability of implementing reservoir computing paradigm on HW/SW platform, this work presents area efficient spiking neurons architectures. These architectures are targeted for large scale implementation of neuro inspired cortical columns for computational related tasks such as sensory fusion. The presented architectures are used as the basic building blocks for fully parallel implementation of multiple cortical columns on FPGAs. The hardware architectures implemented are inspired by 'microcircuits' which plays a fundamental role in cortical computation [1]. The main purpose of these so called microcircuits is to read out information and communicate with

the neighboring microcircuits connected in a columnar fashion. One of the limitations in implementing large scale spiking neural networks on HW/SW platforms is the limited size of the network, its scalability and weight storage for online training. Reservoir computing alleviates the burden of training at the network level where only the readout neurons are used for classification. The proposed architecture fully studies the reconfigurability and scalability of FPGAs at the network level which is targeting on three main areas which including pre-processing, post-processing and reconfigurable neutral reservoir. Pre and post processing is performed in software and fully parallel recurrent neural reservoir or microcircuit is implemented on FPGA hardware. To evaluate the reservoir dynamics, it is tested and benchmarked with an example of isolated spoken digit recognition – Texas Instruments 46-Word (TI46) [15].

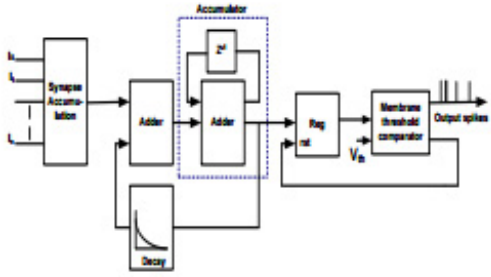

Fig.2. Membrane architecture

II. METHODOLGOY

Biologically plausible neurons are parallel in nature and to exploit this inherent parallelism, reconfigurable hardware architectures were developed. FPGAs offer an interesting alternative to software implementation because software platforms are not sufficient to simulate clusters of spiking neurons in real time and another constraint is scalability. In spiking neurons network, each neuron receives input spike potentials from other neuros within clusters. The input spike potentials believe to have different spike strengths which are accumulated in neuron membrane at different spike arrival times. Each neuron is further connected with clusters of spiking neurons. The neuron clusters are interconnected and the spike firing dynamics depends on synaptic strengths and their corresponding spike firing times. An overview of synaptic interaction is shown in Fig. 1.

There are numerous spiking neuron models, from very detailed to abstract models reported in the literature. In this study, a Leaky Integrate-and-Fire (LIF) neuron model was chosen for neural reservoir implementation. A synaptic integration mechanism was modelled with the following equation:

$$v_s(t) = \sum_{1}^{N_s} w_s x_s(t) \qquad (1)$$

In eq. 1. V_s sums the incoming spike strengths to the membrane, N_s counts the number of synapses, w_s is the weight associated with each synapse and x_s are the incoming binary spikes at specific time intervals t. The incoming synapses are accumulated into the neuron's membrane and when the total potential exceeds a certain threshold, an output spike is generated. The neuron firing dynamics are modelled with the following equation:

$$V_m(t) = \begin{cases} V_{reset} \rightarrow V_m(t) > v_{th} \\ V_m(t-1) + V_s(t) - V_{leakage}(t) \rightarrow otherwise \end{cases} \qquad (2)$$

In eq.(2). V_m is the membrane potential, V_{reset} is the reset potential, V_m $(t-1)$ is the membrane potential at the previous time step, V_s is the sum of synaptic potential and $V_{leakage}$ is the exponentially decreasing leakage voltage with time constant τ. The membrane voltage V_m (t) will be at V_{reset} if V_s $(t) > V_{th}$, otherwise the membrane potential will be equivalent to the second term in eq.(2).

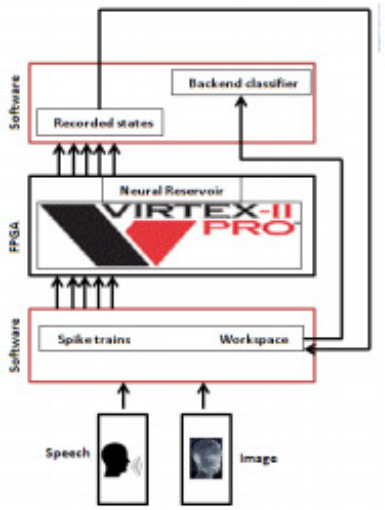

Fig.3. Overview of HW/SW environment for reservior-based recognition

One of the bottlenecks in implementing fully parallel neural reservoirs on reconfigurable hardware is the limited number of embedded multipliers available on a device, hence it is important that the use of area consuming multipliers are minimised so that multiple neural reservoirs with synaptic dynamics are efficiently implemented [13 - 14]. Synaptic mechanism can be implemented by number of ways, the most widely used technique is to multiply inputs with a fixed weight value. This technique requires one embedded multiplier for each synapse and as the number of synapses increase, so is the number of multipliers. This bottleneck limits the realisation of multiple neural reservoirs implemented on a single reconfigurable device. The proposed design offers a technique which could overcome the burden of synaptic implementation. The architecture was split into two sub structures: synapse and membrane. In order to implement synapses, a hardware technique is investigated where random input spikes were generated and converted into spike trains. The numbers of

spikes were counted by the spike counter to model synaptic strength of each spike.

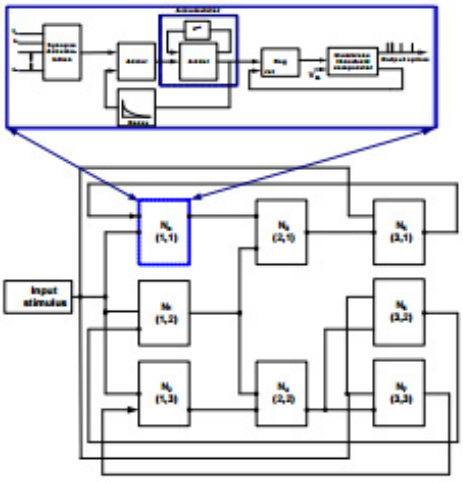

Fig.4. Hardware implementation of a neural reservoir (3 x 2 x 3)

The second half of the architecture is implemented as a neural membrane as shown in Fig. 2. The purpose of this architecture is to accumulate the input spike strengths (earlier encoded as number of spike trains) and when the total membrane potential exceeds a pre-determined fixed threshold, V_{th}, an output spike is generated which is fed to the following neurons in the reservoir. The threshold is modelled with a comparator block and after spike generation, the membrane potential was set to a 'reset' value through a register.

The hardware architectures were implemented with Xilinx System Generator toolbox where a discrete time step of 0.125 *ms* was chosen for simulations. In order to efficiently implement hardware blocks, it is important that appropriate bit resolution is selected. The membrane accumulator bit resolution is chosen as 18_12 (18 bit with 12 binary points). Similar to biological neurons, a threshold value of 0.15 V is selected. As the accumulator reaches the threshold potential, an output spike was generated and the membrane potential was exponentially decayed to the reset value of 0 V. The exponential decay function is implemented on Lookup Tables with a programmable decay constant τ. In order to calculate the maximum clock speed, the worst case delay was calculated and to capture the fully parallel neural dynamics, Xilinx computational blocks were assigned computational latencies accordingly.

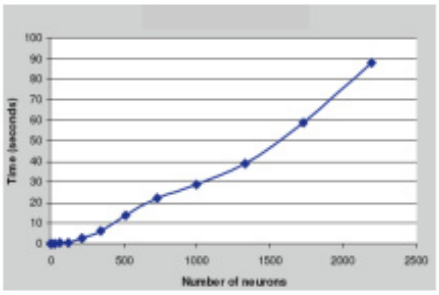

Fig.5. Simulation time verse size of the reservoir (neurons)

III. Results and Discussion

In this section, the T146 dataset [15] was used to test with the proposed reconfigurable architecture described in section II. Fig.3 shows the overview of the integrated HW/SW environment for reservoir-based recognition. This validates the functionality of the neural reservoir. In this case, the input speech signals were initially preprocessed to remove silence parts and features were extracted by implementing the Linear Predictive Coding technique. These features were further transformed into Poisson spike trains as an input stimulus to the reservoir and different states were recorded for post-processing. The state represents the membrane potentials of all the neurons in the reservoir. In this experiment, a reservoir of size 8 neurons is adopted and eight membrane potentials were recorded in one state. In total, 200 spike trains were processed through the reservoir for a total of 10 digits and 20 spike trains were generated for one digit. The 'readout' neurons (feed forward network) were implemented in software for the classification of input digits.

The network is designed where each neuron was connected with a minimum of two inputs spikes which are weighted through fixed weights. To enable the input spike trains interface with neutral reservoir, they have to be converted into Simulink Boolean type through input gateways.

In order to perturb the reservoir, these input spike trains were used and the received responses (membrane potentials) were stored and collected in MATLAB workspace for backend classification. To feed input data into the reservoir, the reservoir has to be simulated for the total time steps which equivalent to the time steps of spike trains. Once the total states were recorded, they were further sampled and only five states were recorded for post-processing. It should be noted that the states were recorded in linear scale from start to the end of states. The readout neurons were trained offline until the algorithm converged to the goal. Then, they were tested with the test samples to evaluate their classification accuracy.

As shown in Fig. 4 that a three-layered recurrent neural reservoir (3x2x3) was implemented where input vectors were directly connected to the neuron cells and each cell had a minimum of two synapses. It should be noted that a total number of 8 neuron cells with 16 synapses were used and it is also possible to increase the number of neurons and synapses

with a chain of adders for synaptic accumulation. The reason why all the neurons in the reservoir work in parallel is because of all the inputs and corresponding random weights were accessed at the same time. A total of 16 fixed weights were stored for 8 neurons where each neuron had minimum two inputs, in the network. The Poisson spike trans where were generated off-chip was selected as the input stimulus to the reconfigurable reservoir. The reservoir states (membrane potentials) were also stored off-chip for backend classification.

An MLP classifying engine was implemented as a backend in software. Total data was split into two sets: training and testing. A training sample is made up by 40 data points which consists of 5 states of total number of eight neurons at five linear time steps from begin to the end, and 10 output neurons were set in the output layer which represents the 10 isolated digits. The network was trained with the training samples. Each training sample was compared with the target and the accuracy is calculated based on this. It was found that the total number of the 30 hidden neurons is the best combination with input layer neurons. Interestingly, the overall accuracy degrades if the number of hidden layer neurons either increases or decreases below or beyond the maximum number of 30 neurons. After carrying out of the testing with the test data and different hidden layers, the results suggested that the overall accuracy of 98% can be achieve on the test data and 100% accuracy was obtained on training data set. Different standard back propagation training algorithms were tested but best results were achieved when the network was trained with the MATLAB Levenberg-Marquardt training algorithm. It was found that the training completed at 124 seconds and converged to the goal after 25 iterations.

In addition, the time required to simulate a reservoir depends on its size and the node type used to construct the reservoir. It will not be an issue to simulate small networks on sequential machines, however considering large scale networks it becomes a significant overhead. The simulation time increases many folds if larger reservoirs are to be simulated. In order to evaluate the simulation time requirement on sequential machines, different reservoirs were simulated on Intel Pentium P4 (3.20 GHz speed and I GB RAM). As shown in Fig. 5, the simulation time increases almost at the order of 2.5 which makes it impractical to simulate large scale reservoirs on software platforms.

IV. Conclusion

This paper has demonstrated a design of Hardware/Software paradigm for developing a reservoir based approach on reconfigurable platform. This will help to analyse, simulate and implement the inherent parallelism of cortical neural networks. The optimized proposed hardware architecture was performed at the network level and the required resources were evaluated. The results confirmed that it is feasible to design an area-efficient synapse processing by avoiding the required multipliers for synapse implementation. Interestingly, the results also suggested that the proposed architecture can be easily scaled on multiple FPGAs to form the distributed compact parallel columns. These attractive features have offered size reduction of circuit and elimination of control circuitry as well as possibly to design and implement large self-contained neural reservoirs for sensory fusion tasks on reconfigurable platforms.

References

[1] W. Maass, T.Natschläger and H.Markram, "Real-time computing without stable states: A new framework for neural computation based on perturbations", Neural Computation, vol.14, no.11, pp.2531-2560, 2002

[2] H. Jaeger and H. Haas, "Harnessing nonlinearity: Predicting chaotic systems and saving energy in wireless communication. Science, 304(5667), pp.78-80, 2004

[3] D. Verstraeten, B. Schrauwen, M.D'Haene, D. Stroobandt, "An experimental unification of reservoir computing methods", Neural Networks 20, pp. 391- 403, 2007

[4] P. Joshi and W. Maass, "Movement generation and control with generic neural microcircuits," BIO-ADIT, 2004.

[5] J. Yin. ,Y.Meng. and Y. Jin, "A developmental approach to structural self-organisation in reservoir computing," IEEE transactions on autonomous mental development, Vol. 4 (4), pp. 273 - 289, 2012

[6] K. Vandoorne1 et al , "Advances in Photonic Reservoir Computing on an Integrated Platform, International Conference on Transparent Optical Networks," pp. 1-4,2011

[7] J. Yin and Y. Meng, "Reservoir Computing Ensembles for Multi-Object Behavior Recognition," IEEE World Congress on Computational Intelligence, pp. 1-8, 2012

[8] M.D. Skowronski and J.G. Harris, " Automatic speech recognition using a predictive echo state network classifier," Neural Networks, vol.20, no.3, pp. 414-423, 2007

[9] I. Uysal, H. Sathyendra and J.G. Harris, "Spike based feature extraction for noise robust speech recognition using phase synchrony coding," ISCAS, pp. 1529 - 1532, 2007

[10] A. Ghani, T.M. McGinnity, L.P. Maguire, J.G.Harkin, "Neuro-inspired speech recognition with recurrent spiking neurons," LNCS 5163, Springer-Verlag, pp. 513-522, 2008

[11] A. Ghani, et al, "Neuro-Inspired Speech Recognition Based on Reservoir Computing," Advances in Speech Recognition, ISBN 978-953-307-097-1, pp. 164, September 2010.

[12] A. Ghani et al, "Neuro-Inspired Reconfigurable Architecture for Hardware/Software Co-design," IEEE international conference on System on Chip, SOCC, pp: 287 - 290,2009

[13] L.P. Maguire ,T.M. McGinnity, B. Glackin, A. Ghani, A. Belatreche, A, J. Harkin,"Challenges for large-scale implementations of spiking neural networks on FPGAs", Elsevier Journal of Neurocomputing, Vol. 71 (1-3), pp. 13-29, 2006

[14] A. Ghani, T.M. McGinnity, L.P. Maguire, J.G. Harkin, "Area efficient architecture for large scale implementation of biologically plausible spiking neural networks on reconfigurable hardware," FPL, pp. 1-2, 2006

[15] G.R. Doddington and T.B. Schalk, T B, "Speech recognition: Turning theory to practice", *IEEE Spectrum*, vol. 18, no.9, pp: 26-32, 1981.

[16] A.Ghani, C.H. See and S.M. Usman Ali, " Step forward to map fully parallel energy efficient cortical columns on field programmable gate arrays," IET SMT, vol.8, no. 6, pp.432-440, 2014

Study On Specific Absorption Rate

R. Asif, R.A. Abd-Alhameed, M Bin-Melha, A. Qureshi, C.H See, Y.I. Abdulraheem, TT Mapuka and J.M. Noras
Antennas and Adv. Electromagnetics Research Group
School of Engineering and Informatics, University of Bradford, Bradford United Kingdom
{r.asif1, r.a.a.abd}@bradford.ac.uk

***Abstract*— In the past fifty years it has been clearly identified that the presence of biological tissues effect the performance of the antenna and considerable effort has been made to improve the characteristics of the mobile phone antenna's but very less effort has been put in to evaluate the effects of the radio frequency and energy absorption by the biological organisms and their effect. In this work as part of a bigger work package we have evaluated the effects of the handset orientation on the values of SAR and radiation efficiency as well as the effect of the distance upon these values. The study has produced some very interesting results showing that the most common way of holding the mobile phone i.e. microphone close to the mouth produces the highest SAR values.**

Keywords—SAR; Electromagnetic radiations; Radio Frequency

I. INTRODUCTION

Recent research activities in the field of radio frequency and microwaves have given birth to a very diverse range of RF equipment's. The fields of telecom, broadcasting, consumer market products and medical devices have been completely revolutionized [1]. When used as a means of communication e.g. in radio or TV broadcasting, including the radar devices the electromagnetic field generally tends to extend over a wide range of area. The industrial and medical devices only spread over a short range. If the devices are short ranged the users tend be more as a general trend but these electromagnetic waves when get reflected and scattered in addition to the simultaneous RF emissions results in a complex system which is simply said to be a multipath and the fields that are non-uniformly distributed in space[2]. The studies that have been conducted to study the negative effects of the RF exposure on the human health has raised some concerns [3] and the limits have been imposed by different governing bodies in order to control, but the exposure outside these limits can cause serious side effects. This effect is not only signal strength dependent or time dependent but there are many other factors that play in to the total effect and can include the frequency, distance from the source and polarization. The electromagnetic radiations do produce a change or a biological in the biological organism but it is not always that it results in side effects and it is very important to understand this concept and the difference between the two terms in order to determine how much exposure is safe [4]. There is exposure in which some physiological change is caused by the electromagnetic radiation, this is referred to as biological effect but if this biological effect falls outside the limitations of the biological body to compensate then it will result in adverse health effects. This paper has been structured in the following manner, Section I gave an introduction into the topic of SAR and Section II will provide an insight on the simulation setup and criteria followed by the Results and Discussion in Section III and the topic will be concluded in the section IV of this paper.

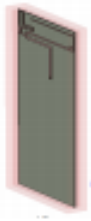

Fig. 1 The geometry of the antenna model (42 x 115 mm).

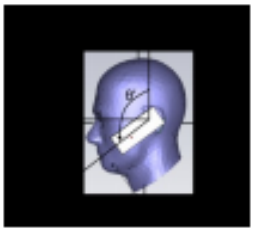

Figure 2: Arrangement of Head and Handset

II. SIMULATION SETUP

The antenna used for this study is multiband planar antenna. The antenna is designed using a two strip monopole and a meandered strip line with an area of 15mm × 42mm as presented in [1]. The geometry of the antenna is detailed in Figure 1. This antenna has been mounted upside down into the handset model in order to keep the radiators away from the biological tissue and then test the SAR. In Figure 2 the return loss of the antenna has been presented for three different scenarios i.e. the red line shows the reflection coefficient of the antenna only and it can be seen that both frequencies of interest i.e. 900MHz an 1800 MHz exhibit acceptable performance. This performance starts to degrade with the addition of the enclosure i.e. the cover of the mobile handset and then considerably decreases when placed in the proximity of the head. The head template was imported from the CST studio Suite and then the electric properties at 900 and 1800 MHz were adopted from [1]. The arrangement of the phone with the head is detailed in the Figure 3. The shortest distance between the handset and the head was denoted by 'd', and orientation angle between the center of the handset and the local z' axis is 'Θ'.

III. RESULTS AND DISCUSSION

The study considers four different distances from the human head i.e. 5mm, 10mm, 15mm and 20mm respectively for three different values of theta Θ i.e. 90 degree, 135 degree and 169 degrees. The reason behind using 169 degrees rather than 180 degrees was the unusual position of the handset. The graphs (shown in Figs 4 and 5) for two classes of SAR, namely SAR averaged over 1g and SAR averaged over 10g

978-1-4799-3662-5/14/$31.00 ©2014 IEEE

have been discussed. Initially consider SAR over 1g at 900MHz. The maximum value of SAR over 1g occurs at Θ = 135 degrees and d = 5mm and roughly equals 12.4W/Kg. The imput power is set at 1 Watt.

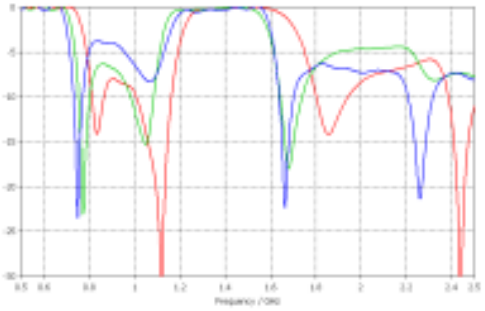

Figure 3: Frequency response of the reflection coefficient; red: antenna only, green: antenna with enclosure, blue: antenna with enclosure and human head.

SAR data for the antenna model given in Figure 1, subject to the orientation angle can be demonstrated by following table/s:

Table 1:
SAR vales for 'θ' = 90 at 900 MHz

D Mm	SAR averaged over 1gm W/kg	SAR averaged over 10gm W/kg	Liner Power Gain	Radiation Efficiency	Power gain dB	Radiated power mW
5	9.85	5.65	0.888	0.383	-0.517	125
10	5.68	4.08	1.1	0.550	0.432	170
15	4.31	3.10	1.39	0.530	1.44	172
20	3.66	2.37	1.65	0.600	2.17	197

The three parameters given in Table 1 and 2 include: Power Gain (dB), Radiated Power and Radiation Efficiency, show a similar trend as distance increases. Radiation efficiency increases from a minimum value of 0.383 at d = 5mm to 0.6 at d = 20mm. Likewise the values of the other two parameters also increase when distance increases.

Table 2:
SAR vales for 'θ' = 135 at 900 MHz

d mm	SAR averaged over 1gm W/kg	SAR averaged over 10gm W/kg	Radiation efficiency	Power gain dB	Radiated power mW
5	12.4	6.50	0.342	-0.493	114
10	6.93	4.58	0.424	0.661	137
15	5.23	3.49	0.515	1.59	166
20	3.96	2.65	0.585	2.35	195

As in Table 1 the three parameters in this table also increase with increasing distance. Power Gain (dB) increases from the lowest negative value of -0.493 to the highest value of 2.35. Radiation efficiency increases from 0.342 to 0.585. There is a rapid increase in radiated power when distance increases d = 10mm to d = 15mm.

Table 3:
SAR vales for 'θ' = 169 at 900 MHz

d mm	SAR averaged over 1gm W/kg	SAR averaged over 10gm W/kg	Radiation efficiency	Power gain dB	Radiated power mW
5	4.41	3.12	0.55	1.79	220
10	3.81	2.68	0.58	2.27	230
15	3.22	2.24	0.64	2.8	250
20	2.87	2.08	0.69	3.24	270

In the Table 3, the Power Gain (dB) increases from the lowest positive value of 1.79 to the highest value of 3.24. Radiation Efficiency also increases but one noticeable fact is that, radiation efficiency will always be less than 1. Maximum radiated power achieved is 270mW at d = 20mm.

Table 4
SAR vales for 'θ' = 90 at 1800 MHz

d mm	SAR averaged over 1gm W/kg	SAR averaged over 10gm W/kg	Radiation efficiency	Power gain dB	Radiated power mW
5	6.20	3.78	0.620	4.01	237
10	4.86	2.99	0.682	4.5	285
15	1.35	0.842	0.743	4.92	260
20	2.55	1.62	0.790	5.34	312

In Table 4 above an irregular pattern can be seen in Radiated Power as distance increases from d = 10mm to d = 15mm. The radiated power at d = 10mm is greater than that at d = 15mm. This difference can occur due to any physical factor. The power gain values are quite high in this table than the values in the previous tables.

Table 5
SAR vales for 'θ' = 135 at 1800 MHz

d mm	SAR averaged over 1gm W/kg	SAR averaged over 10gm W/kg	Radiation efficiency	Power gain dB	Radiated power mW
5	6.11	3.89	0.764	3.58	225
10	3.51	2.19	0.771	4.29	287
15	3.09	2.01	0.779	4.86	285
20	2.51	1.58	0.804	4.95	297

In Table 5 above the SAR values averaged over 1g decrease sharply from 6.11W/Kg to 3.51W/Kg when distance increases from d = 5mm to d = 10mm. We again notice an irregularity in Radiated Power at d = 10mm and d = 15mm. Radiation Efficiency are also quite high in the above table than in the previous tables.

Table 6
SAR vales for 'θ' = 169 at 1800 MHz

d mm	SAR averaged over 1gm W/kg	SAR averaged over 10gm W/kg	Radiation efficiency	Power gain dB	Radiated power mW
5	7.35	4.29	0.742	4.07	265
10	6.84	3.86	0.758	4.29	271
15	3.71	2.23	0.818	5.01	310
20	2.71	1.67	0.833	5.2	329

The results in the Table 6 indicate a similar trend as shown in the previous tables. The three parameters i.e. radiation efficiency, power gain and radiated power, increase with increasing distance. It can be observed that radiation efficiency values are higher in case of 1800MHz than those at 900MHz irrespective of the angle theta.

The averaging volume used to calculate the maximum SAR values is shown in Figure 5.

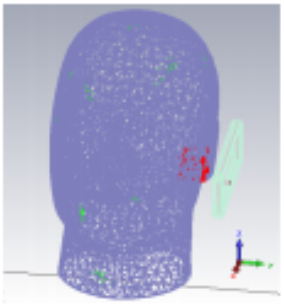

Figure 5: Averaging volume used for max SAR calculation

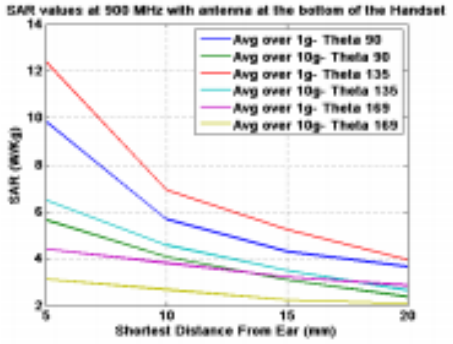

Figure 6: SAR Values at 900 MHz

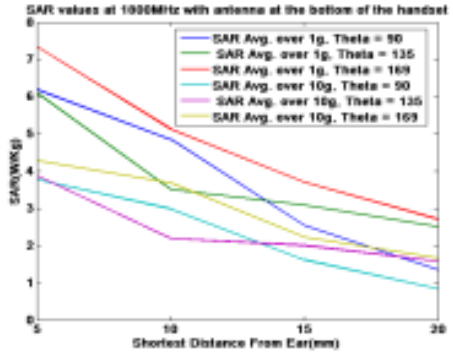

Figure 7: SAR Values at 1800 MHz

The average values of SAR over 1g at Θ = 90 and 169 and d = 5mm equal 9.8W/Kg and 4.5W/Kg respectively. A general decreasing trend in the values of SAR can be seen as the distance of handset from the head increases at the particular angles mentioned above. There is huge decrease in the values of SAR over 1g at theta = 90 and 135 as the distance increases from 5mm to 20mm. The rate of change in the values of SAR with respect to distance decreases for Θ = 90 and 135 as the distance between the handset and head increases. However, a small change occurs in the value of SAR over 1g for Θ =169. The rate of change of SAR with respect to distance for Θ =169 stays fairly constant as the distance between the handset and the head increases. The final values of SAR over 1g and d = 20mm at theta = 90, 135 and 169 are 3.8W/Kg, 4W/Kg and 2.9W/Kg. Now consider the average value of SAR over 10g. The average values of SAR over 10g are less than their 1g counterparts. Again, the max value of SAR over 10g occurs at theta = 135 and d=5mm and roughly equals 6.6W/Kg. The average values of SAR over 10g at theta = 90 and 169 and d=5mm equal 5.8W/Kg and 3.1W/Kg respectively. A general decreasing trend can be seen in the average values of SAR over 10g as the distance between the handset and head increases. The decrease in the SAR values for theta = 90 and 135 is greater compared to that of theta = 169. The rate of decrease of SAR with respect to distance for theta = 90 and 135 decreases as the distance increases. However, the rate of decrease of SAR over 10g for theta = 169 stays fairly constant. The final values of SAR over 10g and d = 20mm at theta = 90, 135 and 169 are 2.4W/Kg, 2.6W/Kg and 2.1W/Kg respectively.

IV. Conclusion

It is concluded that at 900 MHz, 135 degree angle has the highest values of SAR when averaged over 1g or 10g, 90 degree takes the second largest values followed by the 169 degrees and for the 1800 MHz as the properties of the tissues, wavelength of the signal, permittivity and conductivity of the brain matter changes the results quite dramatically change and has very low averaged SAR values over 1g and 10g.

References

1. J. P. Stralka and P. A. Bottomley, "A prototype RF dosimeter for independent measurement of the average specific absorption rate (SAR) during MRI," *Journal of Magnetic Resonance Imaging*, vol. 26, pp. 1296-1302, 2007.
2. R. Asif, R. Abd-Alhameed, O. Anoh, and Y. Dama, "Performance Evaluation of DWT-FDM and FFT-OFDM for Multicarrier Communications Systems using Time Domain Zero Forcing Equalization," *International Journal of Computer Applications*, vol. 51, 2012.
3. E. Piuzzi, P. Bernardi, M. Cavagnaro, S. Pisa, and J. C. Lin, "Analysis of adult and child exposure to uniform plane waves at mobile communication systems frequencies (900 MHz–3 GHz)," *Electromagnetic Compatibility, IEEE Transactions on*, vol. 53, pp. 38-47, 2011.
4. R. F. Cleveland, R. E. Fields, and J. L. Ulcek, "Questions and answers about biological effects and potential hazards of radiofrequency electromagnetic fields," 1999.